Synthesis, substitution kinetics, electrochemistry and phase studies of long-chain alkylated ferrocene-containing rhodium(I) complexes with biomedical applications

A thesis submitted in accordance with the requirements of the degree

Philosophiae Doctor

in the

Department of Chemistry

Faculty of Natural and Agricultural Sciences

at the

University of the Free State

by

Patrick Thabo Ndaba Nonjola

Promoter

Prof. J.C. Swarts

September 2006

TABLE OF CONTENTS

LIST OF ABBREVIATIONS

A	absorbance
Å	angstrom
acac	acetyl acetonato $(CH_3COCHCOCH_3)^-$
$AlCl_3$	Aluminium trichloride
AR	analytical reagent
ArN_2^+	aryl or alkyl diazonium salt
BuLi	*n*-butyllithium
Cc	cobaltocenium $[(C_5H_5)_2Co]^+$
$CDCl_3$	deuterated chloroform
$CHCl_3$	chloroform
CH_2Cl_2	dichloromethane
CH_3CN	acetonitrile
CH_3OH	methanol
CO	carbon monoxide or carbonyl
cod	cyclooctadienyl
CoLo	human colorectal cancer cell line
Cp	cyclopentadienyl $(C_5H_5)^-$
CV	cyclic voltammetry
δ	chemical shift
DCM	dichloromethane
DMF	dimethyl formamide
DMSO	dimethyl sulfoxide
DSC	differential scanning calorimetry
ε	molecular extinction coefficient
E	applied potential
$E^{o/}$	formal reduction potential
E_a	energy of activation
E_{pa}	peak anodic potential

E_{pc}	peak cathodic potential
ΔE_p	separation of peak anodic and peak cathodic potentials
Et	ethyl
eq	equivalents
F	Faraday constant (96485.3 C mol^{-1})
Fc	ferrocene [$(C_5H_5)_2Fe$] or ferrocenyl [$Fe(C_5H_5)(C_5H_4)$]-
Fc^+	ferricenium $[Fe(C_5H_5)(C_5H_4)]^+$
FCS	fetal calf serum
ΔG^*	Gibbs activation energy
HeLa	human cervix epitheloid cancer cancer cell line
ΔH^*	enthalpy activation energy
IC_{50}	mean drug concentration causing 50 % cell death
i_{pa}	peak anodic current
i_{pc}	peak cathodic current
K	equilibrium constant
k_2	second-order rate constant
k_b	Boltzmann constant (1.381 x 10^{-23} J K^{-1})
k_{obs}	observed rate constant
k_s	rate constant of solvation
LDA	lithium diisopropylamide
λ_{exp}	wavelength at maximum absorbance
M	central metal atom
Me	methyl
MTT	3-(4,5-dimethylthiazol-2-yl)-diphenyltetrasodium bromide
n	number of electrons
NaOH	sodium hydroxide
$[NBu_4][PF_6]$	tetrabutylammonium hexafluorophosphate
$[NBu_4][B(C_6F_5)_4]$	tetrabutylammonium tetrakis[pentafluorophenyl]borate
^{1}H NMR	nuclear magnetic resonance spectroscopy
OM	optical microscopy
Ph	phenyl, (C_6H_5)
phen	1,10-phenanthroline

pK_a	-log K_a, K_a = acid dissociation constant
ppm	parts per million
R	gas constant (8.314 J K^{-1} mol^{-1})
Rc	ruthenocene, $[(C_5H_5)_2Ru]$
S	solvent
ΔS^*	entropy of activation
SCE	saturated calomel electrode
T	temperature
THF	tetrahydrofuran
UV/Vis	ultraviolet/visible spectroscopy
ΔV^*	volume of activation
ν(C=O)	infrared carbonyl stretching frequency
X	halogen
χ_R	group electronegativity (Gordy scale) of R group

LIST OF FIGURES

LIST OF SCHEMES

LIST OF TABLES

ACKNOWLEDGEMENTS

I hereby wish to express my sincere gratitude to God Almighty for His grace, strength and wisdom that carried me through this study and towards the following people who all contributed directly or indirectly to the preparation of this thesis.

I would like to thank Prof. J. C. Swarts, my supervisor, for his leadership, support, excellent guidance and the valuable time he devoted during the course of this study. Dr. J. Conradie, for her willingness to render assistance whenever called upon. Mrs Elke Kreft from the Department of Immunology, Institute for Pathology at the University of Pretoria for performing biological tests.

Collectively, all my post-graduate colleagues and the department of chemistry for their interest in my studies as well as their helpful advice in experimental techniques.

Finally to the memory of my mother, Maseitebaleng and my family for their prayers, concern and valuable encouragement during the years of my study. To my girlfriend (Linda) and friends for the constant support and understanding during difficult times and for showing a keen interest in my progress. I am grateful.

For financial assistance during the course of my study I would like to thank NRF.

Patrick Thabo Ndaba Nonjola

September 2006

Abstract

New alkylferrocene-containing β-diketones of the type (Cp-R)-Fe-(Cp-$COCH_2COCH_3$), where R = C_9H_{19}, $C_{10}H_{21}$, $C_{12}H_{25}$, $C_{14}H_{29}$ and $C_{18}H_{37}$ as well as (Cp)-Fe-(R-Cp-$COCH_2COCH_3$), (Cp-R)-Fe-(R-Cp-$COCH_2COCH_3$) and (Cp-R)-Fe-(Cp-$COCH_2CO$-Cp)-Fe-(Cp-R) with R = $C_{10}H_{21}$ or $C_{12}H_{25}$ were prepared by Claisen condensation of acetyl-alkylferrocene derivatives and the appropriate ester under the influence of lithium diisopropylamide. Complexation of all the β-diketones with $[RhCl_2(cod)_2]$ in DMF gave the [Rh(β-diketonato)(cod)] complexes. The $pK_a^{/}$ values of the new β-diketone derivatives were determined spectroscopically in water containing 10 % acetonitrile (v/v). The keto-enol isomerization kinetics of all new β-diketones was studied in $CDCl_3$ by ^1H NMR spectroscopy.

Electrochemical studies revealed that all the β-diketones exhibited an electrochemically and chemically reversible one-electron transfer process for the Fc/Fc^+ couple. The redox active centre of all the β-diketones exhibited $E^{o/}$ values that are independent of the alkyl chain length of the ferrocene-containing β-diketones due to the lack of conjugation between the ferrocenyl group and the alkyl R groups. Cyclic voltammetry results of all the rhodium complexes showed that the Rh^I nucleus exhibited an electrochemically quasi reversible process.

Substitution reactions of the β-diketonato ligand from [Rh(β-diketonato)(cod)] with 1,10-phenanthroline exhibited saturation kinetics. Second-order rate constants, k_2, were determined from the linear plots of $1/k_{obs}$ against 1/[1,10-phenanthroline]. The large negative activation entropy values suggested an association mechanism. All substitution reactions had no observable mechanistic solvent pathway.

Phase studies showed that the ferrocenyl derivatives and free β-diketones exhibited solid state phase changes while the rhodium(I) complexes showed no pronounced melting or crystallization peaks due to very slow crystallization kinetics.

Cytotoxic properties in terms of potential anticancer applications of selected β-diketones and their rhodium complexes are described. Cytotoxicity of these complexes was probed with respect to human colorectal (CoLo) and human cervix epitheloid (HeLa) cancer cell lines. All the drugs that were investigated in this study had lower IC_{50} values than the rhodium complexes without long chain alkyl substituents.

Keywords: Ferrocene, β-diketones, rhodium, $pK_a^{/}$, isomerization kinetics, cyclic voltammetry, substitution kinetics, phase changes and cytotoxicity.

Opsomming

Nuwe alkielferroseen-bevattende β-diketone van die tipe (Cp-R)-Fe-(Cp-$COCH_2COCH_3$), waar R = C_9H_{19}, $C_{10}H_{21}$, $C_{12}H_{25}$, $C_{14}H_{29}$ en $C_{18}H_{37}$ sowel as (Cp)-Fe-(R-Cp-$COCH_2COCH_3$), (Cp-R)-Fe-(R-Cp-$COCH_2COCH_3$) en (Cp-R)-Fe-(Cp-$COCH_2CO$-Cp)-Fe-(Cp-R) met R = $C_{10}H_{21}$ of $C_{12}H_{25}$ is berei deur Claisen kondensasie van asetiel-alkielferroseenderivate en die toepaslike ester onder die invloed van litiumdiisopropielamied. [Rh(β-diketonato)(cod)] komplekse is verkry deur kompleksering van al die β-diketone met [$RhCl_2(cod)_2$] in DMF. Die $pK_a^{/}$ waardes van die nuwe β-diketoonderivate is spektroskopies in water met 10 % asetonitriel (v/v) bepaal. Die keto-enol isomerisasiekinetika van alle nuwe β-diketone is met ^{1}H KMR spektroskopie in $CDCl_3$ bestudeer.

Elektrochemiese studies het gewys dat al die β-diketone 'n elektrochemies- en chemies omkeerbare enkelelektronoordragsproses vir die Fc/Fc^+ koppel vertoon. Die redoksaktiewe sentra van al die β-diketone het $E^{o/}$ waardes getoon wat onafhanklik is van die alkielkettinglengte van die ferroseenbevattende β-diketone weens die gebrek aan konjugasie tussen die ferrosenielgroep en die alkiel R groepe. Sikliese voltammetrie resultate van al die rodiumkomplekse het gewys dat die Rh^I sentrum 'n elektrochemies kwasi-omkeerbare proses vertoon.

Substitusiereaksies van die β-diketonatoligand van [Rh(β-diketonato)(cod)] met 1,10-fenantrolien het versadigingskinetika getoon. Tweede-orde tempokonstantes, k_2, is bepaal vanaf die lineêre grafieke van $1/k_{wg}$ teen 1/[1,10-fenantrolien]. Die groot negatiewe aktiveringsentropiewaardes dui op 'n assosiatiewe meganisme. Tydens al die substitusiereaksies is geen meganistiese oplosmiddelroete waargeneem nie.

Fasestudies het daarop gedui dat die ferrosenielderivate en vrye β-diketone vastetoestand faseveranderinge ondergaan, terwyl die rodium(I)komplekse weens uiters stadige kristallisasiekinetika geen noemenswaardige smeltings- of kristallisasiepieke vertoon het nie.

Sitotoksiese eienskappe, in terme van potensiële antikanker toepassings, van sekere β-diketone en hul rodiumkomplekse word beskryf. Sitotoksisiteit van hierdie komplekse ten opsigte van menslike kolorektale- (CoLo) en menslike servikale epiteloïede (HeLa) kankerseltipes is ondersoek. Al die geneesmiddels wat tydens hierdie studie ondersoek is, het laer IC_{50} waardes as die rodiumkomplekse sonder langketting alkielsubstituente gehad.

Sleutelwoorde: Ferroseen, β-diketone, rodium, $pK_a^{/}$, isomerisasiekinetika, sikliese voltammetrie, substitusiekinetika, faseveranderings en sitotoksisiteit.

Chapter 1

Introduction and aim of study

1.1. Rhodium complexes in catalyses

The platinum group metals are ruthenium, osmium, rhodium, iridium, palladium and platinum.[1] The platinum group metals are extensively used as catalysts in industry.[1] Most of the processes used to convert raw materials such as oil, natural gas and coal into useful products depend on catalytic reactions.[2] Rhodium-based catalytic processes include hydrogenation reactions, hydroformylation of alkenes, the Monsanto acetic acid process and the Wacker process for making acetaldehyde from ethylene. The processes mentioned above represent fundamental reactions that transition metal complexes undergo, reactions such as oxidative addition, insertion reactions, substitution and reductive elimination. This is demonstrated in the scheme below for the synthesis of acetic acid from methanol.

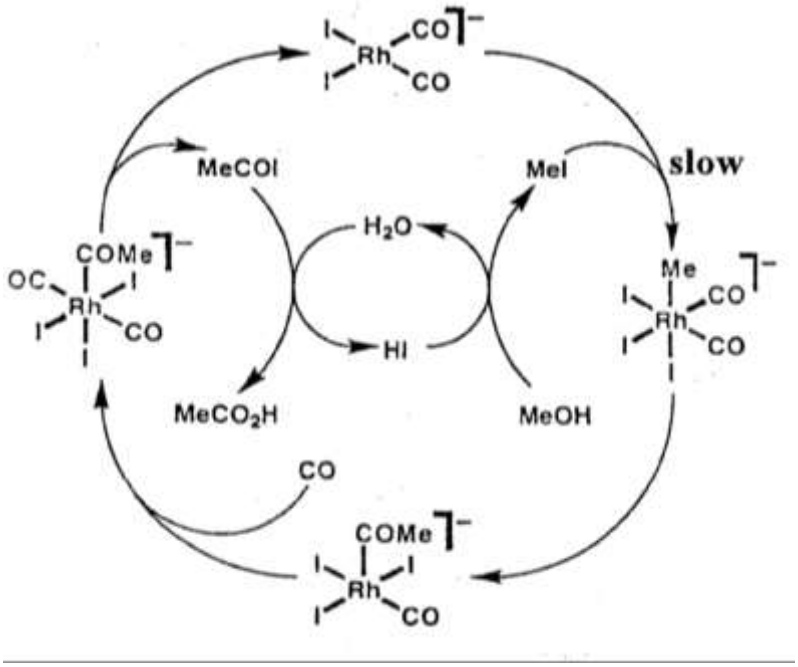

Scheme 1.1: Cycle for the $[Rh(CO)_2I_2]^-$ catalyzed carbonylation of methanol to yield acetic acid.

The rhodium-catalyzed carbonylation of methanol to acetic acid is to date probably the most successful example of an industrial process catalyzed by a metal complex in solution.[3] The rate-determining step of the cycle above is the oxidative addition of methyl iodide to $[Rh(CO)_2I_2]^-$. Just as rhodium, ferrocene and its derivatives have been the subject of many different studies because of their use as colour pigments,[4] high burning rate catalysts in solid fuels,[5] liquid fuel combustion catalysts,[6] smoke suppressant additives[7] and as antineoplastic agent in cancer treatment.[8,9,10]

1.2. Rhodium and iron-containing compounds in medical application

After successful development of *cisplatin* [*cis*$PtCl_2(NH_3)_2$] as an anticancer drug, interest in the use of transition metal complexes, including iron complexes, in medicine and other biological areas grew rapidly.[11] In terms of new antineoplastic material (i.e. compounds that have cytotoxic properties, but are not in clinical use), it was shown in this laboratory that ferrocene-containing β-diketones and alcohols containing a ferrocenyl group have very promising 50 % lethal dosage (LD_{50}) values.[12] The chemotherapeutic effectiveness of ferrocene-containing carboxylic acids and alcohol derivatives was shown to be directly related to the formal reduction potential of the ferrocenyl group.[13] Both the carboxylic acid derivatives and the alcohols showed enhanced anticancer activity as the ferrocenyl group became easier to oxidize.

In addition, it was found that some rhodium(I) complexes showed enhanced antineoplastic activity over *cisplatin*.[14] The antitumor rhodium(I) compounds with the *in vivo* activity were the organometallic neutral and square planar rhodium(I) cyclooctadiene complexes [$(NH_3)Rh^I$(cod)Cl] and [Rh^Ipiperidine(cod)Cl] (cod = cis-1,5-cyclooctadiene). These complexes have antitumor activity against the Ehrlich ascites carcinoma.[15] The acetylacetonato (acac) derivative [Rh^I(cod)(acac)],[16,17] inhibited the growth of leukemia L1210, sarcoma 180, and Ehrlich ascite carcinoma and had antimetastatic activity against the metastasizing Lewis lung carcinoma.

1.3. Liquid crystal properties

The melting of most crystalline solids involves a single well defined transition from crystalline solid to the isotropic liquid phase at a well defined temperature. For some compounds, however, the melting process occurs by way of one or more intermediate phase, called mesophases, over a wide temperature range. All the mesophases represent a liquid crystalline state. The molecular packing order of mesophases lie between the absolute three-dimensional order of crystalline solids and the completely disordered conventional (isotropic) liquids.[18] In many cases, metallomesogens may be created by the introduction of long alkyl chains in the structure of a metal complex. Piechocki [19] and co-workers were the first to report about the metallophthalocyanines displaying thermotropic discotic mesophases. Since the initial discovery, many examples of mesogenic phthalocyanines have been reported with variations in the number, length and position of the substituents.[19] From

this laboratory, Swarts and co-workers showed that by introducing a ferrocene side chain to the phthalocyanine macrocycle, the liquid crystalline temperature range could be substantially enlarged.[20]

Efforts orientated towards the design of new metallomesogens led to ferrocene derivatives displaying rich mesomorphism.[21,22] Deschenaux and co-workers reported the first example of ferrocene-containing thermotropic liquid crystals.[23] Recently unsymmetrical 1,3-disubstituted ferrocene-containing liquid crystals was also reported, where the different substituents at the 1- and 3- position generates structures with planar chirality.[24]

In recent years a new dimension in liquid crystal research developed based on β-diketone, pyrazole and isoxazole derivatives.[25] Few examples of calamatic (rod-like) liquid crystals containing rhodium have been described in the literature and they have *cis*-[RhCl(CO)$_2$L] structures where L is a nitrogen donor promesogenic ligand.[26,27] The liquid crystal properties of rodium complexes containing the rod-like β-diketonate and pyrazole ligands were also investigated.[28]

1.4. Aims of this study

With this background, the following goals were set for this study:

1. Synthesis of ferrocene-containing β-diketones with long-chain alkyl substituents, R, of the type (Cp-R)Fe(Cp-COCH$_2$COCH$_3$) with Cp = cyclopentadienyl and R = C_9H_{19}, $C_{10}H_{21}$, $C_{12}H_{25}$, $C_{14}H_{29}$ and $C_{18}H_{37}$. This implies that this family of the β-diketone ligands has the structure,

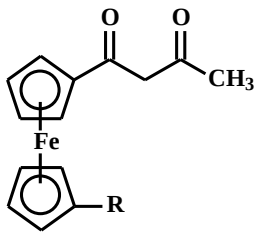

R = C_9H_{19}, $C_{10}H_{21}$, $C_{12}H_{25}$ $C_{14}H_{29}$ and $C_{18}H_{37}$

Figure 1. 1: Long chain alkyl substituents at the 1,1$^/$-position of ferrocene-containing β-diketones.

Other new ligands having structures

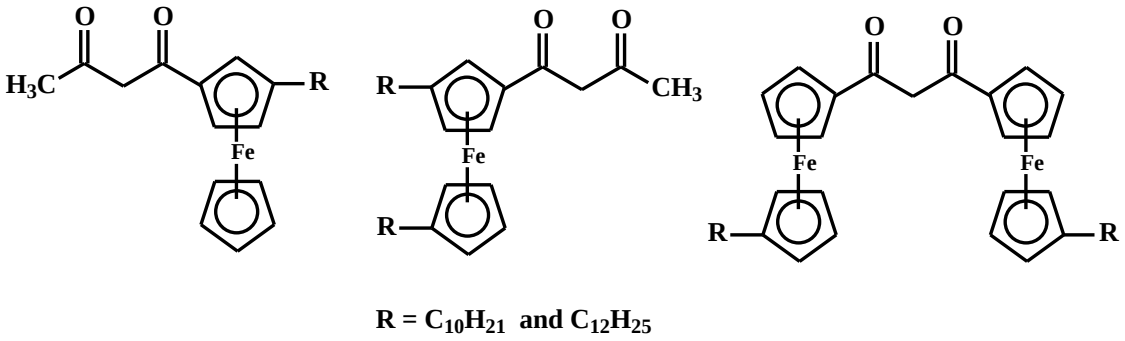

R = $C_{10}H_{21}$ and $C_{12}H_{25}$

Figure 1. 2 Long-chain alkyl substituents at 1,3-, 1,1′,3-position, ferrocene-containing β-diketone derivarives as well as the diferrocenyl β-diketones.

and abbreviated as, (Cp)Fe(R-Cp-$COCH_2COCH_3$), (Cp-R)Fe(R-Cp-$COCH_2COCH_3$) and (Cp-R)Fe(Cp-$COCH_2$CO-Cp)Fe(Cp-R) were also targeted for syntheses. These ligands will probe the influence, if any, of R-substitution on different cyclopentadienyl rings of the ferrocenyl groups.

2. Synthesis of the square planar rhodium(I) complexes [Rh(β-diketonato)(cod)] where cod = cyclooctadiene and β-diketonato is derived from the β-diketones above.
3. Characterization of the β-diketones mentioned in goal 1 in terms of pK_a values, keto-enol equilibrium constants and rate of conversion between the enol and keto isomers.
4. A kinetic study of the substitution of the β-diketonato ligand in [Rh(β-diketonato)(cod)] complexes of goal 2 with 1,10-phenanthroline by means of stopped-flow kinetic techniques.
5. Investigation of the electrochemical properties of the compounds mentioned in goals 1 and 2 above utilizing cyclic, square wave and linear sweep voltammetry techniques. This will allow the determination of formal reduction potentials of the electrochemical irreversible processes of the rhodium(I) centre, as well as the reversible formal reduction potentials of the iron core of the ferrocenyl fragment in the β-diketone ligand for all the complexes synthesized.
6. A thermodynamic phase study to determine the influence that the length of the R alkyl substituents, as well as the position of substitution have on possible mesophase properties of complexes of goals 1 and 2 utilizing the differential scanning calorimetry technique.
7. A cytotoxic study to determine whether the new ligands and rhodium(I) complexes of goals 1 and 2 exhibit antineoplastic activity against cancer cells from a human colorectal cancer cell line (CoLo) and a human cervix epitheloid cancer cell line (HeLa).

[1] Cotton, F. A., Wilkinson, G. and Gaus, P. I., *Basic Inorg. Chem.*, John Wiley and Sons, New York, 1976, 3rd Ed., p. 597.

[2] Cotton, F. A., Wilkinson, G. and Gaus, P. I., *Basic Inorg. Chem.*, John Wiley and Sons, New York, 1976, 3rd Ed., p. 703.

[3] Maitlis, P. M., Haynes, A., Sunley, G. J. and Howard, M. J., *J. Chem. Soc., Dalton Trans.*, 2187 (1996).

[4] Howard, M. J., Jones, M. D., Roberts, M. S. and Taylor, S. A., *Catal. Today*, **18**, 325, (1993).

[5] Nesmeyanov, A. N. and Kotchetkova, N. S., *Russ. Chem. Rev.,* **43**, 710, (1974).

[6] Tompa, A. S., *Thermochim. Acta,* **77**, 133, (1984).

[7] Chittawadgi, B. S. and Voinof, A. N., *Indian J. Technol.*, **6**, 83, (1968).

[8] Neuse, E. W., Woodhouse, J. R., Muntuado, G. and Puglisi,. C., *Appl. Organomet. Chem.*, **2**, 53, (1988).

[9] Köpf-Maier, P., Köpf, H. and Neuse, E. W., *J. Cancer Res. Oncol.*, **108**, 336, (1984).

[10] Neuse, E. W. and Kanzawa, F., *Appl. Organomet. Chem.*, **4**, 19, (1990).

[11] Rosenberg, B., Van Camp, L. and Trosco, J. E., *et al.*, Platinum compounds: a new class of antitumor agents, *Nature*, **222**, 385, (1969).

[12] Swarts, J. C. and van Rensburg, C. E. J., A Substrate or Composition for the Treatment of Cancer, Patent PCT/IB01/02258 in PCT Countries, European Patent 1345951, 2004, p. 1.

[13] Swarts, J. C. Swarts, D. M., Neuse, E. W., La Madeleine, C. and Van Lier, J. E., *Anticancer Res.*, **21**, 2033, (2001).

[14] Sava, G., Zorzet, S., Perissin, L., Mestroni, G., Zassinovich, G. and Bontempi, A., *Inorg. Chim. Acta*, **137**, 69, (1987).

[15] Giraldi, T., Zassinovich, G. and Menstroni, G, Antitumor action of planar organometallic Rh^{I} complexes, *Chem. Biol. Interact*, **9**, 389, (1974).

[16] Giraldi, T., Zassinovich, G., Menstroni, G, Sava, G. and Bertoli, G., Antitumor action of two rhodium and ruthenium complexes in comparison with cis- diammine dichloroplatinum(II), *Cancer Res.*, **37**(8Pt1), 2662, (1977).

[17] Giraldi, T., Zassinovich, G., Menstroni, G, Sava, G. and Stol, A. D., Antitumor action of Rh^{I} and Ir^{I} complexes, *Chem. Biol. Interact*, **22**, 231, (1987).

[18] Collings, P. J. and Hird, M., *An Introduction To Liquid Crystals: Chemistry and Physics:* London: Taylor and Francis, (1997).

[19] Piechocki, C., Simon, J., Skoulios, A., Guillon, D. and Weber, P., *J. Am. Chem. Soc.*, **104**, 5245, (1982).

[20] Swarts, J. C., Langner, E. H. G., Shago, R. F. and Davis, W. L., *Polymer Preprints*, **45(1)**, 452, (2004).

[21] Hudson, S. A. and Maitlis, P. M., *Chem. Rev.*, **93**, 861, (1993).

[22] Deschenaux, R. and Goodby, J. W., in *Ferrocenes*, Ed. Togni, A. and Hayashi, T., VCH, Weinheim, ch. 9, (1995).

[23] Deschenaux, R., Schweissguth, M. and Levelut, A., *Chem. Comm.*, 1275, (1996).

[24] Chaurd, T., Cowlings, S. J., Fernandez-Ciurleo, M., Jauslin, I, Goodby, J. W. and Deschenaux, R., *Chem. Comm.*, 2106, (2000).

[25] Barberá, J., Cativiela, C., Serrane, J. L. and Zurbano, M. M., *Liq. Cryst.*, **11**, 887, (1992).

[26] Espinet, P., Esteruelas, M. A., Oro, L. A., Serrano, J. L. and Sola, E., *Coord. Chem. Rev.*, **117**, 215, (1992).

[27] Bruce, D. W., Lalinde, E., Styring, P., Dunmur, D. A. and Maitlis, P. M., *J. Chem. Soc., Chem. Comm.*, 581, (1986).

[28] Barberá, J., Elduque, A., Gimenez, R., Lahoz, F. J., López, J. A., Oro, L. A., Serrano, J. L., Villacampa, B. and Villalba, J., *Inorg. Chem.*, **38**, 3085, (1999).

Chapter 2

Literature survey

2.1. Ferrocene derivatives

2.1.1. Introduction

As this study is concerned with synthesis, kinetics, electrochemistry and other physical characterization of ferrocene-containing rhodium(I) complexes (see goals 1 – 7, Chapter 1), a preview of pertinent factors related to ferrocene and rhodium chemistry is considered useful.

2.1.2. Ferrocene chemistry

Ferrocene, **1**, has a remarkable geometry in that it possesses a sandwiched structure in which two cyclopentadienyl rings lie parallel to one another with an iron (II) cation buried in the π-electron cloud between them. The Fe^{II} centre is very reluctant to participate in further co-ordination bonds. The ferrocenium cation, **2**, itself a cation-radical species of appreciable stability, interacts readily with free radical precursors and a variety of biologically important electron donor compounds as well as with other nucleophiles.[1] The ferrocenium cation, **2**, undergoes recombination reactions with free radicals, which, after proton elimination, leads to substituted, uncharged ferrocene compounds (**Scheme 2.1**).[2]

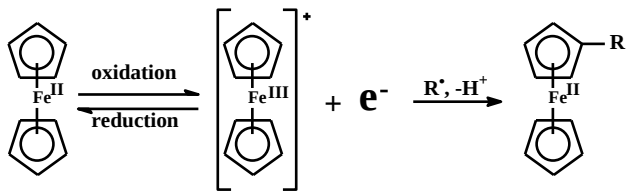

Scheme 2. 1: Oxidation of ferrocene*, 1, to give the ferrocenium cation, 2, which undergoes reductive coupling with radicals, R•, to give substituted ferrocenes 3.

* The structure of ferrocene shown in all figures is in the staggered D_{5d} conformation. It can also exist in the eclipsed D_{5h} conformation.

With respect to this research programme, only selected features of ferrocene will be discussed. One of the objectives of this study is to synthesize a series of ferrocene-containing β-diketones with long alkyl chains attached to the ferrocenyl moiety. The enhanced aromatic reactivity of ferrocene makes possible a wide range of electrophilic substitution reactions, which can often be effected under mild conditions.[2,3] Ferrocene is much more reactive towards Friedel-Crafts acylation,[4,5,6,7] for example the preparation of acetylferrocene, **4**, than either benzene or anisole. Hydrogen substitution of mono-substituted ferrocenes may or may not proceed with ease, depending on whether the existing substituent is an electron donating, such as alkyl, or an electron-withdrawing substituent, such as acetyl. Electron donating substituents activate the ferrocene complex, and substitution takes place preferably on the same cyclopentadienyl ring that contains the activating substituent as shown in the acetylation of ethylferrocene, **6**, to give **7**. Electron withdrawing substituents de-activates the complex, leading almost exclusively to the heteroannular 1,1/-substituted products.[8]

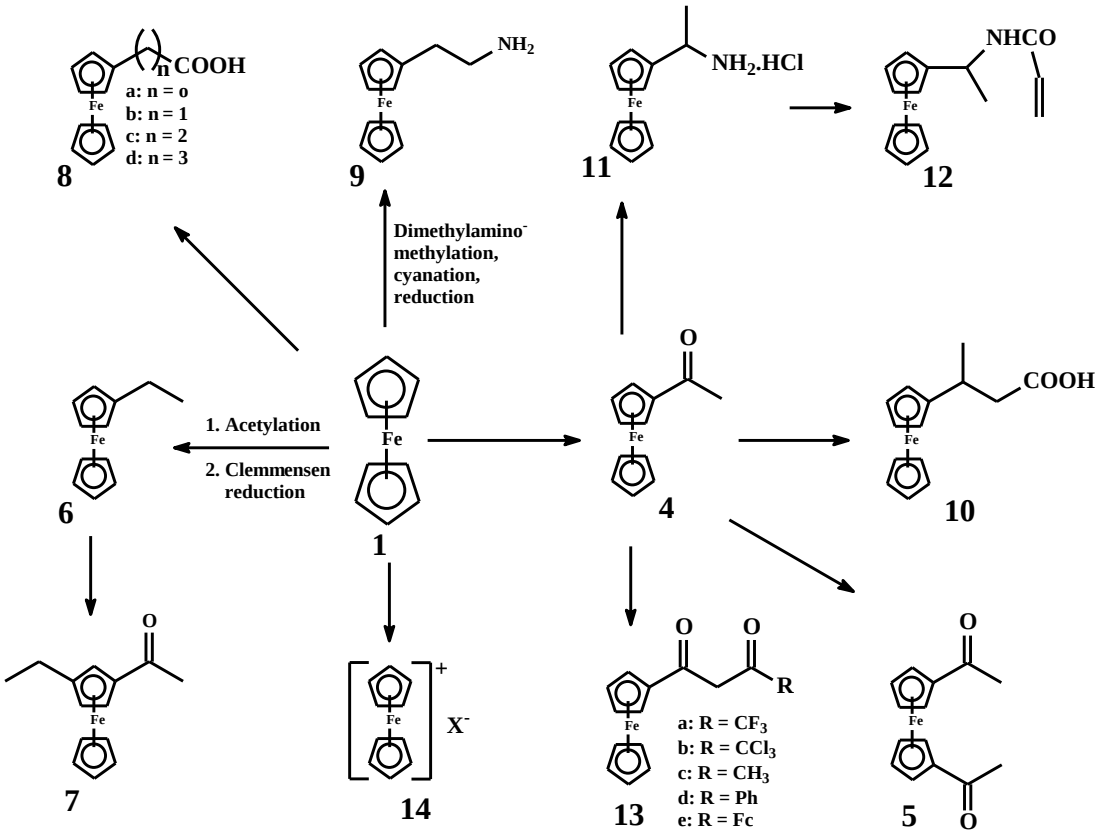

Scheme 2. 2: Syntheses of a variety of ferrocene derivatives. X^- = $[CCl_3COO]^-COOH$ in 14

This is demonstrated by the acylation of acetylferrocene, **4**, to give 1,1′-diacetylferrocene, **5**. Acyl ferrocenes are useful synthetic intermediates towards other ferrocene derivatives,[9] as they are capable of undergoing a large variety of reactions such as Clemmensen reduction to alkanes, lithium aluminium hydride reduction to alcohols and a whole variety of common ketone condensation reactions. Investigation by Carroll and co-workers found that treatment of a range of ferrocenyl ketones, at room temperature, with BH_3.THF resulted in complete deoxygenation of the substrates generating the corresponding ferrocenyl alkanes.[10] Claisen condensation of acetylferrocene with an appropriate ester gave the β-diketones **13** as indicated in **Scheme 2.2**.[11]

Ferrocenoic acid, **8a**, has been prepared in many ways,[12] the most important being carbonation of lithioferrocene[13,14] and by the 2-chlorobenzoyl chloride method.[15] Ferrocenylacetic acid, **8b,** may be prepared from N,N-dimethylaminomethylferrocene methiodide[12,16,17,]after cyanation followed by hydrolysis of the resulting ferrocenylacetonitrile. 3-Ferrocenylpropanoic acid, **8c**, may be prepared from ferrocenecarboxaldehyde, and malonic acid[18] (Doebner condensation), followed by hydrogenation of the intermediate. 4-Ferrocenylbutanoic acid, **8d**, can be prepared by Clemmensen reduction[19] of 3-ferrocenoylpropanoic acid.[20] 3-Ferrocenylbutanoic acid, **10**, was obtained by the Reformatsky reaction between acetylferrocene and malonic acid followed by catalytic hydrogenation of the obtained intermediate 3-ferrocenyl-3-methylacrylic acid.[21]

Reductive amination of acetylferrocene, **4**, with cyanoborohydride, in the presence of ammonium acetate followed by treatment with HCl, gave 1-ferrocenylethylamine hydrochloride, **11**.[22,23] Conversion of **11** to N-(1-ferrocenylethyl)acrylamide, **12**, was achieved by allowing neutralized **11** to react with acryloyl chloride in the presence of triethylamine.[24] The preparation of an amine functionality slightly removed from the ferrocenyl moiety by methylene spacers is demonstrated by the synthesis ferrocenylethylamine, **9**, which is accomplished by the reduction of ferrocenylacetonitrile with $LiAlH_4$.[17] Ferrocenylacetonitrile can be obtained from ferrocenylmethyl(trimethylammonium)iodide. [12,25,26] Finally, Neuse and others[27] have pursued studies in which ferricenium salts, **14**, were prepared and isolated *inter alia* for biological testing.

2.2. The synthesis of β-diketones

2.2.1. Introduction

Most often β-diketones are synthesized by Claisen condensation,[28] involving the replacement of an α-hydrogen atom of a ketone by an acyl group:

$$\mathbf{RCOX + HCH_2COR \rightarrow RCOCH_2COR + HX}$$
$$\mathbf{(X = OR, OCOR, Cl)}$$

The acylation of ketones may also result in oxygen acylation rather than carbon acylation to form oxygen acylation derivatives and these may be rearranged thermally to give a β-diketone.[28] Although Lewis acids, such as BF_3, can be used to promote β-diketone formation, the acylation of ketones with esters is generally effected by means of a basic reagents such as sodium ethoxide, sodium amide,[29] sodium hydride or sodium metal.[30]

2.2.2. Selected examples of β-diketone derivatives

Knochel and co-workers introduced the application of β-diketonate ligands with long perfluoroalkyl (C_7F_{15}) groups for metal catalyzed oxidations under fluoro biphase conditions, which is a potential solution to the catalyst/product separation issues in homogeneous catalysis.[31,32] Croxtall *et al.* prepared a series of fluorinated β-diketones, in reasonable yields by a two-step synthesis.[33] This synthesis involves the reaction of the commercially available perfluoroalkylated carboxylic acids with MeMgBr which readily affords the related methyl ketones.[34] Further reaction with the same or a different perfluoroalkylated ester in the presence of a base gave the desired β-diketones as indicated in **Scheme 2.3**.[33] Treatment of the β-diketones with representative metal (II) salts readily produced the perfluoroalkylated β-diketonato metal complexes L_xM(perfluorinated β-diketones)$_y$ with L an appropriate ligand and x, y < 5.

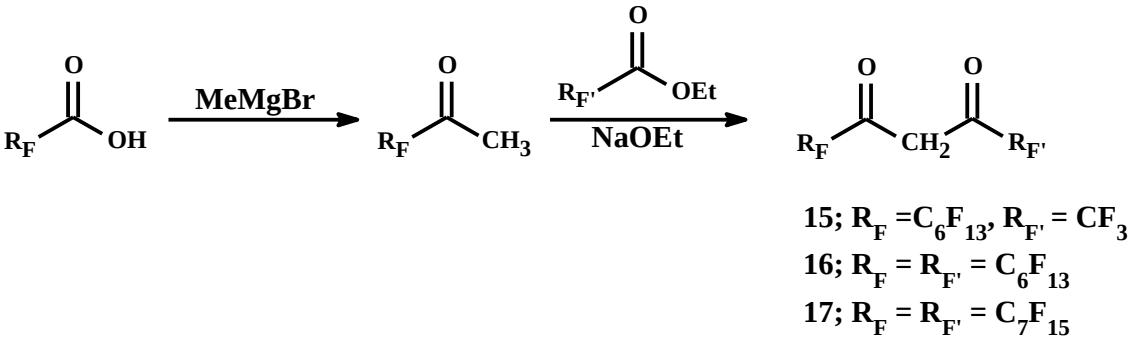

15; R_F =C_6F_{13}, $R_{F'}$ = CF_3
16; R_F = $R_{F'}$ = C_6F_{13}
17; R_F = $R_{F'}$ = C_7F_{15}

Scheme 2. 3: Synthesis of perfluoroalkyl derivatized β-diketones.

Claessen and co-workers as well as other researchers reported efforts to increase the volatility of homoleptic Cu^{II} β-diketonato complexes by incorporation of trialkylsilyl substituents in the supporting ancillary ligands.[35,36,37,38] In particular, the $Cu(tmshd)_2$ complex (where tmshd is the anion of 2,2,6,6-tetramethyl-2-silaheptane-3,5-dione) which sublimes at lower temperatures than its carbon analogue, $Cu(tmhd)_2$ (where tmhd is the anion of 2,2,6,6-tetramethylheptane-3,5-dione) was studied. The silylated Cu(II) materials showed greater stability than the corresponding non-silylated complexes. For the preparation of α-silylketones a synthetic strategy involving 1,3-dithiane chemistry was developed.[39,40] Claessen and co-workers synthesized the sila-β-diketone, 2,2,6,6-tetramethyl-2-silaheptane-3,5-dione (tmshdH), **18**, as shown in **Scheme 2.4**, by the condensation of the anion of 2-trimethylsilyl-1,3-dithiane with 1-bromo-3,3-dimethylbutan-2-one, followed by the deprotection of the latent carbonyl moiety with $HgO/HgCl_2$.[41]

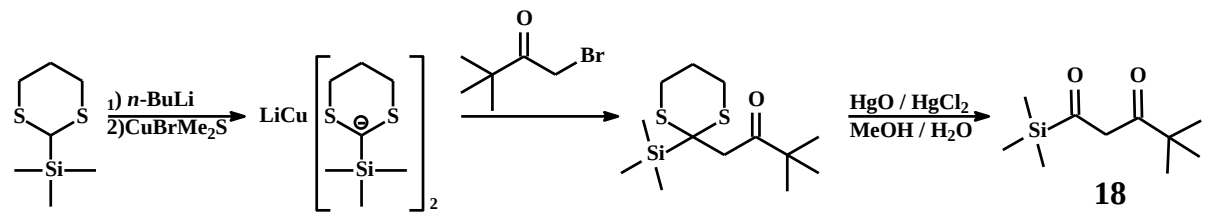

Scheme 2. 4: Preparation of tmshdH, 18, *via* dithiane method.

Functionalized π-conjugated oligomers, such as oligothiophenes, have been extensively studied, owing to their potential use in molecular and organic electronics as active layer in a variety of devices.[42,43] Jaafari and co-workers reported the synthesis and characterization of oligothiophenes

substituted by 1,3-propanedione.[44] The reason behind this concept was to employ β-diketone groups as reactive sites for elaborating π-conjugated oligothiophenes and using them as building blocks to develop coordination-based assemblies, containing multi-nuclear metal complexes with strong interactions.[44] The synthetic procedures to obtain a β-diketone-containing different oligothiophenes are summarized in **Scheme 2.5**. The Claisen condensation of 2-acetylthiophene and 2-thiophenecarboxylic acid ethyl ester leads to 1,3-di-(2-thienyl)propane1,3-dione (TPD), **19,** with a 60 % yield. Almost the same yield was obtained when using bithiophene (BTPD), **20**, instead of thiophene or when introducing a strong electron-donating group, such as ethylenedioxy, onto the thiophene ring (EDOTPD), **21**.

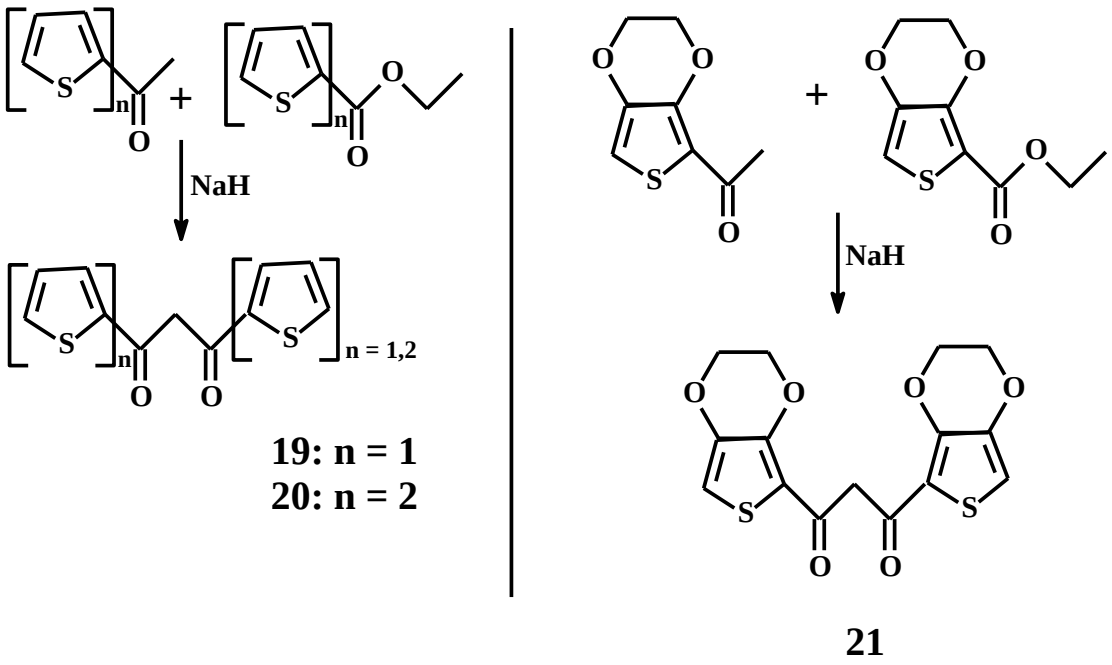

Scheme 2. 5: Synthetic route to β-diketones containing oligothiophenes, *via* Claisen condensation.

Suzuki and co-workers synthesized β-diketones by heating an α,β-epoxyketone at 80 – 140 ^{o}C in toluene with catalytic amounts of $Pd(PPh_3)_4$ and 1,2-bis(diphenylphosphino)ethane.[45] The β-diketone formed by a pinacol rearrangement.[46] The reaction of 2-methyl-3,4-epoxy-5-hexanone under the above conditions gave 2-methylhexane-3,5-dione, **22**, in 80 % yield as shown below in **Scheme 2.6**.

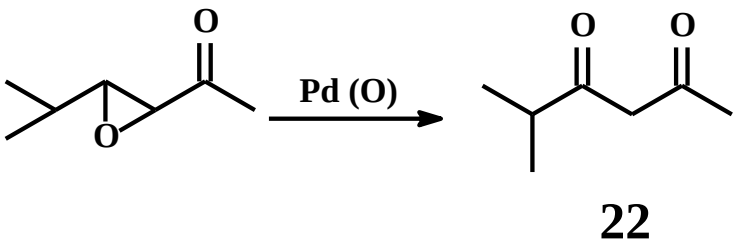

22

Scheme 2. 6: Synthesis of 2-methylheptane-3,5-dione.

Another method for the synthesis of β-diketones, which involves catalyzed condensation, was demonstrated by Manyik and co-workers as indicated in **Scheme 2.7**.[47] The compound *p*-nitro-benzoylacetone, **23**, was obtained by adding a mixture of *p*-nitro-acetophenone and acetic anhydride to an acetic acid-BF_3 complex at 0 ^oC for 30 min and then at 25 ^oC for 24 h.

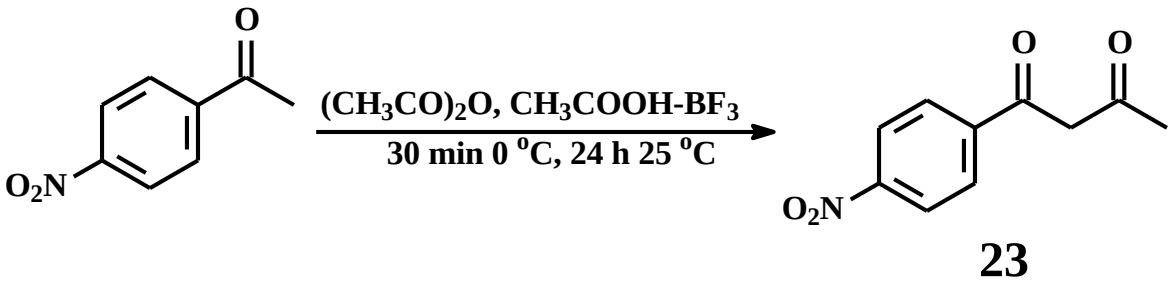

23

Scheme 2. 7: Synthesis of *ρ*-nitro-benzoylacetone.

2.3. Metallocene-containing β-diketones

The β-diketones synthesized in this study all contained a ferrocenyl group. The synthesis of metallocene-containing β–diketones has been achieved by Claisen condensation between acetylferrocene, **4** and the appropriate methyl or ethyl esters in the presence of a strong base to ensure reasonable yields as shown in **Scheme 2.8**.[11]

Hauser and co-workers synthesized various ferrocene-containing β-diketones, including 1-ferrocenylbutane-1,3-dione (ferrocenoylacetone, 65 % yields) and 1-ferrocenyl-3-phenylpropane-1,3-dione (benzoylferrocenoylmethane, 63 % yields), by using potassium amide as the active base additive in liquid ammonia as solvent.[48] Weinmayr and co-workers reported the use of sodium methoxide as basic initiator to prepare both ferrocenoylacetone (29 % yield) and 1-ferrocenyl-4,4,4-trifluorobutane-1,3-dione (ferrocenyltrifluoroacetone), (80 % yield) in diethyl ether.[49] Cullen and co-workers demonstrated the synthesis of ferrocenoylacetone in 38 % yield, by using the sterically hindered base lithium diisopropylamide (LDA).[50] These methods have since been reproduced or slightly adopted by Du Plessis and co-workers to synthesize a variety of ferrocene-containing β-diketones, **Scheme 2.8**.[11]

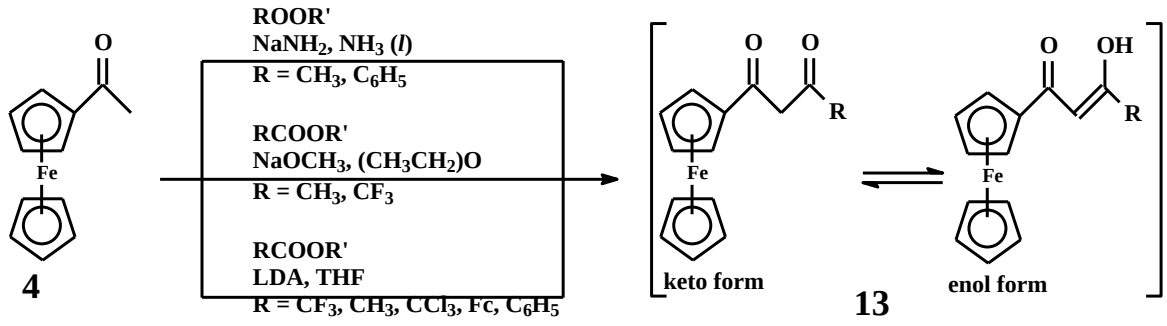

Scheme 2. 8: Claisen condensation of acetylferrocene, 4, utilizing three different bases to give ferrocene-containing β-diketones, 13, (LDA = lithium diisopropylamide, R/ = methyl or ethyl).

2.3.1. Keto-enol tautomerism

The keto-enol tautomerism of a wide variety of β-diketones have been studied over many years, by techniques such as bromine titration,[51] polarographic measurements,[52] energy of enolization,[53,54] kinetics,[55] infra red spectroscopy[56] and ^{1}H NMR spectroscopy.[57,58] Two possible enol forms as represented in **Scheme 2.9** can exist. It was observed that the equilibrium constant, *K*, is highly dependent on the character and position of the R groups.[59]

A ^{1}H NMR study conducted by Du Plessis and co-workers gave the percentages of enolized tautomers in $CDCl_3$ solutions of some β-diketones and were found to be high.[11] Substitution by a bulky group such as an alkyl, at α-position tend to produce steric hindrance between R_3 and R_1 (or

R_2) groups **(Scheme 2.9)** particularly in the enol tautomer, and together with inductive effects of the alkyl groups often brings about a large decrease in the proportion.[60]

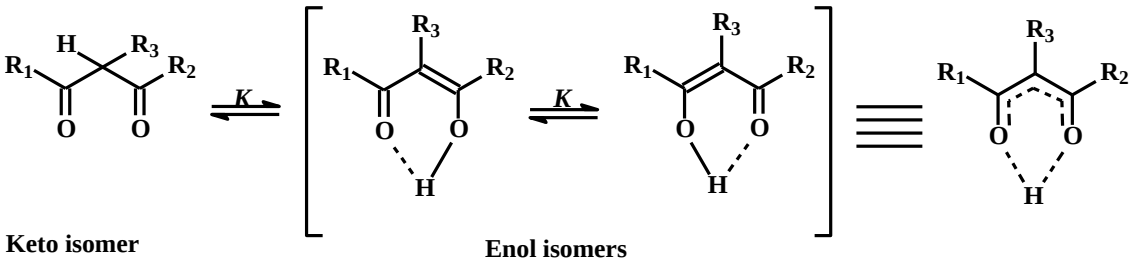

Scheme 2. 9: Schematic representation of tautomerism of β-diketones with the enol forms showing pseudo aromatic character.

Cravero and co-workers reported that the tautomeric equilibrium between the enol forms of *p*-R-benzoylacetone is slightly displaced towards the methyl keto form by electron withdrawing substituents.[61]

Regarding ferrocene-containing β-diketones, enolization in solution was found to be predominantly away from the ferrocenyl moiety.[11] Two driving forces that control the conversion from β-diketone into an enolic isomer were defined. These forces were labelled as electronic and resonance driving forces.[11] In the former, the formation of the preferred enol isomer is controlled by the group electronegativity of the R^1 and R^2 substituents on the β-diketone:

$$\underset{\textbf{(I)}}{\mathbf{R^1\text{-}(OH)C{=}CH\text{-}CO\text{-}R^2}} \rightleftharpoons \underset{\textbf{(k)}}{\mathbf{R^1\text{-}CO\text{-}CH_2\text{-}CO\text{-}R^2}} \rightleftharpoons \underset{\textbf{(II)}}{\mathbf{R^1\text{-}CO\text{-}CH{=}C(OH)\text{-}R^2}}$$

When the group electronegativity of R^1 is larger than that of R^2 the carbon atom of the carbonyl group adjacent to R^2 on the β-diketone, **k**, will be less positive in character than the carbon atom of the other carbonyl, implying that enol (**II**) will dominate. However, many β-diketones were described that did not follow the enolization pattern predicted by the electronic driving force.[11,62] All the cited exceptions had aromatic R^1 or R^2 side groups and hence it was stated that the electronic driving force will always take second priority compared with the resonance driving force.

In addition, it was noted that under certain conditions the keto isomer of ferrocenoylacetone could be observed in large quantities by proton NMR, while under other conditions the keto isomer of the same compound is much less pronounced. The explanation for these apparent discrepancies was at first postulated to be the β-diketone concentration of the solution studied, because at very low concentration hydrogen stabilization of the enol form should be absent. Although it has been shown that very low concentrations slightly favour the keto form in solution, this did not adequately explain why in some cases the keto form of concentrated solutions is observed in appreciable quantities (> 80 %), while in other cases not (< 5 %).[62] Many β-diketones are isolated by isolating solid lithium salts, ($R^1-CO-\overline{C}HLi^+-CO-R^2$) from solution followed by acidification according to Du Plessis and co-workers.[62] This means that the first product that is obtained during a synthetic procedure must be the keto isomer, because the lithium salt exists as a keto isomer. If the solution ^{1}H NMR is obtained very quickly after the isolation and acidification, it follows that the keto content will be high. However, if the solution ^{1}H NMR is obtained several days after synthesis, enough time would have elapsed to allow conversion of the keto form to the equilibrium content. Consequently the keto form will be much less dominant. In contrast, in the solid state, the enol form is the only stable isomer (*i.e.* no keto form) for the ferrocene-containing β-diketones studied.[62]

2.3.2. Acid dissociation constants

The acid dissociation constant is the equilibrium constant for the ionization of a weak acid, as represented in reaction below:[63]

$$HA(aq) + H_2O(l) \underset{}{\overset{K_c}{\rightleftharpoons}} H_3O^+(aq) + A^-(aq)$$

From this reaction the equilibrium constant (K_c) is given as;

$$K_c = \frac{[H_3O^+][A^-]}{[HA][H_2O]}$$

which can be rewritten to give

$$K_a = K_c[H_2O] = \frac{[H^+][A^-]}{[HA]}$$

with $pK_a = -\log K_a$

For the ferrocene-containing β-diketones, as described in **Scheme 2.10**, the terminology "apparent $pK_a^{/}$ values" and not pK_a was preferred since there was no attempt to partition the obtained $pK_a^{/}$ values between the separate pK_a's for the enol and keto tautomers.[11]

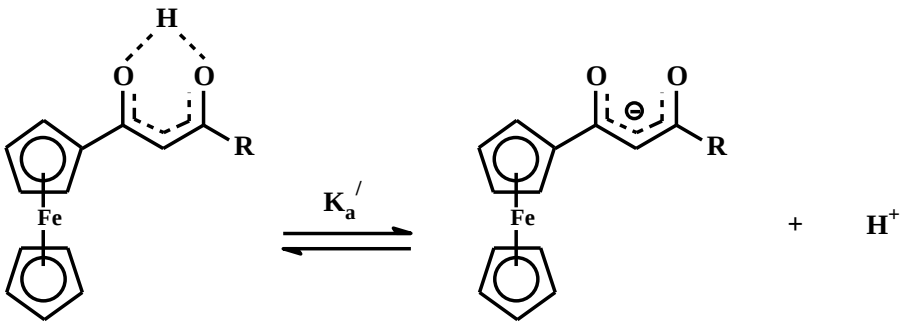

Scheme 2. 10: Acid dissociation constant equilibrium for ferrocene-containing β-diketones.

The most common methods that are used to determine pK_a values are the spectroscopic monitoring of an acid-base titration and the conductometric method. There are some other methods that can be used in the determination of pK_a, such as Raman spectroscopy, proton nuclear magnetic resonance (NMR), thermotropic methods and NMR using labelled atoms.[62] Du Plessis and co-workers adapted the absorbance method in the determination of $pK_a^{/}$ values for their research in ferrocene-containing β-diketones, $FcCOCH_2COR$ (with R = CCl_3, CH_3, C_6H_5, Fc; with Fc = ferrocenyl), by inserting the pH data into the following equation utilizing the fitting program MINSQ.[11,64]

$$A_T = \frac{A_{HA}10^{-pH} + A_A 10^{-pK_a^{/}}}{10^{-pH} + 10^{-pK_a^{/}}} \qquad \textbf{equation 2.1}$$

Here A_T = total absorbance, A_{HA} = the absorbance of the free β-diketone, (the acidic form) and A_A = absorbance of of the deprotonated (basic) form. A plot of A_T *versus* pH (**Figure 2.1**) has an S-shaped curve with $pK_a^{/}$ at the middle of the steep increase.[11]

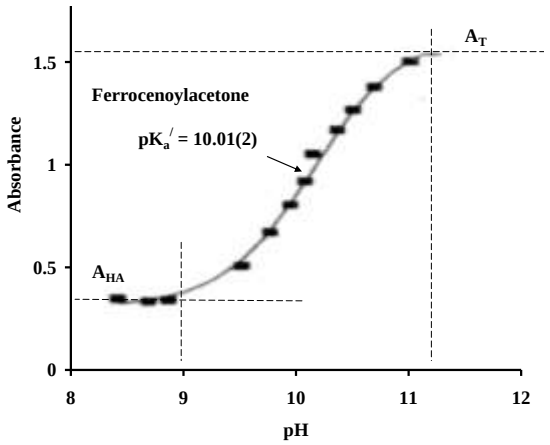

Figure 2. 1 Absorbance dependence on pH of ferrocenoylacetone (0.1059 mmol dm^{-3}, 326 nm), in water containing 10 % acetonitrile solution with ionic strength (*I*) 0.100 mol dm^{-3} ($NaClO_4$). Acetonitrile is added to assist the solubility of ferrocenoylacetone in aqueous media.

For the ferrocene β-diketone, Fc-$COCH_2CO$-CF_3, two $pK_a^{/}$ values were observed. The second $pK_a^{/}$ value was suspected to be due to the attachment of a hydroxide group onto the β-diketone at the carbonyl group to which the CF_3 group was attached as described in **Scheme 2.11**. The $pK_a^{/}$ values for the Fc-$COCH_2CO$-CF_3 were obtained by inserting the pH data utilizing the fitting program MINSQ according to the equation below.

$$A_T = \frac{A_{HA}(10^{-pH})^2 + A_A(10^{-pK_a^{/}})(10^{-pH}) + A_F(10^{-pK_a^{/}})(10^{-pK_{a2}^{/}})}{(10^{-pH})^2 + (10^{-pH})(10^{-pK_a^{/}}) + (10^{-pK_a^{/}})(10^{-pK_{a2}^{/}})} \qquad \textbf{equation 2.2}$$

The constants A_T, A_{HA} and A_A have the same meaning as mentioned in **Equation 2.1** with A_F = final absorption.

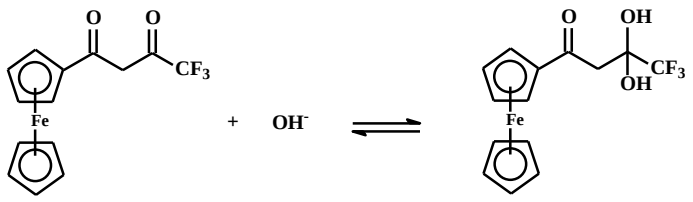

Scheme 2. 11: Reversible hydroxylation of 1-ferrocenyl-4,4,4-trifluorobutane-1,3-dione.

2.4. Metal β-diketonato complexes

The rhodium complexes containing β-diketonato ligands, [Rh(β-diketonato)(cod)], **24**, where cod = cyclooctadiene, were synthesized in high yields (> 75 %) in DMF from the rhodium (I) dimer $[Rh_2Cl_2(cod)_2]$ as shown **Scheme 2.12**.[48] Two routes were utilized to obtain dicarbonyl rhodium(I) complexes, **25**.[65] The first route consisted of the direct interaction between $[Rh_2(Cl)_2(CO)_4]$ and the β-diketones to give $[Rh(\beta\text{-diketonato})(CO)_2]$. An alternative synthetic method involving the [Rh(β-diketonato)(cod)], **24**, which in an equilibrium process can undergo carbon monoxide exchange to liberate, in the presence of an excess CO, rhodium (I) complexes, **25**. The [Rh(β-diketonato)(CO)(PPh_3)] complexes, **26**, were obtained by reacting an equivalent amount of PPh_3 with $[Rh(\beta\text{-diketonato})(CO)_2]$ in *n*-hexane medium.

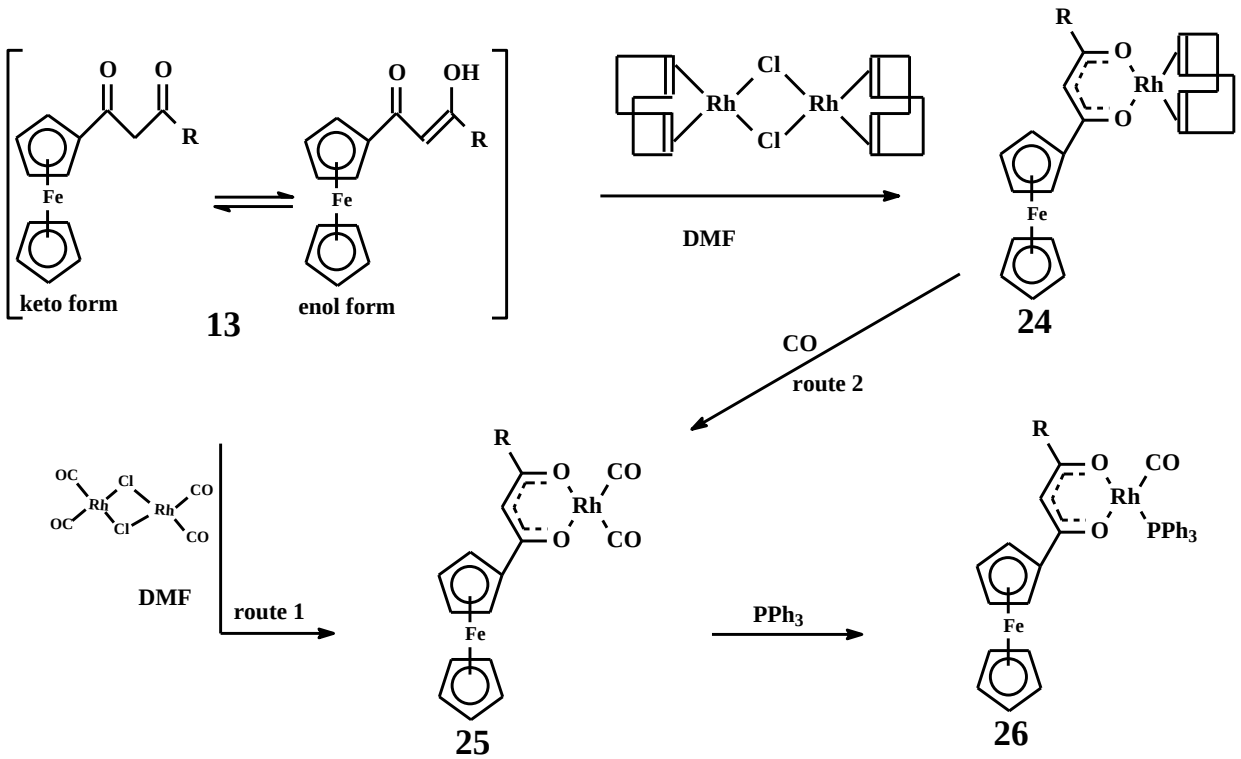

Scheme 2. 12: Synthetic routes for the synthesis of the [Rh(β-diketonato)(cod)] complexes, 24, [Rh(β-diketonato)(CO)$_2$], 25 and [Rh(β-diketonato)(CO)(PPh$_3$)], 26, with R = CF$_3$, CH$_3$, C$_6$H$_5$ and Fc. Fc = ferrocenyl.

This study is particularly concerned with the influence of long chain alkyl substituents on new β-diketones and their rhodium β-diketonato complexes where alkyl chain length varies between nC_9H_{19} and $nC_{18}H_{37}$.

2.5. Substitution kinetics of square planar complexes

2.5.1. Introduction

The influence of different substituent positions on the β-diketones of **Figure 1.1** and **1.2**, and their rhodium(I) complexes on the rate of β-diketonato substitution was the key study field in this research programme (goal 3, Chapter 1). Related to this goal, the following section provides a clear literature survey of related studies in this field.

2.5.2. Mechanism of substitution reactions

Substitution reactions or ligand exchange are usually divided into three main groups; (i) nucleophilic substitution, (ii) electrophilic substitution and (iii) oxidative addition followed by reductive elimination.[66] Type (iii) substitution reactions involve the interaction between 18-electron and 16-electron species. These substitution reactions generally proceed *via* one of the three pathways, a dissociative and associative mechanism or a hybrid of these two pathways.[67,68]

2.5.2.1. Dissociative mechanism

In a dissociative mechanism, the ligand to be replaced dissociates from the metal center and the vacancy in the coordination sphere is taken by the ligand. This is represented below:

$$[L_3M\text{-}X] \xrightarrow{k} [L_3M] + X \qquad \text{(slow step)}$$

$$[L_3\text{-}M] + Y \longrightarrow [L_3M\text{-}Y] \qquad \text{(fast step)}$$

Here M = metal ion, L = substitution inert ligand, X = leaving ligand and Y = entering ligand. Y can also be a solvent species. The important feature of such a mechanism is that the first step (dissociation of the leaving group) is the rate determining step. Once formed by cleavage of the bond to the leaving group, X, the three-coordinate intermediate will react with the new ligand, Y, almost immediately. This mechanism for ligand substitution is comparable to the S_N1 mechanism in organic systems.[68]

The kinetic rate law in this mechanism takes the form of

$$\text{Rate} = k[L_nM\text{-}X]$$

The rate law is independent of the concentration of the incoming ligand. The entropy of activation (ΔS^*) is positive because the transition state is less ordered than the starting material. However, the stereochemistry may be retained or allow racemization,[69,70] depending on the size of k.

2.5.2.2. Associative mechanism

In the associative mechanism, the incoming ligand, Y, directly attacks the original complex to form a five-coordinate intermediate in the rate determining step, as shown below:

$$[L_3M\text{-}X] + Y \xrightarrow{k} [L_3MX\text{-}Y] \qquad \text{(slow step)}$$

$$[L_3MX\text{-}Y] \longrightarrow [L_3M\text{-}Y] + X \qquad \text{(fast step)}$$

After rate-determining association between the entering ligand, Y, and the metal complex, the leaving group, X, is lost in a fast step. This mechanism for ligand substitution is comparable to the S_N2 mechanism in organic systems.[68]

A different kinetic rate law applies to this mechanism and has the general form

$$\text{Rate} = k[L_nM\text{-}X][Y]$$

The entropy (ΔS^*) is negative, which implies that the transition state is more ordered than the starting materials. Electron deficient complexes (*e.g.* 16 or 17 valence electron compounds) favour the associative mechanism, but some 18 electron compounds also follow the associative mechanism.[70] The associative mechanism often involves solvolysis as indicated in **Scheme 2.13**, especially if the solvent is polar or has a tendency to solvate (*e.g.* acetonitrile or DMSO). If solvolysis takes place, the kinetic rate law changes to

$$\text{Rate} = (k_s + k_2[Y])[L_nM\text{-}X] = k_{obs}[L_nM\text{-}X]$$

where $k_{obs} = k_s + k_2[Y]$, with k_s = rate constant of the solvent pathway and k_2 = rate constant of the direct pathway.

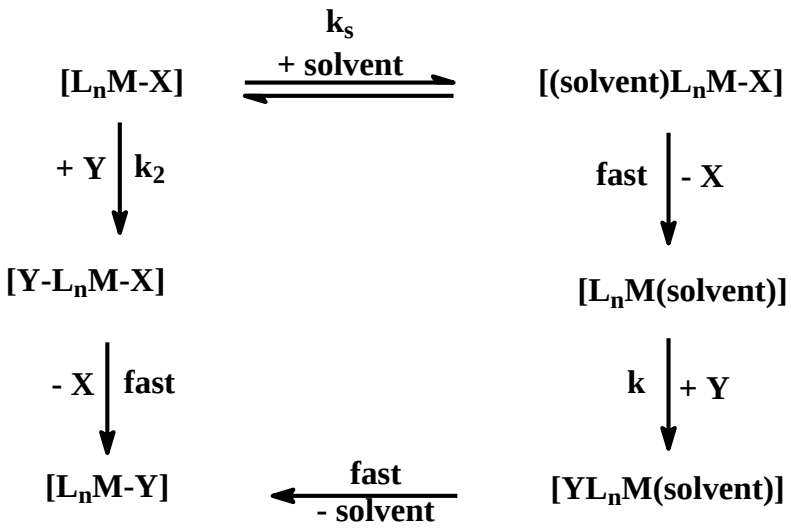

Scheme 2. 13: Schematic representation of the direct and solvent pathways for the associative mechanism.

2.5.3. Substitution kinetics of β-diketonato metal complexes

(i) Effect of the entering ligand

As expected for an associative mechanism, the entering ligand has a large influence on the reaction rate. This mostly depends on the nucleophilicity of the incoming ligand, which is the measure of the readiness of an entering ligand to attack the positive metal center of a complex, or its readiness to supply the electrons needed for the reaction to proceed. This was confirmed by the determination of the rate constants for the substitution of Cl by a large variety of ligands from *trans*-$[Pt(py)_2(Cl)_2]$.[71,72]

The basicity of the incoming ligand (in contrast to the nucleophilicity) has a rather small effect on the rate of associative substitution reactions. Leipoldt and co-workers as well as Swarts and co-workers confirmed this by the substitution reaction of β–diketonato ligand in [Rh(cod)(acac)] and [Rh(cod)(fca)] with derivatives of 1,10-phenanthroline and 2,2'-dipyridyl as illustrated in **Scheme 2.14**.[73,74,75]

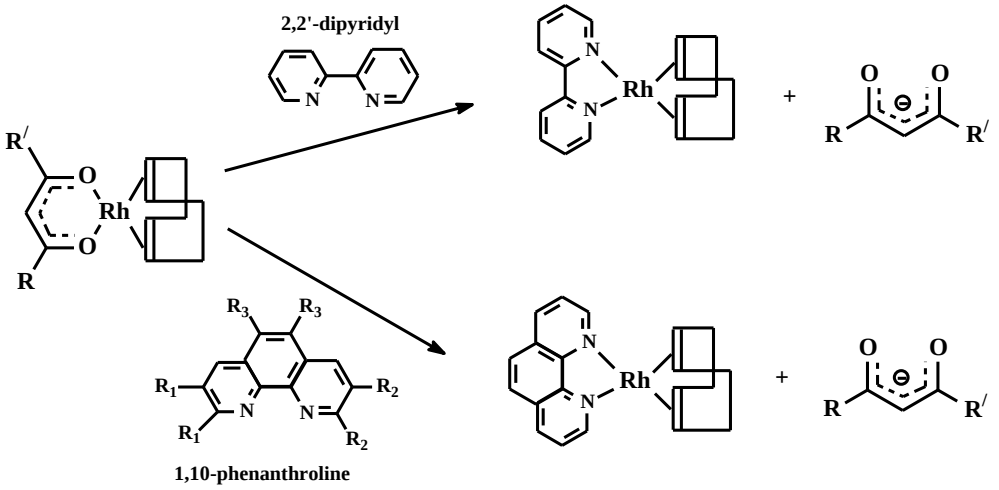

Scheme 2. 14: Substitution reaction of β-diketonato ligand by various derivatives of 1,10-phenanthroline and 2,2/-dipyridyl form [Rh(cod)(acac)], (for acac; R = R/ = CH_3) and [Rh(cod)(fca)] (for fca; R = ferrocenyl and R/ = CH_3). R_1, R_2 and R_3 were combinations of H, CH_3, NO_2 and Cl.

Table 2.1 (page 27) summarizes the second order rate constants, k_2, for the substitution reactions in **Scheme 2.14**. Over the pK_a range of 3.57 to 6.31 for substituted 1,10-phenanthroline derivatives, the slowest rate constant was 12.4 and the fastest was 29 dm^3 mol^{-1} s^{-1} in the case of the [Rh(cod)(acac)] reactions. The rate constants varied between 5.46 and 17.8 dm^3 mol^{-1} s^{-1} in the case of [Rh(cod)fca)]. The much faster reaction of 2,2/-dipyridyl compared to reactions of derivatives of 1,10-phenanthroline was attributed to the fact that 2,2/-dipyridyl is much less rigid than 1,10-phenanthroline implying free rotation of the two pyridyl groups is possible.

(ii) Effect of the leaving group

The effect of the leaving group is often related to the strength of the M-X bond (metal-ligand bond, where X = leaving group). A stronger M-X bond makes it more difficult for X to be substituted by another ligand, resulting into a decrease in the substitution rate, whereas the opposite applies to the weaker M-X bond. Substitution kinetics studied by Leipoldt and co-workers of the β-diketonato metal complexes of the type [Rh(β-diketone)$(CO)_2$] by cyclooctadiene was to observe the effect of the substituents R_1 and R_2 of the different β-diketones (R_1-$COCH_2CO$-R_2) on the *trans* effect of the oxygen atoms of the β-diketones as represented in (**Table 2.2**).[76] They showed that the reactivity of the β-diketone complexes is dependent on the group electronegativities of the terminal substituents (CH_3 (χ_{CH3} = 2.34), Ph (χ_{Ph} = 2.21) and CF_3 (χ_{CF3} = 3.10))

(smallest k_2) BA < DBM << TFAA < TFBA << HFAA (largest k_2),

(here BA = benzoylacetone, DBM = dibenzoylmethane, TFAA = 1,1,1-trifluoropentane-2,4-dione, TFBA = 1,1,1-trifluoro-5-phenylpentane-2,4-dione, HFAA = 1,1,1-trifluoro-5,5,5-trifluoropentane-2,4-dione).

Therefore, the influence that the terminal side groups of the β-diketonato ligands have on the kinetic *trans*-effect is to increase the rate of substitution with increase of the group electronegativities of individual side groups. It is of interest to note that the group electronegativities of the CH_3 and the Ph group are almost equal. This implies that either of the CO groups in {Rh(PhCOCHCOCH$_3$)$(CO)_2$] may be substituted by PPh_3. This was actually found by Preston and

co-workers in a crystallographic study, both isomers were observed *within the same* crystal with a ratio 1:1.[77]

Table 2. 1: Second order rate constants (k_2 dm^3 mol^{-1} s^{-1}) and activation parameters for the substitution of β-diketonato ligands with derivatives of 1,10-phenanthroline and 2,2-dipyridyl in methanol.

Incoming ligand	pK_a[a]	[Rh($CH_3COCHCOCH_3$)(cod)][b]			[Rh(fcCOCHCOCH$_3$)(cod)][b]		
		k_2 dm^3 mol^{-1} s^{-1}	ΔH* kJ mol^{-1}	ΔS* kJ mol^{-1}	k_2 dm^3 mol^{-1} s^{-1}	ΔH* kJ mol^{-1}	ΔS* kJ mol^{-1}
5-nitro-1,10-phenanthroline	3.57	12.4	30.8	-121	5.46	25	-146
1,10-phenanthroline	4.96	29.0	32.6	-108	17.8	29	-123
5,6-dimethyl-phenanthroline	5.20	19.9	38.7	-90	13.7	23	-143
4,7-dimethyl-phenanthroline	5.97	18.8	36.7	-97	13.2	22	-149
3,4,7,8-tetramethyl-phenanthroline	6.31	19.6	40.7	-84	15.7	27	-128
2,2-dipyridyl	4.30	124	26.8	-115	118	31.2	-100

a) pK_a values of the conjugate acid in water from reference [78]

b) in methanol at 25 ºC.

Table 2. 2: The sum of the group electronegativities of the β-diketonato side groups and second order rate constants, k_2, for the substitution reaction of cod in [Rh(β-diketonato)$(CO)_2$] complex to illustrate the *trans* effect of various β-diketonato ligands $R_1COCH_2COR_2$ at 25 ºC.

β-diketone	R_1	R_2	$\chi_{R1} + \chi_{R2}$	k_2 / dm^3 mol^{-1} s^{-1}
BA	CH_3	C_6H_5	4.55	0.10
DBM	C_6H_5	C_6H_5	4.42	0.36
TFAA	CH_3	CF_3	5.35	2.30
TFBA	C_6H_5	CF_3	5.22	4.10
HFAA	CF_3	CF_3	6.02	200

(iv) Effect of the central metal atom

The effect of a central metal atom on the rate of substitution is determined by the ease with which the metal enhances the replacement of the ligand attached to it, by another ligand, and such a metal needs to be able to form a five co-ordinate complex. The easier a metal can form a five co-ordinate complex (intermediate) in a square planar substitution reaction, the more stable is the transition state in an associative mechanism, and hence substitution is enhanced. The results of the substitution reactions between [M(β-diketonato) (cod)] and 1,10-phenanthroline (M = Rh[79] or Ir[74]) given in **Table 2.3** indicate that the rate constant k_2 for Ir^I complexes is, except for slow reactions, much higher than k_2 for Rh^I complexes. These results are unexpected if compared to the general trend of the relative rate of substitution of a ligand to isostructural square planar metal complexes with metal centers from the same triad.[69,80]

Table 2. 3: Rate constants at 25 °C and the activation parameters for the reaction between [M (β-diketonato) (cod)] and 1,10-phenanthroline (M = Rh or Ir).

β-diketonato	pK_a [a]	[Rh(β-diketonato) (cod)] [b]			[Ir(β-diketonato) (cod)] [c]		
	pK_a [a]	k_2 / dm^3 mol^{-1} s^{-1}	H* kJ mol^{-1}	S* kJ mol^{-1}	k_2 / dm^3 mol^{-1} s^{-1}	H* kJ mol^{-1}	S* kJ mol^{-1}
$CH_3COCHCOCH_3^-$	8.95	29.0	32.6	-108	13.6	29.5	-125
$C_6H_5COCHCOCH_3^-$	8.70	51.2	31.6	-106	85.8	31.5	-102
$C_6H_5COCHCOC_6H_5^-$	9.35	61.4	27.3	-119	413	26.3	-106
$CF_3COCHCOCH_3^-$	6.30	1330	30.5	-83	17100	24.0	-83
$CF_3COCHCOC_6H_5^-$	6.30	2420	26.2	-93	25100	23.1	-81
$CF_3COCHCOCF_3^-$	4.35	276000	23.2	-63	3000000	-	-

a) pK_a values used are those published in references 91 and 71.

b) in methanol at 25 °C.

c) in acetone at 25 °C.

(iii) Influence of the solvent

The solvent's role lies mainly in the solvolysis steps of the reaction as represented in **Scheme 2.13** (page 26). For the solvent to act as a nucleophile, it must have an ability to donate electrons and

supply them to the metal centre, therefore, coordinating to the metal. Studies by Pearson and co-workers found that a large k_s value is observed in solvents that are capable of good coordination with Pt^{II} complexes.[81] Rate constants depend on the coordination power of the solvent in the following way:

(largest k_s values)$(CH_3)_2SO > CH_3NO_2$, $H_2O >$ ROH(lowest k_s values).

Solvents that are poor coordinators such as C_6H_6 and CCl_4, have no influence on the reaction rate. The order of nucleophilicities does not change in different solvents.

(v) Steric effects of the ligands

This refers to the influence of different bulky ligands coordinated to the same metal centre. Basolo and co-workers demonstrated that in sterically crowded complexes, bulky ligands shield the metal centre by blocking the approach of the incoming ligand, in the hydrolysis of *cis*-$[Pt(Cl)L(PEt_3)_2]$ with L = pyridine, 2-methylpyridine or 2,6-dimethylpyridine.[80] The reaction rate decreases as more bulky ligands are used.

2.5.4. Activation parameters

The rate of chemical reactions improves with increasing temperature. Generally the dependence of the rate constant, k, on temperature, T in Kelvin degrees, follows the Arrhenius equation:

$$k = Ae^{-E_a / RT}$$

Here, A is the frequency factor, E_a is the activation energy of the reaction and R the gas constant. The higher the activation energy, the slower the reaction at any given temperature.[82] The magnitude and the sign of the E_a values, ΔH^*, ΔS^*, ΔG^* and ΔV^*, are often useful in interpreting the reaction mechanism. The theory of reaction rates postulates that in the rate-determining step,

the reacting species combine reversibly to form an activated complex, which can then decompose into reaction products. For the reaction

$$A + B \underset{}{\overset{K_c^*}{\rightleftharpoons}} [A\cdot B]^* \xrightarrow{k} \text{product} \qquad \textbf{Equation 2.3}$$

the following equilibrium constant is valid

$$K_c^* = \frac{[A\ B]^*}{[A][B]} \qquad \textbf{Equation 2.4}$$

The rate constant, k, of any reaction is given by the expression

$$k = \frac{RT}{Nh} K_c^* \qquad \textbf{Equation 2.5}$$

where K_c^* is an equilibrium constant, h is the Planck's constant and N the Avogadro's number. The free energy of activation, ΔG^*, can the be defined thermodynamically as

$$\Delta G^* = -RT \ln K_c^*$$
$$= \Delta H^* - T\Delta S^* \qquad \textbf{Equation 2.6}$$

where ΔH^* is the enthalpy of activation and ΔS^* the entropy of activation. Therefore, k can be obtained by substituting **Equation 2.5** and **Equation 2.6** into **Equation 2.4**:

$$\ln k = \ln\left(\frac{RT}{Nh}\right) + \frac{\Delta S^*}{R} - \frac{\Delta H^*}{RT} \qquad \textbf{Equation 2.7}$$

When k and ΔH^* of a reaction are known at a given temperature, ΔS^* can be determined. If ΔS^* is large negative, it implies that the reaction mechanism is associative in nature. The volume of activation can be considered as two components, an intrinsinct part ΔV^*_{intr}, and the solvation part, ΔV^*_{solv}.[83]

$$\Delta V^* = \Delta V^*_{intr} + \Delta V^*_{solv}$$ **Equation 2.8**

Large negative ΔV* values point mainly to an associative mechanism, whereas a small negative ΔV* values are most likely an indication of a dissociative interchange process.[84]

2.5.5. Saturation kinetics

The above kinetic treatment is for systems where limited excess to the reactive site of reacting molecules does not hinder reactions. While this is normally true for small molecules, the same cannot be said for large molecules such as proteins or enzymes. The reduction of the R2 subunit of the enzyme, ribonucleotide reductase, which have an active tyrosil radical demonstrate this well.[85] Swarts and co-workers showed R2 tyrosil reduction with glutamic acid-γ-monohydroxamate (GluHA) follow the mechanism.[85]

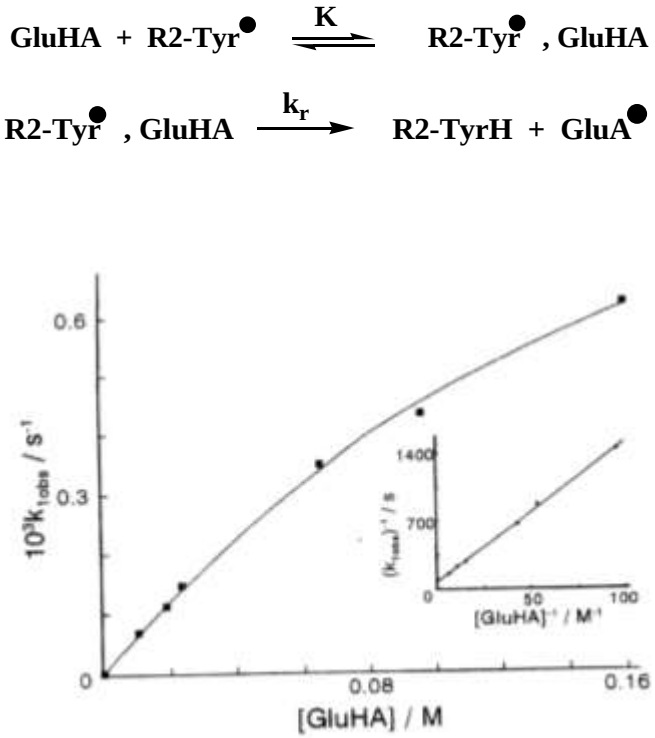

Figure 2. 2: The dependence of rate constants k_{1obs} (25 ºC) for the L-Glutamic-γ-monohydroxamate, $^-O_2CCH(NH_3^+)(CH_2)_2CONHOH$ (GluHA), reduction of the tyrosil radical of active *E. coli* ribonucleotide reductase (410 nm) at pH 7.6, I = 0.100 mol dm^{-3} (NaCl). A linear reciprocal plot is obtained (inset) consistent with saturation kinetic behaviour.

This mechanism gives rise to saturation kinetics and the rate dependence

$$k_{1obs} = \frac{k_r K[GluHA]}{1 + K[GluHA]}$$ was obtained.

Plots of k_{1obs} *vs.* [GluHA] show the saturation kinetic trend **Figure 2.2**. The rate constant k_r and equilibrium constant *K* can be separated by an inverse plot of $1/k_{1obs}$ *vs.* 1/[GluHA] as shown in the insert of **Figure 2.2**. By converting the equation above

$$\frac{1}{k_{1obs}} = \frac{1}{k_r K[GluHA]} + \frac{1}{k_r}$$

The slope of this graph is $1/k_rK$ while the y-intercept is $1/k_r$ implying *K* = intercept/slope.

The present long chain alkyl substituents with R = C_9H_{19} – $C_{18}H_{37}$ in complexes of the type shown below introduced for the first time a saturation kinetic effect on the mechanism of substitution in [Rh(β-diketonato)(cod)] complexes.

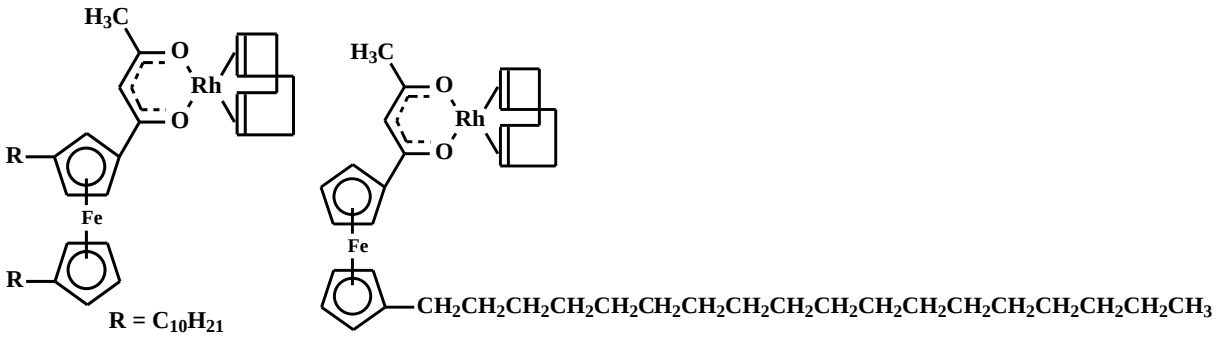

Figure 2. 3: Some of the long chain alkyl substituted ferrocene-containing rhodium complexes of this study.

2.6. Cyclic voltammetric studies

2.6.1. Introduction to cyclic voltammetry

Ferrocene is known for its electrochemical reversible one-electron transfer process, while the rhodium nucleus normally is associated with 2-electron oxidative addition and 2-electron reductive elimination processes which are seldom electrochemically reversible. As this study focuses on the electrochemical behaviour of rhodium / ferrocene complexes of the type [Rh(β-diketonato)(cod)] (see goal 4, Chapter 1), a short discussion of the electrochemical properties of the ferrocene derivatives and rhodium complexes is considered important.

Voltammetry is a group of analytical methods in which only a small portion of the bulk volume of a material is electrolytically reduced or oxidized at the surface of an electrode in a stationary solution.

$$Fe^{3+} + e \underset{\text{oxidation}}{\overset{\text{reduction}}{\rightleftharpoons}} Fe^{2+}$$

Cyclic voltammetry (CV) is one of the most used techniques for examining the electrochemical properties of a chemical substance or material. CV has also been applied to the study of biosynthetic pathways and to study electrochemically generated radicals.[86,87] Knowledge of the electrochemistry of a metal complex can be useful in the selection of the proper oxidizing agent to oxidize or reduce the metal in the metal complex to an intermediate oxidation state. Electrochemical methodology has also been exploited as a novel means of introducing functional groups and removing protective groups.[88]

Cyclic voltammetry consists of cycling the potential of an electrode, which is immersed in an unstirred solution, and measuring the resulting current. The potential of this working electrode is controlled *versus* a reference electrode such as a saturated calomel electrode (SCE) or a silver/silver chloride electrode (Ag/AgCl). By IUPAC convention, potentials are always recalibrated to be referenced to an internal standard, the ferrocene/ferrocenium couple if possible in organic media.

The excitation signal for a CV is a linear potential scan with a triangular waveform. The potential at which the sweep changes direction is known as the switching potential.[89,90]

2.6.2. Parameters of a CV

For an electrochemically reversible reaction the separation between the two peak potentials, ΔE_p, for a process which involves transfer of electrons, as shown in **Figure 2.4**, is given by the equation

$$\Delta E_p = E_{pa} - E_{pc} \cong \frac{0.059V}{n} \qquad \textbf{Equation 2.9}$$

with E_{pa} = cathodic peak potential, E_{pc} = anodic peak potential and n = number of electrons transferred. Many systems are reversible when the voltage is scanned slowly, but at higher scan rates ΔE_p becomes larger than $59/n$ mV. This implies that the rate of electron transfer between substrate and electrode are comparable to or slower than the scan rate.[89,90,91] Experimentally, due to electrode imperfections, ΔE_p values of 90 mV or less are often taken to imply electrochemical reversibility.

Electrochemical reversibility means that the rate of electron transfer between the electrode and substrate is fast enough to maintain the concentration of the oxidized and reduced forms in equilibrium with each other at the electrode surface as required by the Nernst equation. The average of the forward and return peak potentials is called the formal reduction potential, $E^{o/}$, and can be obtained by applying the following equation:

$$E^{o/} = \frac{E_{pa} + E_{pc}}{2} \qquad \textbf{Equation 2.10}$$

The relationship between peak current and concentration is particularly important in analytical applications and in studies of electrode mechanisms. For a chemically reversible reaction that is not accompanied by any further reaction sequences, the ratio between the peak currents is unity as shown by the following equation:

$$\frac{i_{pa}}{i_{pc}} = 1$$ **Equation 2.11**

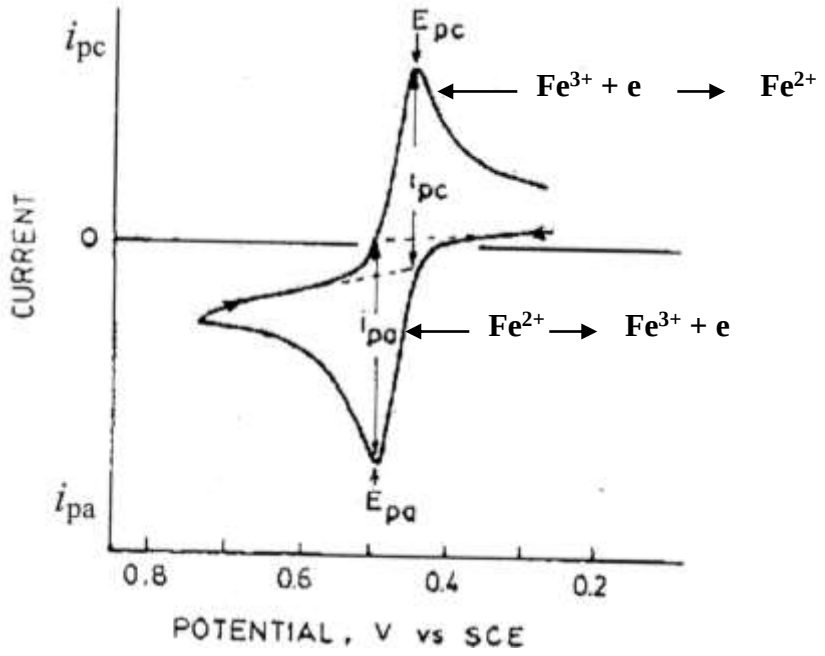

Figure 2. 4: **Cyclic voltammogram of a 1.00 mmol dm^{-3} Fe^{2+} solution in H_2SO_4 on a carbon paste working electrode. The scan initiated at +0.25V *versus* SCE in a positive direction at scan rate 0.1 V s^{-1}.**

Systems can also be electrochemically irreversible or quasi-reversible. The latter term is often used for a system where the electrochemical kinetics are slow, but the electron transfer process still takes place at a rate that allows experimental $90 < \Delta E_p < 150$ mV measurements. Electrochemical irreversibility is assigned when ΔE_p, measures > 150 mV. Measured ΔE_p values also become larger with faster scan rate. These three electrochemical process types (or classes) are summarized in **Figure 2.5**. Electrochemical irreversibility is caused by a slow electron exchange of redox species with the working electrode. **Equations 2.9, 2.10,** and **2.11** are not applicable to irreversible and quasi irreversible electrochemical processes. A complete chemical and electrochemical irreversible system is one where the scan rate of the experiment cannot be made so slow that ΔE_p <150 mV.[92]

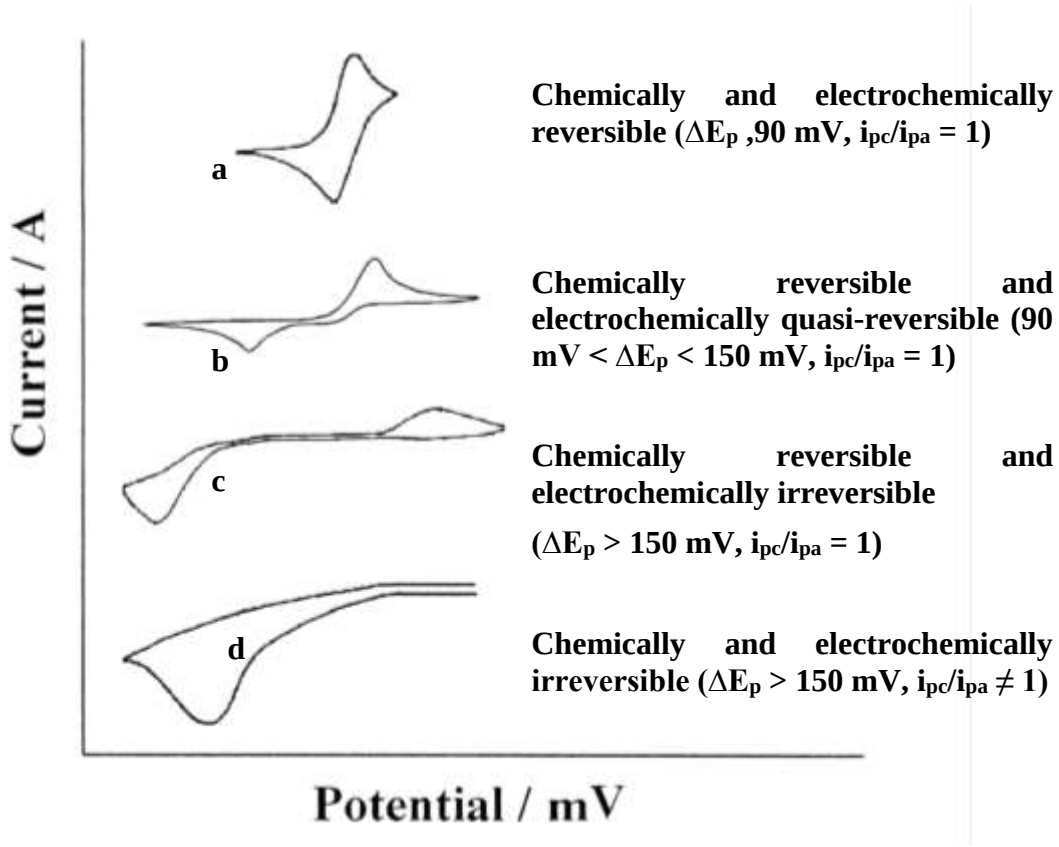

Figure 2. 5: A Schematic presentation of the cyclic voltammogram expected for (a) an electrochemical reversible process, (b) an electrochemical quasi-reversible process, (c) an electrochemical irreversible process (if ΔE_p > 150 mV) and (d) an electrochemical and chemical irreversible process.

2.6.3. Solvents and electrolytes

Non-aqueous solvents have found wide application in studies of redox reactions of organic, organometallic and coordination compounds.[93] Electrochemical phenomenon occurs in a suitable medium, which generally consists of a solvent containing a supporting electrolyte. An ideal electrochemical solvent should possess an electrochemical and chemical inertness over a wide potential range. The solvents that are often used are polar aprotic solvents. Reasons for performing electrochemical measurements in such solvents include; increased solubility of non-polar compounds, elimination of proton transfer reactions, suppression of adsorption, effects of solvent ligation and high conductivity. For example, acetonitrile, CH_3CN, which has a dielectric constant of 37 is commonly used. If a strictly non-coordinating solvent is needed, dichloromethane, CH_2Cl_2, which has a dielectric constant of 8.9, is then preferred.

The choice of supporting electrolyte is crucial in that this "chemically indifferent, but charge conducting salt" affects not only mass transport and solution resistance, but possibly determines the chemical fate of the electrolysis products.[94,95] Supporting electrolytes are used to increase conductivity in the majority of electroanalytical and electrosynthetic experiments. Tetrabutylammonium hexafluorophosphate, $[NBu_4][PF_6]$, is widely used as a supporting electrolyte.[89]

Recent developments of new supporting electrolytes and use of non-traditional solvents have increased options in electrochemical studies. Ohrenberg and Geiger demonstrated that by using the non-coordinating solvent α,α,α-trifluorotoluene or (trifluoromethylbenzene) and the electrolyte tetrabutylammonium(tetrakispentafluorophenyl)borate, $[NBu_4][B(C_6F_5)_4]$, reversible electrochemistry could be achieved for nickelocene and cobaltocene as shown in **Figure 2.6 (a) and (b)** respectively.[96]

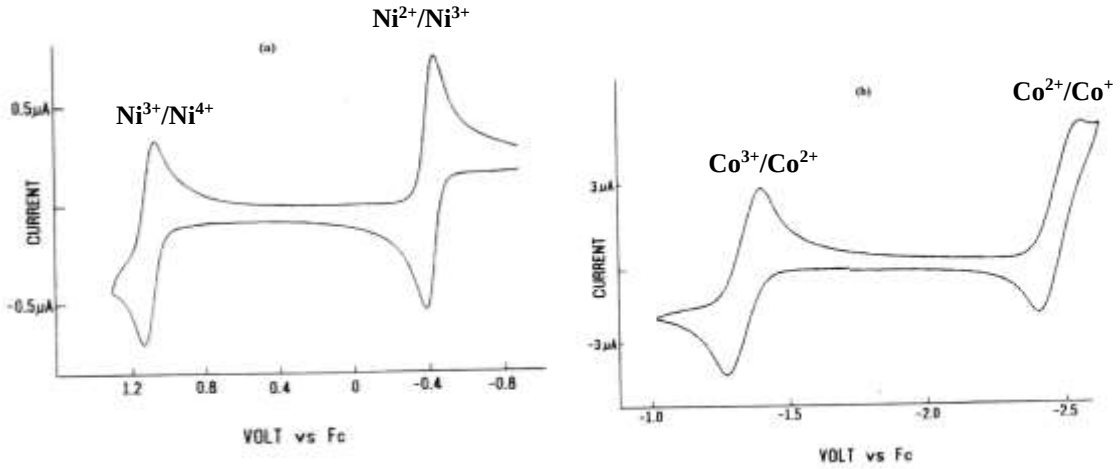

Figure 2. 6: The cyclic voltammograms of 0.5 mmol dm^{-3} solutions nickelocene (left side), (a) and and 1 mmol dm^{-3} cobaltocene(right side), (b) measured in α,α,α-trifluorotoluene containing 0.1 mol dm^{-3} of $[NBu_4][B(C_6F_5)_4]$ on a glassy carbon electrode at a scan rate of 0.1 V s^{-1}.

These findings led LeSuer and Geiger to establish that;

(1) The $[B(C_6F_5)_4]^-$ anion is extremely uncoordinating with respect to positively charged species produced in anodic reactions.

(2) Voltammetric measurements are now possible in solvents having very low dielectric constants, including aliphatic ethers.[97]

(3) Better peak resolutions of closely overlapping signals are possible.

They also discovered that although dichloromethane is a preferred solvent, precipitate formation at the electrode often complicates voltammetric scans for polycationic products. Examples of this are found in the study of polyferrocenyl compounds in low-polarity solvents.[98] **Figure 2.7** compares cyclic voltammetry scans of the triferrocenyl compound, $[Fe(\eta\text{-}C_5H_4)_4]_3(SiMe_2)_2$ in CH_2Cl_2 containing 0.1 mol dm^{-3} $[NBu_4][PF_6]$ with those of the same system with 0.1 mol dm^{-3} $[NBu_4][B(C_6F_5)_4]$.

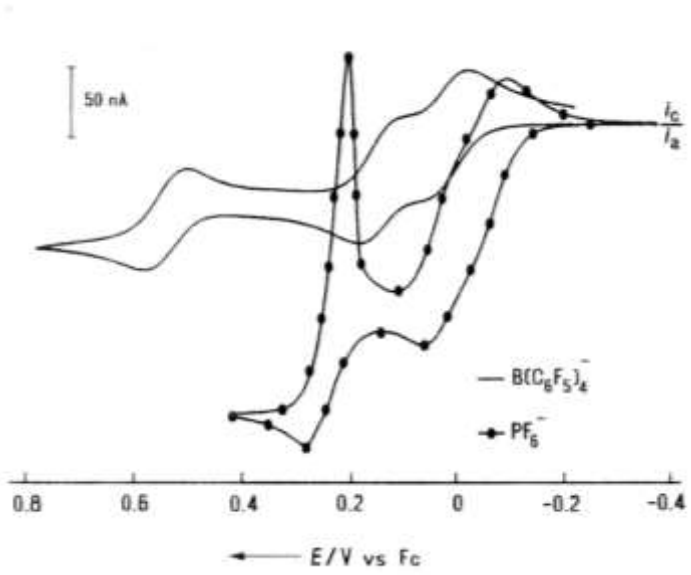

Figure 2. 7: Comparison of cyclic voltammograms of 1.0 mmol dm^{-3} solution of $[Fe(\eta\text{-}C_5H_4)_4]_3(SiMe_2)_2$ in CH_2Cl_2 measured with different supporting electrolytes, (•) 0.1 mol dm^{-3} $[NBu_4][PF_6]$; (-) 0.1 mol dm^{-3} $[NBu_4][B(C_6F_5)_4]$ at a scan rate of 0.2 V s^{-1}, with Fc = ferrocenyl.

The diffusion-controlled shapes of all three waves for the experiment with $[NBu_4][B(C_6F_5)_4]$ media (**Figure 2.7**) attest the fact that even the trication $\{[Fe(\eta\text{-}C_5H_4)_4]_3(SiMe_2)_2\}^{3+}$ is soluble in contrast to the precipitation of the trication and subsequent cathodic stripping wave on the sweep in $[NBu_4][PF_6]$-containing media.[97] Mann and co-workers showed that the oxidation of ruthenocene is a reversible one-electron process when the supporting electrolyte anion in use is tetrakis[3,5-bis(trifluoromethyl)phenyl]borate, $[B\{C_6H_3(CF_3)_2\}_4]^-$, whereas an irreversible two-electron process was found when the more traditional anions $[ClO_4]^-$, $[BF_4]^-$ or $[PF_6]^-$ were used.[95] The supporting electrolyte $[NBu_4][B\{C_6H_3(CF_3)_2\}_4]$ is more effective to prevent precipitation of multiple charged oxidized species such as the dimer Rc^+-Rc^+, than $[NBu_4][B(C_6F_5)_4]$ (Rc = ruthenocenium).

2.6.4. Ferrocene-containing β-diketone cyclic voltammetry

Cyclic voltammetric results of previously studied ferrocene-containing β-diketones (Fc-$COCH_2CO$-R) are important within the context of this study.[99] The difference in peak anodic, E_{pa}, and peak cathodic, E_{pc}, potentials, ΔE_p, for all the ferrocene-containing β-diketones, of the type Fc-$COCH_2CO$-R with R = CF_3, CCl_3, CH_3, Ph and Fc, indicates reasonable electrochemical reversibility as indicated in **Table 2.4** and are represented in **Figure 2.8**.

Table 2. 4: Peak anodic potentials, E_{pa} (*vs.* Fc/Fc^+); difference in peak anodic and peak cathodic potential, ΔE_p; formal reduction potentials, $E^{o/}$; peak anodic current, i_{pa}; and peak cathodic/anodic ratios, i_{pc}/i_{pa}, for 2.0 mmol dm^{-3} solutions of β-diketones, (Fc-$COCH_2CO$-R), measured in 0.1 mol dm^{-3} $[NBu_4][PF_6]/CH_3CN$ on a Pt electrode at 25 °C at a scan rate of 50 mV s^{-1}.

β-diketone R group	E_{pa} /V	ΔE_p /V	$E^{o/}$ /V	i_{pa} / μA	i_{pc}/i_{pa}
Fc-1st ferrocenyl group	0.220	66	0.187	10.00	1.00
Ph	0.267	73	0.230	11.58	0.97
CH_3	0.279	86	0.240	12.46	0.99
Fc-2nd ferrocenyl group	0.333	72	0.297	12.14	1.02
CCl_3	0.332	78	0.293	12.08	0.98
CF_3	0.354	74	0.317	10.53	0.96

All $E^{o/}$ values remained constant between scan rates of 50 and 200 mV s^{-1}. The large spread in $E^{o/}$ values was the result of good communication between the ferrocenyl group and the R substituents having different group electronegativities on the β-diketones *via* the backbone of the pseudo-aromatic β-diketone core. All i_{pc}/i_{pa} ratios approached unity as listed in **Table 2.4**, implying that the electrochemical oxidation of the iron (II) nucleus of the ferrocenyl groups was not followed by a chemically induced reduction of the iron (III) nucleus of the ferrocenium group by the hydroxyl group of the enol form of the β-diketone.[88,100] Two formal reduction potentials, $E^{o/}$, one at 0.266 and another at 0.297 V *vs.* Fc/Fc^+ were observed for Fc-$COCH_2CO$-Fc. This observed inequality was due to the improbability of both ferrocenyl groups not oxidizing simultaneously at the surface of the electrode to invoke two simultaneous one electron transfer processes. Therefore one ferrocenyl group is first oxidized according to the reaction

$$Fc - COCH_2CO - Fc \rightarrow Fc - COCH_2CO - Fc^+ + e^- \qquad E^{o/} = 0.187 \text{ V } vs. \text{ Fc/Fc}^+$$

Good communication between Fc and Fc^+ leads to oxidation of the second ferrocenyl group at a different potential than observed for the first ferrocenyl oxidation according to the reaction

$$Fc - COCH_2CO - Fc^+ \rightarrow Fc^+ - COCH_2CO - Fc^+ + e^- \qquad E^{o/} = 0.297 \text{ V } vs. \text{ Fc/Fc}^+$$

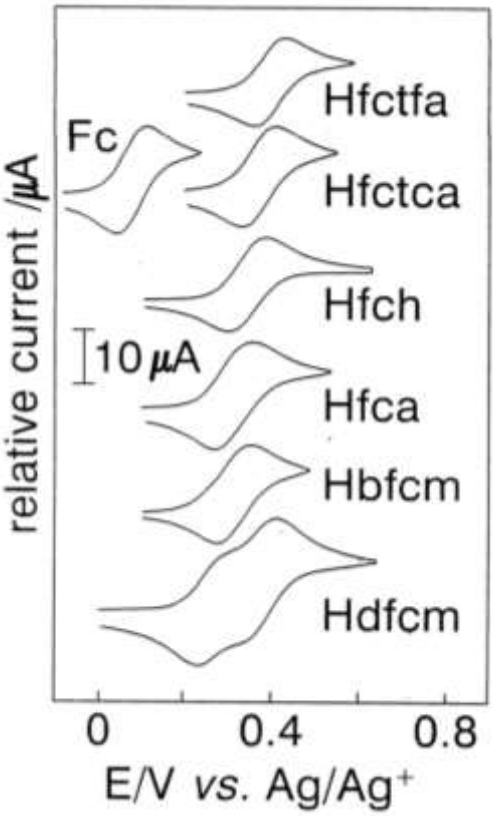

Figure 2. 8: Cyclic voltammograms of 2.0 mmol dm^{-3} solutions of ferrocene, Fc, and β-diketones in 0.1 mol dm^{-3} $[NBu_4][PF_6]/CH_3CN$ on a Pt electrode at 25 ºC at a scan rate of 50 mV s^{-1}.

2.6.5. Rhodium(I) complexes cyclic voltammetry

Rhodium complexes have been studied in order to gain more knowledge of the electronic and steric factors influencing the oxidative addition reactions. Oxidative addition reactions are important

steps in the functioning of compounds as homogenous catalysts.[101] The formal reduction potential obtained by means of cyclic voltammetry of the various β-diketones coordinated onto the rhodium is expected to be independent of steric parameters. In contrast, the relation between the chemical oxidation by means of CH_3I and the pK_a values of the various β-diketones coordinated onto the rhodium is influenced by steric parameters.[102]

Conradie and co-workers reported that the ferrocenyl group of ferrocene-containing Rh^I complexes of the type $[Rh(FcCOCHCOR)(CO)_2]$ with R = CF_3, CH_3, C_6H_5 and Fc were oxidized reversibly at less positive potentials than the rhodium nucleus, while a slow equilibrium process allows rhodium(I) oxidation at potentials associated with those of ferrocene oxidation as well as at substantially more positive potentials (**Figure 2.9**).[103]

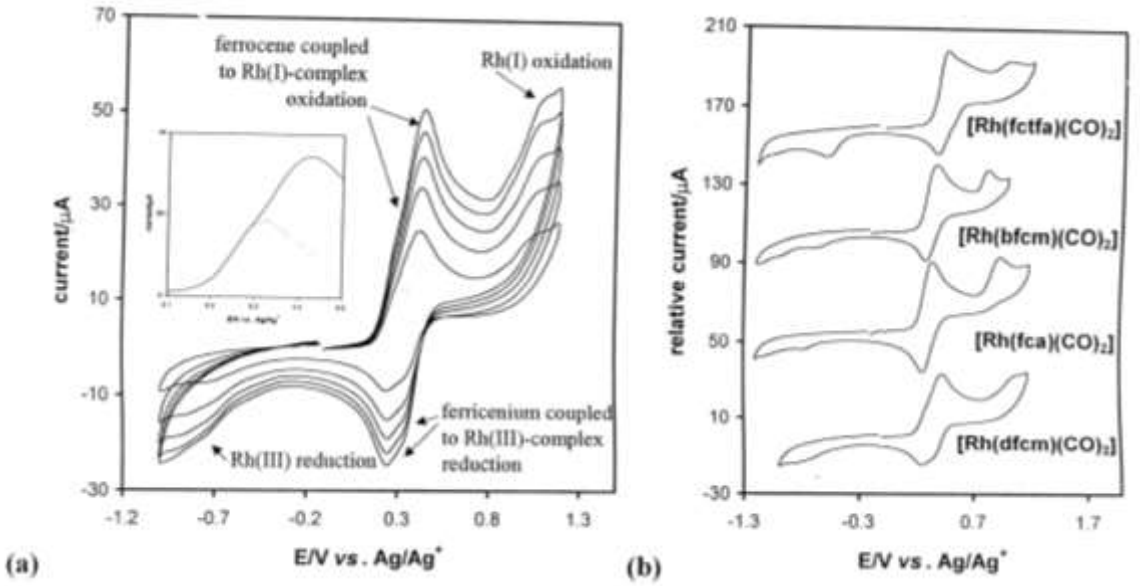

Figure 2. 9 (a) Cyclic voltammograms of 0.5 mmol dm^{-3} solution of $[Rh(FcCOCHCOFc)(CO)_2]$ measured in 0.1 mol dm^{-3} $[NBu]_4[PF_6]$ at scan rates 50 – 250 mVs^{-1} on a glassy carbon working electrode at 25.0 °C. Insert indicates an enlargement of the ferrocene coupled to Rh^I complex oxidation for the 100 mVs^{-1} scan. (b) CV's of 1.2 mmol dm^{-3} solutions of different $[Rh(FcCOCHCOR)(CO)_2]$ complexes ($[Rh(FcCOCHCOFc)(CO)_2]$ = 0.5 mmol dm^{-3}) at a scan rate 100 mVs^{-1} measured under the same conditions as (a).

Figure 2.9 shows the highest Rh^I oxidation potential at 1.022 V *vs.* Ag/Ag^+ for the [Rh(Fc-COCHCO-Fc)$(CO)_2$] and also illustrates the much larger drift in the Rh^I oxidation potentials compared to that observed for formal reduction potentials, $E^{o/}$, for the Fc/Fc^+ couple when changing R from Fc to CF_3 in complexes of the type [Rh(Fc-COCHCO-R)$(CO)_2$].

The present study especially focused on the influence of supporting electrolyte and R-groups substitution on β-diketones of the type shown in **Figure 1.1** and **Figure 1.2** (Chapter 1, page 5) and their rhodium complexes.

2.7. Classification of liquid crystal properties

2.7.1. Introduction

As this study is concerned with complexes having long chain alkyl substituents, C_9H_{19} – $C_{18}H_{37}$, it was expected that most of the new complexes of this study might have liquid crystal or mesophase behaviour (see goal 6, Chapter 1). Alternatively, complex solid state phase behaviour may be observed.

2.7.2. General concept

In the field of liquid crystals, molecular structure and molecular order play a fundamental role. However, it is sufficient to familiarize oneself with a few relatively simple terms in order to fully understand the general principle which applies to liquid crystals. Liquid crystals (or mesogens) are materials which exhibit liquid crystalline behaviour (or mesomorphism). This behaviour appears under given conditions, when phases occur in which the molecular order is intermediate between that of an ordered solid crystal and a disordered liquid or solution. These intermediate phases are called mesophases. Liquid crystals have been defined as "orientationally ordered" liquids or positionally disordered crystals[104] and combine properties of both the crystalline state (*e.g.* optical and electrical anisotropy) and the liquid state (molecular mobility and fluidity). There are two different ways in which a mesophase can be formed and these gave rise to the main classes of liquid crystals:

a) Mesophases can be formed by pure compounds (or mixture of compounds) under the influence of temperature. In this case the liquid crystal is termed a thermotropic mesophase (those that are formed by heating solid crystals or by cooling to the isotropic liquid crystal phase).

b) Mesophases can also be observed as a result of certain species (*e.g.* amphiphiles) forming anisotropic aggregates in the presence of a solvent, usually water. These mixtures are known as lyotropic liquid crystals.

The latter class does not fall within the scope of this study. The intermolecular forces responsible for the molecular arrangement in liquid crystals are essentially the same as those predominant in molecular solids. However, only molecules containing certain structural elements exhibit liquid crystalline behavior. Mesogenic molecules need to meet a series of structural and electronic criteria so that a satisfactory packing of molecules is achieved which allows appropriate interactions between neighbouring molecules. The existence of a permanent dipole moment, its magnitude, or the anisotropy of the molecular polarizability, can be the determining factors in the promotion of liquid crystallinity.[105]

Thermotropic liquid crystals are divided into two main groups depending on their structural features; (i) **calamitic** (rod-like) and (ii) **discotic** (disc-like). Many compounds whose structures are rather different from rod-like are capable of showing calamitic phases.[106] Conversely, compounds with an elongated molecular shape can give rise to columnar mesophases usually associated with disc-shaped molecules.[107] This phenomenon is commonly observed for metallomesogens, where molecules with the same mesogenic core unit can exhibit calamitic or discotic phases depending on the number and position of aliphatic chains.[108] There are two types of calamitic mesophases: the *nematic* and the *smectic* (or lamellar) mesophases[109,110] as indicated in **Figure 2.10**. The least ordered mesophase is the nematic phase (N). In this phase, the molecules align parallel in a preferred direction which is called the director ($\vec{n}$). The molecules can move within the nematic phase and are able to rotate around the molecular long axis. In spite of this freedom of movement the molecules are, on average, aligned in one direction (**Figure 2.10a**), so that they possess orientation, but no positional order. Smectic mesophases (S) show higher degree of order than the nematic phase. The molecules are organized into layers. Within a layer the molecules tend to align parallel to each other. A number of smectic phases exist which differ in the degree of order both within and between the layers. Each smectic modification is denoted by a letter, for example the smectic A phase (in which the molecules are aligned parallel to the layer normal without having a positional order within the layer). Smectic phases are often represented by the letter S with the corresponding subscript letter (*e.g.* the S_A phase). The normal to the layers can be aligned parallel to the director (as in the smectic A) or tilted (as in the smectic C phase). Smectic A and C phases are the least ordered smectic phases and are also the most commonly observed.

Due to the molecular mobility inherent in these phases and their low viscosities, they are called fluid mesophases. Other types of smectic phases show three dimensional order, restricted mobility and higher viscosities.[110]

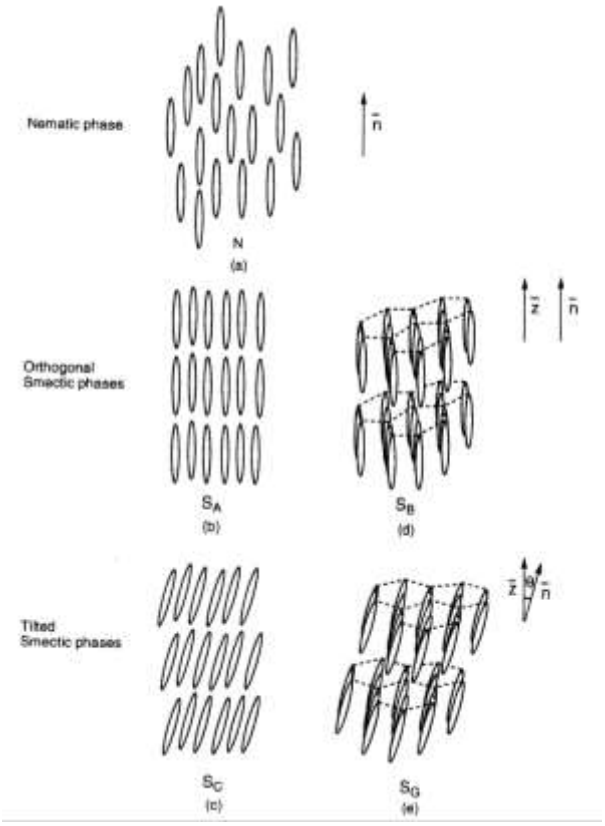

Figure 2. 10: Schematic representation of calamitic mesophases: a) N, nematic; b) S_A, smectic A; c) S_C, smectic C; d) S_B, smectic B; e) S_G, smectic G.

In cases where the molecules are chiral, the structure of fluid mesophases can have an additional property. Chirality in nematogenic molecules can cause a twist in the director alignment, giving rise to the chiral nematic (N*), or cholesteric (Ch) phase. In the chiral nematic phase the director has a helical shape, this is caused by molecules aligning parallel to the director at any position of it, as schematically illustrated in **Figure 2.11a** above (although only layers are represented in this illustration, a chiral nematic does not form layered structure). In the chiral smectic C* phase the helical alignment is caused by the tilt plane of the angle, which changes its direction from layer to layer thus forming a helix (**Figure 2.11b**). Chiral nematic and smectic phases show optical activity and the smectic C* phase can additionally give rise to ferro-, ferri-, or antiferroelectric properties.[111]

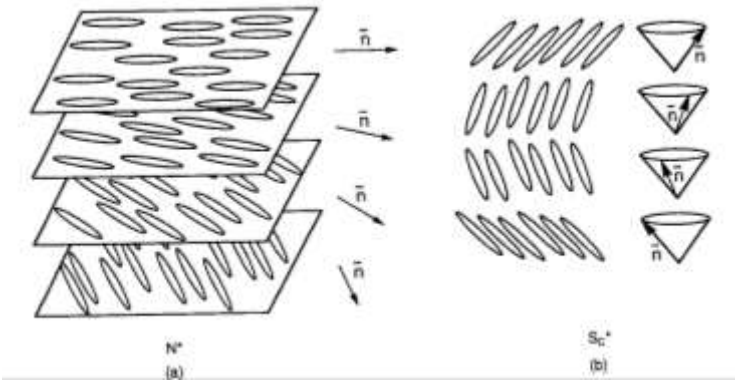

Figure 2. 11: Schematic representation of two chiral mesophases: (a) N*, chiral nematic (cholesteric); (b) S_C*, chiral smectic C.

When the term discotic is applied to mesophases, it does not necessarily imply that the molecules have the geometric shape of a disc. Three different classes of discotic mesophase have been defined: *nematic*, *columnar* and *lamellar* (**Figure 2.12**).[112]

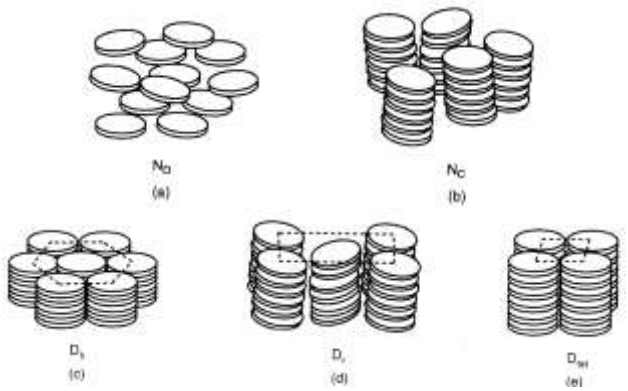

Figure 2. 12: Schematic representation of five discotic phases: (a) N_D, nematic discotic; (b) N_C, columnar nematic; (c) D_h, discotic hexagonal; (d) D_r, discotic rectangular; (e) D_{tet}, discotic tetragonal.

In the discotic nematic phase (N_D), the arrangement of the disc-like molecules is similar to that in the nematic phase formed by calamitic molecules in columnar mesophases (**Figure 2.12a**). The molecules tend to stack in columns which could give rise to a different type of arrangement. In the nematic columnar phase (N_C), the columnar superstructure acts like the rod-like molecules in the nematic calamitic phase (**Figure 2.12b**). In the lamellar discotic phase (D_L), a smectic-like organization of molecules, it has been suggested that the molecules are tilted with respect to the layers.[113]

2.8. The effect of the spacer length on mesophases

Studies of the liquid crystal properties of polymers have been conducted, revealing that the effect of the length of the flexible spacer was considerable. Two main features were observed. Firstly, within a homologous series of polymers, isotropization temperature (T_i) decreases as the number of atoms forming the backbone chain (*i.e*. the length) of the flexible segment increases.

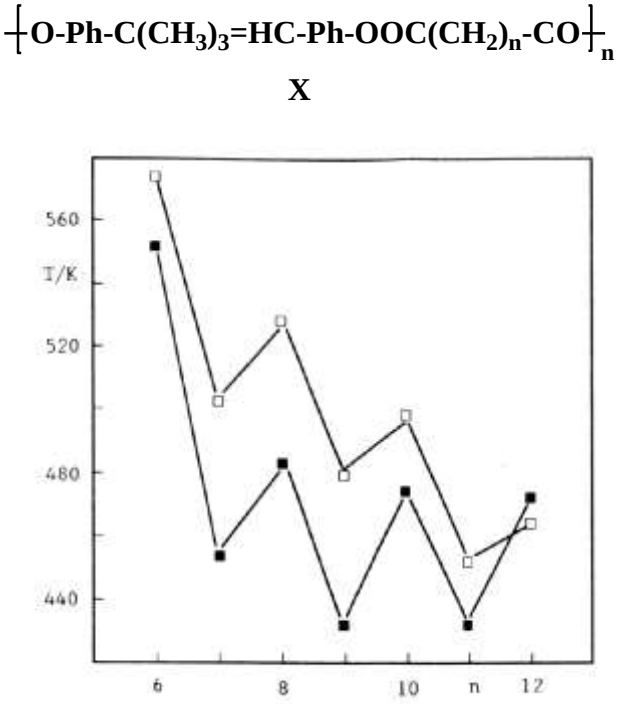

Figure 2. 13: Melting (■) and isotropization (□) temperatures for nematic polyester (X) as a function of number (*n*) of CH_2 groups in the spacer.[115]

Secondly, T_i fluctuates with amplitude depending on the chemical nature of the polymer, according to the even or odd parity of the number (*n*) of atoms forming the backbone chain of the flexible segment. In general, $T_i(n) > [T_i(n-1) + T_i(n+1)]/2$ for *n* = even. This behaviour has been observed both for nematic[114,115,116] and smectic polymers[117,118,119] or even in some cases in which both mesomorphic forms are present.[120] A typical example of regular behavior is shown in **Figure 2.13** for a homologous series of nematic polyesters, **X**, containing α-methylstilbene as a mesogenic segment.[115] Melting temperature (T_m) and isotropization temperature (T_i) fluctuate with a parallel odd-even effect but they decrease for increasing *n* with different gradient. For shorter spacers (*n* <

10 in this specific example), $dT_m/d_n < d\ T_i/d_n$, for both even and odd values of *n* and for longer spacers the trend is inverted.

2.9. Organometallic liquid crystals

2.9.1. Introduction

The great stability of the ferrocene system led to its incorporation into metal-containing liquid crystals. First attempts to introduce the ferrocene unit into mesogenic materials were carried out years ago, and a large number of ferrocene derivatives which are liquid crystalline have been described.[121] The largest number of examples within the group of organometallic liquid crystals, in which the metal is bonded to a π –system in the organic ligand, contains the ferrocene moiety. Other metal- π- bonded complexes which incorporate a ruthenocene unit[122] or a butadiene iron group have also been reported.[123]

2.9.2. Metallocene derivatives

Efforts oriented towards the design of new metallomesogens[124] led to ferrocene derivatives displaying rich mesomorphism.[125] Chiral and polymeric liquid crystalline ferrocenyl systems with potential applications in the development of ferroelectric liquid crystal devices and processable materials were also described.[126,127] Parallel to investigations devoted to thermotropic metallomesogens, metal-containing lyotropic liquid crystals have also been described.[128] Ferrocene proved to a be a valuable unit for constructing thermotropic liquid crystal,[125,129,130] Langmuir and Langmuir-Blodget films:[131] the molecular organization could be controlled as a function of the nature, number, and position of the substituents located on the ferrocene core. With this information, Donnio and co-workers reported the synthesis and thermotropic and lyotropic liquid-crystalline behaviour of the amphiphilic ferrocene derivative, **27**, (**Figure 2.14**), which is substituted at the 1,1′-positions by a sugar moiety (1-amino-1-deoxy-D-sorbitol) and a long alkyl chain (14 carbon atoms).[132] The substituents, in particular the sugar framework, were selected in

view of successful investigations performed with organic-type amphiphilic carbohydrates surfactants.[133,134]

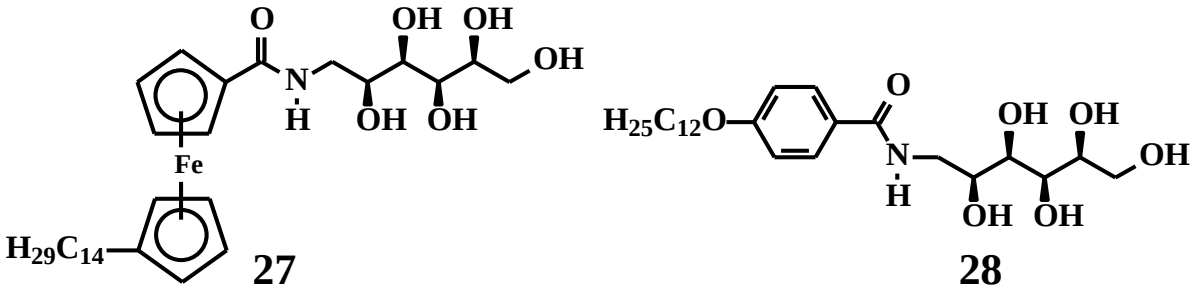

Figure 2. 14: Example of ferrocenyl, 27, and phenyl, 28, derivatives possessing liquid crystal properties.

Comparison of thermotropic properties of **27** with those reported for the ferrocene-free analogue **28**,[133,135] revealed that replacement of the benzene ring by the ferrocene unit led to a decrease of the clearing point, *i.e.*, to destabilize the liquid-crystalline phase (the influence of the alkyl chain length, 14 carbon atoms for **27** and 12 carbon atoms for **28** can be neglected). This result was in agreement with literature data reported for ferrocene-containing thermotropic liquid crystals[125] and for ferrocene-based Langmuir and Langmuir-Blodgett films.[131] It was noteworthy that despite its bulkiness, the ferrocene unit did not completely disrupt the H-bonded network either in the bulk (thermotropic behaviour) or in solution (lyotropic behaviour). Polarized optical microscopy (POM) and differential scanning calorimetry (DSC) investigations for the thermotropic behaviour provided a liquid crystalline phase characterized by fanlike and homeotropic textures. From these observations, the mesophase was identified as a smectic A phase. Two models were postulated to explain the organization of **27** within the smectic A phase.[136,137] In the first model (**Figure 2.15a**),[136] the aliphatic chains are interdigitated and placed in the interior of the layers, whereas the sugar moieties self-assemble in the outer regions of the bilayers. In the second model (**Figure 2.15b**),[137] there is a microphase separation of the alkyl chains and the sugar moieties into a fluid bilayer. In the latter both the alkyl chains and the carbohydrate residues form a disordered packing array, with carbohydrate groups held together through H-bonds.

The lyotropic behaviour of **27** in water indicated the formation of a lamellar (Lα) phase, in agreement with the structure of **27**. Two models were also looked into for the structure of the Lα phase derived from **Figures 2.15a** and **2.15b** respectively. In the first case (**Figure 2.15c**), the alkyl

chains remain interdigitated as the water penetrates the polar groups. The second possibility was that the lamellar (Lα) phase consists of fluid surfactant bilayers separated by thin layers of water (**Figure 2.15d**).

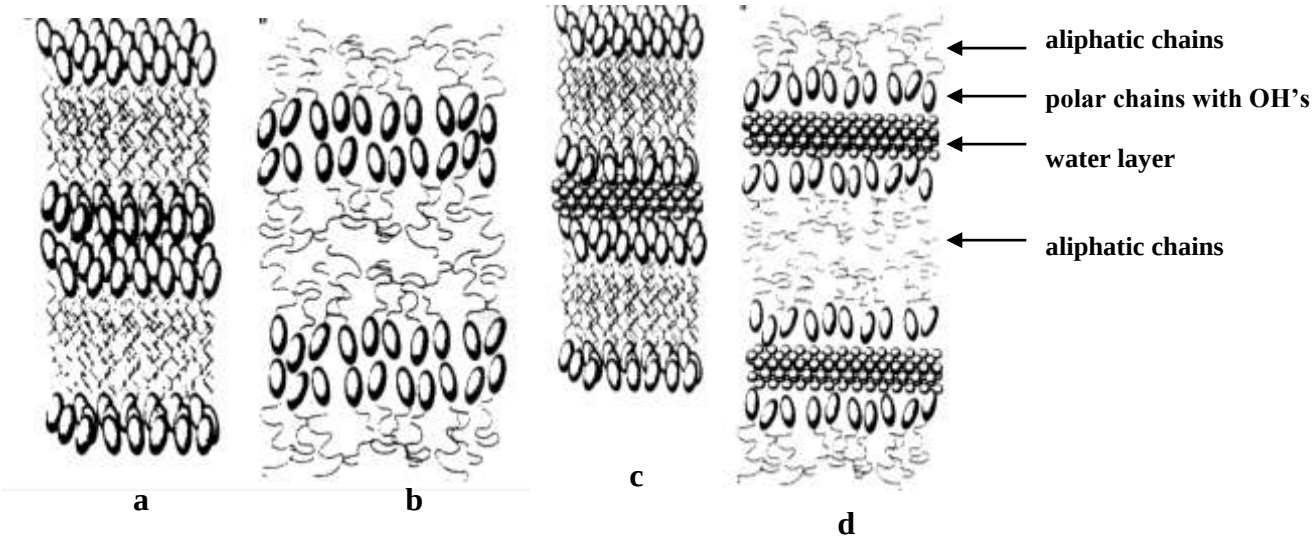

Figure 2. 15: Possible molecular organizations of 28 within the smectic phase: (a) the aliphatic chains are interdigitated, and (b) microphase separation of the alkyl chains and sugar moieties. For 27, within the L_α phase: (c) fluid bilayers with interdigitated aliphatic chains and (d) fluid bilayers without chain interdigitation.

Deschenaux and co-workers described the synthesis and thermal properties of the persubstituted ferrocene derivatives, **29** and of its oxidized complex, **30**, as outlined in **Scheme 2.15**.[138] The latter represents the first example of ferrocene-containing thermotropic liquid crystals. A peralkylated ferrocene derivative was selected as an electron donor because of the ease of oxidation of such species (and related peralkylated compounds) in comparison with less substituted compounds.[139] No mesomorphism was observed from ferrocene derivative **29**, only for **30. Figure 2.16** shows the DSC thermogram from which the liquid crystalline behaviour of compound **30** can be seen.

Deschenaux and co-workers concluded that electron transfer can be exploited for controlling supramolecular organization within the liquid-crystalline state for the ferrocene-ferrocenium redox system.[138]

Chaurd and co-workers synthesized unsymmetrical 1,3-disubstituted ferrocene-containing liquid crystal moeities, where the different substituents at the 1- and 3-positions generate structures with chirality as shown in **Figure 2.17**.[140] A representative example is illustrated by compound **32** (see **Scheme 2.16**), the two substituents are differentiated by the length of the alkyl chains and the

orientation of the outer ester groups. Compound in **Scheme 2.16**, smectic C (SmC) and smectic A (SmA) phases were reported, and in some cases, an additional nematic phase was observed.

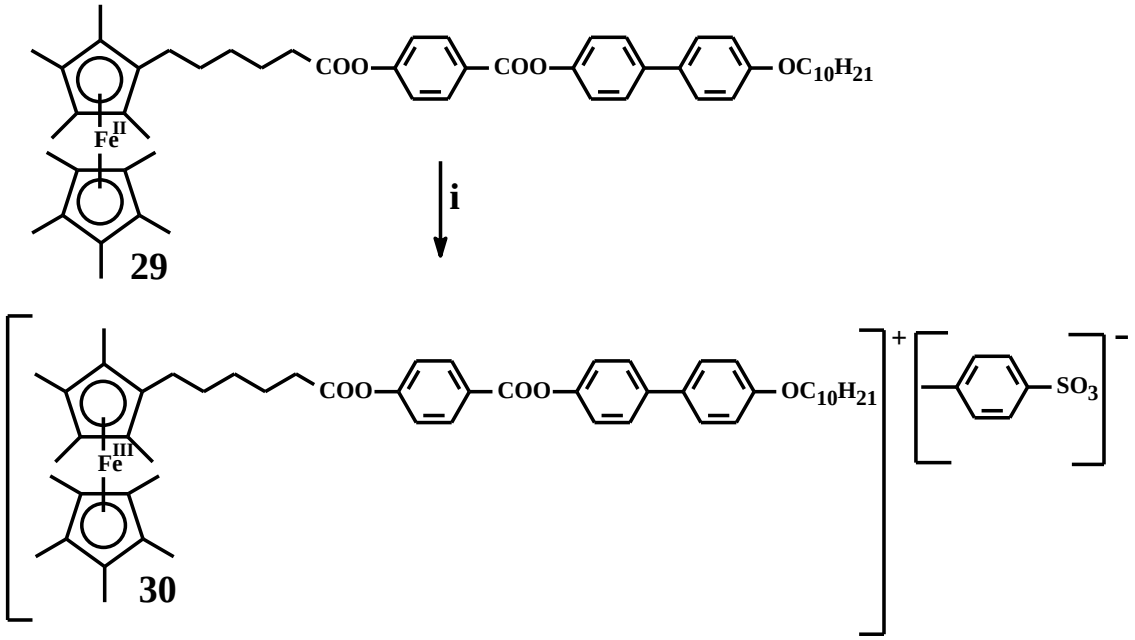

Scheme 2. 15: Example of a ferrocenium salt having thermotropic liquid crystal properties.

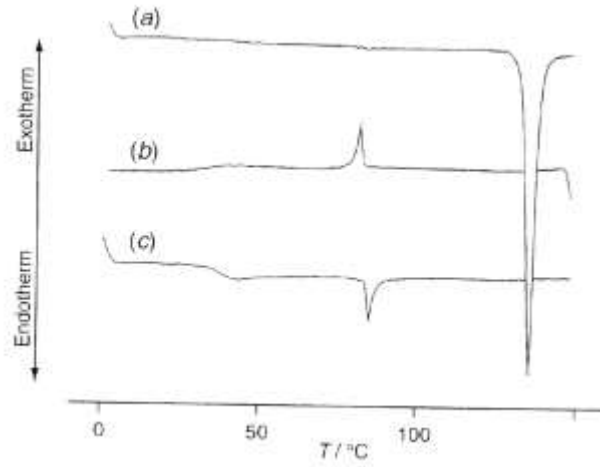

Figure 2. 16: Differential scanning calorimetry thermograms of 30 registered during the (a) first heating (melting and molecular reorganization), (b) first cooling (transition from isotropic liquid to mesophase) and (c) second heating run (transition from mesophase to isotropic liquid).[138]

The presence of the SmC phase in this family of compounds provided a unique challenge to make the materials optically active (SmC*) and thereby ferroelectric. For ferrocenyl liquid crystals, SmC* phases have been reported only for two mono-substituted derivatives.[126,141]

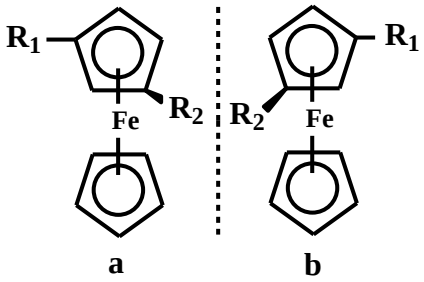

31

Figure 2. 17: Planar chirality in unsymmetrically 1,3-disubstituted ferrocene derivatives. Planar chirality is chirality resulting from the arrangement of out-of-plane groups with respect to a reference plane called the chiral plane.[142]

In addition to the investigation of the dependency of ferroelectricity on planar chirality, Chaurd and co-workers probed the influence of the chiral unit, which is imbedded in the central region of the molecular structure, on the self-organization process and mesophase formation.[140] Malthête and co-workers exploited planar chirality by reporting optically-active butadienetricarbonyliron liquid crystal complexes. [143]

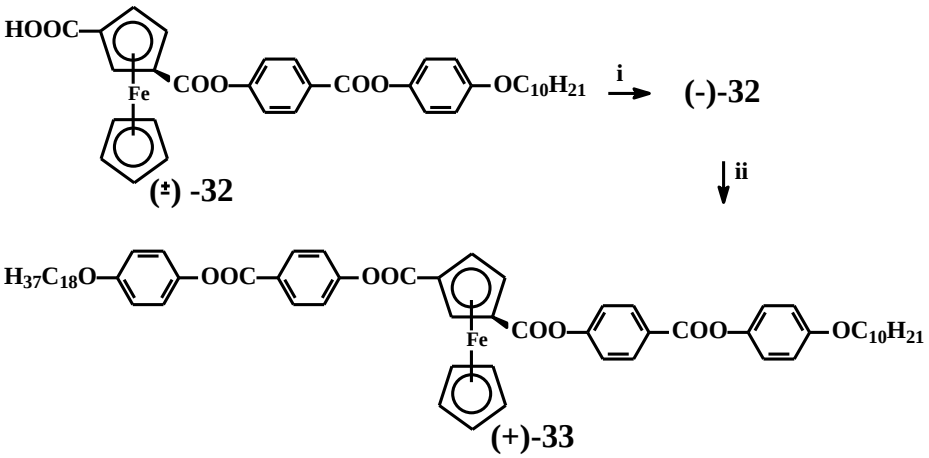

Scheme 2. 16: Unsymmetrically 1,3-disubstituted ferrocene-containing liquid crystal.

The mesomorphic behaviour and ferroelectric properties of compound **(+)-33**, was selected because the corresponding racemic analogue gave the broadest SmC range among the family of homologues studied.[126] The results obtained are shown in **Figure 2.18.**[140] It firstly indicated that planar chirality can induce ferroelectric properties. Secondly, the induced effects are weak, revealing a poor coupling between the chirality associated with ferrocenyl moiety at the centre of the structure, the strongly polar functional groups in the material, and the liquid crystalline environment. Finally, Chaurd and co-workers concluded that the weak ferroelectric properties were probably linked to the fact that the arms attached to the ferrocenyl unit are not greatly different in length or polarity.[140]

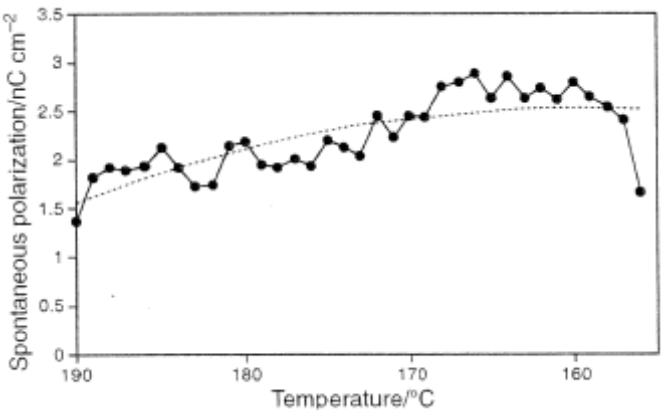

Figure 2. 18: The spontaneous polarization measured as a function of temperature from the Curie point for (+)-33.

2.9.3. Rhodium-complexes containing β-diketonate

β-diketonate complexes have been subjected to extensive work in the field of metallomesogens, with the scope of the research concerning calamatic as well as non-calamatic systems.[144] The mesomorphic properties of this kind of β-diketonate complexes changed drastically depending on the number of aliphatic chains substituted on the phenyl rings. Few examples of calamatic (rodlike) liquid crystals containing rhodium have been described.[145,146,147] The mesogenicity of certain β-diketones (**Scheme 2.17,** ligands **34 - 36**)[148] and their ability to coordinate metal atoms motivated Barberá *et al.* to investigate the liquid crystal properties of new rhodium complexes containing these rodlike β-diketonate ligands (**Scheme 2.17,** complexes **37 - 39**).[149]

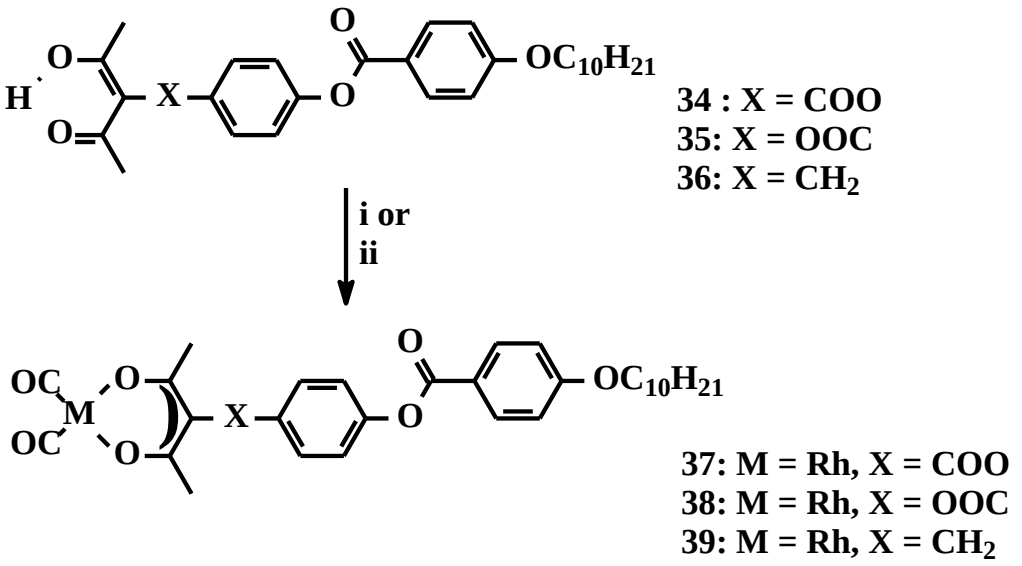

Scheme 2. 17 Rhodium complexes containing β-diketonate ligands with liquid crystal properties. Here, i = KOH, ½ [M(μ-Cl)(cod)]$_2$, 2CO and ii = NaOAc, ½ [Rh(μ-Cl)(CO)$_2$]$_2$.

These compounds exhibit conjugated structures in which the metal environment, [M(CO)$_2$] or [RhCl(CO)$_2$], act as a terminal polar group and the decyloxy group, at the other end of the molecule, could play the role of an electron-donor substituent. Mesomorphic properties of complexes **(37 - 39)** were characterized by optical microscopy (OM) with polarized light.[149]

Columnar mesophases can *inter alia* be obtained when the attractive forces between aromatic cores of a compound causes a degree of stacking of molecules on top of each other. This would lead to a crystalline state. However, when long side chains are bound to the aromatic core, these may melt when heat is applied to the system without disturbing the order generated by the attractive forces keeping the aromatic core stacked in columnar fashion.

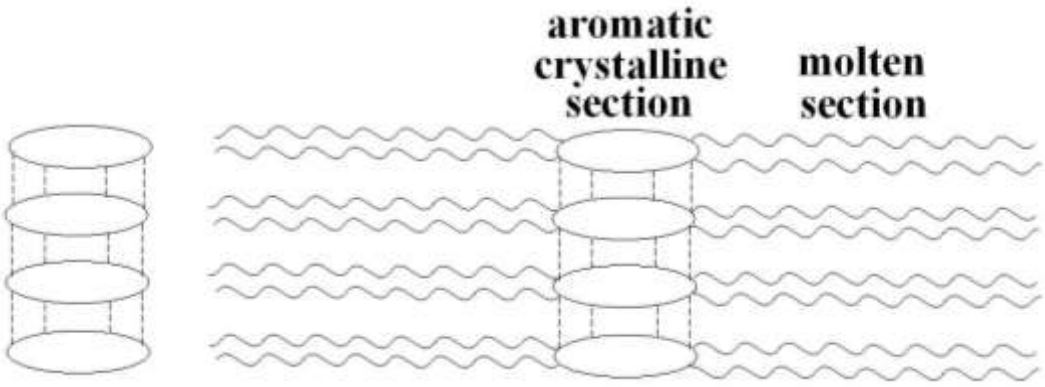

This in essence would lead to a liquid crystal state. If the attractive forces between the aromatic cores are broken before side chain melting occurs no liquid crystal state will be observed. However, upon cooling the isotropic liquid state of such a system, phase changes may be observed at lower temperature than the melting point. This will be the results of different packing patterns of the side chains of the system at different temperature. Such apparent solid phase changes may also be the result of slow kinetics causing the long side chains of such a system first to freeze into an amorphous solid at the melting point before, at lower temperatures and at a slow rate, these side chains rearrange into different crystal packing mode. It will manifest as a solid state phase change during a phase study. Such liquid crystal and solid state phase changes are conveniently observed by differential scanning calorimetry.

With respect to this study it becomes of interest to see if metallocene β-diketones and their rhodium complexes may exhibit any thermotropic columnar mesophase or solid state phase change behaviour (**Figure 2.19**).

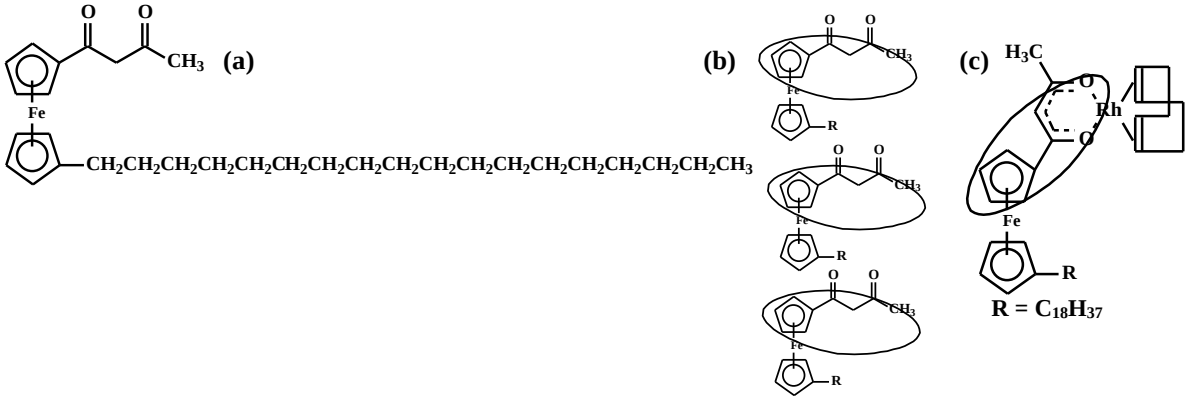

Figure 2. 19: Ferrocene-containing β-diketone showing the pseudo aromatic core that (b) may induce a thermotropic columnar mesophase. (c) Rhodium β-diketonato complexes that may show mesophase or solid state phase changes.

2.10. Cytotoxic studies

2.10.1. Introduction

It was previously shown that some ferrocene-containing rhodium complexes have superior anticancer activity over *cisplatin*.[150] As this study concerns complexes of the type [Rh((Cp-

R^2)Fe(Cp-R^1-1,3-$COCHCOCH_3$))(cod)], a short review of the anticancer activity of ferrocene derivatives and rhodium(I) complexes is very important.

2.10.2. Ferrocene derivatives in cancer treatment

Since the discovery of *cisplatin* in the treatment of cancer, there have been various studies on its effectiveness against different tumours, its pharmacokinetics, its distribution in the body, the mechanism by which it destroys cancer cells as well as the studies on dose intensity.[151,152] However, this highly effective and frequently used chemotherapeutic drug often finds limited clinical use, owing to the many negative medical and physical side effects it shows. For *cisplatin*, these negative side-effects or undesired chemical and physical properties include *inter alia* lack of aqueous solubility, high toxicity especially to the kidneys and bone marrow, it induces a loss of appetite (anorexia) in many patients and it is excreted at a very high rate from the body.[153] In addition, the development of drug resistance after a continued drug dosage limits the long-term use of this drug. The reason for all the detrimental side-effects of any chemotherapeutic drug, including *cisplatin*, is centered on the drug's inability to distinguish between healthy and cancerous cells. To overcome these negative aspects surrounding *cisplatin* and other chemotherapeutic drugs, new antineoplastic materials are continuously being synthesized and evaluated. New methods of delivering an active drug to a cancerous growth are being developed[154] and combination therapy has been investigated in the hope of finding synergistic effects.[155]

.

In 1984 Köpf-Maier and co-workers were the first to show that the ferricenium species has appreciative activity against cancer.[156] Further to this study, it was shown by Neuse and co-workers that ferrocenylacetic acid induced good to excellent cure rates against human *adenocarcinoma*, squamous cell *carcinoma* and large-cell *carcinoma* of the lung in *in vitro* human tumour clonogenic assays.[157] Osella and co-workers determined the mechanism of action of the ferrocenyl moiety in chemotherapy. It is based on electron transfer processes.[158] The Fe^{II}-containing ferrocenyl group needs first to be activated by oxidation to a Fe^{III}-containing ferrocenium species by redox-active enzymes in a particular body compartment. The ferrocenium species then interacts with water and oxygen to generate a hydroxyl radical ($OH^{\bullet}$), which is the cytotoxic species.

The cytotoxic capabilities of ferrocene compounds studied in this laboratory, showed, for example, that 3-ferrocenylbutanoic acid, **10**, is one order of magnitude more active against Murine EMT-6 cancer cells when anchored on the water-soluble polymer conjugate shown in **Figure 2.20** compared to its cytotoxicity when it is a free monomeric drug.[159] In a world wide patent from this laboratory it was reported that the IC_{50}-values of the $FcCOCH_2COCF_3$ β-diketone was much more favourable than that of *cisplatin*, even against platinum resistant cell lines such as COR L23, a sensitive human lung large cell *carcinoma*.[150] Also, the therapeutic index (TI) of these compounds exceeds 8 compared to the 2 for *cisplatin*. The most impressive cytotoxic results for ferrocene-containing rhodium complexes to date, though, were obtained for the $[RhFcCOCHCOCF_3(cod)]$ complexes, which showed an IC_{50} value of 0.39 μM/kg mass of test animal when irradiated with a radiation dose of 5 Gy. The corresponding value for *cisplatin* is 4.5 μM/kg mass test animal.

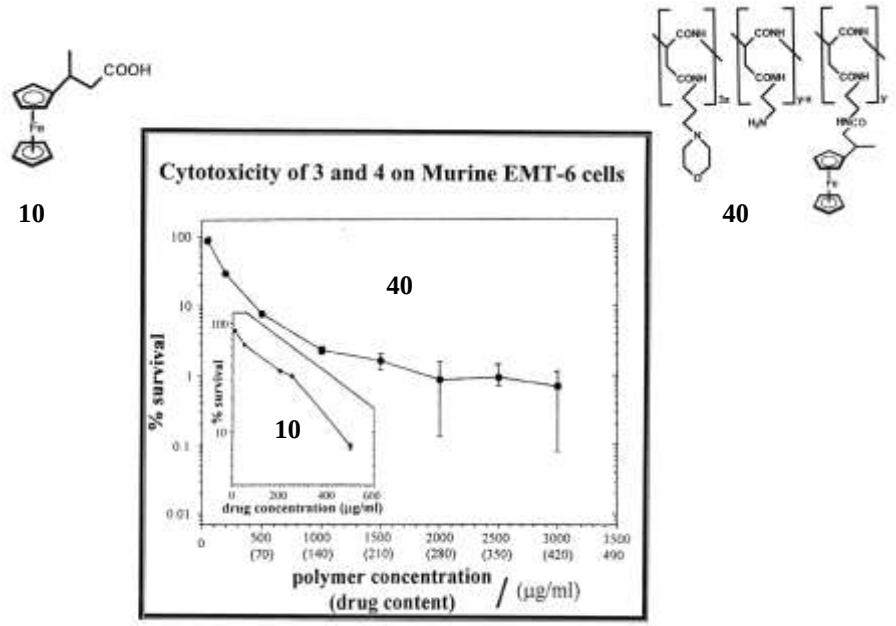

Figure 2. 20: 3-Ferrocenylbutanoic acid, 10, and water-soluble polymer conjugate, 40. The diagram shows the % survival of murine EMT-6 cells after 24 hours of incubation with 40, and in the insert diagram, shows the % survival at the indicated concentration with compound 10.

Bohm and co-workers also investigated the apoptosis and abnormal morphology of *cisplatin*, ferrocene-containing β-diketone ($FcCOCH_2COCF_3$) and the rhodium complex $[RhFcCOCHCOCF_3(cod)]$.[160] It was discovered that the three drugs showed similar toxicities in the 1-10 (μM) range in prostate cell lines and differ significantly in the activation of death pathways as indicated in **Table 2.5**.

Table 2. 5: IC_{50} values (μM) for *cisplatin*, the ferrocene-containing β-diketone $FcCOCH_2COCF_3$ and the rhodium complex $[RhFcCOCHCOCF_3(cod)]$ determined by the MTT assay.

Cell lines	$FcCOCH_2COCF_3$	$[RhFcCOCHCOCF_3(cod)]$	Cisplatin
1542T	4.52	4.14	0.88
1542N	13.20	10.11	1.32
Caco-2	4.85	5.15	1.01

However, no detailed information on the mechanism of action of rhodium complexes in chemotherapy is currently available. What follows in this dissertation is a discussion of all research results (Chapter 3), followed by the experimental procedures, (Chapter 4). A summary of results and future perspective (Chapter 5) concludes this chapter.

1 Nefedov, V. A. and Tarygina, L. K., *Russ. J. Org. Chem. (Eng. Transl.)*, **12**, 1960, (1976).

2 Rosenblum, M., *Chemistry of the Iron Group Metallocenes*, Part I, Wiley-Interscince, New York, p.201, (1965).

3 Bublitz, D. E. and Rinehart Jr., K. L., *Organic Reactions*, **17**, 1 (1969).

4 Hofmann, V., Ringsdorf, H. and Maucevic, G., *Makromol. Chem.*, **176**, 1929, (1975).

5 Rosenblum, M., Barnejee, A., K, Danieli, N., Fisch, R. W. and Schlatter, V., *J. Am. Chem. Soc.*, **85**, 316, (1963).

6 Schögl, K., *Mh. Chem.*, **88**, 601, (1957).

7 Schögl, K. and Egger, H., *Mh. Chem.*, **94**, 376, (1963).

8 Benkeser, A., Nagai, Y. and Hooz, J., *J. Am. Chem. Soc.*, **86**, 1450, (1964).

9 Buell, G. R., McEwen, W. E. and Kleinberg, J., *J. Am. Chem. Soc.*, **84**, 40, (1962).

10 Carrol, M. A., White, A. J. P., Widdowson, D. A. and Williams, D. J., *J. Chem. Soc., Perkin Trans.* **1**, 1551, (2000).

11 Du Plessis, W. C., Vosloo, T. G. and Swarts, J. C., *J. Chem. Soc., Dalton Trans.*, 2507, (1998).

12 D. E. Bublitz and K. L. Rinehart, *Org. Reactions*, 21, (1968).

13 Benkeser, R. A., Goggin, D. and Schroll, G., *J. Am. Chem. Soc.*, **76**, 4025, (1954).

14 Seyferth, D. and Helling, J. F. *Chem. Ind. (London)*, 1568, (1961).

15 Reeves, P. C., *Org. Synth.*, **56**, 28, (1977).

16 Lednicer, D. and Hauser, C. R., *Org. Synth.*, **40**, 31, (1961).

17 Lednicer, D., Lindsay, J. K. and Hauser, C. R., *J. Org. Chem.*, **23**, 653, (1958).

18 Broadhead, G. D., Osgerby, J. M. and Pauson, P. L., *J. Chem. Soc.*, 650, (1958).

19 Blom, N. F., Neuse, E. W. and Thomas, H. G., *Transition Met. Chem.*, **12**, 301, (1987).

20 (a) Rinehart Jr., K. L., Curby Jr., R. J. and Sokol, P. E., *J. Am. Chem. Soc.*, **79**, 3420, (1957); (b) Weinmayr, V., *J. Am, Chem. Soc.*, **77**, 3029, (1955).

21 Da Re, P. and Sianesi, E., *Experientia*, **21**(11), 648, (1965).

22 Hofmann, V., Ringsdorf, H. and Maucevic, G., *Makromol. Chem.*, **176**, 1929, (1975).

23 Hudson, R. F. and Moss, G. E., *J. Chem. Soc.*, 5157, (1962).

[24] Neuse, E. W. and Perwiltz in *Polyamides as Drug Carriers*: *Water Soluble Polymers;* eds. Shalaby, S. W., McCormick, C. L. and Butler, G. B., *American Chemical Society,* Washington DC, ch. 25, p. 395, (1991).

[25] Lindsay, J. K. and Hauser, C. R., *J. Org. Chem.,* **22**, 355, (1957).

[26] Seyferth, D., Hoffman, H. P., Burton, R. and Helling, J. F., *Inorg. Chem.,* **1**, 227, (1962).

[27] Köpf-Maier, P., Köpf, H. and Neuse, E. W., *J. Cancer Res. Clin. Oncol.,* **108**, 336, (1984)

[28] Hauser, C. R., Swamer, F. W. and Adams, J. T., *Organic Reactions,* John Wiley and Sons, New York, **8**, chapter 3, p. 59, 98, (1954).

[29] Adams, J. T. and Hauser, C. R., *J. Am. Chem. Soc.*, **66**, 1220, (1944).

[30] Swamer, F. W. and Hauser, C. R., *J. Am. Chem. Soc.*, **68**, 2647, (1946).

[31] Klement, L., Lütjens, H. and Knochel, P., *Angew. Chem. Int. Ed. Engl.*, **36**, 1454, (1997).

[32] Betzemeier, B., Lhermitte, F. and Knochel, P., *Tetrahedron Lett.*, **39**, 6667, (1998).

[33] Croxtall, B., Fawcett, J., Hope, E. G. and Stuart, A. M., *J. Fluorine Chem.,* **119**, 65, (2003).

[34] Kondo, A. and Iwatsuki, S., *J. Fluorine Chem.,* **26**, 59, (1984).

[35] Claessen, R. U., Welch, J, T., Toscano, P. J., Banger, K. K., Kornilov, A. M., Eisenbraun, E. T. and Kaloyeros, A. E., *Mater. Res. Soc. Symp. Proc.,* **612**, D6, (2000).

[36] Banger, K. K, Korlinov, A., Claessen, R. U., Eisenbraun, E. T., Kaloyeros, A. E., Toscano, P. J. and Welch, J. T., *Inorg. Chem. Commun.,* **4**, 496, (2001).

[37] Higashiya, S., Banger, K. K., Ngo, S. C., Lim, P. N., Toscano, P. J. and Welch, J. T., *Inorg. Chim. Acta,* **351**, 291, (2003).

[38] Banger, K. K., Ngo, S. C., Higashiya, S., Claessen, R. U., Bousman, K. S., Lim, P. N., Toscano, P. J. and Welch, J. T., *J. Organomet. Chem.*, **678**, 15, (2003).

[39] Corey, E. J., Seebach, D. and Freedman, R., *J. Am. Chem. Soc.*, **89**, 434, (1967).

[40] Brook, A. G., Duff, J. M., Jones, P. F. and Jones, N. R., *J. Am. Chem. Soc.,* **89**, 431, (1967).

[41] Claessen, R. U., Korlinov, A. M., Banger, K. K., Ngo, S. C., Higashiya, S., Wells, C. C., Dikarev, E. V., Toscano, P. J. and Welch, J. T., *J. Organomet. Chem.*, **689**, 71, (2004).

[42] Katz, H. E., *J. Mater. Chem.,* **7**, 369, (1997).

[43] (a) Graf, D. D., Day, N. C. and Mann, K. R., *Inorg. Chem.,* **34**, 1562, (1995); (b) Graf, D. D. and Mann, K. R., *Inorg. Chem.*, **36**, 141, (1997); (c) Jones, L. Ch. and Higgins, S. J., *J. Mater. Chem.*, **9**, 865, (1999).

[44] Jaafari, A., Ouzeau, V., Ely, M., Rodriguez, F., Chane-Ching, K., Yassar, A. and Aaron, J. J., *Synthetic Metals,* **147**, 183, (2004).

[45] Suzuki, M., Watanabe, A. and Noyori, A., *J. Am. Chem. Soc.,* **102**, 2095, (1980).

[46] March, J., *Advanced Organic Chemistry, (4th ed.),* John Wiley and Sons Inc., New York, p. 1072, (1992).

[47] Manyik, R. M., Frostick Jr., F. C., Sanderson, J. and Hauser, C. R., *J. Am. Chem. Soc.,* **75**, 5030, (1953).

[48] (a) Hauser, C. R and Cain, C. E., *J. Org. Chem.*, **23**, 1142 (1958); (b) Cain, C. E., Mashburn, T. A. and Hauser, C. R., *J. Org. Chem.*, **26**, 1030, (1961).

[49] Weinmayr, V., *Naturwissenschaften,* **45**, 311, (1958).

[50] Cullen, W. R., Rettig, S. J. and Wickenheiser, E, B., *J. Mol. Catal.,* **66**, 251, (1991).

[51] Gero, A., *J. Org. Chem.,* **19**, 469, (1954).

[52] Semerano, G. and Chisini, A., *Gazz. Chim. Ital.,* **66**, 504, (1936).

[53] Conant, J. B. and Thompson Jr., A. F., *J. Am. Chem. Soc.,* **54**, 4039, (1932).

[54] Wheland, G. W., *Advance Organic Chemistry,* (3rd edition), John Wiley and Sons, New York, 1960.

[55] Irving, R. J. and Riberio da Silva, M. A. V., *J. Chem. Soc. Dalton Trans,* 798 (1998).

[56] Bratoz, S., Hadzi, D. and Rossmy, G., *Trans. Faraday Soc.,* **52**, 464, (1954).

[57] Jarret, H. S., Sadler, M. S. and Shoolery, J. N., *J. Chem. Phys.,* **21**, 2092 (1953).

[58] Reeves, L. W., *Can. J. Chem.,* **35**, 1351, (1957).

[59] Moon, S. and Kwon, Y., *Magn. Reson. Chem.,* **39**, 89, (2001).

[60] Klose, G., Thomas, P., Uhlemann, E. and Marki, J., *Tetrahedron,* **22**, 2695, (1966).

[61] Cravero, R. M., González-Sierra, M. and Olivieri, A., *J. Chem. Soc., Perkin Trans 2,* 1067, (1993).

[62] Du Plessis, W. C., Davis, W. L., Cronje, S. J. and Swarts, J. C., *Inorg. Chim. Acta,* **314**, 97, (2001).

[63] Albert, A. and Sejeant, E. P., *The Determination of Ionization Constants, (3rd edition),* Chapman and Hall, Ltd., p. 110, (1984).

[64] Helm, L., MINSQ, non-linear parameter estimation and model development, least squares parameter optimisation V3.12, MicroMath Scientific Software, Salt Lake City, UT, 1990.

[65] Conradie, J., Lamprecht, G. J., Otto, S. and Swarts, J. C., *Inorg. Chim. Acta*, **328**, 191, (2002).

[66] Cross, R. J., *Chem. Soc. Rev.*, **14**, 197, (1985).

[67] Rodgers, G. E., Introduction to Coordination, Solid State, and Descriptive Inorganic Chemistry, McGraw-Hill, 1994, pp 94-116.

[68] Cotton, F. A., Wilkinson, G. and Gaus, P. L., *Basic Inorganic Chemistry, (3rd edition)*, John Wiley and Sons, Inc., p. 187, (1995).

[69] Wilkinson, R. G., *Kinetics and mechanism of reactions of Transition Metal Complexes, 2nd* thoroughly revised edition, CVH, Weinhein, p. 103, 232, (1991).

[70] Mathey, F. and Servin, A., *Molecular Chemistry of the Transition Elements*, John Wiley and Sons, Chichester, p 28, (1996).

[71] Belluco, U. Cattalini, L., Pearson, R. G. and Turco, A., *J. Am. Chem. Soc.*, **87**, 241, (1965).

[72] Swain, C. G. and Scott, C. B., *J. Am. Chem. Soc.*, **75**, 141, (1953).

[73] Leipoldt, J. G., Lamprecht, G. J. and Steynberg, E. C., *J. Organomet. Chem.*, **402**, 259, (1991).

[74] Leipoldt, J. G., Basson, S. S., van Zyl, G. J. and Steyn, G. J. J., *J. Organomet. Chem.*, **418**, 241, (1991).

[75] Vosloo, T. G. and Swarts, J. C., *Trans. Met. Chem.*, **27**, 411, (2002).

[76] Leipoldt, J. G., Basson, S. S., Schlebusch, J. J. J. and Grobler, E. C., *Inorg. Chim. Acta.*, **62**, 113, (1982).

[77] Purcell, W., Basson, S. S., Schelbusch, J. J. J. and Preston, H., *Inorg. Chim. Acta*, **234**, 153, (1995).

[78] Robb, W. and Nicholson, C. G., *S. Afr. J. Chem.*, **31**, 1, (1978).

[79] Leipoldt, J. G. and Grobler, E. C., *Trans. Met. Chem.*, **11**, 110, (1986).

[80] Basolo, F., Chatt, J., Gray, H. B, Pearson, R. G. and Shaw, B. L., *J. Chem. Soc.*, 2207, (1961).

[81] Pearson, R. G., Gray, H. B. and Basolo, F., *J. Am. Chem. Soc.*, **82**, 787, (1960).

[82] Cotton, F. A., Wilkinson, G. and Gaus, P. L., *Basic Inorganic Chemistry, (3rd edition)*, John Wiley and Sons, Inc., p 21, (1995).

[83] Stranks, D. R., *Pure Appl. Chem.*, **38**, 303, (1974).

[84] Whalley, E., *J. Chem. Phys.*, **38**, 303, (1974).

[85] Swarts, J. C., Aquino, M. A. S., Han, J-Y., Lam, K-U. and Sykes, A. G., *Biochim. Biophys. Acta*, **1247**, 215, (1995).

[86] Bobbitt, J. M. and Wills, J. P., *J. Org. Chem.*, **45**, 1978, (1980).

[87] Nelsen, S. F., Kessel, C. R., Brein, D. J. and Weinhold, F., *J. Org. Chem.*, **45**, 2116, (1980).

[88] Mabbot, G. A., *J. Chem. Ed.*, **60**, 697, (1983).

[89] Kissinger, P. T. and Heineman, W. R., *Laboratory Techniques in Electroanalytical Chemistry*, Marcel Dekker, Inc., New York, p. 86, 297, (1984).

[90] Kissinger, P. T. and Heineman, W. R., *J. Chem. Ed.*, **60**, 702, (1983).

[91] Bard, A. J. and Faulkner, L. R., *Electrochemical Methods: Fundamentals and Applications*, Wiley, New York, chapter 6, 1980.

[92] Christensen, P. A. and Hammet, A., *Techniques and Mechanism in Electrochemistry*, Blackie Academic and Professional, London, p. 55, 170, (1994).

[93] Mann, K., *Nonaqueous Solvents for Electrochemical Use*, in: *Electroanalytical Chemistry*, Bard, A. J.(Ed.), Series of Advances, **3**, M. Dekker, New York, p. 37, (1969).

[94] Stone, N. J. and Sweigart, A. M., *Organometallics*, **5**, 2553, (1986).

[95] Hill, M. G., Lamanna, W. M. and Mann, K. R., *Inorg. Chem.*, **30**, 4687, (1991).

[96] Ohrenberg, C. and Geiger, W. E., *Inorg. Chem.*, **39**, 2948, (2000).

[97] LeSuer, R. J. and Geiger, W. E., *Angew. Chem. Int. Ed.*, **39**, 248, (2000).

[98] (a) Rulkens, R., Lough, A. J., Manners, I., Lovelace, S. R., Grant, C. and Geiger, W. E., *J. Am. Chem. Soc.*, **118**, 12683, (1996); (b) Grossmann, B., Heinze, J., Herdtweck, E., Koehler, F. H., Noeth, H., Schwenk, H., Spiegler, M., Watcher, W. and Weber, B., *Angew. Chem. In. Ed.*, **36**, 387, (1997).

[99] Du Plessis, W. C., Erasmus, J. C., Lamprecht, G. J., Conradie, J., Cameron, T. S., Aquino, M. A. S. and Swarts, J. C., *Can. J. Chem.*, **77**, 378, (1999).

[100] Swarts, J. C., Neuse, E. W. and Lamprecht, G. J., *J. Inorg. Organomet. Polym.*, **4**, 143, (1994).

[101] Foster, D., *Adv. Organomet. Chem.*, **17**, 255, (1979).

[102] Steyn, J. J. G., Roodt, A. and Leipoldt, J. G., *Inorg. Chem.*, **31**, 3477, (1992).

[103] Conradie, J., Cameron, T. S., Aquino, M. A. S., Lamprecht, G. J. and Swarts, J. C., *Inorg. Chim. Acta.*, **358**, 2530, (2005).

[104] Paleos, C. M., Margomenou-Leonidopoulou, G, Anastassoupoulou, J. D. and Papaconstantinou, E., *Mol. Cryst., Inc. Nonlin. Opt.*, **161**, 373, (1988).

[105] Serrano, J. L., *Metallomesogens: Synthesis, Properties and Applications*, Weinheim, New York, Basel, Cambridge, Tokyo, VCH, p. 5, (1996).

[106] Holm, R. H. and O'Connor, M. J., *Prog. Inorg. Chem.,* **14**, 241, (1971).

[107] Galyametdinv, Y. G., Ovchinnikov, I. V., Bolotin, B. M., Etingen, N. B., Ivanova, G. I. and Yagfarova, L. M., *Izv. Akad. SSSR, Ser. Khim.,* **10**, 2379, (1984).

[108] Roviello, A., Sirigu, A., Iannelli, P. and Immirzi, A., *Liq. Cryst.,* **3**, 115, (1988).

[109] Demus, D. and Richter, L., *Texture of Liquid Crystals,* VCH, Weinheim, New York, (1984).

[110] Gray, G. W. and Goodby, J. W. G., *Smectic Liquid Crystals,* Leonard Hill, Glasgow, London, (1984); Pershan, P. S., *Structure of Liquid Crystal Phases,* World Scientific, Singapore, (1988).

[111] Serrano, J. L., *Metallomesogens: Synthesis, Properties and Applications,* Weinheim, New York, Basel, Cambridge, Tokyo, VCH, p. 31, (1996).

[112] Serrano, J. L., *Metallomesogens: Synthesis, Properties and Applications,* Weinheim, New York, Basel, Cambridge, Tokyo, VCH, p. 14, (1996).

[113] (a) Ohta, K., Muroki, H., Takagi, A., Hatada, K. I., Ema, H., Yamamoto, I. and Matsuzaki, K., *Mol. Cryst. Liq. Cryst.,* **140**, 131, (1986); (b) Sakashita, H., Nishitani, A., Sumiya, Y., Terauchi, H., Ohta, K. and Yamamoto, I., *Mol. Cryst. Liq. Cryst.,* **163,** 211, (1988).

[114] Galli, D., Chiellini, E., Angeloni, A. S. and Laus, M., *Macromolecules,* **22**, 1120, (1989).

[115] Roviello, A. and Sirigu, A., *Makromol. Chem.,* **183**, 895, (1982).

[116] Griffin, A. C. and Havens, S. J., *Mol. Cryst. Liq. Cryst. Lett.,* **49**, 239, (1979).

[117] Watanabe, J. and Hayashi, M., *Macromolecules,* **21**, 278, (1988).

[118] Kricheldorf, H. R. and Pakull, R., *Macromolecules,* **21**, 551, (1988).

[119] Koide, N., Ohta, R. and Iimura, K., *Polym. J.,* **16,** 505, (1984).

[120] Asrar, A., Toriumi, H., Watanabe, J., Krigbaum, W. R. and Ciferri, A., *J. Polym. Sci. Polym. Phys. Ed.,* **21**, 1119, (1983).

[121] Serrano, J. L. and Sierra, T., in *Metallomesogens: Synthesis, Properties and Applications,* ed. Serrano, J. L., Weinheim, New York, Basel, Cambridge, Tokyo, VCH, ch. 3, p. 117, (1996).

[122] Deschenaux, R. and Santiago, J., *J. Mater. Chem.,* **3**(2), 219, (1993).

[123] Serrano, J. L. and Sierra, T., in *Metallomesogens: Synthesis, Properties and Applications,* ed. Serrano, J. L., Weinheim, New York, Basel, Cambridge, Tokyo, VCH, ch. 3, p. 120, (1996).

[124] (a) Hudson, S. A. and Maitlis, P. M., *Chem. Rev.,* **93,** 861, (1993); (b) Bruce, D. W., *Inorganic Material,* eds. Bruce, D. W. and O'Hare, D., Wiley Chichester, ch. 8, (1992); (c) Espinet, P, Esteruelas, M. A., Oro, L. A., Sorrane, J. L. and Sola, E., *Coord. Chem. Rev.,* **117**, 215, (1992); (d) Giroud-Godquin, A. M. and Maitli, P. M., *Angew. Chem. Int. Ed. Engl.,* **30**, 375, (1975).

[125] Deschenaux, R. and Goodby, J. W., in *Ferrocenes: Homogenoues Catalysis. Organic Synthesis. Material Science,* eds. Togni, A and Hayashi, T., VCH, Weinheim, ch. 9, p. 471, (1995).

[126] Deschenaux, R. and Santiago, J., *Tetrahedron lett.,* **35**, 2169, (1994); Imrie, C. and Loubser, C., *J. Chem. Soc., Chem. Commun.,* 2159, (1994).

[127] (a) Deschenaux, R., Kosztics, I., Scholten, U., Gullion, D.and Ibn-Elhaj, M., *J. Mater. Chem.*, **4**, 1351, (1994); (b) Deschenaux, R, Izvolensky, V., Turpin, R., Gullion, D. and Heinrich, B., *J. Chem. Soc., Chem. Commun.,* 439, (1996).

[128] (a) Bruce, D. W., Denby, I. R., Tiddy, G. J. T. and Watkins, J. M., *J. Met. Chem.*, **3**, 911, (1993); (b) Bruce, D. W.,Holbrey, J. D., Tajbakhsh, A. R. and Tiddy, G. J. T., *J. Met. Chem.*, **3**, 905, (1993); (c) Holbrey, J. D., Tiddy, G. J. T. and Bruce, D. W., *J. Chem. Soc., Dalton Trans.,* 1769, (1995).

[129] Deschenaux, R., Jauslin, I., Scholten, U., Turpin, F., Guillon, D. and Heinrich, B., *Macromolecules,* **31**, 5647, (1998).

[130] (a) Deschenaux, R., Serrano, E. and Levelut, A. M., *J. Chem. Soc.,Chem. Commun.,* 1577, (1997); (b) Dardrl, B., Deschenaux, R., Even, M. and Serrano, E., *Macromolecules,* **32**, 5193, (1999).

[131] Deschenaux, R., Megert, S., Zumbrunn, C., Ketterer, J. and Steiger, R., *Langmuir,* **13**, 2363, (1999).

[132] Donnio, B., Seddon, J. M. and Deschenaux, R., *Organometallics,* **19**, 3077, (2000).

[133] Tschierske, C., *J. Mater. Chem.,* **8**, 1485, (1998).

[134] Jeffrey, G. A. and Wingert, L. M., *Liq. Cryst.,* **12**, 179, (1992); Prade, H., Meithchen, R. and Vill, V., *J. Prakt. Chem.,* **337**, 427, (1995).

[135] Borisch, K., Diele, S., Goring, P., Muller, H. and Tschierske, C., *Liq. Cryst.,* **22**, 427, (1997).

[136] Goodby, J. W., Haley, A. J., Meckenzie, G., Watson, M. J., Plusquellec, D. and Ferrieres, V., *J. Mater. Chem.,* **5**, 2209, (1995).

[137] Goodby, J. W., Meckenzie, G., Watson, M. J, Kelly, S. M., Bachir, S., Bault, P., Gode, P., Goethals, G., Martin, P., Ronco, G. and Villa, P., *Liq. Cryst.,* **25**, 139, (1998).

[138] Dechenaux, R., Schweissguth, M. and Levelut, A., *J. Chem. Soc., Chem. Commun.,*1275, (1996).

[139] Togni, A., in *Ferrocenes,* eds. Togni, A. and Hayashi, T., VCH, Weinheim, ch. 9, (1995).

[140] Chaurd, T., Cowling, S. J., Fernandez-Cuirleo, M., Jauslin, I., Goodby, J. W. and Deschenaux, R., *J. Chem. Soc., Chem. Commun.,* 2109, (2000).

[141] Seshadri, T. and Haupt, H. J., *J. Chem. Soc., Chem Commun.,* 735, (1998).

[142] Elliel, E. L. and Wilen, S. H., in *Stereochemistry of Organic Compounds*, Wiley, New York, (1994).

[143] (a) Malthête, J. and Ziminsky, L., *J. Chem. Soc., Chem Commun.*, 1495, (1990); (b) Malthête, J. and Jacq, P., *Liq. Cryst.*, **21**, 291, (1996).

[144] Barberá, J., in *Metallomesogens: Synthesis, Properties and Applications*, ed. Serrano, J. L., Weinheim, New York, Basel, Cambridge, Tokyo, VCH, ch. 4, p. 132, (1996).

[145] Espinet, P., Esteruelas, M. A., Oro, L. A., Serrano, J. L. and Sola, E., *Coord. Chem. Rev.*, **117**, 215, (1992).

[146] Serrano, J. T and Sierra, T., in *Metallomesogens: Synthesis, Properties and Applications*, ed. Serrano, J. L., Weinheim, New York, Basel, Cambridge, Tokyo, VCH, ch. 3, (1996).

[147] (a) Berdagué, P., Courtieu, J. and Maitlis, P. M., *J. Chem. Soc., Chem. Commun.*, 1313, (1994); (b) Bruce, D. W., Hudson, S. A. and Marsden, J. R., *Liq. Cryst.*, **250**, 373, (1994).

[148] Cativiela, C., Serrano, J. L. and Zurbano, M. M., *J. Org. Chem.*, **60**, 3074, (1995).

[149] Barberá, J., Elduque, A., Giménez, R. Lahoz, F. J., López, J. A., Oro, L. A., Serrano, J. L., Villacampa, B. and Villalba, J., *Inorg. Chem.*, **38**, 3085, (1999).

[150] Swarts, J. C., and van Rensburg, C. E. J., A Substrate or Composition for the Treatment of Cancer, Patent PCT/IB01/02258 in PCT Countries, European Patent 1345951, p. 1, (2004).

[151] Rozencweig, M, Von Hoff, D. D., Slavik, M. and Muggia, M. F., *Ann. Int. Med.*, **86**, 803, (1977).

[152] Ozols, R. F., *Semin. Oncol.*, **16**, 22, (1989).

[153] Wallace, H. J. and Higby in *Platinum coordination complexes in cancer therapy*; eds. Conners, T. A. and Roberts, J. J., Springer-Verlag, Heidelberg, p. 128 , 167, (1974).

[154] Swarts, J. C., Neuse, E. W., Perlwitz, A. G., Stephanou, A. S. and Lamprecht, G. J., *Angew. Makromol. Chem.*, **207**, 123, (1993).

[155] Gale, G. R., Atkins, L. M. and Meischen, S. J., *Cancer Treat. Rep.*, **61**, 336, (1984).

[156] Köpf-Maier, P, Köpf, H. and Neuse, E. W., *J. Cancer Res. Clin. Oncol.*, **108**, 336, (1984).

[157] Neuse, E. W. and Kanzawa, F., *Appl. Organomet. Chem.*, **4**, 19, (1990).

[158] Osella, D., Ferrali, M., Zanello, P., Laschi, F., Fontani, M., Nervi, C. and Cavigiolio, G., *Inorg. Chim. Acta*, **306**, 42, (2000).

[159] Swarts, J. C., Swarts, D. M., Neuse, E. W., La Madeleine, C. and Van Lier, J. E., *Anticancer Res.*, **21**, 2033, (2001).

[160] Weber, B, Serafin, A, Michie, J., Van Rensburg, C. E. J., Swarts, J. C. and Bohm, L., *Anticancer Res.*, **24**, 763, (2004).

Chapter 3

Results and discussions

3.1. Introduction

In this chapter, the results presented from this study include synthesis and characterization of a series of ferrocene-containing β-diketones substituted with long chain alkyl substituents, R, of the type (Cp-R)Fe(Cp-CO-CH_2-CO-CH_3), with Cp = cyclopentadienyl and R = C_9H_{19}, $C_{10}H_{21}$, $C_{12}H_{25}$, $C_{14}H_{29}$ and $C_{18}H_{37}$ *via* suitable ferrocene precursors. The new ligands abbreviated as (Cp)Fe(R-Cp-CO-CH_2-CO-CH_3), (Cp-R)Fe(R-Cp-CO-CH_2-CO-CH_3) and (Cp-R)Fe(Cp-CO-CH_2-CO-Cp)Fe(Cp-R) with R = $C_{10}H_{21}$ and $C_{12}H_{25}$ were also prepared and characterized. Characterization and determination of the properties of these β-diketones included use of techniques such as ^{1}H NMR, pK_a determination, elemental analysis (C,N,H), cyclic, linear and square wave voltammetry. Complexation reactions of these β-diketones with [$Rh_2(Cl)_2(cod)_2$] to give a square planar rhodium(I) complexes of the type [Rh(β-diketonato)(cod)] have also been investigated. Substitution kinetics of the β-diketonato ligand in [Rh(β-diketonato)(cod)] with 1,10-phenanthroline as well as cyclic, linear and square wave voltammetry of the rhodium complexes are described. Thermodynamic phase studies were also conducted to determine the influence of the length of the R = C_nH_{2n+1} alkyl substituents, as well as the position of substitution on the phase transition properties of these complexes, utilizing differential scanning calometry techniques. In addition, some cytotoxic properties of selected compounds on cancer cells are presented in the final section of this chapter.

3.2. Synthetic aspects and identification of compounds

3.2.1. Acyl and alkyl ferrocene derivatives

In pursuing goal 1 (Chapter 1) of this study, the synthesis of acyl ferrocene derivatives in **Scheme 3.1**, is first described. The substitution pattern aimed for included the 1,1′, (series **42**) and 1,3,1′-substituent positions (series **43**) by an acyl and/or long chain alkyl substituents (series **44** and **45**). Methyl ferrocenoate, **41**, prepared *via* the lithium intermediate as described elsewhere,[1] was acylated with the acyl chlorides, RCOCl where R = C_8H_{17}, C_9H_{19}, $C_{11}H_{23}$, $C_{13}H_{27}$ and $C_{17}H_{35}$ under Friedel-Crafts reaction conditions to give 1,1′-acylferrocene esters, 1-carbomethoxy-1′-(nonanoyl)ferrocene, **42a**, in 48 % yield, 1-carbomethoxy-1′-(decanoyl)ferrocene, **42b**, in 86 % yield, 1-carbomethoxy-1′-(dodecanoyl)ferrocene, **42c**, in 76 % yield, 1-carbomethoxy-1′-

(tetradecanoyl)ferrocene, **42d** , in 51 % yield and 1-carbomethoxy-1′-(octadecanoyl)ferrocene, **42e**, in 48 % yield. All these compounds were characterized by both infrared and ^{1}H NMR spectroscopy. The telling characteristic ^{1}H NMR signals for compound series **42** is the triplet at ~δ 2.70 ppm which is assigned to the –CO$\underline{CH_2}$- group, and the singlet signal of the O-methyl group in COOMe at δ 3.85 ppm. The 1,3,1′-substituted compounds, 1-carbomethoxy-3,1′-di(decanoyl)ferrocene, **43a**, was obtained in 54% yield, while 1-carbomethoxy-1,1′-di(dodecanoyl)ferrocene, **43b**, was obtained in 70% yield. The essential factor in these reactions is the correct ratio or equivalents of $AlCl_3$ in relation to the methylferrocenoate, as well as the purity and freshness of $AlCl_3$. To synthesize the mono-acylated ferrocene series **42**, a molar ratio of 1:1 of $AlCl_3$ and acyl chlorides with methylferrocenoate is required. Di-acylated compound series **43** were obtained by reacting methylferrocenoate with $AlCl_3$ and acyl chlorides in a molar ratio of 2:2. $AlCl_3$ is a hygroscopic reagent; it must be tightly sealed and kept in a dessicator to avoid decomposition. Friedel-Crafts reactions with decomposed $AlCl_3$ are unsuccessful.

Clemmensen reduction of the acylferrocenyl methanoate gave the corresponding alkyl derivatives, as illustrated in **Scheme 3.1**. 1-Carbomethoxy-1′-(nonyl)ferrocene, **44a**, was obtained in 88% yield, 1-carbomethoxy-1′-(decyl)ferrocene, **44b**, in 55% yield, 1-carbomethoxy-1′-(dodecyl)ferrocene, **44c**, in 54% yield, 1-carbomethoxy-1′-(tetradecyl)ferrocene, **44d**, in 60% yield and 1-carbomethoxy-1′-(octadecyl)ferrocene, **44e**, in 56% yield. However, Clemmensen reduction was unsuccessful in obtaining the 1,3,1′-substituted dialkyl monocarbomethoxy ferrocene derivatives. In our hands one acyl group was cleaved during the reduction reaction. Reaction conditions giving dialkyl monocarbomethothxy ferrocene derivatives was not searched any further because an alternative approach to dialkylated monomethyl ferrocene derivatives were found to be useful (see section **3.2** for compound series **52**). The appendix at the end of this thesis shows the ^{1}H NMR spectra of all compounds. The absence of a –CO$\underline{CH_2}$- ^{1}H NMR signal at ~2.70 ppm indicated that there was no observable acyl group in the side chain's backbone. All the esters were solids for compounds **44c, 44d** and **44e**, and oily liquids for compounds **44a** and **44b**.

The carboxylic acid derivatives, 1-carboxy-1′-(nonyl)ferrocene, **45a**, (66 % yield), 1-carboxy-1′-(decyl)ferrocene, **45b**, (52 %), 1-carboxy-1′-(dodecyl)ferrocene, **45c**, (69 %), 1-carboxy-1′-(tetradecyl)ferrocene, **45d**, (62 %) and 1-carboxy-1′-(octadecyl)ferrocene, **45e**, (86 %), were obtained by the hydrolysis of the methyl ester precursors, **44a - 44e**, under alkaline alcoholic conditions.[2] The ester series **44** were then set aside for future β-diketone synthesis in this study.

The acid series **45** was shared with a Canadian collaborator (Professor M. A. S. Aquino from Saint Francis Xavier University) for ruthenium coordination chemistry research.

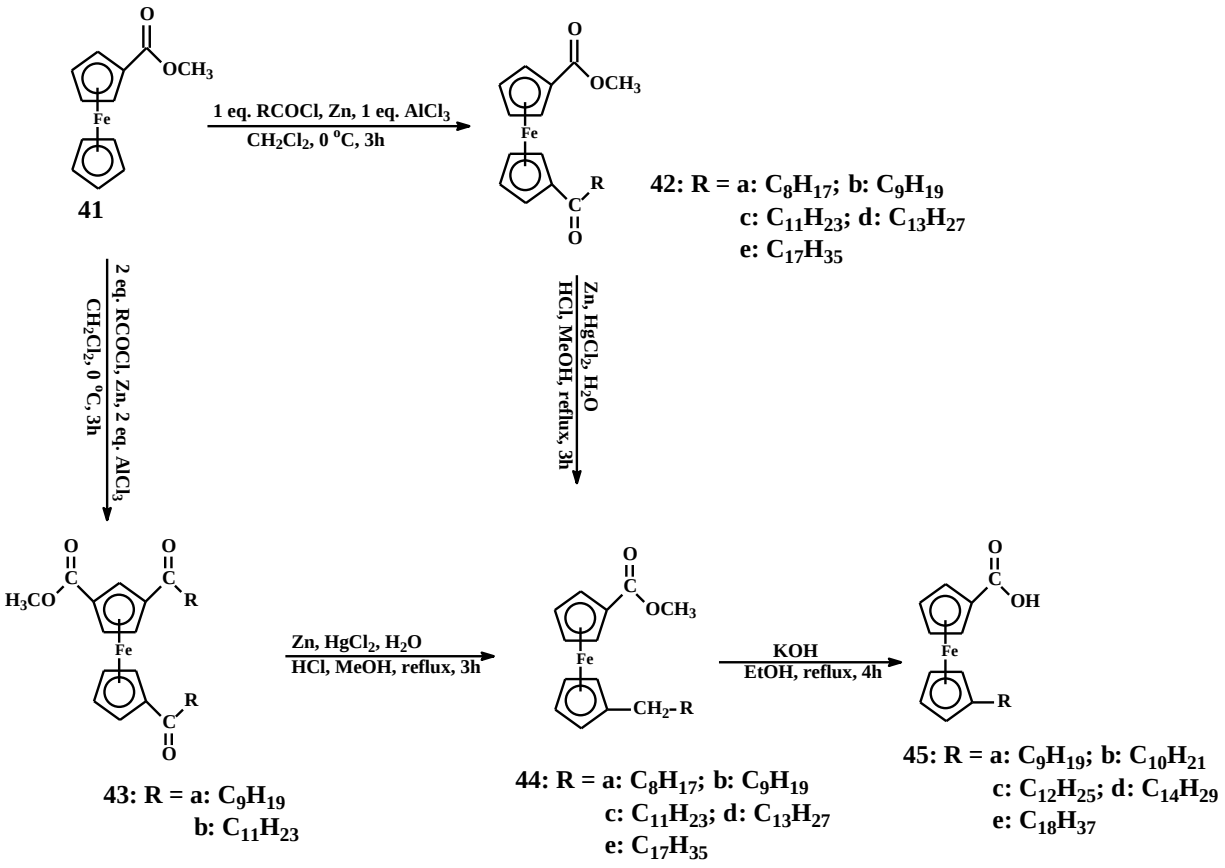

Scheme 3. 1: Friedel-Crafts acylation of ferrocenylmethanoate with acylchlorides, RCOCl and subsequent Clemmensen reduction to give corresponding alkylferrocene derivatives, 44a – 44e. Carboxylic acid derivatives, 45a -45e, were obtained by hydrolysis of 44a – 44e, under alkaline alcoholic conditions.

A series of mono- and diacyl derivatives of alkylated ferrocenes were then prepared according to **Scheme 3.2**. In the first step, ferrocene, **1**, was treated with a suspension of the appropriate acyl chloride RCOCl (R = C_8H_{17}, C_9H_{19}, $C_{11}H_{23}$, $C_{13}H_{27}$ and $C_{17}H_{35}$), and aluminium chloride in dichloromethane at 0 ^oC and then at room temperature to produce the mono-acylferrocenes, 1-nonanoylferrocene, **46a**, in 91 % yield as a dark brown oil, 1- decanoylferrocene, **46b**, in 95 % yield as brown solid, 1-dodecanoylferrocene, **46c**, in 92 % yield as a yellow solid, 1-tetradecanoylferrocene, **46d**, in 79 % yield, as a brown solid and 1-octadecanoylferrocene, **46e**, in 59 % yield as a yellow solid after column chromatography.[3] The diacyl ferrocenes, 1,1$^/$-di(decanoyl)ferrocene, **50a**, (50 % yield, a brown solid) and 1,1$^/$-di(dodecanoyl)ferrocene, **50b**, (41 % yield, a red solid) were obtained by treating ferrocene with 2 equivalents of RCOCl and 2 equivalents of $AlCl_3$, while the mono-acetylated series **46** were obtained by using a 1:1

stoichiometric quantity of acyl chloride and $AlCl_3$ over ferrocene. These compounds were all characterized by ^1H NMR spectroscopy (spectra are shown in the appendix).

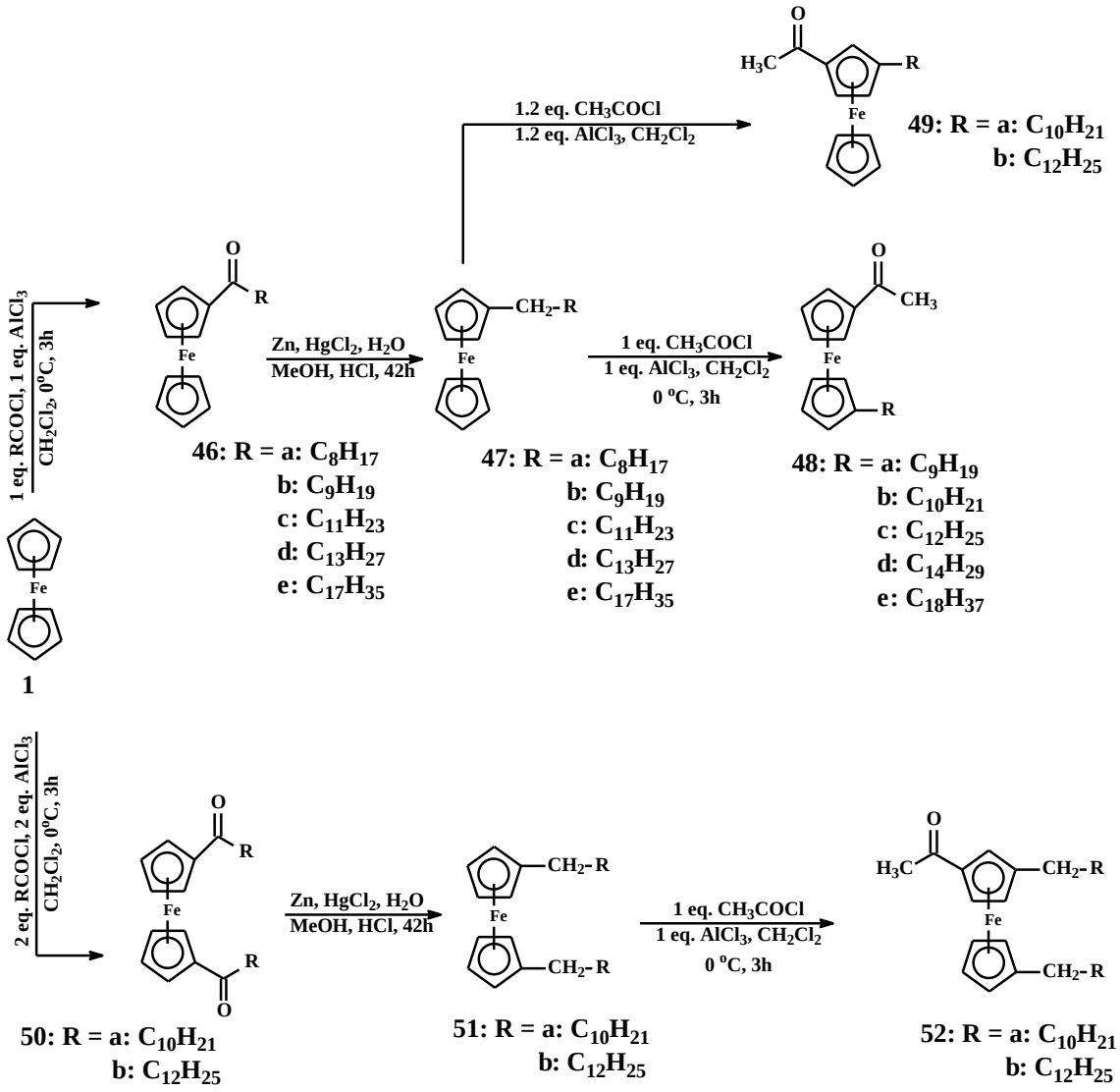

Scheme 3. 2: General synthetic route towards mixed alkyl/acyl ferrocene derivatives.

The acylferrocenes were then reduced by Clemmensen reduction (**Scheme 3.2**) to the corresponding alkylferrocenes, 1-nonylferrocene, **47a**, in 88 % yield, as a brown solid, 1-decylferrocene, **47b**, in 86 % yield, as brown solid, 1-dodecylferrocene, **47c**, in 80% yield, as a yellow solid, 1-tetradecanoylferrocene, **47d**, in 76 % yield, as a brown solid and 1-octadecanoylferrocene, **47e**, in 94 % yield, as a yellow solid. The isolation and purification of 1,1$^{/}$-di(decyl)ferrocene, **51a**, (92 % yield, a brown oil), 1,1$^{/}$-di(dodecyl)ferrocene, **51b**, (86 % yield, a brown oil) was also achieved after Clemmensen reduction of **50a** and **50b** and column chromatography.

The acetyl-alkylferrocene derivatives, **48, 49** and **52**, were synthesized utilizing Friedel-Crafts acylation techniques as described in the preceding paragraph. The reactions are shown in **Scheme 3.2**. Acetylation of the mono alkylated ferrocene series **47** to the 1-alkyl-1$^{/}$-acetyl derivatives, **48a – 48e**, was achieved in ~60 % yields. Acetylation of the dialkylated series **51** to the 1,1$^{/}$-dialkylated-3-acetyl derivatives **52a** and **52b** was achieved in 33 and 37 % yield respectively. This method of synthesizing acyl-dialkylated ferrocenes is in contrast with the one used in **Scheme 3.1**. It is concluded that in order to obtain dialkyl-carbomethoxy compounds, alkylation of the species has to be performed first and then followed by acylation as indicated in **Scheme 3.2**. The 1-alkyl-3-acetyl derivatives, **49a** and **49b**, were obtained in 59 and 55 % yields respectively, by reacting the alkylferrocenes, **47b** and **47c**, in a molar ratio of both the acid chloride and aluminum chloride to alkylferrocene greater than 1.2:1. The crude product consisted of a mixture of compounds and required column chromatographic purification techniques to purify compounds **49a** and **49b**.

3.2.2. Ferrocene-containing β-diketones

The ferrocene-containing β-diketones, 1-[1-(nonyl)ferrocenyl-1$^{/}$-]-butane-1,3-dione, **53a**, 1-[1-(decyl)ferrocenyl-1$^{/}$-]-butane-1,3-dione, **53b**, 1-[1-(dodecyl)ferrocenyl-1$^{/}$-]-butane-1,3-dione, **53c**, 1-[1-(tetradecyl)ferrocenyl-1$^{/}$-]-butane-1,3-dione, **53d**, 1-[1-(octadecyl)ferrocenyl-1$^{/}$-]-butane-1,3-dione, **53e**, 1-[3-(decyl)ferrocenyl-1-]-butane-1,3-dione, **54a**, 1-[3-(dodecyl)ferrocenyl-1-]-butane-1,3-dione, **54b**, 1-[-1,1$^{/}$-di(decyl)ferrocenyl-3-]-butane-1,3-dione, **55a**, 1-[-1,1$^{/}$-di(dodecyl)ferrocenyl-3-]-butane-1,3-dione, **55b**, as 1,3-di-[-(1-decyl)ferrocenyl-1$^{/}$-]-propane-1,3-dione, **56a** and 1,3-di-[-(1-dodecyl)ferrocenyl-1$^{/}$-]-propane-1,3-dione, **56b**, were prepared according to **Scheme 3.3**, by Claisen condensation of the acetyl- alkylferrocene derivatives, **48, 49, 50** and **51**, with the appropriate ester, R-FcCOOMe (**44**, Fc = ferrocenyl) or CH_3COOEt, under the influence of the strong base lithium diisopropylamide (LDA). For the synthesis of compound series **53, 54, 55** and **56**, freshly distilled and dried ethylacetate (CH_3COOEt) had to be used because wet ethylacetate destroys LDA.

Yields varied between 27 and 41 %. Compounds **53a, 55a, 56a** and **56b** were obtained as red-oils. The other ligands were red solids. All ferrocene-containing β-diketones were purified by chromatographic separation on silica gel using ether/hexane mixture as eluent in a ratio of 1:3.

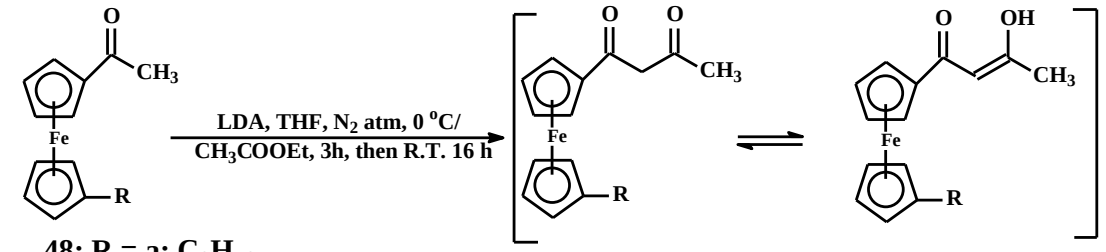

48: R = a: C_9H_{19}
b: $C_{10}H_{21}$
c: $C_{12}H_{25}$
d: $C_{14}H_{29}$
e: $C_{18}H_{37}$

53: R = a: C_9H_{19}
b: $C_{10}H_{21}$
c: $C_{12}H_{25}$
d: $C_{14}H_{29}$
e: $C_{18}H_{37}$

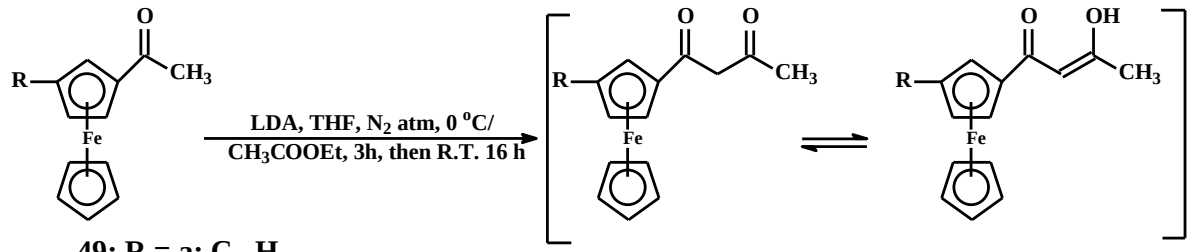

49: R = a: $C_{10}H_{21}$
b: $C_{12}H_{25}$

54: R = a: $C_{10}H_{21}$
b: $C_{12}H_{25}$

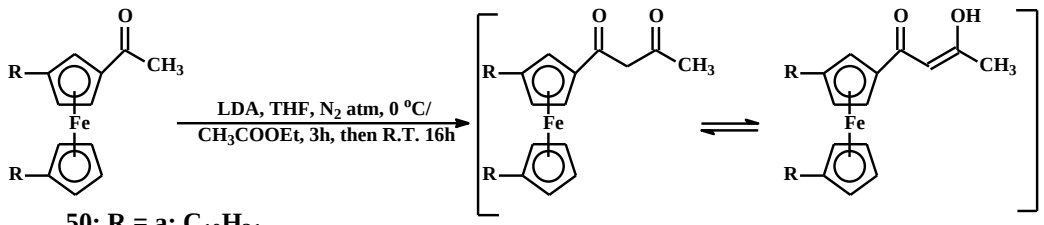

50: R = a: $C_{10}H_{21}$
b: $C_{12}H_{25}$

55: R = a: $C_{10}H_{21}$
b: $C_{12}H_{25}$

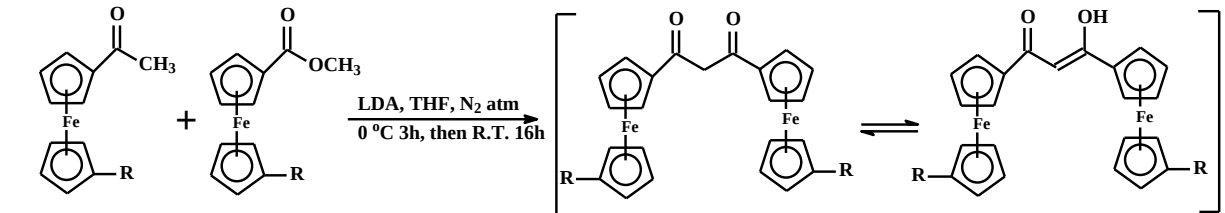

51: R = a: $C_{10}H_{21}$
b: $C_{12}H_{25}$

44: R = a: $C_{10}H_{21}$
b: $C_{12}H_{25}$

56: R = a: $C_{10}H_{21}$
b: $C_{12}H_{25}$

Scheme 3. 3: Reaction scheme for the preparation of new ferrocenyl-containing β-diketones, 53, 54, 55 and 56, by Claisen condensation of acetylferrocenes, 48, 49, 50 and 51 with the appropriate ester in the presence of lithium diisopropylamide (LDA). R. T. = room temperature.

3.2.3. Complexation of ferrocene-containing β-diketones with rhodium(I)

The rhodium dimer, $[Rh_2Cl_2(cod)_2]$, **57**, was synthesized by refluxing $RhCl_3.H_2O$ and cyclooctadiene (cod), in the presence of ethanol for 2.5 hours at 78 ^oC, in yields up to 65% as a yellow powder.[4] Complexation of the β-diketones, **53 - 56**, with $[Rh_2Cl_2(cod)_2]$, in stirred dimethylformamide (DMF) at room temperature for 16 hours according to **Scheme 3.4**, lead to the rhodium β-diketonato complexes of the type $[Rh^I(\beta\text{-diketonato})(cod)]$ with yields of 45% for [(η^4-1,5-cyclooctadiene){(1-((-1-nonyl)ferrocenyl-1′-)-butane-1,3-dionato-κ^2O,O')}rhodium(I)], **58a**, 75% for [(η^4-1,5-cyclooctadiene){(1-((-1-decyl)ferrocenyl-1′-)-butane-1,3-dionato-κ^2O,O')}rhodium(I)] **58b**, 77% for [(η^4-1,5-cyclooctadiene){(1-((-1-dodecyl)ferrocenyl-1′-)-butane-1,3-dionato-κ^2O,O')}rhodium(I)], **58c**, 86% for [(η^4-1,5-cyclooctadiene){(1-((-1-tetradecyl)ferrocenyl-1′-)-butane-1,3-dionato-κ^2O,O')}rhodium(I)] **58d**, 78% for [(η^4-1,5-cyclooctadiene){(1-((-1-octadecyl)ferrocenyl-1′-)-butane-1,3-dionato-κ^2O,O')}rhodium(I)], **58e**. Compounds **59a** and **59b** were obtained in 77% and 52% yields respectively. The compound series **60** and **61** were obtained in yields as high as 71 %.

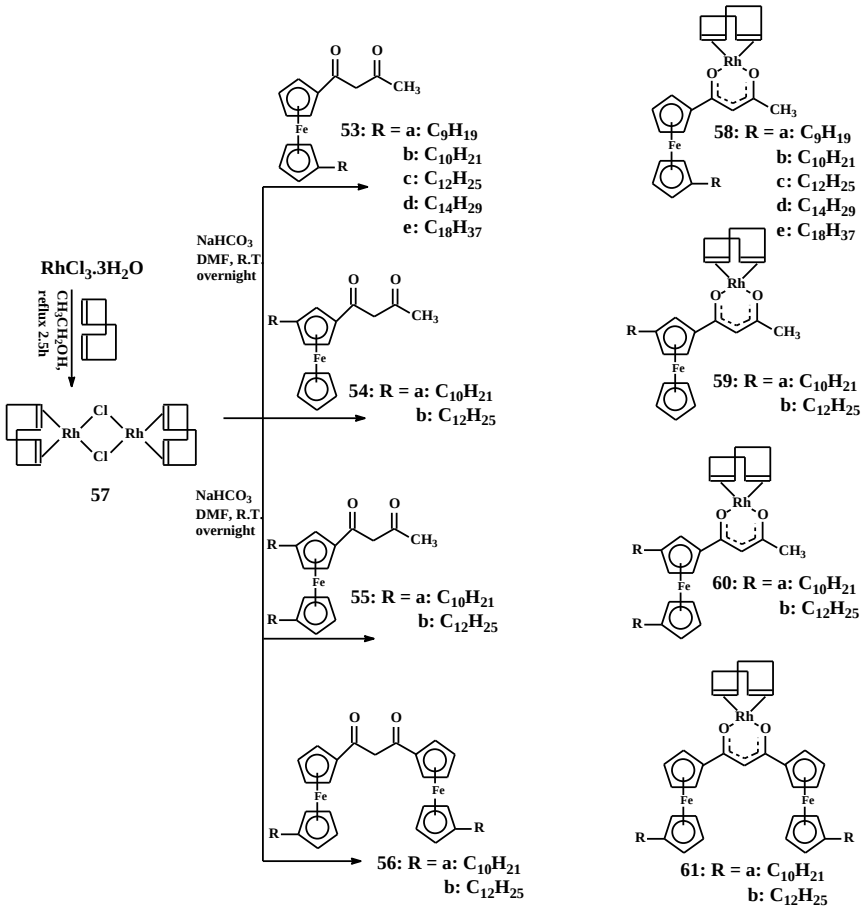

Scheme 3. 4: Synthesis of $[Rh_2Cl_2(cod)_2]$ and complexation of ferrocene-containing β-diketones with $[Rh_2Cl_2(cod)_2]$, 57, to give rhodium(I) complexes, 58, 59, 60 and 61. R. T. = room temperature.

The base, $NaHCO_3$, added in stoichiometric amounts to the ferrocene-containing ligand, was used to abstract the methine proton from the enol form of the β-diketone to form a β-diketonato anion, which is a more effective complexing agent than the free β-diketone ligand. The reaction mixture was stirred for 16 hours, due to the slow formation kinetics for all the ferrocene-containing β-diketones, to allow complex formation to proceed to a maximum. Complexation reactions where no long-chain substituents were present (*i.e.* R = H) were completed in 5 min.[5]

3.3. $pK_a^{/}$ determination

Characterization of the new β-diketones from this study in terms of $pK_a^{/}$ values according to goal 3 (Chapter 1) were performed next. Having synthesized the new β-diketone series **53 – 56**, their $pK_a^{/}$ values were determined. The reaction during $pK_a^{/}$ determination refers to the process as illustrated in **Scheme 3.5**:

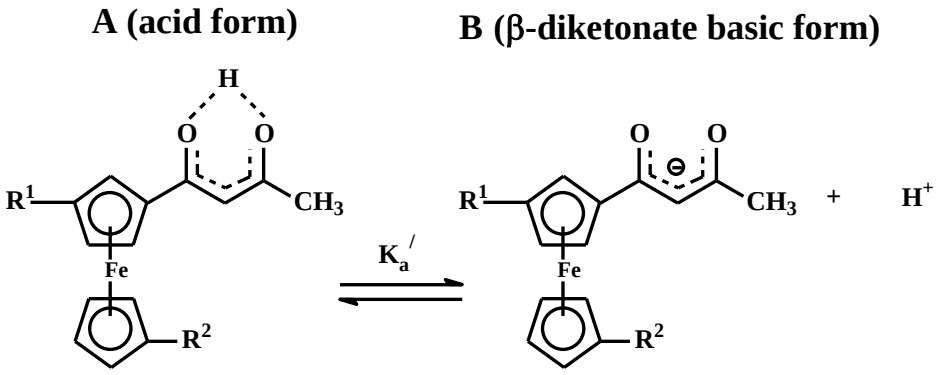

53: R^1 = H; R^2 = C_9H_{19}, $C_{10}H_{21}$, $C_{12}H_{25}$, $C_{14}H_{29}$ or $C_{18}H_{37}$
54: R^1 = H; R^2 = $C_{10}H_{19}$, $C_{12}H_{25}$
55: R^1 = H; R^2 = $C_{10}H_{19}$, $C_{12}H_{25}$
56: The β-diketonato CH_3 group is replaced by a substituted ferrocenyl group to give the symmetrical β-diketone with R^1 = H and R^2 = $C_{10}H_{19}$ or $C_{12}H_{25}$

Scheme 3. 5: Schematic representation that takes place in the determination of the $pK_a^{/}$ showing the acid (A) and (B) the basic form of the β-diketones, 53 - 56.

In this study we refer to the apparent pK_a, or $pK_a^{/}$, rather than thermodynamic pK_a values, since no attempt was made to distinguish between the experimentally observed pK_a and the pK_a values for the keto and enol tautomers. Since the β-diketones of this study were not soluble in water, the $pK_a^{/}$ values were determined in 10 % acetonitrile/water (v/v), with the ionic strength, μ = 0.1 mol dm^{-3}

($NaClO_4$) at 21 ^oC. Since $pK_a^/$ is effected by ionic strength, it was decided to report $pK_a^/$ values at μ = 0.1 mol dm^{-3}. The $pK_a^/$ values were obtained by monitoring absorption of β-diketone solutions as a function of pH. The wavelengths used for the spectroscopic $pK_a^/$ determination of the β-diketones were decided upon from the UV/Visible spectra of the free β-diketone (acidic) and deprotonated (β-diketonato anions, the conjugated base) forms of each ligand, four examples of which are shown in **Figure 3.1**.

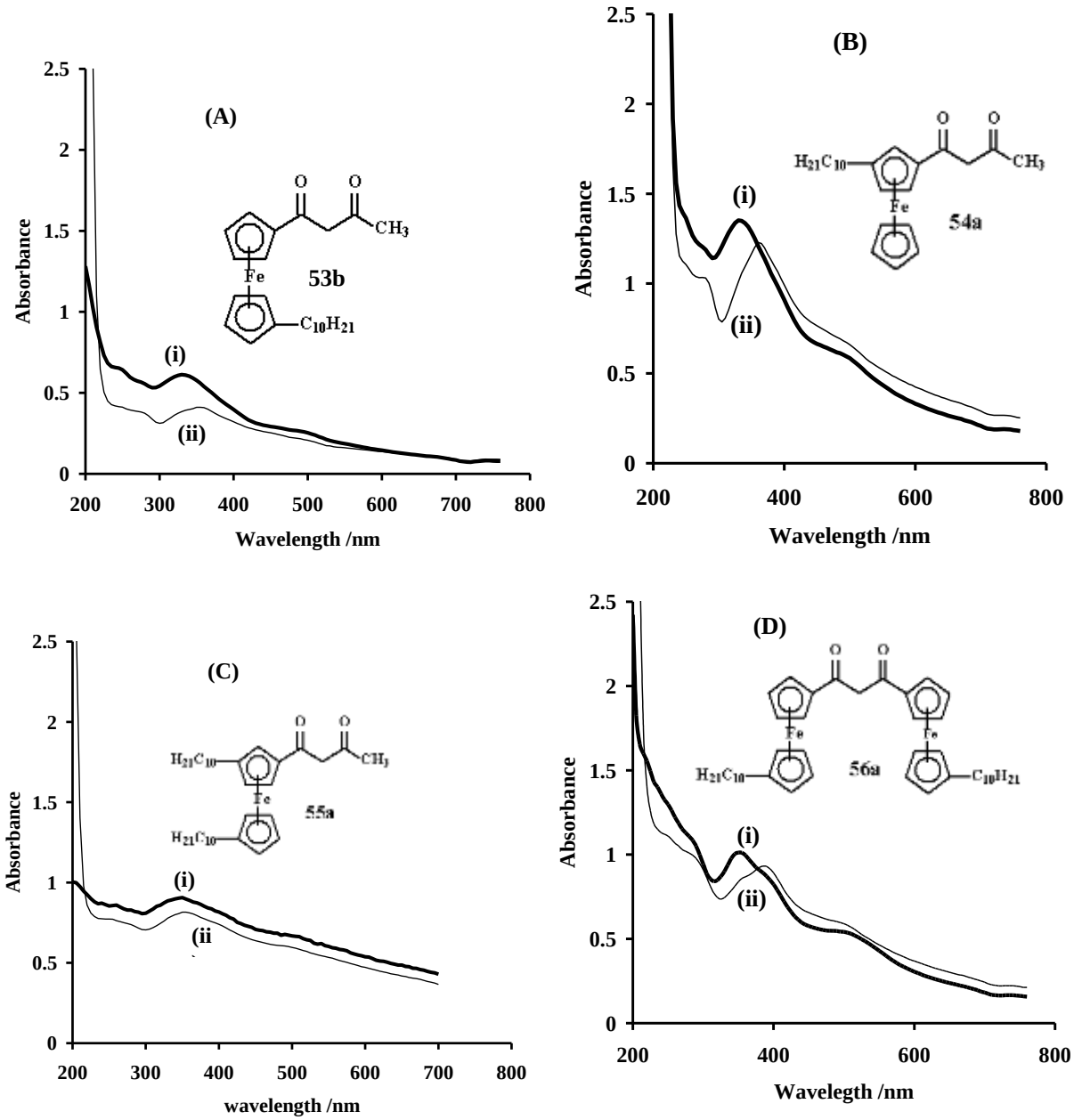

Figure 3. 1: UV/Visible spectra of the free β-diketone (i, —) and the deprotonated β-diketonato anion (ii, □) of β-diketones, (A) (Cp-$C_{10}H_{21}$)Fe(Cp-$COCH_2COCH_3$); 53b, (B) (Cp)Fe(Cp-$C_{10}H_{21}$-$COCH_2COCH_3$); 54a, (C) (Cp-$C_{10}H_{21}$)Fe(Cp-$C_{10}H_{21}$-$COCH_2COCH_3$); 55a and (D) (Cp-$C_{10}H_{21}$)Fe(Cp-$COCH_2CO$-Cp)Fe(Cp-$C_{10}H_{21}$); 56a in water containing 10 % acetonitrile (v/v), μ = 0.100 mol dm^{-3} ($NaClO_4$) at 21 ^0C. [β-diketone] = 0.1000 mmol dm^{-3}.

Once a wavelength was identified that showed a convenient difference in absorbance for free β-diketone and β-diketonato anion solution, a pH titration was performed to follow how the absorbance of a species changed with pH. **Figure 3.2** shows some examples of pH absorbance measurements for **53b, 54a, 55a** and **56a**. The concentrations of each species during the titration are given in **Table 3.1**. It was observed in **Figure 3.1**, that at pH 12, the enolate form of (Cp-$C_{10}H_{21}$)Fe(Cp-$C_{10}H_{21}$-$COCH_2COCH_3$)**, 55a** and (Cp-$C_{10}H_{21}$)Fe(Cp-$COCH_2CO$-Cp)Fe(Cp-$C_{10}H_{21}$), **56a**, respectively did not give large differences in absorbance. It was concluded that the β-diketones that are substituted with more than one alkyl group suppress absorption differences between free β-diketones and the enolate anion ligand.

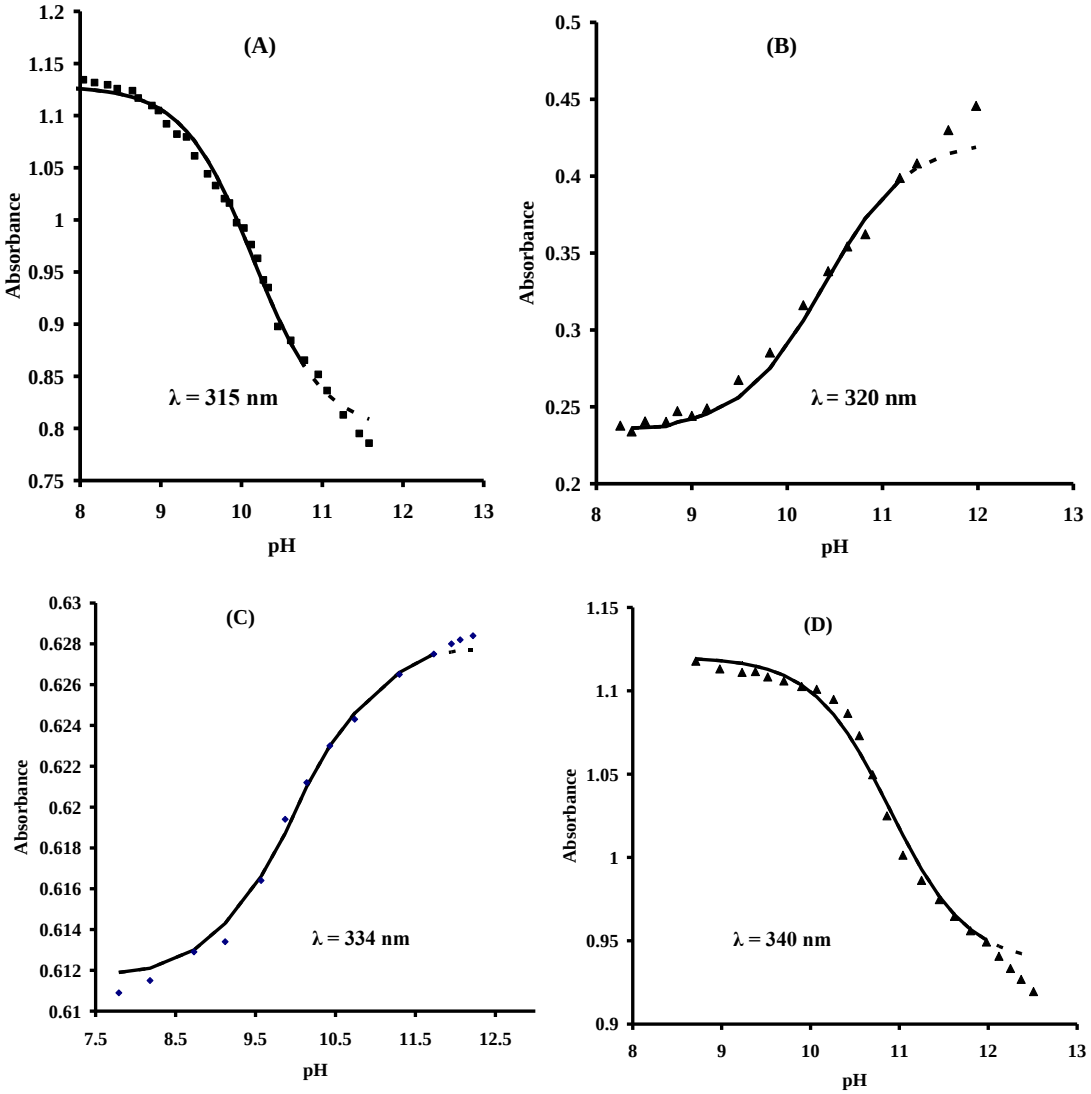

Figure 3. 2: Absorbance dependence on pH for (A) (Cp-$C_{10}H_{21}$)Fe(Cp-$COCH_2CO$-CH_3); 53b, (B) (Cp)Fe(Cp-$C_{10}H_{21}$-$COCH_2CO$-CH_3); 54a, (C) (Cp-$C_{10}H_{21}$)Fe(Cp-$C_{10}H_{21}$-$COCH_2CO$-CH_3); 55a and (D) (Cp-$C_{10}H_{21}$)Fe(Cp-$COCH_2CO$-Cp)Fe(Cp-$C_{10}H_{21}$); 56a, in water containing 10 % acetonitrile mixture, μ = 0.100 mol dm^{-3} ($NaClO_4$) at 21 ^{0}C. Degradation of the β-diketonato anion at high pH explains why the "S" curves veers off from the experimental points at high pH.

The titrated absorbance/pH data from **Figure 3.2**, as well as from the other new β-diketones of this study, were fitted to **equation 3.1** to determine the $pK_a^{/}$ value of each β-diketonato derivative.

$$A_T = \frac{A_{HA}10^{-pH} + A_A 10^{-pK_a^{/}}}{10^{-pH} + 10^{-pK_a^{/}}} \qquad \textbf{equation 3. 1}$$

In **equation 3.1** A_T = measured absorbance; A_{HA} = absorption of the free β-diketone form and A_A = absorption of the deprotonated (basic) β-diketonato form.

A key feature of each pH titration, including those shown in **Figure 3.2** is that at pH > 12, measurements become very erratic. This is in part regarded as the consequence of the interaction of the negative charge on the β-diketonato anion with the hydrophobic long alkyl chain on each ligand, but β-diketonato decomposition also plays a significant role in this erratic behaviour at high pH.

Table 3. 1: $pK_a^{/}$ values determined (at λ_{exp}) and molar extinction coefficients, ε, (at λ_{max} nm) of the β-diketones, 53 – 56, in water containing 10 % acetonitrile mixture, μ = 0.100 mol dm^{-3} ($NaClO_4$) at 21 ^{0}C. Values in brackets are molar extinction coefficients in dm^3 mol^{-1} cm^{-1}. c = bulk concentration of the β-diketonate during the experiment

Compound	β-diketone λ_{max} /nm	β-diketonato λ_{max} /nm	λ_{exp}[(a)] nm	10^3 c / mol dm^{-3} (ε /dm^3 mol^{-1} cm^{-1})	$pK_a^{/}$
53a, R = C_9H_{19}	320	325	315	1.02 (575)	10.31(2)
53b, R = $C_{10}H_{21}$	330	355	315	0.987 (594)	10.14(2)
53c, R = $C_{12}H_{25}$	335	365	320	1.01 (938)	10.35(1)
53d, R = $C_{14}H_{29}$	330	365	320	1.06 (1503)	10.69(4)
53e, R = $C_{18}H_{35}$	350	350	350	1.12 (729)	10.02(2)
54a, R = $C_{10}H_{21}$	330	360	320	0.965 (1359)	10.47(5)
54b, R = $C_{12}H_{25}$	330	325	330	1.04 (599)	10.15(2)
55a, R = $C_{10}H_{21}$	350	350	334	0.972 (911)	9.97(4)
55b, R = $C_{12}H_{25}$	330	325	325	0.984 (765)	ppt[(b)]
56a, R = $C_{10}H_{21}$	350	385	340	1.11 (880)	10.89(1)
56b, R = $C_{12}H_{25}$	355	355	355	1.04 (200)	10.32(7)

(a) wavelength utilized during $pK_a^{/}$ determination
(b) under the specified conditions **55b** precipitated and/or degraded, no $pK_a^{/}$ determination was possible.

A further complicating factor is the precipitation of the ligands at high pH, as well as the cleavage of the β-diketonato anions into esters and ketones in basic aqueous media. **Figure 3.3** shows the effect these processes have on absorbance measurements during a pH titration in a solvent system

containing 9 % acetonitrile and 1 % THF mixture in water. The drift in $pK_a^{/}$ when the solvent medium changes from 10 % acetonitrile to 9 % acetonitrile/1 % THF mixed with 90 % water is due to the presence of the stronger coordinating THF species and has been observed many times before in this laboratory.[5] The problems surrounding accurate absorbance measurements at high pH is the reason why $pK_a^{/}$ determination obtained for titrations starting at low pH with an alkali solution is regarded as more correct.

From **Table 3.1** it can be seen that $pK_a^{/}$ values of compound series **53** varies from 10.02 – 10.69. This is not a significant drift implying that increasing alkyl side chain length from C_9H_{19} – $C_{18}H_{37}$ had no appreciable electronic influence on the ligand. Most $pK_a^{/}$ values were 10.30 or larger. When the R-group was completely omitted, to result in β-diketone, Fc-CO-CH_2-CO-CH_3, **13c**, the $pK_a^{/}$ was determined as 10.01.[5] This means that by adding an alkyl side chain to the ferrocenyl groups, only a very small increase in electron density is effected on the pseudo aromatic β-diketonato core, which accounts for the slightly larger $pK_a^{/}$ values in compound series **53** compared to that of **13c**. The effect alkyl groups seem to have on $pK_a^{/}$ values is, however, for the present series of compounds, minimal. The substitution position also does not play a significant role, because the compound series **53** and **54** gave essentially the same $pK_a^{/}$ values. The double alkyl-substituted compound series **55** gave $pK_a^{/}$ values of about 10. This is certainly lower than was expected but the same result was obtained from multiple titrations.

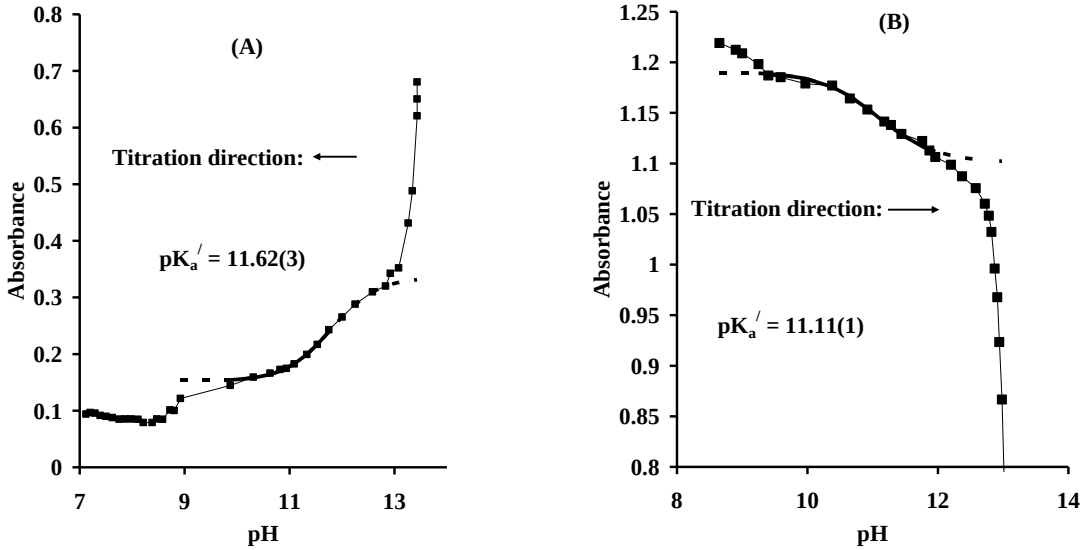

Figure 3. 3: Absorbance dependence on pH for (Cp-$C_{10}H_{21}$)Fe(Cp-$COCH_2COCH_3$), 53a, where graph (A) shows titration from basic pH to acidic pH and (B) indicates titration from acidic to basic pH, containing 9 % acetonitrile and 1 % THF mixture in water, μ = 0.100 mol dm^{-3} ($NaClO_4$) at 21 ^{0}C. All dotted points (----) are artificial, but had to be used to approximate the desired $pK_a^{/}$. The line (—) corresponds to fit if all data points were indiscriminately used during a fit to equation 3.1.

The double-ferrocene-containing compound series **56** did give pK_a' values which are marginally higher than the compound series **53**, but still the pK_a' of 10.89(1) for **56a** is much lower than the pK_a' value that was found for Fc-COCH2CO-Fc (13.1).[5] This unexpected result is contributed to the extreme hydrophobic properties of **56**. The unusually low pK_a' values are consistent with molecules forming micelles and the ^-OH ion only reacts with molecules at the surface of the micelles. However, further research about the solution behaviour of series **56** is required before a clearer understanding of this pK_a' result will be possible.

3.4. Keto-enol equilibra in β-diketones

3.4.1. The observed solution phase equilibrium constant, K_c

All β-diketones can exist in principle as a mixture of keto and enol forms as indicated in **Scheme 3.6**. Although two enol isomers for the β-diketones, (Cp-R)Fe(Cp-$COCH_2COCH_3$) are possible, only one set of enol isomer signals together with the keto isomer set of signals are observed in ^1H NMR spectra. This implies that either the conversion from one enol tautomer to the other is fast on the ^1H NMR time scale, or that only one isomer exists. In analogy with previous crystallographic studies we propose that **isomer B** probably dominates in the present compound series as well.[5] In addition it was found that in the solid state, compound series **53**, with time converts completely to the enol **isomer B**. No trace of keto isomers could be found in aged solid samples of the present β-diketone series.

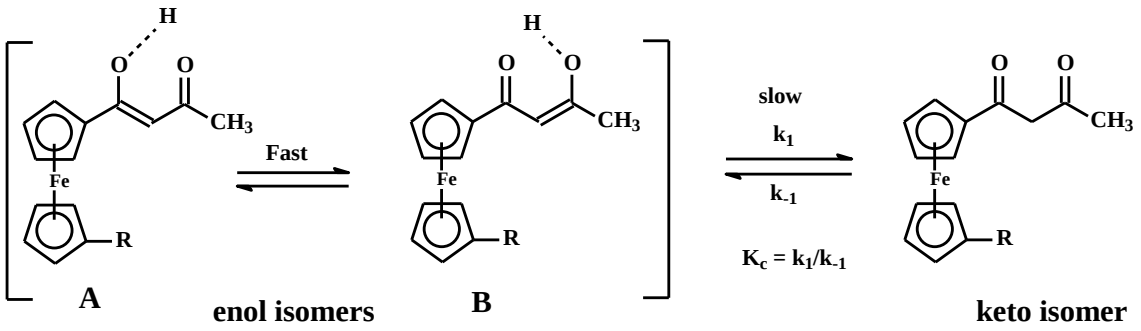

Scheme 3. 6: The keto-enol equilibrium for the ferrocene-containing β-diketones that was studied. k_1 is a rate constant for the forward reaction, k_{-1} is a rate constant for the reverse reaction, and $K_c = k_1/k_{-1}$ = equilibrium constant for the overall process.

Hence, the isomerization kinetics between the keto- and the enol-isomers could be followed by ^{1}H NMR in $CDCl_3$ as a solvent at 20 ^oC. A portion of the ^{1}H NMR spectrum of compound **53c** obtained 145 seconds after dissolving an aged solid sample in $CDCl_3$ and the equilibrium spectrum after 8 hours are shown in **Figure 3.4**.

Upon interpreting ^{1}H NMR spectra of the keto and enol tautomers, the measured integral values of the enol and keto isomers would be indicative of the relative enol and keto content in solution.

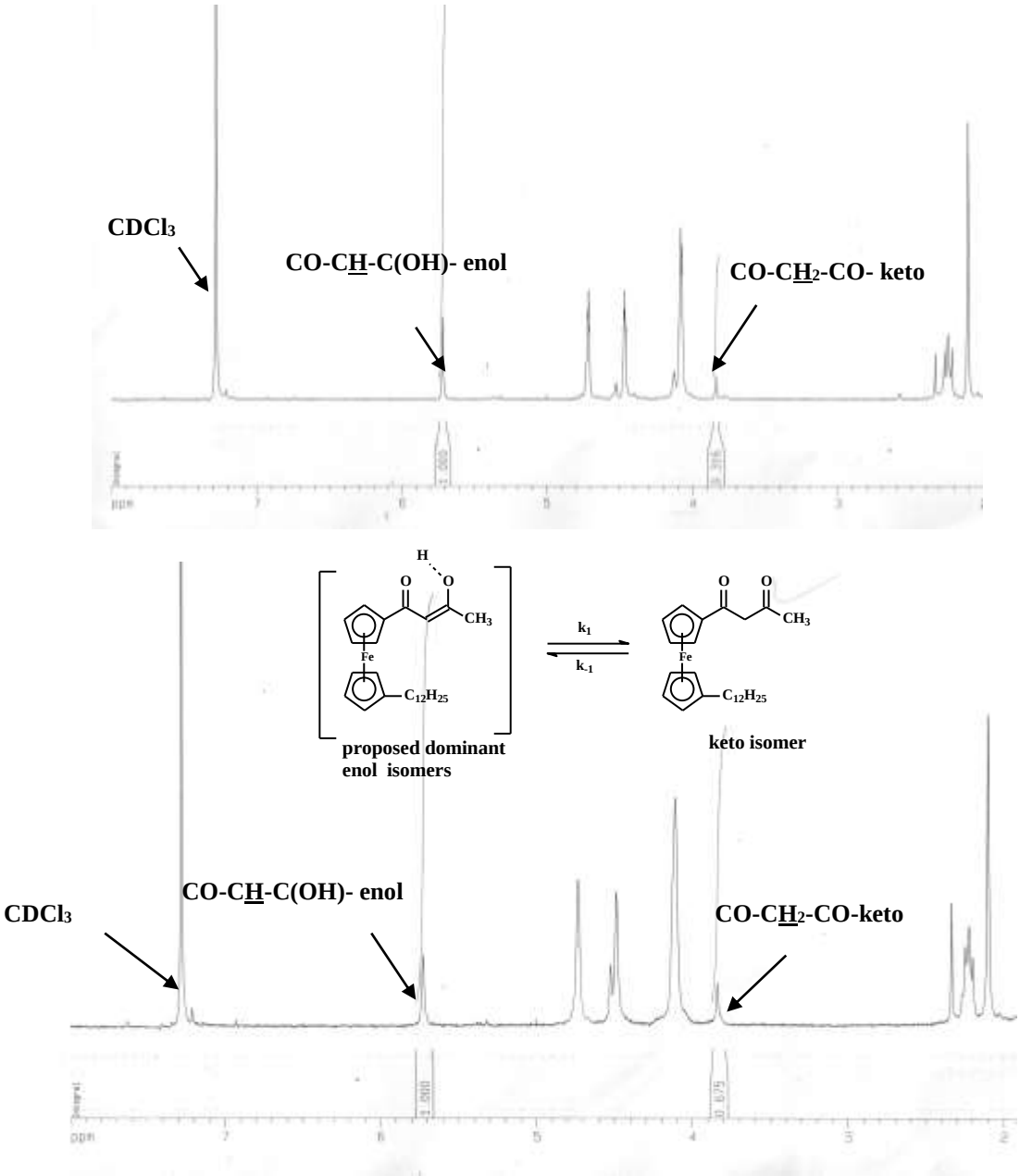

Figure 3. 4: A portion of the ^{1}H NMR spectra of 53c in $CDCl_3$ at 20°C, 145 s after dissolving the sample in $CDCl_3$ (Top) and at equilibrium (after 8 hours) (Bottom).

This implies the equilibrium constant, K_c, which applies to the equilibrium shown in **Scheme 3.6** could be determined conveniently by utilizing integral values for suitable ^{1}H NMR signals (**Equation 3.2**). Integration of all ^{1}H NMR spectra were done in such a way that the methine proton of the enol isomer, (Cp-$C_{12}H_{25}$)Fe(Cp-COC**H**=C(OH)CHCH_3), was assigned an integral value of one (**Figure 3.4**).

K_c = (integral value of ^{1}H NMR signal of a suitable keto molecular fragment) / (integral value of ^{1}H NMR signal of a suitable enol molecular fragment) **equation 3. 2**

Utilizing, the CO-C**H$_2$**-CO- signal integral value of (Cp-$C_{12}H_{25}$)Fe(Cp-COC**H$_2$**$COCH_3$) of 0.675 at 3.85 ppm (keto isomer) and the (Cp-$C_{12}H_{25}$)Fe(Cp-COC**H**=C(OH)CH_3) signal integral value of 1.00 at 5.72 ppm (enol isomer) the equilibrium constant could be calculated as K_c = (0.675/2)/(1.00) = 0.337. The integral value of 0.675 for the keto isomer is divided with two to compensate for the fact that the keto isomer has two protons between the carbonyl groups and the enol isomer has only one methine proton. However, for evaluating kinetic data it was more convenient to use isomer percentages in determining equilibrium constants (**Equation 3.3**).

K_c = (% keto isomer)/(% enol isomer) = k_1/k_{-1} **equation 3. 3**

Once again, K_c applies to the equilibrium shown in **Scheme 3.6**. The percentage keto-isomer at any given time during the course of the conversion between the keto- and enol isomers can be calculated using **Equation 3.4**.

% keto isomer = (*I* of keto signal)/{(*I* of keto signal) + (I of enol signal)} x 100 **equation 3. 4**

Here, I = integral value of the ^{1}H NMR signal.

For example, from the methine proton signals (Cp-$C_{12}H_{25}$)Fe(Cp-COC**H**=C(OH)CH_3) and (Cp-$C_{12}H_{25}$)Fe(Cp-COC**H$_2$**-$COCH_3$)

the equilibrium % keto isomer = (0.675/2)/{(0.675/2+1.00)} x 100 = 25.2 %.
Thus using **Equation 3.3**

K_c = (25.2 %)/(74.8 %) = 0.337

which is for all practical purposes the same as 0.337 found using **Equation 3.2**. In a similar fashion, by determining the % keto isomer for compound series **53, 54, 55** and **56** using appropriate unambiguously definable ^{1}H NMR signals, K_c values for all β-diketones could be calculated. Results are summarized in **Table 3.2**.

From **Table 3.2** it is strikingly evident that the enol isomer is the dominant isomer at equilibrium in $CDCl_3$ solutions. It can be seen that K_c values of compounds **53a - 53e** are approximately the same. This implies that increasing alkyl side chain length from C_9H_{19} – $C_{18}H_{37}$ had no appreciable electronic influence on the ligand. Even when the R-group is completely omitted, to give β-diketone Fc-CO-CH_2-CO-CH_3, **13c**, K_c was determined as 0.282 in $CDCl_3$.[6] As can be seen from the present series of compounds, the effect alkyl groups have on β-diketonato K_c values are minimal.

Table 3. 2 Equilibrium constant, K_c, the % keto isomer at equilibrium for the keto-enol equilibrium, shown in Scheme 3.6 and the Gibb's free energy for this equilibrium for different β-diketones and $FcCOCH_2COCH_3$, 13c, in $CDCl_3$ at 20 °C.

Compounds	% keto at equilibrium	K_c in $CDCl_3$	ΔG /kJ mol^{-1}
53a: R = C_9H_{19}	20.5	0.257	3.31
53b: R = $C_{10}H_{21}$	23.1	0.300	2.93
53c: R = $C_{12}H_{25}$	25.2	0.337	2.65
53d: R = $C_{14}H_{29}$	21.6	0.276	3.13
53e: R = $C_{18}H_{37}$	24.8	0.329	2.71
54a: R = $C_{10}H_{21}$	20.3	0.254	3.33
54b: R = $C_{12}H_{25}$	24.9	0.331	2.69
55a: R = $C_{10}H_{21}$	26.5	0.360	2.49
55b: R = $C_{12}H_{25}$	25.9	0.350	2.56
56a: R = $C_{10}H_{21}$	20.4	0.256	3.31
56b: R = $C_{12}H_{25}$	20.9	0.264	3.24
$FcCOCH_2COCH_3$[6]	22.0	0.282	3.08

The Gibbs free energy for the keto-enol isomerization process shown in **Scheme 3.6** can be obtained by utilizing **Equation 3.5**.

$$\Delta G = -RT\ln K_c \qquad \textbf{equation 3. 5}$$

The Gibb's free energy was calculated to be in the same range for all compounds in **Table 3.2** above. There is also a correlation observed between ΔG and % keto isomer of the β-diketones. As ΔG becomes larger positive, the % keto content becomes smaller. This means that the thermodynamic driving force of the equilibrium favours the enol isomer in solution.

3.4.2. Isomerization kinetics

By plotting a time trace of % keto isomer versus time (**Figure 3.5**) the rate of conversion from enol to keto isomers could be determined. This was achieved by fitting the equation

$$C_t = C_\infty + (C_0 - C_\infty)e^{-(k_{obs})t} \qquad \textbf{equation 3. 6}$$

to experimentally determined concentration (here % keto isomer) and time data. Here C_0 = initial concentration expressed as % initial keto isomer, C_t = concentration at time t expressed as % keto content at time t and C_∞ = equilibrium % keto content.

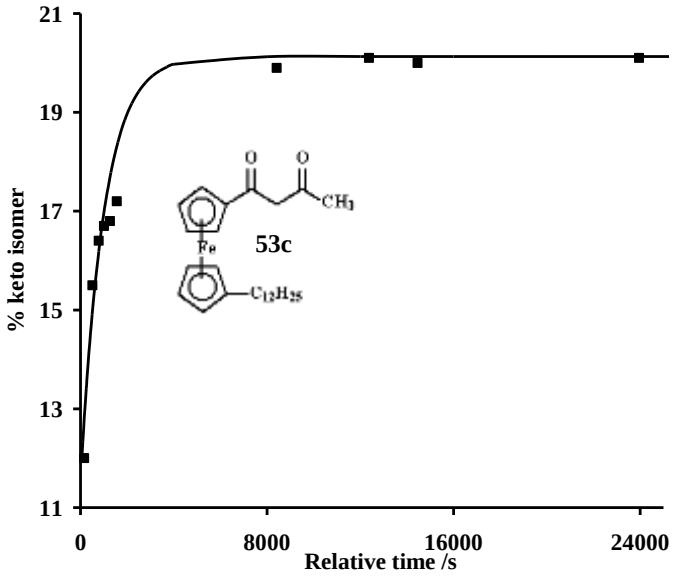

Figure 3. 5: Time trace showing the conversion from enol to keto isomer for (Cp-$C_{12}H_{25}$)Fe(Cp-$COCH_2COCH_3$), 53c, at 20 °C in $CDCl_3$.

The obtained first order rate constant, k_{obs}, is actually the sum of the forward and reverse rate constants in **Scheme 3.6**.[6] This means

$$k_{obs} = k_1 + k_{-1} \qquad \textbf{equation 3. 7}$$

By simultaneously solving $k_{obs} = k_1 + k_{-1}$ (**equation 3.7**) and $K_c = k_1/k_{-1}$ (**equation 3.3**) rate constants k_1 and k_{-1} can be separated. **Figure 3.6** shows time traces for all compounds. The kinetic data obtained for β-diketones **53, 54, 55** and **56** is summarized in **Table 3.3**.

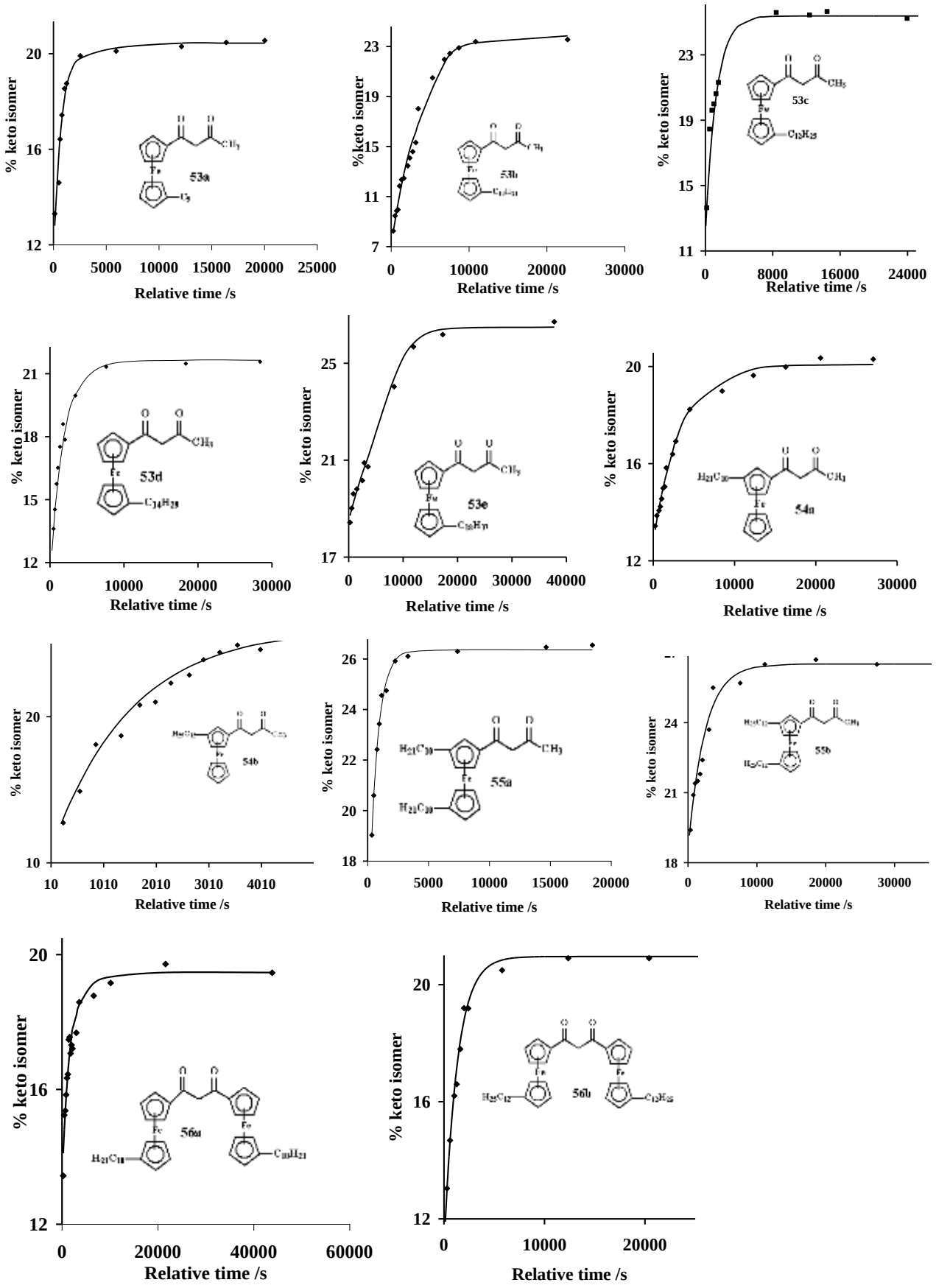

Figure 3. 6 Time traces showing the conversion from enol- to keto tautomer for the β-diketone series, 53, 54, 55 and 56 at 20 ºC.

From **Table 3.3**, in terms of how fast the equilibrium sets in, k_{obs} values indicated that isomerization is largely independent of the R-substituents. It also shows that the rate constants of compounds **53a – 53e**, are approximately the same and that K_c values are also in the same range. Compound series **54, 55** and **56** showed the same trend that is observed for compound series **53**.

Table 3. 3 Equilibrium constant, K_c, for the keto-enol equilibrium of (R-Cp)Fe(Cp-$COCH_2COCH_3$) in $CDCl_3$ at 20 °C. The first order rate constants, k_{obs}, k_1 for the keto to enol half reaction are also listed.

Compound	% keto isomer at equilibrium	10^4 k_{obs} s^{-1}	K_c in $CDCl_3$	10^4 k_1 s^{-1}	10^4 k_{-1} s^{-1}
53a: R = C_9H_{19}	20.5	0.12(4)	0.257	0.025	0.10
b: R = $C_{10}H_{21}$	23.1	2.5(2)	0.300	0.57	1.92
c: R = $C_{12}H_{25}$	25.2	5.6(3)	0.337	1.41	4.19
d: R = $C_{14}H_{29}$	21.6	5.7(5)	0.276	1.23	4.47
e: R = $C_{18}H_{37}$	24.8	1.4(5)	0.329	1.40	4.26
54a: R = $C_{10}H_{21}$	20.3	2.9(2)	0.254	0.59	2.31
b: R = $C_{12}H_{25}$	24.9	6.6(3)	0.331	1.64	4.96
55a: R = $C_{10}H_{21}$	26.5	0.14(3)	0.360	0.037	0.10
b: R = $C_{12}H_{25}$	25.9	4.1(2)	0.350	1.06	3.04
56a: R = $C_{10}H_{21}$	20.4	6.0(5)	0.256	1.22	4.78
b: R = $C_{12}H_{25}$	22.0	7.6(4)	0.282	1.67	5.93

We concluded therefore, that the R-substituents with chain length varying from C_9H_{19} – $C_{18}H_{37}$, and with one or more than one R-group substituent, had very little effect on the rate of keto/enol conversions.

3.5. Cyclic Voltammetry

3.5.1. Introduction

In this section, cyclic voltammetric (CV) results are reported for all the new ferrocene-containing β-diketones, **53 - 56**. The objective of the present electrochemical study was to determine the effect that the R substituent size and its substitution position on each β-diketone have on the electrochemistry of the iron centre in the ferrocenyl moiety. In section **3.6.3**, the interaction between the rhodium metal centre and the ferrocenyl moiety is discussed.

Cyclic voltammetric experiments were conducted in dry CH_2Cl_2 utilizing 0.05 mol dm^{-3} tetrabutylammonium tetrakispentafluorophenylborate ($[NBu_4][B(C_6F_5)_4]$) as supporting electrolyte.

This solvent electrolyte system minimized any solvation or electrolyte ion pairing interactions with the β-diketone substrate. In each CV experiment, a Pt wire was utilized as auxiliary electrode, a glassy carbon electrode (surface area = 2.0 mm^2) as working electrode and a Ag/AgCl reference electrode. To prevent signal overlapping, decamethylferrocene (Fc*) was used as an internal standard. Under our conditions decamethylferrocene exhibited a ΔE_p value of 82 mV and $E^{o/}$ = -41 mV *vs.* Ag/AgCl, while ferrocene (Fc) itself gave a ΔE_p value of 76 mV and $E^{o/}$ = 588 mV *vs.* Ag/AgCl at scan rate 100 mVs^{-1}. This value could drift with more than 200 mV from experiment to experiment. However, no drifting versus an internal standard, e.g. free ferrocene could be detected. Under our conditions, the $(Fc^*)/(Fc^*)^+$ couple was found to be at -619 mV *vs.* Fc/Fc^+. Electrochemical reversible one electron transfer processes are characterized theoretically by peak potential differences of $\Delta E_p = E_{pa} - E_{pc} = 59/n$ mV and is independent of scan rate, with n = number of electrons transferred, E_{pa} = peak anodic potential and E_{pc} = peak cathodic potential. In this study, experimentally determined ΔE_p values up to 90 mV were considered still to imply electrochemical reversibility. Larger ΔE_p values (> 90 mV) were considered to indicate quasi-reversible behaviour, while ΔE_p > 150 mV were considered to indicate electrochemical irreversibility.

3.5.2. Cyclic voltammetry of β-diketones, 53 – 56

3.5.2.1. Cyclic voltammetry of β-diketones of the type (Cp-R)-Fe(Cp-$COCH_2COCH_3$) complexes, with R = C_9H_9, 53a; $C_{10}H_{21}$, 53b; $C_{12}H_{25}$, 53c; $C_{14}H_{29}$, 53d and $C_{18}H_{37}$, 53e

Cyclic voltammograms of compounds **53b** (left) and unsubstituted β-diketone Fc-$COCH_2COCH_3$ (**13c**, right) at scan rates 100, 200, 300, 400, 500 and 1000 mVs^{-1} are shown in **Figure 3.7**. Cyclic voltammograms of the β-diketones, **53a – 53e**, at scan rates 100 mVs^{-1}, are compared in **Figure 3.8**.

All showed a one-electron electrochemically reversible ferrocenyl-based electron transfer wave with ΔE_p values smaller than 90 mV at a scan rate of 100 mVs^{-1}. ΔE_p became progressively larger at faster scan rates. A complicating factor in the interpretation of the CV's of **Figure 3.8** is the broadening of the anodic peak. Especially **53a, 53b, 53c** and **53d** showed there are two E_{pa} potentials, labeled I and II. The source of these two peaks is attributed to the existence of enol and keto isomers in the solution on which cyclic voltammetry was performed (see section **3.4**). Except for **53e**, this made accurate determinations of $E^{o/}$ difficult.

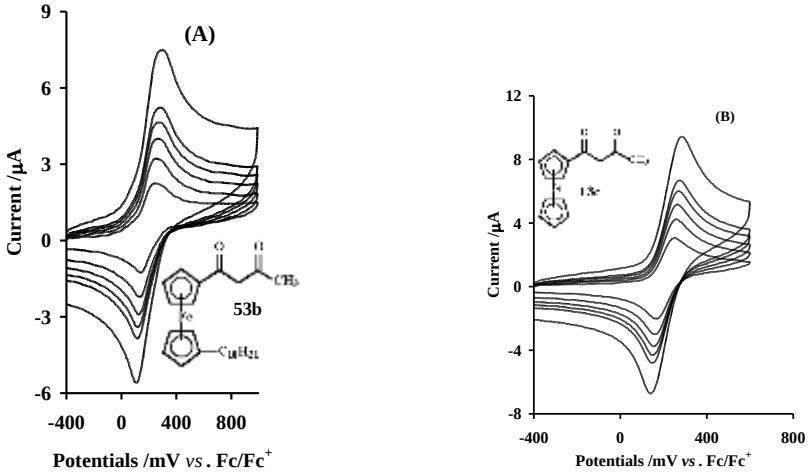

Figure 3. 7: (A) Cyclic voltammograms of 0.5 mmol dm^{-3} solutions of compounds 53b and (B) $FcCOCH_2COCH_3$, 13c, measured in 0.05 mol dm^{-3} $[NBu_4][B(C_6F_5)_4]/CH_2Cl_2$ on a glassy carbon working electrode at 25 ºC *vs.* Fc/Fc^+ at scan rates of 100, 200, 300, 400, 500 and 1000 mVs^{-1}.

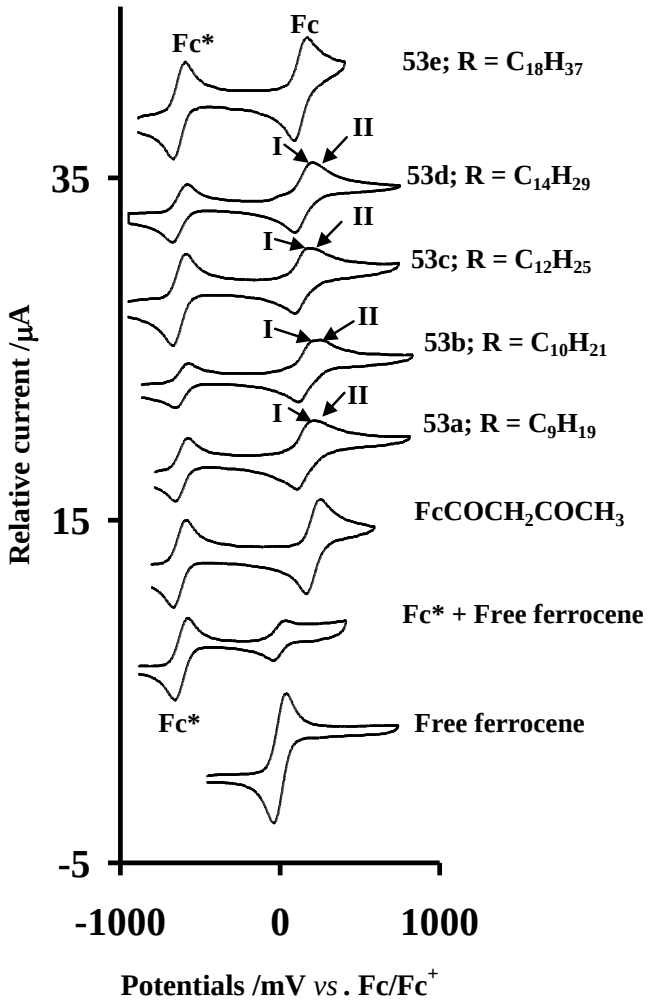

Figure 3. 8: Cyclic voltammograms of 0.5 mmol dm^{-3} solutions of ferrocene and ferrocene-containing β-diketones of the type (Cp-R)Fe($COCH_2COCH_3$) measured in 0.05 mol dm^{-3} $[NBu_4][B(C_6F_5)_4]/CH_2Cl_2$ on a glassy carbon working electrode at 25 ºC *vs.* Fc/Fc^+ at scan rate of 100 mVs^{-1}. Fc* = decamethylferrocene as internal standard.

Table 3. 4: Electrochemical data of 0.5 mmol dm^{-3} solutions of β-diketones, 53a – 53e, measured in 0.05 mol dm^{-3} [NBu$_4$][B(C$_6$F$_5$)$_4$]/CH$_2$Cl$_2$ on a glassy carbon working electrode at 25 °C *vs*. Fc/Fc$^+$ at scan rates between 100 and 1000 mVs^{-1}. E_{pa} = anodic peak potentials, $\Delta E_p = E_{pa} - E_{pc}$ (E_{pc} = cathodic peak potentials), formal reduction potentials, $E^{o\prime} = (E_{pa} + E_{pc})/2$, i_{pa} = anodic peak currents and i_{pc}/i_{pa} = peak current ratios with i_{pc} = cathodic peak currents.

ν / mV s^{-1}	E_{pa},I[a] / mV	ΔE_p / mV	$E^{o\prime}$ / mV	i_{pa} / μA	i_{pc}/i_{pa}	E_{pa},I[a] / mV	ΔE_p / mV	$E^{o\prime}$ / mV	i_{pa} / μA	i_{pc}/i_{pa}
(Cp-C$_9$H$_{19}$)Fe(Cp-COCH$_2$COCH$_3$) {53a}						**(Cp-C$_{10}$H$_{21}$)Fe(Cp-COCH$_2$COCH$_3$) {53b}**				
100	194	90	149	2.00	0.96	189	77	150	1.86	0.90
200	204	106	151	3.67	1.00	200	92	154	2.57	0.95
300	223	124	161	4.34	1.02	220	144	148	3.36	0.94
400	229	138	160	5.20	1.02	228	148	154	3.79	0.94
500	233	144	171	5.92	1.03	234	160	154	4.29	0.92
1000	242	169	148	7.86	1.02	253	198	154	5.71	0.98
(Cp-C$_{12}$H$_{25}$)Fe(Cp-COCH$_2$COCH$_3$) {53c}						**(Cp-C$_{14}$H$_{29}$)Fe(Cp-COCH$_2$COCH$_3$) {53d)**				
100	186	89	141	1.88	1.06	193	90	148	1.88	0.85
200	195	112	139	2.53	0.93	204	102	153	3.00	1.00
300	197	114	140	3.06	0.96	218	128	154	3.45	1.04
400	203	128	139	3.47	0.98	228	152	152	4.27	0.99
500	208	140	138	3.88	0.94	232	164	150	5.00	0.99
1000	216	156	138	5.18	0.93	250	193	153	6.68	0.98
(Cp-C$_{18}$H$_{37}$)Fe(Cp-COCH$_2$COCH$_3$) {53e}						**Fc-COCH$_2$CO-CH$_3$**				
100	167	80	127	3.31	1.03	246	85	209	2.60	0.96
200	178	88	134	5.98	1.01	258	95	210	3.73	0.94
300	180	90	135	7.68	1.03	263	106	210	4.47	0.96
400	190	104	140	9.03	1.02	266	111	210	5.17	0.92
500	194	104	142	10.65	0.98	273	123	211	5.71	0.91
1000	203	125	138	15.01	0.98	284	142	213	7.65	0.91

[a] E_{pa} II is 259 mV (**53a**), 251 mV (**53b**), 234 mV (**53c**) and 243 mV (**53d**). **53e** does not show a second peak anodic wave at a scan rate of 100 mVs^{-1}.

In accordance with recent studies on ruthenocene-containing β-diketones,[7] peak I is considered to be associated with the enol form and peak II with the keto form. The reduction cycle only showed one peak, not two. Since it is known that β-diketones exist almost exclusively in the enol form when R-group are electron-withdrawing in nature, the absence of two cathodic peaks for compound series **53** is expected. This is so because the ferrocenyl group with $\chi_{Fc} = 1.86$ becomes almost as electron withdrawing as a CF_3 group ($\chi_{CF3} = 3.01$) after oxidation during an anodic half cycle. The group electronegativity of the ferrocenium species is $\chi_{Fc+} = 2.89$.[8] Data that could be extracted from

the CV's are summarized in **Table 3.4**. Cited potentials are corrected to be referenced against Fc/Fc^+, as required by IUPAC.[9]

It was found that peak current ratios, i_{pc}/i_{pa}, (the conversion used is to calculate current ratios always as the current of the reverse scan divided by the current of the forward scan) for the β-diketones, **53a – 53e**, were found to be approximately 1 at the indicated scan rates (**Table 3.4)**. This implies that the electrochemical oxidation of the ferrocenyl species ($CpFe^{II}Cp$) to generate the ferricenium species $(CpFe^{III}Cp)^+$, in the anodic sweep results in a chemically stable ferricenium species which is reduced quantitatively in the cathodic reduction halfwave.

From **Table 3.4**, $E^{o/}$ was found to follow a decreasing trend as side chain length increased from C_9 through C_{18}. However, when R is not an alkyl group but a proton, *i.e.* $Fc\text{-}COCH_2COCH_3$, $E^{o/}$ was found to be 209 mV. This trend is graphically highlighted in **Figure 3.9**.

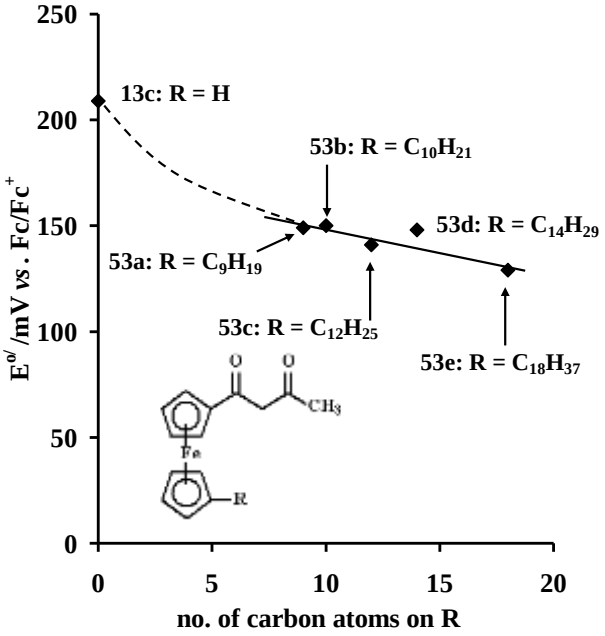

Figure 3. 9: Relationship between the formal reduction potentials, $E^{o/}$, of the ferrocenyl group and the number of carbon atoms on R substituent at a scan rate of 100 mV s^{-1}.The broken line represents an imaginative trend for shorter chain alkyl substituent, but experimental data is not yet available.

The increase in the number of carbon atoms on the R substituent in moving from C_9H_{19} through $C_{18}H_{37}$ showed a small effect on the formal reduction potential due to the lack of conjugation between the ferrocenyl group and the alkyl R groups (see **Figure 3.9**) and also because any electronic effects induced by electron donating long chain alkyl substituents are so small that they cannot be quantified with great accuracy by cyclic voltammetry.

3.5.2.2. Cyclic voltammetry of β-diketones (Cp)Fe(Cp-$C_{10}H_{21}$-$COCH_2COCH_3$) and (Cp)Fe(Cp-$C_{12}H_{25}$-$COCH_2COCH_3$)

The electrochemistry of the ferrocene-containing β-diketones, **54a** and **54b**, was also investigated using the cyclic voltammetric technique. **Figure 3.10(A)** shows cyclic voltammograms of **54b** at scan rates 100, 200, 300, 400, 500 and 1000 mVs^{-1} and the cyclic voltammograms of **54a** and **54b** are shown in **Figure 3.10(B)** at a scan rate of 100 mVs^{-1}. The electrochemical data relevant to the β-diketones, **54a** and **54b**, is summarized in **Table 3.5**. Under the present conditions, for compound series **54**, no anodic peak potentials could be detected that distinguished between enol and keto isomers.

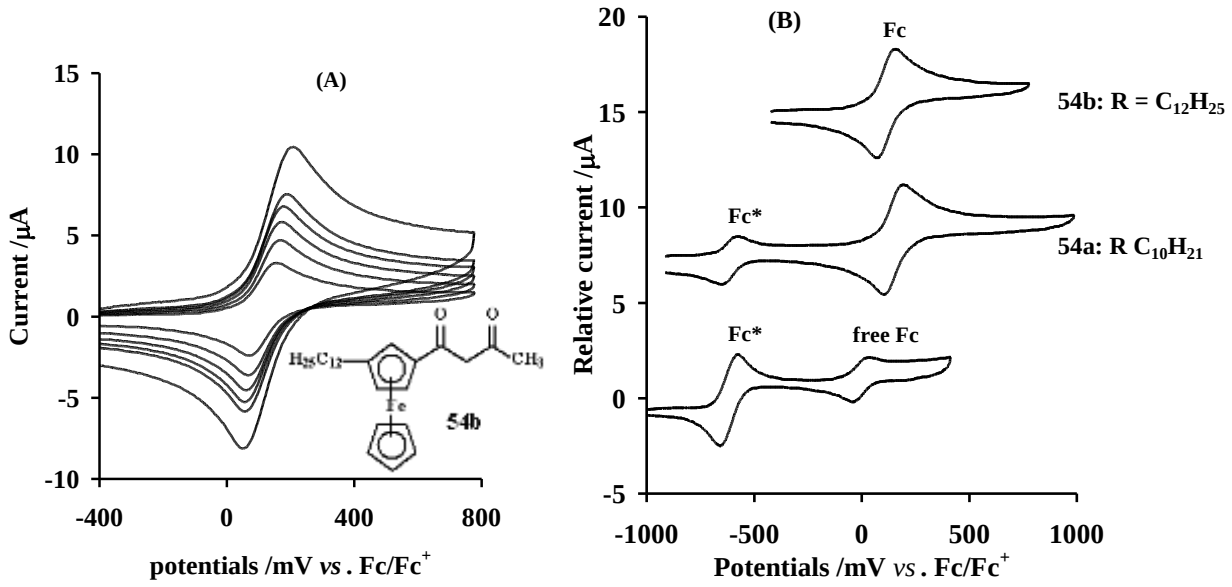

Figure 3. 10: (A) Cyclic voltammograms of *ca.* 0.5 mmol dm^{-3} solutions of the ferrocene-containing β-diketones, 54b, in CH_2Cl_2 containing 0.05 mol dm^{-3} $[NBu_4][B(C_6F_5)_4]$ at 25 ºC on a glassy carbon working electrode at scan rates 100, 200, 300, 400, 500 and 1000 mVs^{-1}. (B) Cyclic voltammograms of the ferrocene-containing β-diketones, 54a and 54b, at scan rate 100 mVs^{-1} under the same conditions as (A) with Fc* = decamethylferrocene.

The redox process associated with compounds, **54a** and **54b**, exhibited ΔE_p = 80 mV and 88 mV respectively at slow scan rate 100 mVs^{-1}. The average peak current ratios (i_{pc}/i_{pa}) observed lies close to one as indicated in **Table 3.5**. Thus, one-electron transfer redox processes associated with compound series **54** are considered as electrochemically and chemically reversible.

From **Table 3.5**, it can be seen that the formal reduction potentials, $E^{o/}$, of **54a** and **54b** are 151 and 114 mV respectively at a scan rate of 100 mVs^{-1}. For compounds **53b** and **53c** in **Table 3.4** values for $E^{o/}$ of 150 and 141 mV respectively at slow scan rate (100 mVs^{-1}) were tabulated. It follows that in moving from 1,1/-hetero cyclopentadienyl ring substituents to 1,3-homo ring substituents, peak potentials were within *ca*. 30 mV of compound **54b**. These results showed that the position of the R-substituent on a cyclopentadienyl ring had very little effect on the electrochemical properties of the above mentioned compounds.

Table 3. 5: Electrochemical data of 0.5 mmol dm^{-3} solutions of β-diketones, 54a and 54b, measured in 0.05 mol dm^{-3} $[NBu_4][B(C_6F_5)_4]/CH_2Cl_2$ on a glassy carbon working electrode at 25 ºC *vs.* Fc/Fc^+ at scan rates between 100 and 1000 mVs^{-1}. Symbols are defined in Table 3.3.

ν / mV s^{-1}	E_{pa} / mV	ΔE_p / mV	$E^{o/}$ / mV	i_{pa} / μA	i_{pc}/i_{pa}	E_{pa} / mV	ΔE_p / mV	$E^{o/}$ / mV	i_{pa} / μA	i_{pc}/i_{pa}
(Cp)Fe(1,3-$C_{10}H_{21}$-Cp-$COCH_2COCH_3$) {54a}						**(Cp)Fe(1,3-$C_{12}H_{25}$-Cp-$COCH_2COCH_3$) {54b}**				
100	191	80	151	3.78	1.12	158	88	114	3.14	0.95
200	197	92	151	5.78	1.04	167	99	117	4.41	0.95
300	199	100	149	6.78	1.03	173	112	117	5.34	0.95
400	203	104	151	7.78	1.06	181	126	118	6.16	0.97
500	207	110	152	8.67	0.97	188	131	122	6.74	0.94
1000	215	124	153	8.78	0.97	210	161	129	8.83	0.96

3.5.2.3. Cyclic voltammetry of β-diketones (Cp-$C_{10}H_{21}$)Fe(Cp-$C_{10}H_{21}$-$COCH_2COCH_3$) and (Cp-$C_{12}H_{25}$)Fe(Cp-$C_{12}H_{25}$-$COCH_2COCH_3$)

Cyclic voltammograms of ferrocene-containing β-diketones, **55a** and **55b**, are shown in **Figure 3.11**. Once again, no distinction could be made between keto and enol isomers for these samples. This is probably because in the solid state the complexes slowly convert exclusively to the enol form. When aged samples are taken, it takes several days before the equilibrium position is obtained. Electrochemical results are summarized in **Table 3.6**. The difference in peak anodic, E_{pa} and peak cathodic, E_{pc}, potentials, ΔE_p, < 90 mV, indicates an electrochemical reversible process at a scan rate 100 mVs^{-1} for both **55a** and **55b**, but quasi-electrochemical reversibility to full electrochemical irreversibility (ΔE_p > 120 mV) are observed at faster scan rates. **Table 3.6** shows that the current ratios i_{pc}/i_{pa} is in both compounds close to a unity, thus indicating chemical reversibility.

The formal reduction potential, $E^{o/}$, for both β-diketones, **55a** and **55b**, in **Table 3.6** with values of 79 and 86 mV at scan rate 100 mVs^{-1} respectively, showed a large difference (*ca*. 80 mV lower for **55a** and 50 mV for **55b**) when compared to the corresponding compounds **53b** and **53c** in **Table 3.4**, and **54a** and **54b** in **Table 3.5**. Upon recognizing that the C_{10} and C_{12} alkyl substituents are weakly electron donating this was expected. Two electron donating alkyl substituents will obviously increase the electron density on the iron(II) centre of the ferrocenyl group more than just one. The result of this will be a lowering in the formal reduction potentials of compound series **55** compared to compound series **53** and **54**.

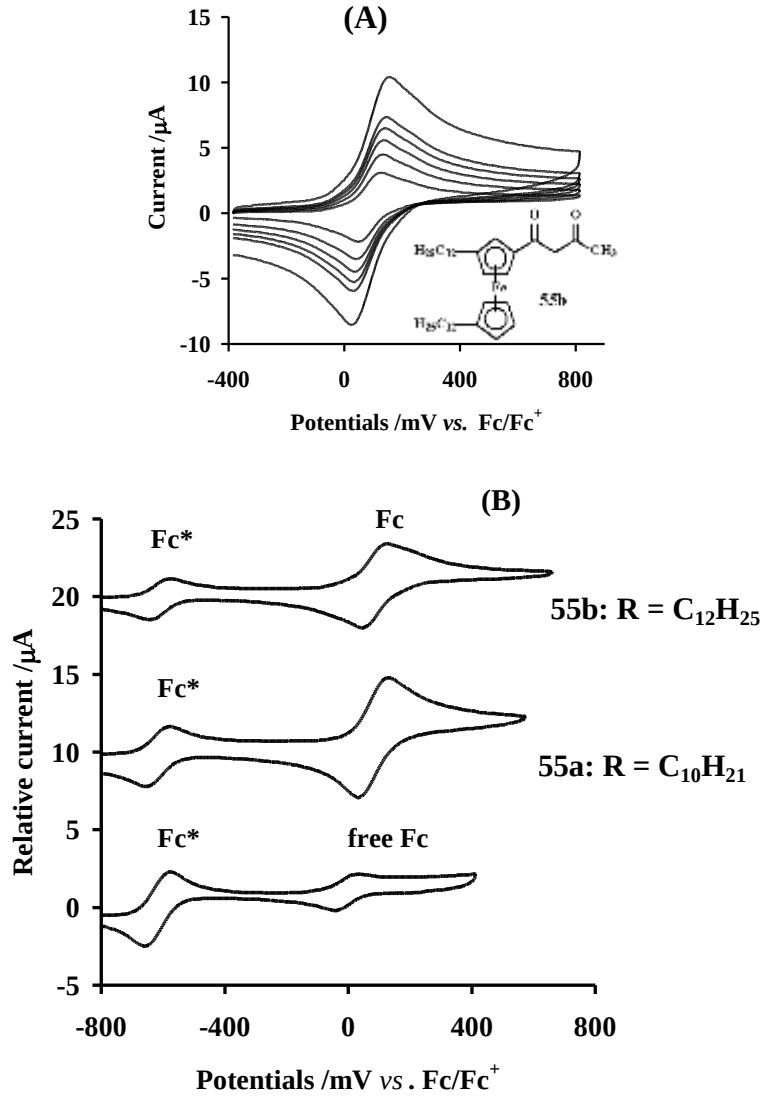

Figure 3. 11: (A) Cyclic voltammograms of *ca.* 0.5 mmol dm^{-3} solution of ferrocene-containing β-diketone, 55b, in CH_2Cl_2 containing 0.05 mol dm^{-3} $[NBu_4][B(C_6F_5)_4]$ at 25 ºC on a glassy carbon working electrode at scan rates 100, 200, 300, 400, 500 and 1000 mVs^{-1}. (B) Cyclic voltammograms of the ferrocene-containing β-diketones 55a and 55b at scan rate of 100 mVs^{-1} under the same conditions as (A). Fc* = decamethylferrocene.

Table 3. 6: Electrochemical data of 0.5 mmol dm^{-3} solutions of β-diketones, 55a and 55b, measured in 0.05 mol dm^{-3} [NBu$_4$][B(C$_6$F$_5$)$_4$]/CH$_2$Cl$_2$ on a glassy carbon working electrode at 25 ^{o}C *vs.* Fc/Fc$^+$ at scan rates between 100 and 1000 mVs^{-1}.

ν / mV s^{-1}	E_{pa} / mV	ΔE_p / mV	$E^{o/}$ / mV	i_{pa} / μA	i_p/i_{pa}	E_{pa} / mV	ΔE_p / mV	$E^{o/}$ / mV	i_{pa} / μA	i_{pc}/i_{pa}
(Cp-C$_{10}$H$_{21}$)Fe(1,3-C$_{10}$H$_{21}$-Cp-COCH$_2$COCH$_3$) {55a}						**(Cp-C$_{12}$H$_{25}$)Fe(1,3-C$_{12}$H$_{25}$-Cp-OCH$_2$COCH$_3$) {55b}**				
100	124	89	79	3.89	0.96	127	81	86	2.79	0.97
200	145	124	83	5.56	0.95	133	91	87	3.79	1.07
300	149	133	82	6.81	0.94	137	100	87	5.11	0.94
400	151	148	77	7.78	0.96	142	109	87	5.52	1.05
500	151	160	71	8.61	1.00	145	115	87	6.52	0.98
1000	158	188	64	11.67	1.00	156	134	89	8.75	0.97

3.5.2.4. Cyclic voltammetry of β-diketones (Cp-C$_{10}$H$_{21}$)Fe(Cp-COCH$_2$CO-Cp)Fe(Cp-C$_{10}$H$_{21}$) and (Cp-C$_{12}$H$_{25}$)Fe(Cp-COCH$_2$CO-Cp)Fe(Cp- C$_{12}$H$_{25}$)

Cyclic voltammetry experiments conducted in a coordinating solvent, acetonitrile, with 0.1 mol dm^{-3} tetrabutylammonium hexafluorophosphate {[NBu$_4$][PF$_6$]} as supporting electrolyte for unsubstituted β-diketone **13e** (Fc-COCH$_2$CO-Fc) showed two poorly resolved ferrocene based waves (**Figure 3.12,** left), with the difference in formal reduction potentials, $\Delta E^{o/}$ = 109 mV *vs.* Ag/AgCl at scan rate 100 mVs^{-1}.[10e] When the same experiment was repeated utilizing the uncoordinative and poorly nucleophilic salt tetrabutylammonium tetrakispentafluorophenylborate {[NBu$_4$][B(C$_6$F$_5$)$_4$] as a supporting electrolyte in the solvent system CH$_2$Cl$_2$/0.5 mol dm^{-3} {[NBu$_4$][B(C$_6$F$_5$)$_4$], two very well-defined reversible cyclic voltammograms were clearly observed with $\Delta E^{o/}$ = 197 mV *vs*. Fc/Fc$^+$ at scan rate 100 mVs^{-1} (**Figure 3.12**, middle). **Figure 3.12** (right) shows the cyclic voltammogram of **13e** with decamethylferrocene (Fc*) as internal standard at 100 mVs^{-1}.

Cyclic voltammograms of β-diketones, **56a** and **13e** at scan rates 100, 200, 300, 400, 500 and 1000 mVs^{-1} are shown in **Figure 3.13**. Cyclic voltammetry experiments carried out with the β-diketones, **56a** and **56b**, also showed two redox waves, labelled as peaks I and II as indicated in **Figure 3.14** for each compound. Linear sweep voltammetry (LSV), confirmed peaks I and II both represent a one-electron transfer process, **Figure 3.14** shows this. The two well-defined peaks I and II were

much better resolved by Osteryoung square wave voltammetry (OSWV), **Figure 3.14** shows this for **56a**.

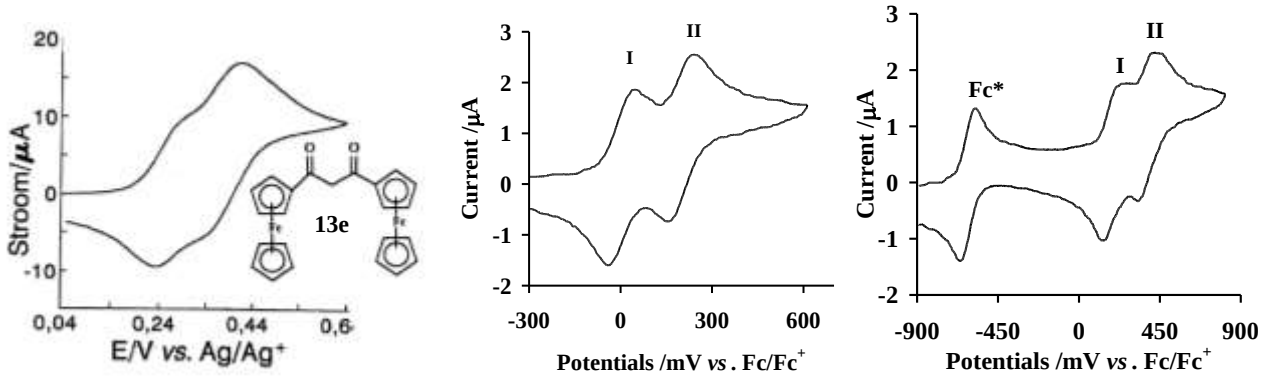

Figure 3. 12 Cyclic voltammograms of 0.5mmol dm^{-3} solutions of Fc-COCH$_2$CO-Fc, 13e, measured in 0.1 mol dm^{-3} [NBu$_4$][PF$_6$]/CH$_3$CN (left, CV is taken from reference 10e) and in 0.05 mol dm^{-3} [NBu$_4$][B(C$_6$F$_5$)$_4$]/CH$_2$Cl$_2$ (middle) as well as the cyclic voltammograms with internal standard under the same conditions as the latter (right) on a glassy carbon working electrode at 25 ºC *vs.* Fc/Fc$^+$ at scan rate of 100 mVs^{-1}. Fc* = decamethylferrocene.

The two observed peaks I and II in CV, LSV and OSWV in **Figure 3.14**, are typical of those associated with a symmetrical dimer, which generates a mixed valent intermediate upon oxidation or reduction. Different formal reduction potentials for side groups on symmetrical complexes in which mixed-valent intermediates are generated are well known in systems that allow electron delocalization, either through bridge mediated paths or from a through-space metal-metal interaction.[10] The inequivalence of the ferrocenyl and ferrocenium groups of such mixed valent intermediate are highlighted in terms of their group electronegativities, with χ_{Fc} = 1.86 and χ_{Fc+} = 2.89.[10a.11] The electrochemical scheme associated with peaks I and II is therefore

$$\mathbf{(R\text{-}Cp)\text{-}Fe^{II}\text{-}(Cp\text{-}COCH_2CO\text{-}Cp)\text{-}Fe^{II}\text{-}(Cp\text{-}R)}$$

$$\mathbf{+e^- \rightleftharpoons -e^-}$$

$$\mathbf{(R\text{-}Cp)\text{-}Fe^{III}\text{-}(Cp\text{-}COCH_2CO\text{-}Cp)\text{-}Fe^{II}\text{-}(Cp\text{-}R)}$$

$$\mathbf{+e^- \rightleftharpoons -e^-}$$

$$\mathbf{(R\text{-}Cp)\text{-}Fe^{III}\text{-}(Cp\text{-}COCH_2CO\text{-}Cp)\text{-}Fe^{III}\text{-}(Cp\text{-}R)}$$

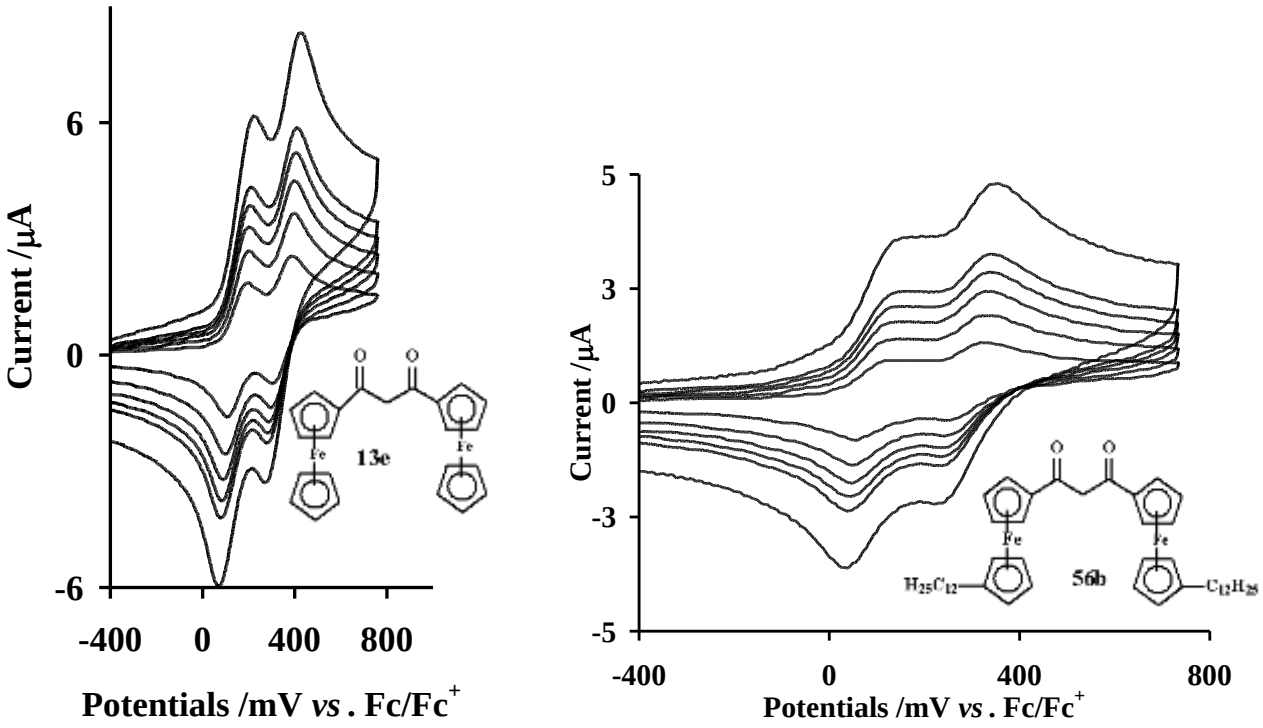

Figure 3. 13 Cyclic voltammograms of 0.5 mmol dm^{-3} solutions of β-diketone, 13e and 56a, in CH_2Cl_2 containing 0.05 mol dm^{-3} $[NBu_4][B(C_6F_5)_4]$ at 25 ºC on a glassy carbon working electrode at scan rate 100, 200, 300, 400, 500 and 1000 mVs^{-1}.

In the first ferrocene-based wave, peak I, of compounds **56a** and **56b**, the redox couple is considered electrochemically reversible and chemically reversible due to peak potential differences, ΔE_p being less than 90 mV, and a current ratio (i_{pc}/i_{pa}) approximately 1, at scan rates below 200 mVs^{-1}. As the scan rate increased to 300 400, 500 and 1000 mVs^{-1} the redox process became electrochemically quasi-reversible (**Table 3.6**). Similar results were observed for peak II, the second ferrocene-based wave, where $83 \geq \Delta E_p \geq 79$ mV and $0.98 \geq i_{pc}/i_{pa} \geq 0.94$, defining the second ferrocene-based system as also electrochemically reversible at scan rates below 200 mVs^{-1}.

From **Table 3.7**, formal reduction potential values, $E^{o/}$, for both peaks I and II, for the β-diketones **56a** and **56b** are approximately in the same range at different scan rates. Upon comparing these results with those obtained for the β-diketone without any R substituent, Fc-$COCH_2CO$-Fc, we observed that $E^{o/}$ for peak I is *ca*. 100 mV more positive for **13e** than for **56a** or **56b**. Peak II is almost 80 mV more positive for **13e** than for **56a** and **56b**. We concluded therefore, that the weakly electron donating R-substituents have lower $E^{o/}$ values compared to the unsubstituted complex **13e**, because it increases the electron density on the Fe^{II} nucleus of the ferrocenyl group.

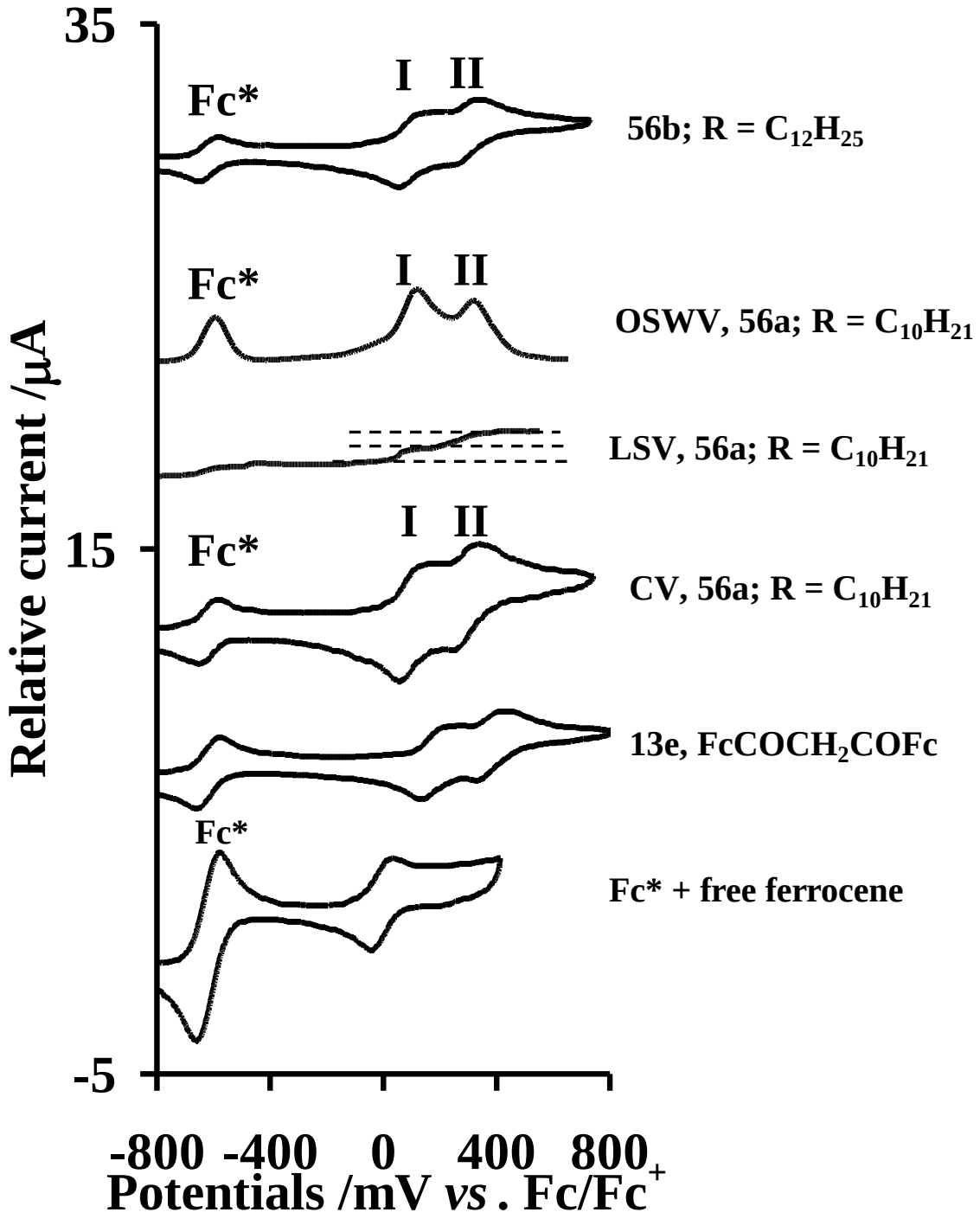

Figure 3. 14: Cyclic voltammograms of 0.5 mmol dm^{-3} solutions of β-diketone, 13e, 56a and 56b, in CH_2Cl_2 containing 0.05 mol dm^{-3} $[NBu_4][B(C_6F_5)_4]$ at 25 ºC on a glassy carbon working electrode at scan rate 100 mVs^{-1}. Linear sweep voltammetry at 2 mVs^{-1} and Osteryoung square wave voltammogram at 10 Hz of 56a are also shown. Fc* = decamethylferrocene.

Upon comparing $E^{o/}$ values of compound series **56** with compound series **53, 54** and **55** it was found that $E^{o/}$ for peak I is substantially (30 – 70 mV) lower. It follows that the electron donating

power of the second substituted ferrocenyl group of **56a** and **56b** is stronger than that of the CH_3 group of compound series **53 – 55**.

Table 3. 7: Electrochemical data for the ferrocene-containing β-diketones, 56a and 56b, in CH_2Cl_2 containing 0.05 mol dm^{-3} tetrabutylammonium tetrakispentafluorophenylborate as a supporting electrolyte at 25 °C.

ν / mV s^{-1}	E_{pa} / mV	ΔE_p / mV	$E^{o/}$ / mV	i_{pa} / μA	i_{pc}/i_{pa}	E_{pa} / mV	ΔE_p / mV	$E^{o/}$ / mV	i_{pa} / μA	i_{pc}/i_{pa}
(Cp-$C_{10}H_{21}$)Fe(Cp-$COCH_2CO$-Cp)Fe(Cp-$C_{10}H_{21}$) peak I {56a}						**(Cp-$C_{10}H_{21}$)Fe(Cp-$COCH_2CO$-Cp)Fe(Cp-$C_{10}H_{21}$) peak II {56a}**				
100	128	74	91	0.981	0.96	331	79	292	1.040	0.94
200	136	90	91	1.478	0.95	332	83	291	1.120	0.98
300	149	106	96	1.777	0.95	339	93	293	1.440	1.04
400	153	112	97	2.043	0.94	341	97	293	1.680	1.03
500	154	109	93	2.296	0.95	343	102	292	1.92	0.99
1000	156	126	93	3.045	0.97	348	111	292	2.52	0.99
(Cp-$C_{12}H_{25}$)Fe(Cp-$COCH_2CO$-Cp)Fe(Cp-$C_{12}H_{25}$) peak I {56b}						**(Cp-$C_{12}H_{25}$)Fe(Cp-$COCH_2CO$-Cp)Fe(Cp-$C_{12}H_{25}$) peak II {56b}**				
100	116	71	81	0.772	0.99	331	78	292	0.667	1.01
200	124	87	81	1.168	0.98	333	88	289	1.095	0.95
300	141	102	90	1.244	0.97	338	96	287	1.238	0.97
400	142	110	84	1.643	0.96	339	99	290	1.476	0.97
500	144	115	85	1.785	0.95	342	102	291	1.524	0.98
1000	147	110	82	2.035	0.95	355	111	299	1.905	0.98
Fc-$COCH_2CO$-Fc Peak I						**Fc-$COCH_2CO$-Fc Peak II**				
100	210	86	167	1.63	1.00	411	71	376	1.41	1.06
200	217	103	166	1.93	0.97	417	96	374	1.70	1.08
300	217	112	165	2.67	0.86	421	111	374	2.00	1.04
400	219	118	166	3.03	0.92	428	115	376	2.22	1.09
500	224	128	166	3.33	0.93	431	125	374	2.52	1.03
1000	233	154	166	4.67	0.86	442	139	377	3.10	1.00

In addition, $E^{o/}$ for peak II is 200 mV (or more) larger than that of peak I and also *ca*. 150 mV larger than for compound series **53** to **55**. This is consistent with the electron withdrawing capability of the $(Cp\text{-}Fe^{III}\text{-}Cp)^+$ group being substantially larger than that of a CH_3 group and that electron delocalization ensures that this effect is communicated to the second redox species of the ligands **56a** and **56b.**

3.6. Substitution Reactions

This section focuses on the kinetics of substitution of the β-diketonato ligands, (Cp-R^2)Fe(R^1-Cp-$COCHCOCH_3$)$^-$ from complexes, **58, 59, 60,** and **61** by 1,10-phenanthroline to give [Rh(phen)(cod)]$^+$ as suggested in goal 5 (Chapter 1) and as illustrated in **Scheme 3.7**.

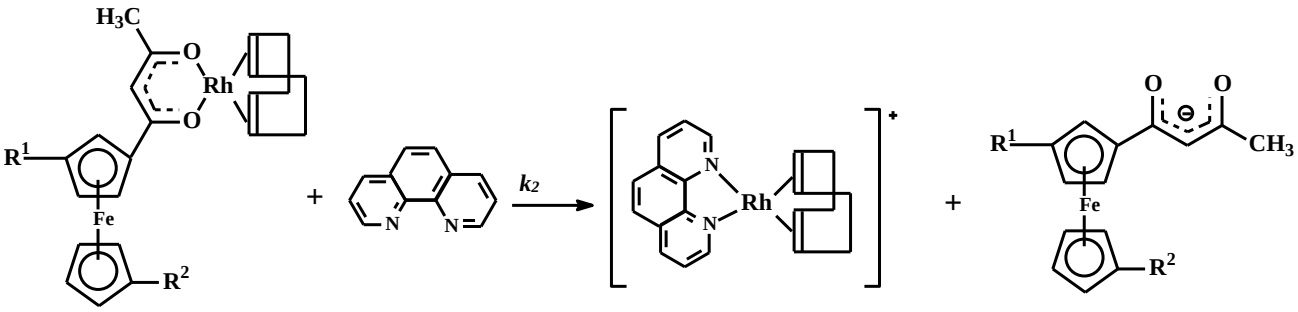

58a: R^1 = H; R^2 = C_9H_{19}, 58b: R^2 = $C_{10}H2_{21}$, 58c: R^2 = $C_{12}H_{25}$, 58d: R^2 = $C_{14}H_{29\ and}$ 58e: R^2 = $C_{18}H_{35}$
59a: R^1 = $C_{10}H_{21\ and}$ 59b: R^1 = $C_{12}H_{25}$; R^2 = H
60a: R^1 = R^2 = $C_{10}H_{21}$ or 60b: R^1 = R^2 = $C_{12}H_{25}$
61a: CH_3 is replaced with ferrocenyl where both ferrocenyls have R^1 = H; R^2 = $C_{10}H_{21}$ or 61b: R^2 = $C_{12}H_{25}$

Scheme 3. 7: Schematic representation of the substitution of (Cp-R^2)-Fe(R^1-Cp-$COCHCOCH_3$)$^-$ ligand from [Rh(β-diketonato)(cod)] complex with 1,10-phenanthroline to liberate [Rh(phen)(cod)]$^+$ with various groups.

3.6.1. The Beer Lambert law

Figures 3.15 – 3.18 show the UV spectra of examples of the four different classes of rhodium complexes **58b, 59a, 60a** and **61a**, and the product of the substitution reaction between [Rh((Cp-R^2)-Fe(R^1-Cp-$COCHCOCH_3$))(cod)] and 1, 10-phenanthroline, namely [Rh(phen)(cod)]$^+$, in acetone at 25 ^oC. From these spectra, and others for the other complexes, the wavelengths where the reaction could conveniently be followed kinetically were determined.

The linear relationships between the absorbance, A, and concentration, c, of [Rh(β-diketonato)(cod)] complex series, **58, 59, 60** and **61** at the experimental wavelengths confirmed the validity of the Beer Lambert law ($A = \varepsilon c l$, with ε = extinction coefficient and l = path length = 1 cm) for each one of these complexes. ε-Values from these plots are summarized in **Table 3.8**. Examples of such linear relationship for [Rh((Cp-R^2)-Fe(R^1-Cp-$COCHCOCH_3$))(cod)] complexes are shown in **Figures 3.15 – 3.18**.

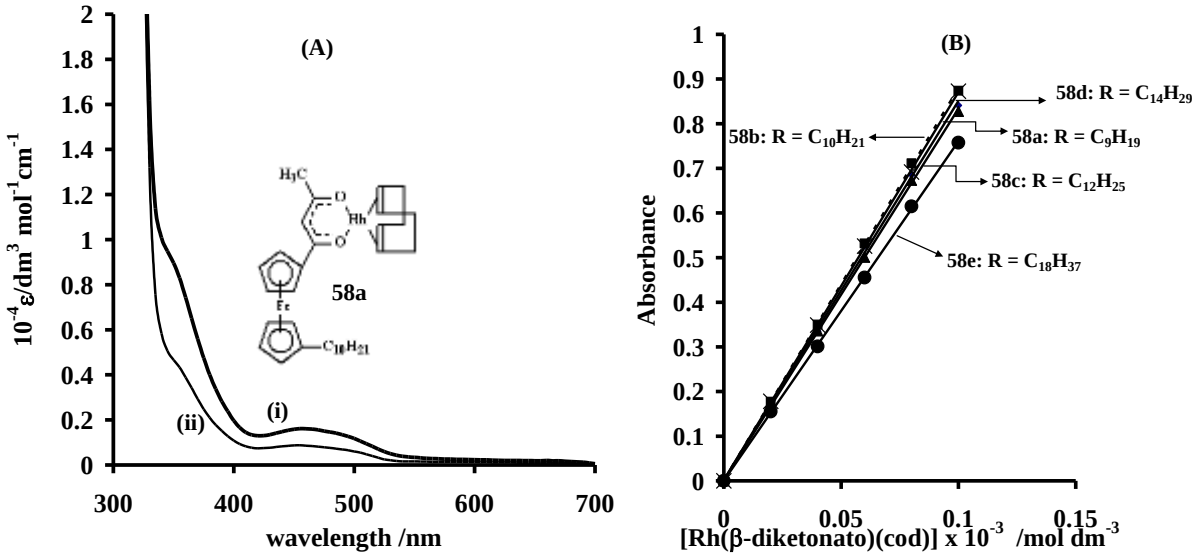

Figure 3. 15: (A) UV spectra of (i, —) [Rh((Cp-$C_{10}H_{21}$)-Fe(Cp-$COCHCOCH_3$))(cod)], 58b and (ii, −) [Rh(phen)(cod)]$^+$ in acetone at 25 ºC. (B) The linear relationship between absorbance and concentration of compound series [Rh((Cp-R)-Fe(Cp-$COCHCOCH_3$))(cod)] complexes at wavelengths reported in Table 3.5 confirm the validity of the Beer Lambert law.

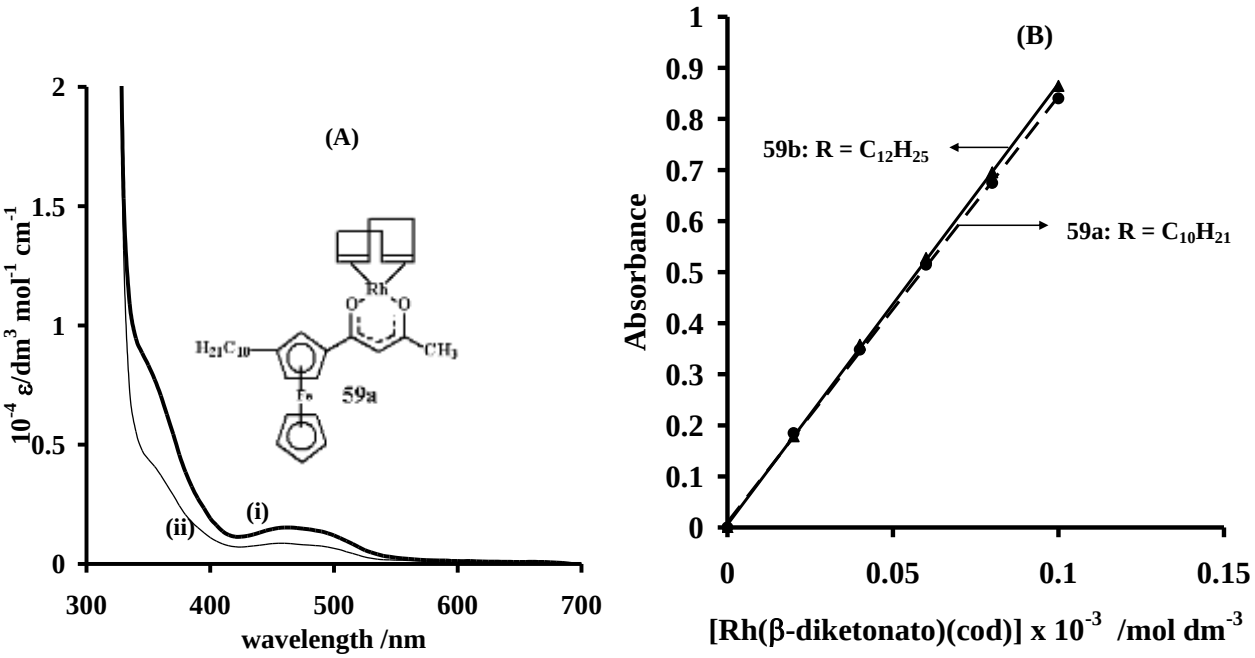

Figure 3. 16: (A) UV spectra of (i, —) [Rh((Cp)-Fe(Cp-$C_{10}H_{21}$-$COCHCOCH_3$))(cod)] and (ii, −) [Rh(phen)(cod)]$^+$ in acetone at 25 ºC. (B) The linear relationship between absorbance and concentration of 59a and 59b complexes at 360 nm confirm the validity of the Beer Lambert law.

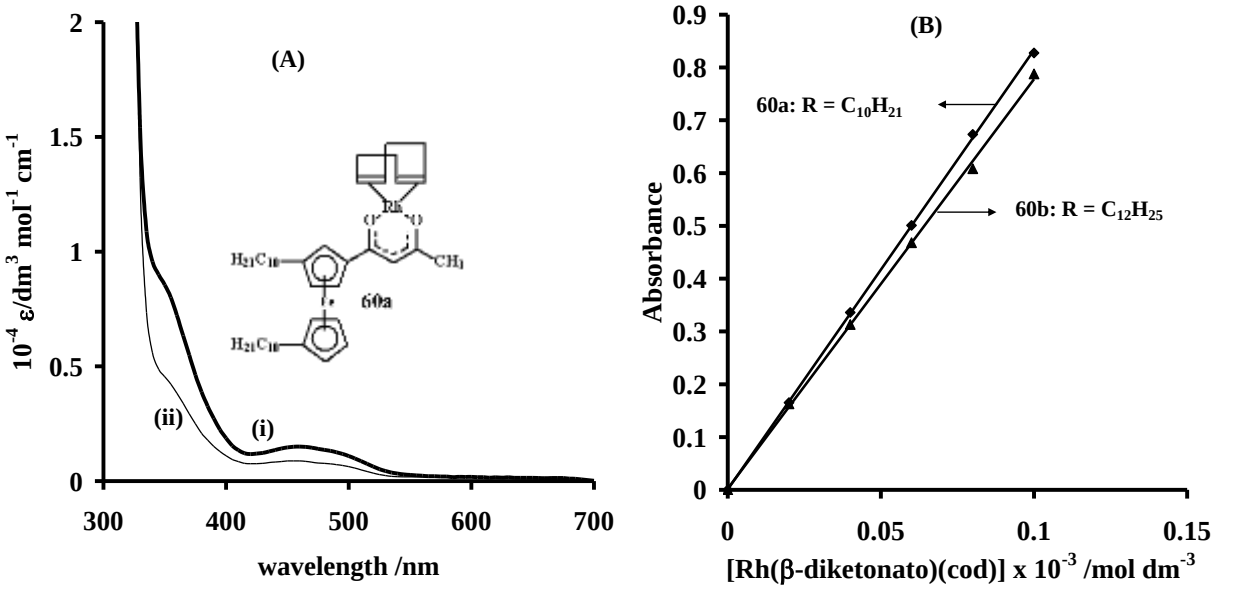

Figure 3. 17: (A) UV spectra of (i, —) [Rh((Cp-$C_{10}H_{21}$)-Fe(Cp-$C_{10}H_{21}$-COCHCOCH$_3$))(cod)] and (ii, −) [Rh(phen)(cod)]$^+$ in acetone at 25 ºC. (B) The linear relationship between absorbance and concentration of 60a and 60b complexes at 360 and 355 nm respectively confirm the validity of the Beer Lambert law.

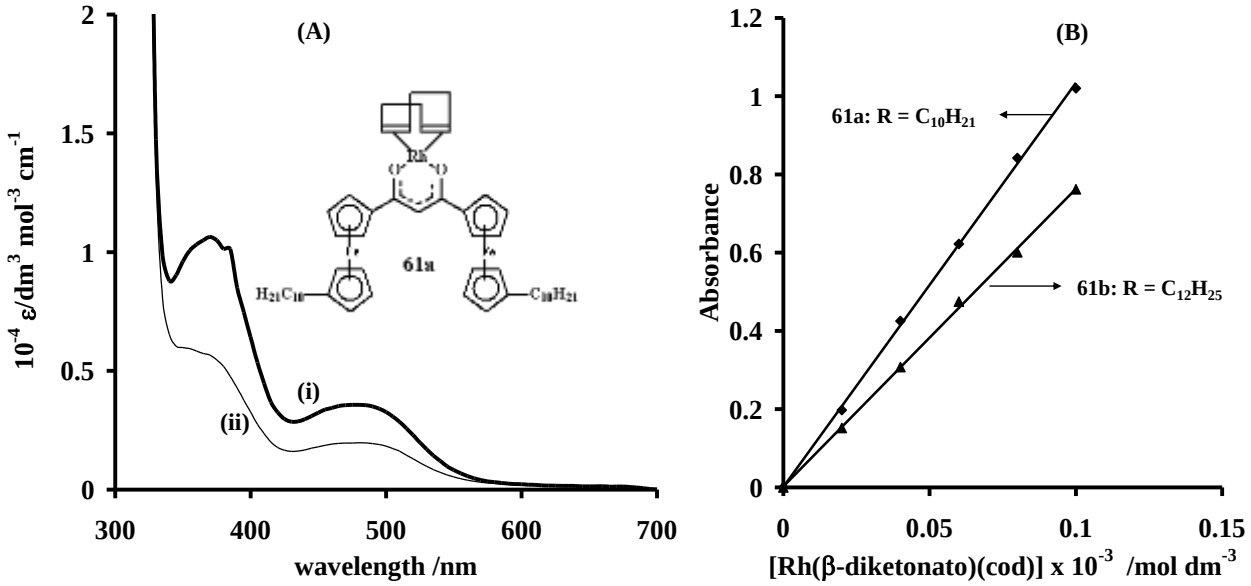

Figure 3. 18: (A) UV spectra of (i, —) [Rh((Cp-$C_{10}H_{21}$)Fe(Cp-COCHCO-Cp)Fe(Cp-$C_{10}H_{21}$))(cod)] and (ii, −) [Rh(phen)(cod)]$^+$ in acetone at 25 ºC. (B) The linear relationship between absorbance and concentration of 61a and 62b complexes at 355 and 360 nm respectively confirm the validity of the Beer Lambert law.

Table 3. 8: Molar extinction coefficients, ε, in brackets at indicated wavelengths, λ_{exp} and λ_{max} for [Rh((Cp-R^2)-Fe(R^1-Cp-$COCHCOCH_3$))(cod)] complexes.

Compound	λ_{exp} /nm (ε /mol^{-1} dm^3 cm^{-3})	λ_{max} /nm (ε /mol^{-1} dm^3 cm^{-3})
58a	355 (7693)	455 (1618)
58b	355 (8302)	455 (1618)
58c	360 (7425)	460 (1619)
58d	360 (7462)	455 (1620)
58e	360 (6778)	460 (1520)
59a	360 (7064)	465 (1529)
59b	360 (7225)	460 (1601)
60a	360 (7237)	460 (1507)
60b	360 (6709)	460 (1478)
61a	355 (10061)	370 (10636) 475 (3575)
61b	355 (6968)	365 (7133) 465 (2368)

3.6.2. Substitution kinetics of [Rh((Cp-R^2)Fe(R^1-Cp-$COCHCOCH_3$))(cod)] with 1,10-phenanthroline

Since rhodium complexes **58 – 61** each obey the Beer Lambert law, the fast kinetics of the substitution of β-diketonato ligands from the [Rh(β-diketonato)(cod)] with 1,10-phenanthroline could be studied spectrophotometrically utilizing a stopped-flow spectrophotometer. The reaction rate constants for the reaction in **Scheme 3.7**, were obtained by following the formation of $[Rh(phen)(cod)]^+$ at wavelengths indicated in **Table 3.8**. All reactions were studied under pseudo first-order conditions with 1,10-phenathroline concentration = (8-80) [Rh(β-diketonato)(cod)] concentration.

For each kinetic run, a plot of volt *vs*. time data was collected and the observed pseudo-first order reaction rate constants, k_{obs}, were determined (**Figure 3.19**). The stopped-flow spectrophotometer that was used in this study uses "volt" as a measurement quantity, "volt" is directly proportional to rhodium complex concentration. Since the reactions are performed under pseudo first-order conditions, "volts" need not be calibrated to concentration because whatever the proportionality

constant is to convert "volts" to concentration, for first-order reactions it cancels during rate constant determination as follows:

$$\ln\frac{(C_0 - C_\infty)}{(C_t - C_\infty)} = \ln\left[\frac{k_v(V_0 - V_\infty)}{k_v(V_t - V_\infty)}\right] = \ln\left(\frac{V_0 - V_\infty}{V_t - V_\infty}\right) = k_{obs}t$$

Here k_v is the proportionality constant that links V with C, and k_{obs} is the pseudo first-order rate constant.

The pseudo first-order rate constants determined experimentally by fitting volt/time data to the equation

$$\ln\left(\frac{V - V_\infty}{V_t - V_\infty}\right) = k_t \text{ (as linear fit)} \qquad \text{or} \qquad V = V_t - (V_t\text{-}V_\infty)e^{-kt} \text{ (an exponential fit)}$$

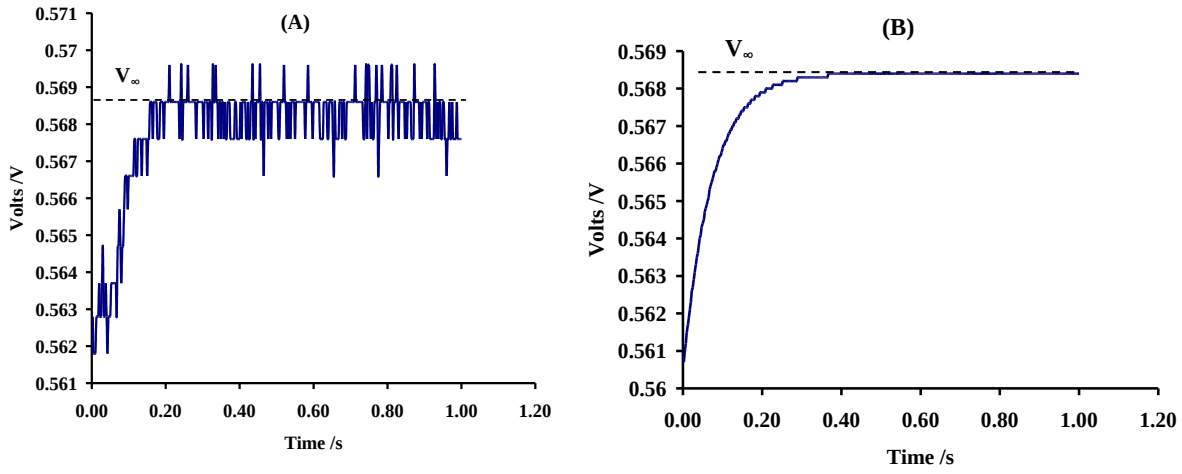

Figure 3. 19: An example of graphs of (A) raw "volt" data and (B) smoothed "volt" data from which the k_{obs} values were determined by the fitting program of the 8X. 18MV applied photophysics stopped flow spectrophotometer. The data shown in the graphs is for the substitution reaction between [Rh((Cp-$C_{10}H_{21}$)Fe(Cp-COCHCOCH$_3$))(cod)], 58b, with 1,10-phenanthroline.

The second-order rate constant, k_2, could not be determined from plots of k_{obs} *vs.* [1,10-phenanthroline] because saturation kinetics were observed (**Figures 3.20(A) – 3.23(A)**). It implied that $k_{obs} \neq k_2$[1,10-phenanthroline], with k_2 a second-order constant.

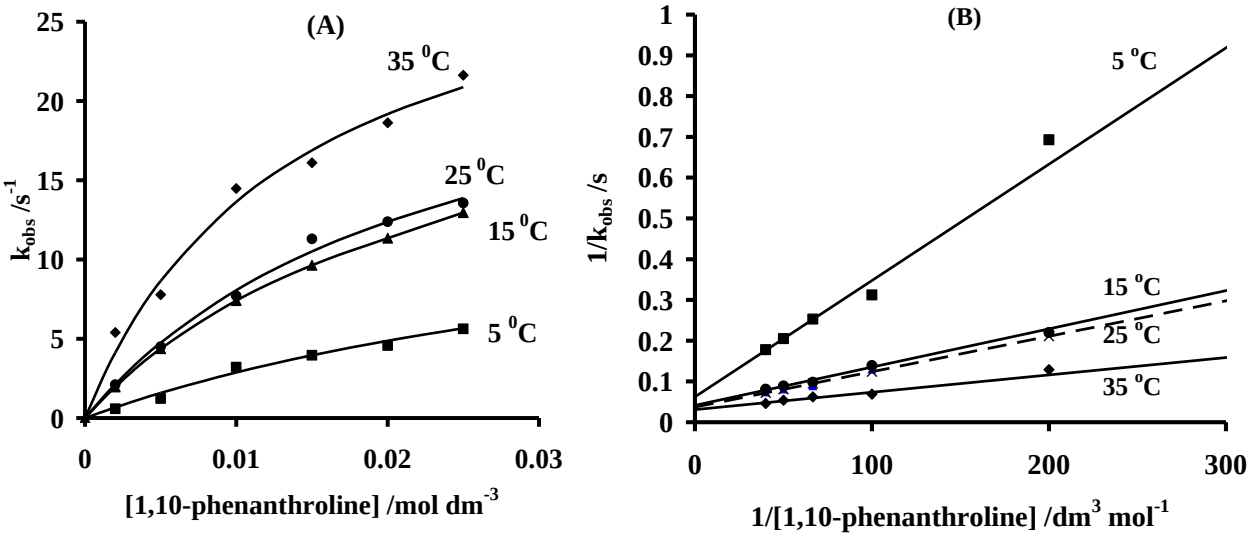

Figure 3. 20: (A) Graphs of pseudo-first order rate constant, k_{obs}, *vs.* [1,10-phenanthroline] over a temperature range of 5, 15, 25 and 35 °C for the [Rh((Cp-$C_{10}H_{21}$)Fe(Cp-$COCHCOCH_3$))(cod)] complex, 58b, pass through the origin implying $k_s \approx 0$. (B) Graphs of $1/k_{obs}$ *vs.* 1/[1,10-phenanthroline] at various temperatures (5, 15, 25 and 35 °C) for the same complex.

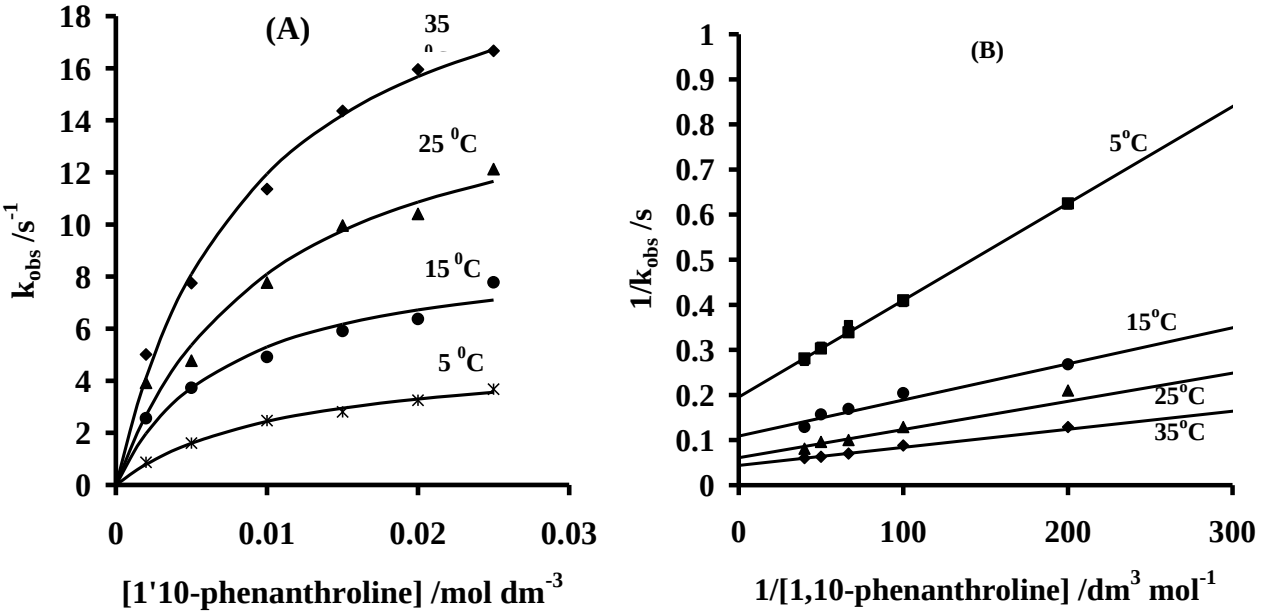

Figure 3. 21: (A) Graphs of pseudo-first order rate constant, k_{obs}, *vs.* [1,10-phenanthroline] over a temperature range of 5, 15, 25 and 35 °C for the [Rh((Cp)Fe(Cp-$C_{10}H_{21}$-$COCHCOCH_3$))(cod)] complex, 59a, pass through the origin implying $k_s \approx 0$. (B) Graphs of $1/k_{obs}$ *vs.* 1/[1,10-phenanthroline] at various temperatures (5, 15, 25 and 35 °C) for the same complex.

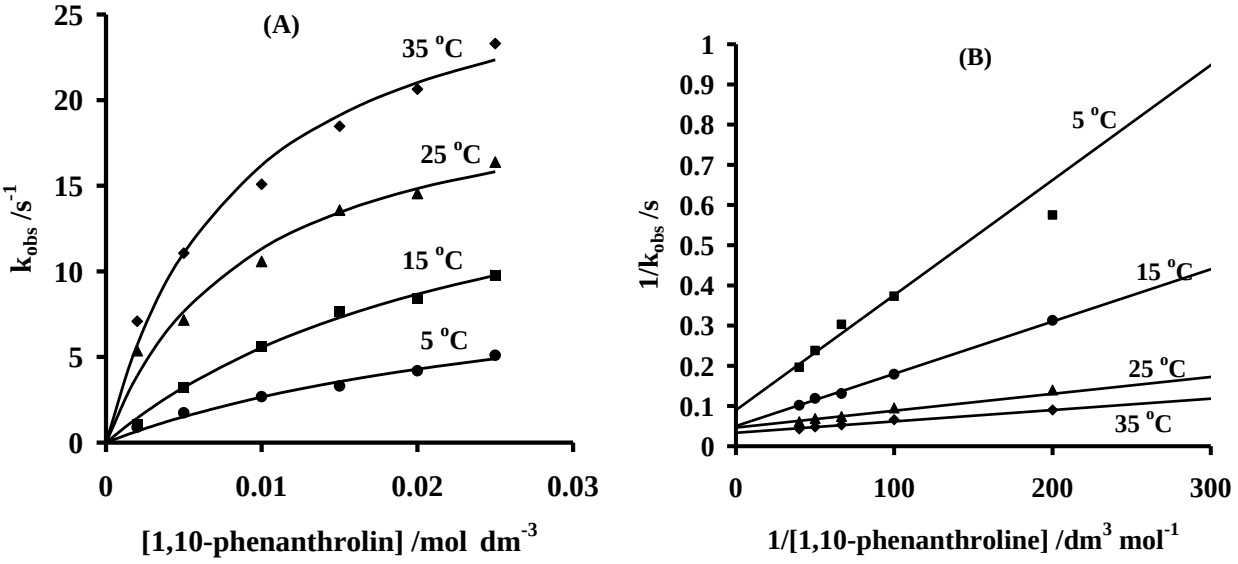

Figure 3. 22: (A) Graphs of pseudo-first order rate constant, k_{obs}, *vs.* [1,10-phenanthroline] over a temperature range of 5, 15, 25 and 35 °C for the [Rh((Cp-$C_{10}H_{21}$)Fe(Cp-$C_{10}H_{21}$-$COCHCOCH_3$))(cod)] complex, 60a, pass through the origin implying $k_s \approx 0$. (B) Graphs of $1/k_{obs}$ *vs.* 1/[1,10-phenanthroline] at various temperatures (5, 15, 25 and 35 °C) for the same complex.

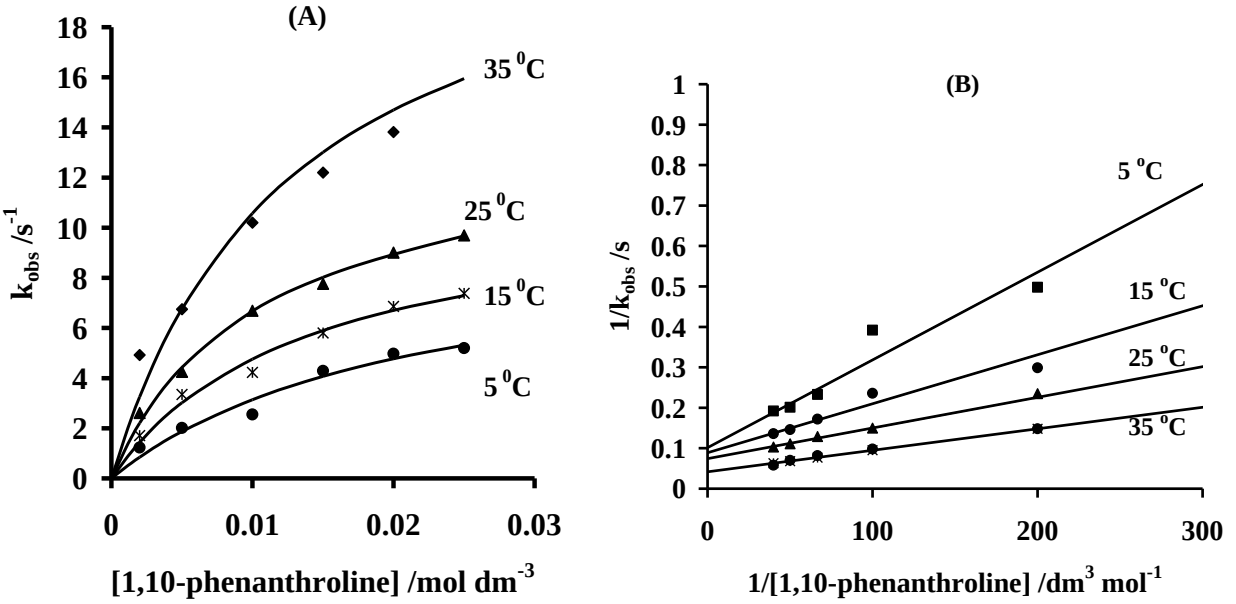

Figure 3. 23: (A) Graphs of pseudo-first order rate constant, k_{obs}, *vs.* [1,10-phenanthroline] over a temperature range of 5, 15, 25 and 35 °C for the [Rh((Cp-$C_{10}H_{21}$)Fe(Cp-COCHCO-Cp)Fe(Cp-$C_{10}H_{21}$))(cod)] complex, 61a, pass through the origin implying $k_s \approx 0$. (B) Graph of $1/k_{obs}$ *vs.* 1/[1,10-phenanthroline] at various temperatures (5, 15, 25 and 35 °C) for the sane complex.

Figures 3.20(A) – 3.23(A) show the non-linear relationship between k_{obs} and [1,10-phenanthroline] for selected complexes. This implies that 1,10-phenanthroline, like reaction centres in proteins, probably does not have unlimited free access to the rhodium nucleus, and more importantly,

apparently forms an intermediate [Rh(β-diketonato)(cod)]·[1,10-phenanthroline] adduct which are so stable that they have a long lifetime to lead to the saturation effect above. This kind of saturation kinetic results was to our knowledge never before detected for simple β-diketonato substitution by 1,10-phenanthroline for complexes of the type [Rh(β-diketonato)(cod)] and must be a consequence of the long chain alkyl substituents on the present complexes. These non-linear k_{obs}-1,10-phenanthroline graphs are consistent with a mechanism involving saturation kinetics. That saturation kinetics actually was observed were confirmed by the linear plots of $1/k_{obs}$ against 1/[1,10-phenanthroline], see **Figures 3.20 – 3.23(B)**.

To explain the observed saturation kinetics the normally accepted rate law for square planar substitution reactions has to be reconsidered. As discussed in Chapter 2, square-planar substitution reactions with incoming ligand 1,10-phenanthroline normally obey the general rate law

$$\text{Rate} = (k_s + k_2[\text{1,10-phenanthroline}])[\text{Rh}(\beta\text{-diketonato})(\text{cod})] = k_{obs}[\text{Rh}(\beta\text{-diketonato})(\text{cod})] \qquad \textbf{equation 3. 8}$$

for the stoichiometric reaction

$$1,10-phenanthroline + [Rh(\beta-diketonato)(cod)] \xrightarrow{k_2} [Rh(1,10-phenanthroline)(cod)]^+ + (\beta-diketonato)^-$$

In **equation 3.8**, k_2, is the second-order reaction rate constant. The first-order rate constant, k_s, refers to the bimolecular attack of the solvent, in this case acetone, on the [Rh(β-diketonato)(cod)] complexes. For the reactions studied, all plots of k_{obs} *vs*. 1,10-phenanthroline concentration passes through the origin, suggesting k_s is approximately zero for acetone as solvent. The observed zero intercept was expected because the displacement rate of the bidentate β-diketonato ligand by a monodentate solvent would be much slower or even approach zero compared to the displacement rate by the bidentate ligand 1,10-phenanthroline. To accommodate saturation kinetics, though, it means the substitution reaction must follow the following general mechanism:

$$\text{Rh}(\beta\text{-diketonato})(\text{cod}) + \text{1,10-phenanthroline} \underset{}{\overset{K}{\rightleftharpoons}} \text{Rh}(\beta\text{-diketonato})(\text{cod})\bullet(\text{1,10-phenthroline})$$

$$\text{Rh}(\beta\text{-diketonato})(\text{cod})\bullet(\text{1,10-phenthroline}) \xrightarrow{k_2} \text{Rh(1,10-phenanthroline)(cod)}^+ + (\beta\text{-diketonato})^-$$

Under ordinary substitution conditions, K would be slow and k_2 fast (Chapter 2). The present system involving long-chain alkyl substituents on the β-diketonato ligand have influenced the

mechanism to change, with K being fast and k_2 the rate determining step. The rate law for the above mechanism can be derived as follows.[12]

$$\text{Rate} = \frac{k_2 K[1,10-phenanthroline][Rh(\beta-diketonato]}{1+K[1,10-phenanthroline]}$$

$$= k_{obs}[Rh(\beta-diketonato)(cod)]$$

$$\text{with } k_{obs} = \frac{k_2 K[1,10-phenanthroline]}{1+K[1,10-phenanthroline]} \qquad (\mathbf{1})$$

if [1,10-phenanthroline] >> [Rh(β-diketonato)(cod)]. This is the case under pseudo first-order conditions. By inverting expression (**1**) it follows that

$$\frac{1}{k_{obs}} = \frac{1}{k_2 K[1,10-phenanthroline]} + \frac{1}{k_2}$$

implying plots of $1/k_{obs}$ *vs*. 1/[1,10-phenanthroline] should be linear with slope $1/k_2K$ and y-intercept $1/k_2$. **Figures 3.20(B) – 3.23(B)** shows this to be the case.

Scheme 3.8 attempts to structurally visualize the mechanism above. It is proposed that the breaking of β-diketonato Rh-O bond adjacent to the ferrocenyl group is slow and that this slow bond breaking step is the result of the long chain alkyl substituents on the ferrocenyl group. If the rate determining step involves the carbonyl group adjacent to the methyl group, it is difficult to understand why the mechanism changed to a process where the rate determining step following the formation of the first five coordinate intermediate, rather than the rate determining step being the formation of the five coordinate intermediate itself.

The rate constants for the respective substitution reactions between the [Rh(β-diketonato)(cod)] complex and 1,10-phenanthroline are dependent on the ability of 1,10-phenanthroline to associate with the square planar [Rh(β-diketonato)(cod)]. Fast rotation of the cyclopentadienyl ring with the R^2 substituent blocks access for the 1,10-phenanthroline to rhodium from the bottom. The R^1 substituent may also fold in such a way to block access to the rhodium centre. Hence, it can only attack from the top or one side. This means not all approaches of 1,10-phenanthroline to the rhodium complex will necessary lead to a reaction. This is also consistent with a saturation

mechanism. Rate constants k_2 and equilibrium constants, K for each reaction at 25 °C are summarized in **Table 3.9**.

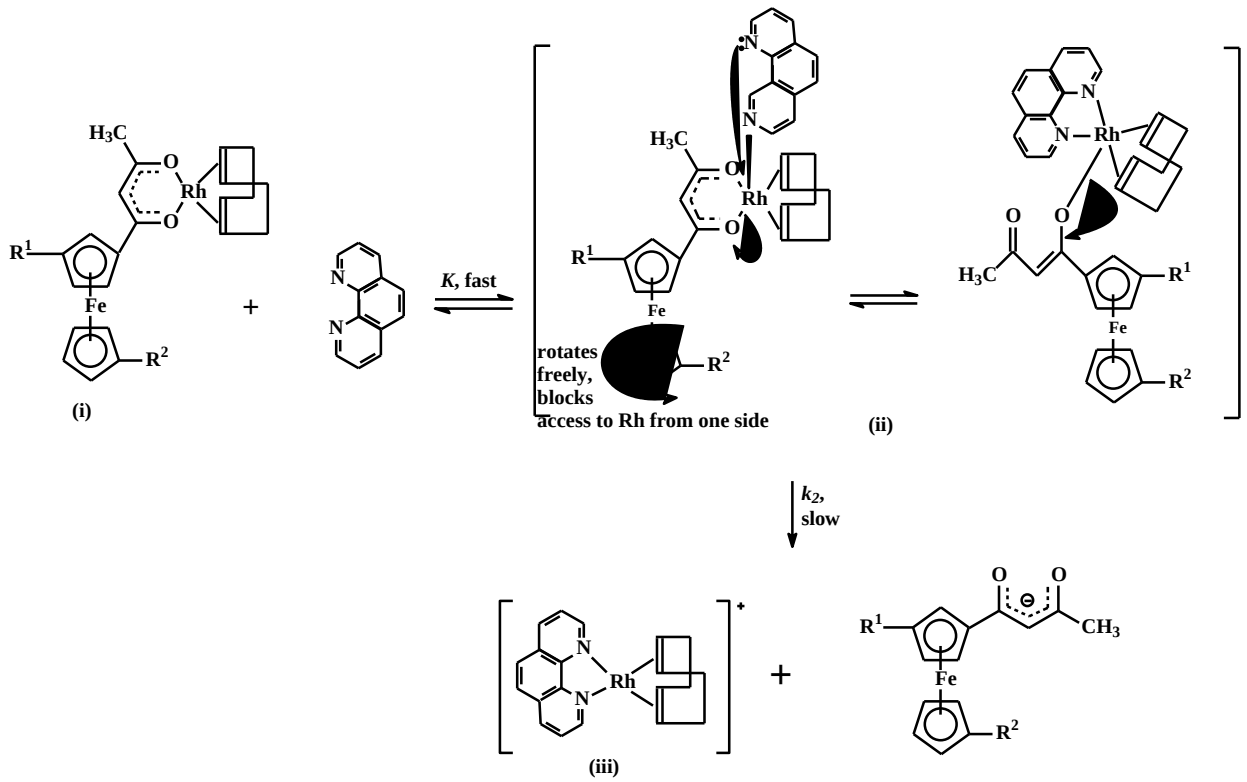

R^1 = H; 58a: $R^2 = C_9H_{19}$, 58b: $R^2 = C_{10}H2_{21}$, 58c: $R^2 = C_{12}H_{25}$, 58d: $R^2 = C_{14}H_{29}$ and 58e: $R^2 = C_{18}H_{35}$
R^2 = H; 59a: $R^1 = C_{10}H_{21}$ and 59b: $R^1 = C_{12}H_{25}$
60a: $R^1 = R^2 = C_{10}H_{21}$ or 60b: $R^1 = R^2 = C_{12}H_{25}$
61a: CH_3 is replaced with ferrocenyl where both ferrocenyls have R^1 = H; $R^2 = C_{10}H_{21}$ or 61b: $R^2 = C_{12}H_{25}$

Scheme 3. 8: Schematic representation of the proposed association mechanism for the substitution reaction between the [Rh((Cp-R^2)Fe(R^1-Cp-COCHCOCH$_3$))(cod)] complexes with 1,10-phenanthroline.

From **Table 3.9**, it is clear that the second-order rate constants, k_2, of complexes **58a – 58e**, are approximately the same and that K values are also in the same range. Complexes **59a** and **59b** showed faster second-order kinetics than compounds **58b – 58c**. The second-order rate constant, k_2, for complexes **60a** and **60b** were a factor of 2 higher than for both **58** and **59** species, but a factor of 2 rate enhancement is not large enough to be considered kinetically important. Compounds **61a** and **61b**, k_2, were also observed to react at a rate not significantly different from the other complexes.

We concluded therefore, that the effect R-substituents with chain length varying from C_9H_{19}–$C_{18}H_{37}$, and with one or more than one R-group substituent, had very little effect on the reaction rate. The fastest reaction, that is for **60b**, was barely four times faster than the slowest reaction, that for **61b**.

Table 3. 9: The second-order rate contants, k_2 as well as the equilibrium constant, K, for the substitution of the ligand $((Cp\text{-}R^2)Fe(R^1\text{-}Cp\text{-}COCHCOCH_3))^-$ with 1,10-phenanthroline in $[Rh((Cp\text{-}R^2)Fe(R^1\text{-}Cp\text{-}COCHCOCH_3))(cod)]$ complexes at 25 °C. R substituents are indicated in the table. For 61a and 61b, the CH_3 group was replaced with a second ferrocenyl group where both ferrocenyl groups have the indicated substituents on the second cyclopentadienyl ring.

Compound	k_2 $dm^3\ mol^{-1}\ s^{-1}$	K ratio
58a: $R^2 = C_9H_{19}$, $R^1 = H$	1798	0.0158
58b: $R^2 = C_{10}H_{21}$, $R^1 = H$	1157	0.0376
58c: $R^2 = C_{12}H_{25}$, $R^1 = H$	1191	0.0301
58d: $R^2 = C_{14}H_{29}$, $R^1 = H$	1753	0.0430
58e: $R^2 = C_{18}H_{37}$, $R^1 = H$	1234[j]	0.0315
59a: $R^1 = C_{10}H_{21}$, $R^2 = H$	1594	0.0606
59b: $R^1 = C_{12}H_{25}$, $R^2 = H$	1643	0.0386
60a: $R^1 = R^2 = C_{10}H_{21}$	2377	0.0460
60b: $R^1 = R^2 = C_{12}H_{25}$	2678	0.0483
61a: $R^2 = C_{10}H_{21}$, $R^1 = H$	1321	0.0742
61b: $R^2 = C_{12}H_{25}$, $R^1 = H$	612	0.0502

In order to eliminate the possibility that something other than the long chain alkyl substituents was the cause for the saturation kinetics, such as solvent, the substitution of the β-diketonato ligand $(Fc\text{-}COCHCOCH_3)^-$ from $[Rh(Fc\text{-}COCHCOCH_3)(cod)]$, **24c**, by 1,10-phenanthroline was also investigated.

It was found in previous research that β-diketonato substitution from $[Rh(FcCOCHCOCH_3)(cod)]$, **24c**, by 1,10-phenanthroline in methanol has a linear 1,10-phenanthroline dependency passing through the origin.[11] This means methanol does not take part in the substitution reaction. Compounds of the present study do not dissolve in methanol, because these compounds possess extreme lipophylic characteristics. Hence acetone was utilized as solvent during substitution reaction.

To prove acetone was not the cause of the saturation kinetics, $(Fc\text{-}COCHCOCH_3)^-$ substitution from $[Rh(Fc\text{-}COCHCOCH_3)(cod)]$ was re-investigated in acetone as solvent. **Figure 3.24** shows plots of k_{obs} against [1,10-phenanthroline] for this reaction. In contrast to the results found for compound series **58 – 61**, non-zero intercepts were observed from these graphs indicating that the solvent acetone does contribute in a solvent substitution path towards the reaction mechanism of $[Rh(FcCOCHCOCH_3)(cod)]$. Rate constants, k_s, associated with the solvent path are indicated in **Figure 3.24**.

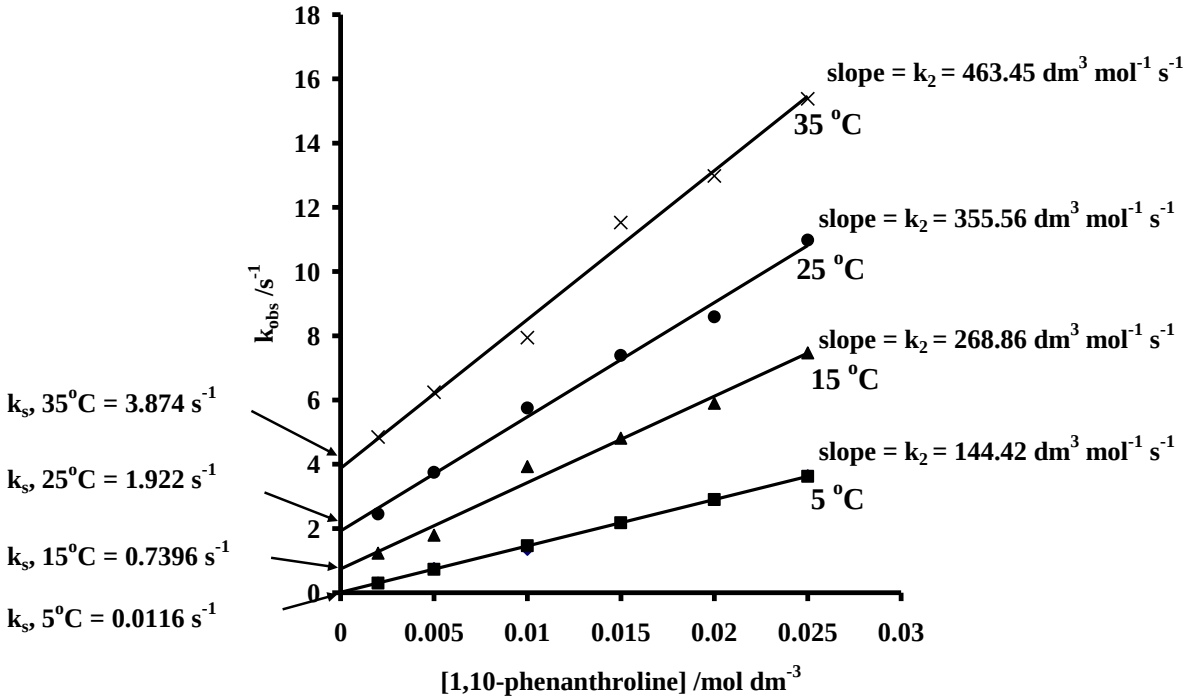

Figure 3. 24: Graphs of k_{obs} *vs.* [1,10-phenanthroline] at various temperatures for the [Rh(FcCOCHCOCH$_3$)(cod)] complex in acetone, had intercept of 0.0116 at 5 ºC, 0.739 at 15 ºC, 1.922 at 25 ºC and 3.869 at 35 ºC. Fc = ferrocenyl.

The long chain alkyl substituted complexes of this study showed no solvent path. This observation is considered consistent with the view that the long chain alkyl substituted complexes are so lipophylic that they tend to form minute micelles which interact favourably with 1,10-phenanthroline, but not with hydrophilic acetone. If this argument is correct, one would expected substitution reaction rates of rhodium complexes, **58 – 61**, to be faster than for the [Rh(FcCOCHCOCH$_3$)(cod)] complex. This was actually found; see **Table 3.9** and **Figure 3.24**.

Additional proof for the micelle theory proposed to explain our results, is that the [Rh(β-diketonato)(cod)] complex of this study is more reactive in cancer treatment than [Rh(FcCOCHCOCH$_3$)(cod)] complex (cytotoxic results are discussed later in this Chapter). This is consistent with lipid solubility of rhodium complex series **58 – 61** being higher than that of [Rh(FcCOCHCOCH$_3$)(cod)].

Activation parameters were obtained from a fit of k_2 and temperature data to the Eyring equation[13] **(equation 3.9)**. All the mathematical fits were carried out using the fitting program MINSQ.[14]

$$\ln (k_2/T) = -\Delta H^* /(RT) + \Delta S^* /R + \ln (R/Nh) \qquad \textbf{equation 3. 9}$$

The Eyring plots of ln (k_2/T) *vs*. 1/T for the substitution reaction for the rhodium complexes **58c, 59b, 60b** and **61b** as selected examples, over a temperature range of 5 to 35 ^{o}C, are given in **Figures 3.25 – 3.28**. A summary of the second-order rate constant, k_2, the equilibrium constant, *K*, as well as the entropy of activation ΔS*, activation enthalpy ΔH* and the Gibbs activation free energy ΔG*, which were determined from the temperature study, are given in **Table 3.10**. The Gibbs activation free energy was obtained from **equation 3.10**.

$$\Delta G^* = \Delta H^* - T\Delta S^* \qquad \textbf{equation 3. 10}$$

The entropy values obtained from the temperature study have large negative values for all the substitution reactions. The negative entropy values also suggest an association mechanism, just as the saturation mechanism data did, and it thus provides more credibility to the mechanism suggested in **Scheme 3.8**. The values obtained for the Gibbs free energy were also found to be roughly in the same range for all the compounds indicating the transition state in **Scheme 3.8** forms with equal ease and independent of side chain length and substitution position for complexes having alkyl substituent chain length C_9H_{19} – $C_{18}H_{37}$.

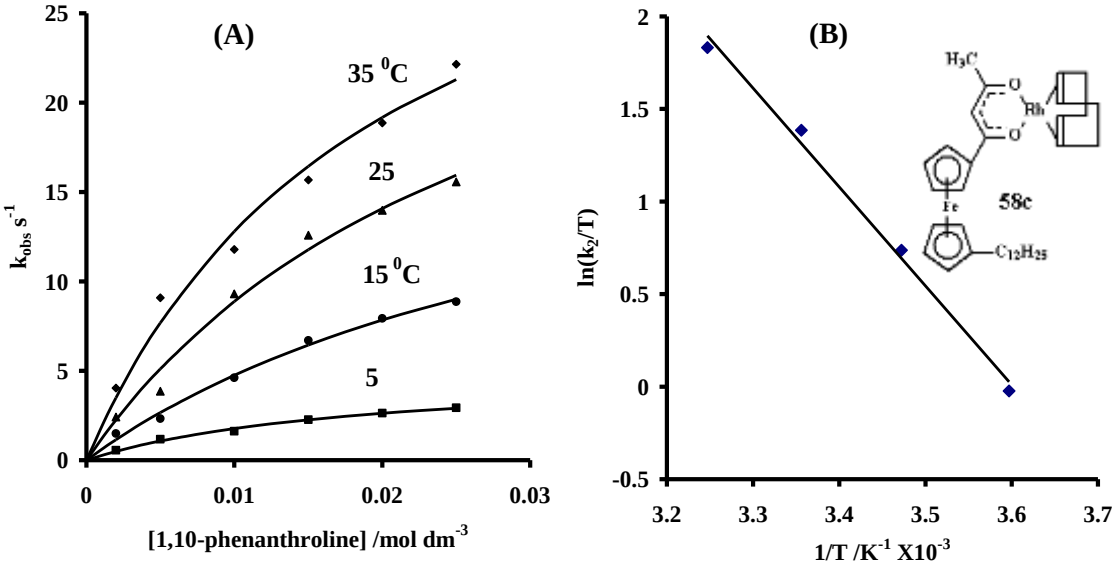

Figure 3. 25: (A) Graphs of pseudo-first order rate constant, k_{obs}, *vs*. [1,10-phenanthroline] at temperatures of 5, 15, 25 and 35 ^{o}C for the [Rh((Cp-$C_{12}H_{25}$)Fe(Cp-COCHCOCH$_3$))(cod)] complex, 58c. (B) The Eyring plots of ln(k_2/T) *vs.* 1/T for the substitution reaction of [Rh((Cp-$C_{12}H_{25}$)Fe(Cp-COCHCOCH$_3$))(cod)] with 1,10-phenanthroline at various temperatures (5, 15, 25 and 35 ^{o}C).

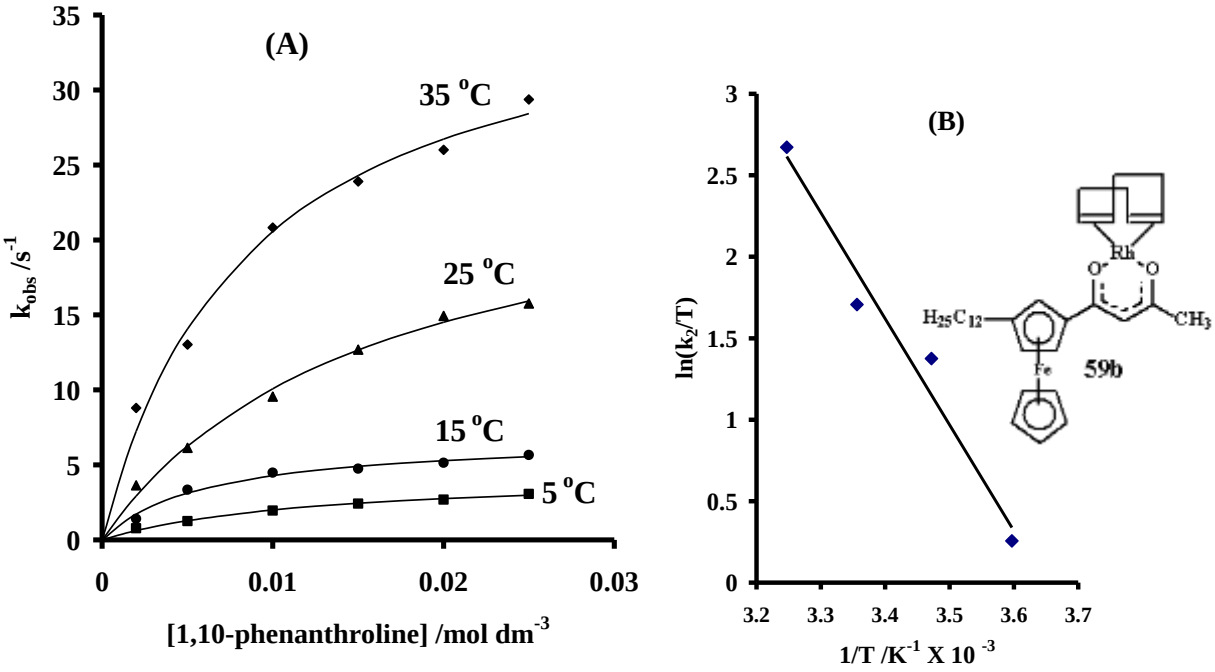

Figure 3. 26: (A) Graphs of pseudo-first order rate constant, k_{obs}, *vs.* [1,10-phenanthroline] at temperatures of 5, 15, 25 and 35 ºC for the [Rh((Cp)Fe(Cp-$C_{12}H_{25}$-COCHCOCH$_3$))(cod)] complex. (B) The Eyring plots of ln(k_2/T) *vs.* 1/T for the substitution reaction of [Rh((Cp)Fe(Cp-$C_{12}H_{25}$-COCHCOCH$_3$))(cod)] with 1,10-phenanthroline at various temperatures (5, 15, 25 and 35 ºC).

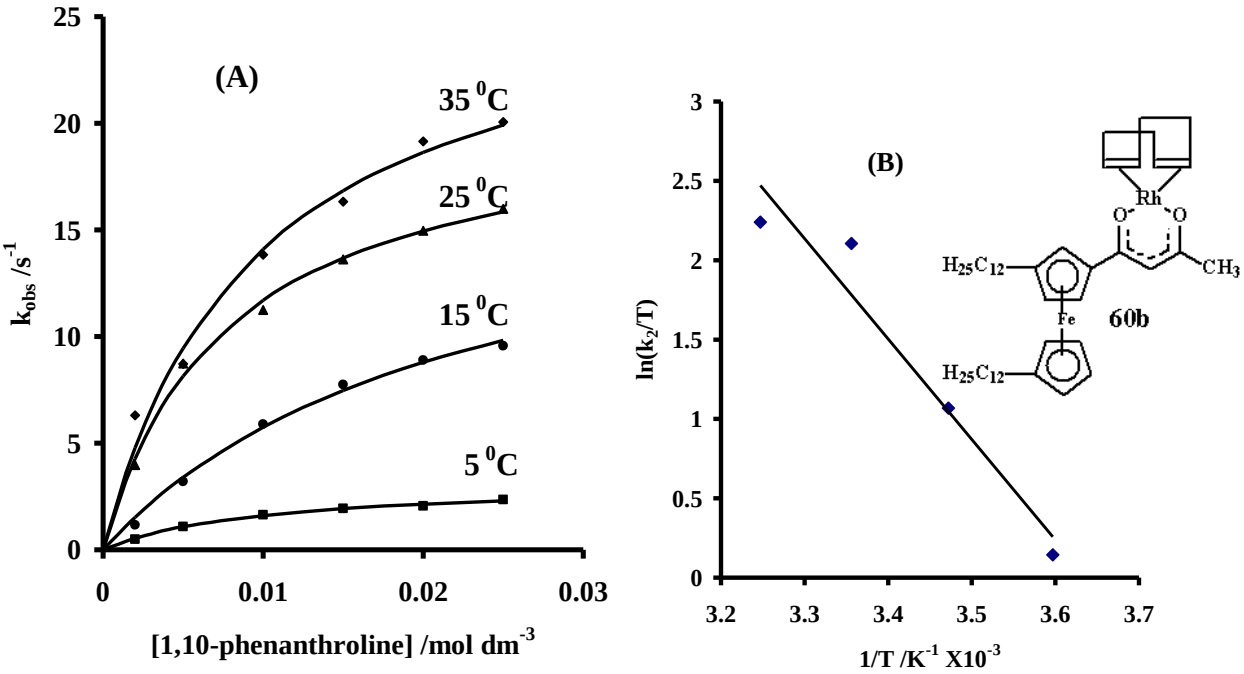

Figure 3. 27: (A) Graphs of pseudo-first order rate constant, k_{obs}, *vs.* [1,10-phenanthroline] at temperatures of 5, 15, 25 and 35 ºC for the [Rh((Cp-$C_{12}H_{25}$)Fe(Cp-$C_{12}H_{25}$-COCHCOCH$_3$))(cod)] complex. (B) The Eyring plots of ln(k_2/T) *vs.* 1/T for the substitution reaction of [Rh((Cp-$C_{12}H_{25}$)Fe(Cp-$C_{12}H_{25}$-COCHCOCH$_3$))(cod)] with 1,10-phenanthroline at various temperatures (5, 15, 25 and 35 ºC).

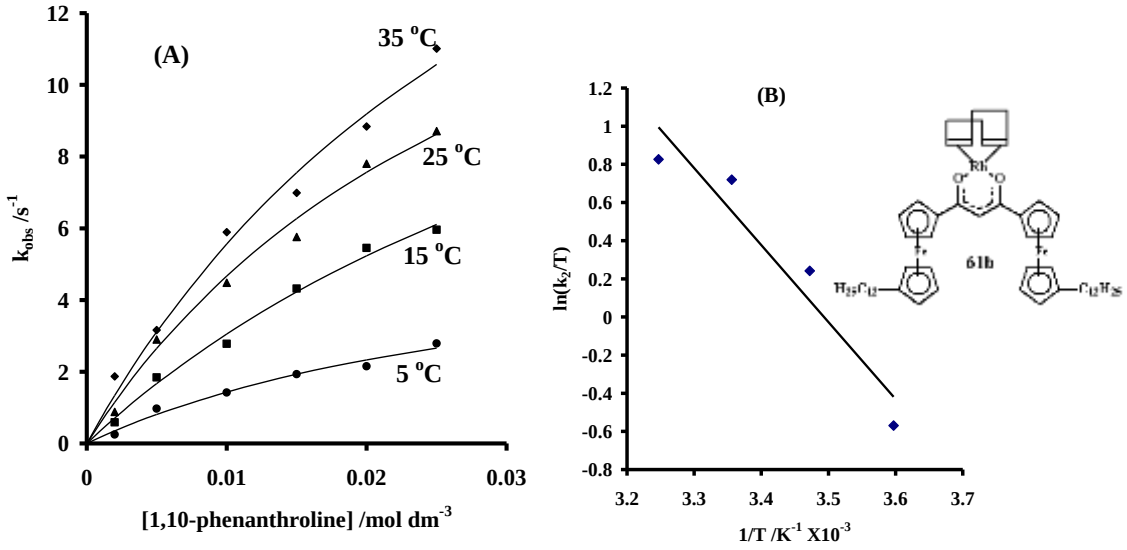

Figure 3. 28: **A) Graphs of pseudo-first order rate constant, k_{obs}, *vs.* [1,10-phenanthroline] at temperatures of 5, 15, 25 and 35 °C for the [Rh((Cp-$C_{12}H_{25}$)Fe(Cp-COCHCO-Cp)Fe(Cp-$C_{12}H_{25}$))(cod)] complex passing through the origin implying $k_s \approx 0$. (B) The Eyring plots of ln(k_2/T) *vs.* 1/T for the substitution reaction of [Rh((Cp-$C_{12}H_{25}$)Fe(Cp-COCHCO-Cp)Fe(Cp-$C_{12}H_{25}$))(cod)] with 1,10-phenanhtroline at various temperatures (5, 15, 25, 35 °C).**

Table 3. 10: **Values of the second-order rate constants, k_2, and the activation parameters, activation enthalpy, ΔH*, activation entropy, ΔS* and Gibbs activation free energy, ΔG* of the reaction of different [Rh((Cp-R^2)Fe(Cp-R^1-$COCHCOCH_3$))(cod)] complexes, 58, 59, 60 and 61 with 1,10-phenanthroline in acetone medium at 25 °C.**

Compound	k_2 dm^3 mol^{-1} s^{-1}	*K* ratio	ΔH* kJ mol^{-1}	ΔS* JK^{-1} mol^{-1}	ΔG* kJ mol^{-1}
58a	1798	0.0158	68.47	-168.37	118.64
58b	1157	0.0376	39.12	-180.22	92.83
58c	1139	0.030	44.34	-178.33	97.48
58d	1753	0.0430	59.49	-171.82	110.69
58e	1234	0.0315	61.32	-168.47	111.52
59a	1594	0.0606	35.87	-181.37	89.92
59b	1643	0.0386	54.01	-173.83	105.81
60a	2377	0.046	55.06	-173.47	106.75
60b	2678	0.0483	53.18	-174.27	105.11
61a	1321	0.0742	31.02	-183.57	85.72
61b	612	0.0502	33.52	-183.46	88.19

3.6.3. Cyclic voltammetry of [Rh(β-diketonato)(cod)] complexes

The main focus of this section was to investigate, by means of cyclic voltammetry, the electrochemical behaviour of the ferrocenyl fragment of the β-diketonato ligand coordinated to rhodium as well as that of the rhodium centre itself. Analyses of the structure of the [Rh(β-diketonato)(cod)] complex series **58, 59, 60** and **61**, show two redox centres: the iron centre of the ferrocenyl group that behaves electrochemically as shown in **equation 3.11**, as well as the square planar rhodium(I) centre that behaves electrochemically according to **equation 3.12**.

$$\mathbf{Fc} \rightleftharpoons \mathbf{Fc^+ + e^-} \qquad \textbf{equation 3. 11}$$

$$\mathbf{Rh^I} \rightleftharpoons \mathbf{Rh^{II} + e^-} \qquad \textbf{equation 3. 12}$$

The overall reaction sequence observed during a cyclo voltammetric sweep is

$$\mathbf{Fc\ Rh^I} \rightleftharpoons \mathbf{Fc^+\ Rh^I} \rightleftharpoons \mathbf{Fc^+\ Rh^{II}} \qquad \textbf{equation 3. 13}$$

3.6.3.1. Cyclic voltammetry of [Rh((Cp-R)Fe(Cp-COCHCOCH$_3$))(cod)] complexes with R = C$_9$H$_{19}$, 58a; C$_{10}$H$_{21}$, 58b; C$_{12}$H$_{25}$, 58c; C$_{14}$H$_{29}$, 58d and C$_{18}$H$_{37}$, 58e

Figure 3.29 shows the cyclic voltammograms of **58b** (left) and [Rh(Fc-COCHCOCH$_3$)(cod)], **24c** (right). They demonstrate the general trend observed for all [Rh(β-diketonato)(cod)] complexes at different scan rates and also clearly indicate that Rh(I) is oxidized at more positive potentials than where the ferrocenyl fragment is redox active. Cyclic voltammograms of [Rh((Cp-R)Fe(Cp-COCHCOCH$_3$))(cod)], **58a – 58e**, at 100 mVs^{-1} are shown in **Figure 3.30**. Results are summarized in **Table 3.11**.

From **Table 3.11** it can be seen that for [Rh((Cp-R)Fe(Cp-COCHCOCH$_3$))(cod)] complexes **58a – 58e**, ΔE_p < 90 mV and current ratios (i_{pc}/i_{pa}) approached 1 for the ferrocenyl wave. This indicated that the Fc/Fc$^+$ couple is an electrochemically and chemically reversible one-electron transfer redox process at slow scan rates (100 mVs^{-1}). However, at higher scan rates the Fc/Fc$^+$ couple showed

electrochemically quasi-reversible behaviour with ΔE_p < 150 mV and chemically irreversible behaviour with current ratios in the range $0.91 \geq i_{pc}/i_{pa} \geq 0.70$.

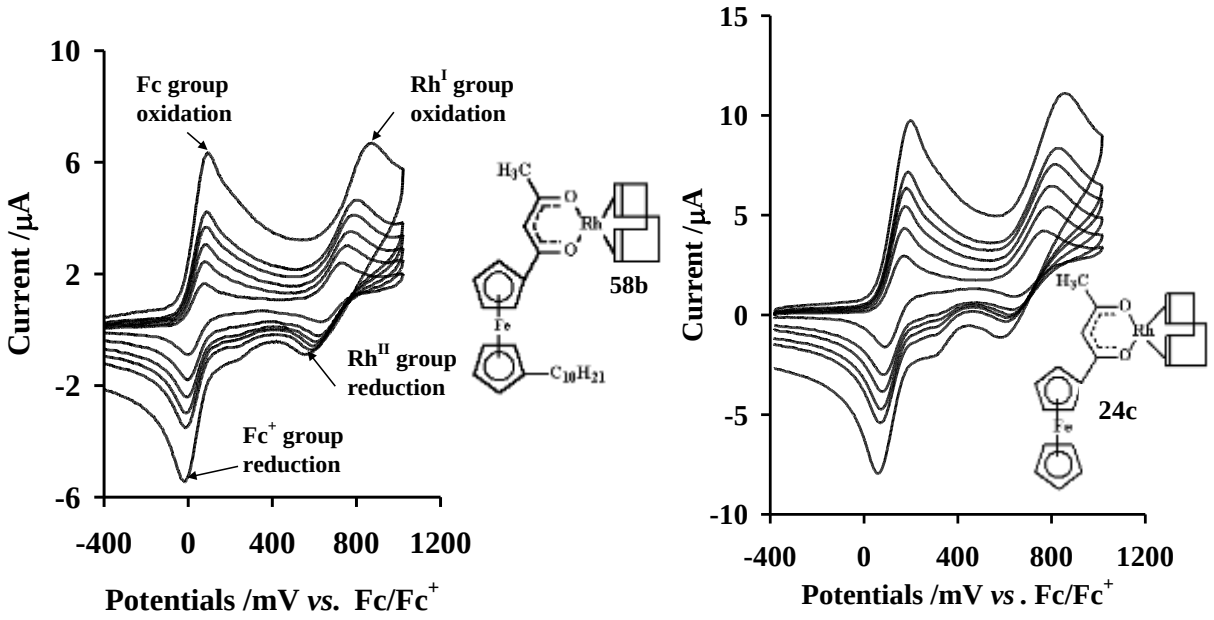

Figure 3. 29: Cyclic voltammograms of 0.5 mmol dm^{-3} solution of rhodium complexes 58b (left) and [Rh(Fc-COCHCOCH$_3$)(cod)], 24c (right) measured in 0.05 mol dm^{-3} [NBu$_4$][B(C$_6$F$_5$)$_4$]/CH$_2$Cl$_2$ on a glassy carbon working electrode at 25 ºC *vs.* Fc/Fc$^+$ at scan rates 100, 200, 300, 400, 500 and 1000 mVs^{-1}.

The Rh^I nucleus of complexes **58a – 58e** is electrochemically quasi reversible oxidized to Rh^{II} at E_{pa} > 500 mV because ΔE_p is smaller than 150 mV but larger than 90 mV. Current ratios i_{pc}/i_{pa} < 0.60 at different scan rates (**Table 3.11**) indicated chemically irreversible redox processes.

From **Table 3.11**, it was observed that the ferrocenyl-based formal reduction potentials remained in the same range as the R substituents on ferrocenyl group increases from C_9H_{19} to $C_{18}H_{37}$ (**58a – 58e**). Scientifically, a mere difference in formal reduction potential value of approximately 5 mV is regarded as insignificant. Ferrocene-based formal reduction potential values of complexes **58a - 58e** were compared to that of the rhodium complex **24c** which has no alkyl substituent on the ferrocenyl group, [Rh(Fc-COCHCOCH$_3$)(cod)]. It was found that $E^{o/}$ for **24c** was 129 mV, approximately 100 mV more positive than the alkyl substituted rhodium complex series **58**. This trend is graphically indicated in **Figure 3.31** (left). The fall of $E^{o/}$ values upon moving from **24c** to **58a** and analogous complexes is consistent with the R substituents being weakly electron donating alkyl groups. However, no significant distinguishable different electronic effects could be

identified that clearly indicated that the $C_{18}H_{37}$ chain has a different electron donating power than the C_9H_{19} chain.

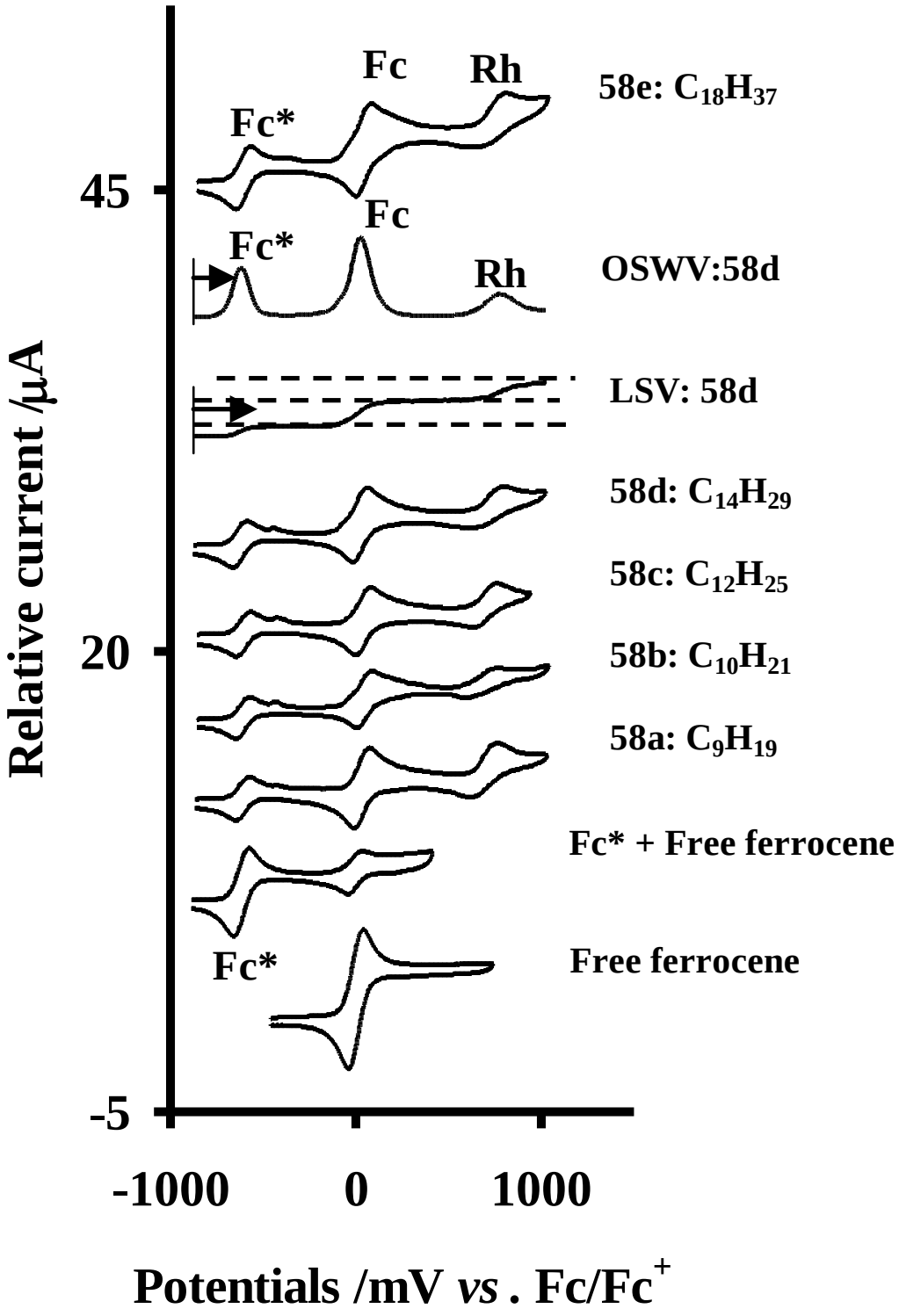

Figure 3. 30: Cyclic voltammograms of 0.5 mmol dm^{-3} solutions of [Rh((Cp-R)Fe(Cp-COCHCOCH$_3$))(cod)] complexes, 58a – 58e, measured in 0.05 mol dm^{-3} [NBu$_4$][B(C$_6$F$_5$)$_4$]/CH$_2$Cl$_2$ on a glassy carbon working electrode at 25 ºC *vs*. Fc/Fc$^+$ at scan rate 100 mVs^{-1}. Osteryoung square wave voltammogram (OSWV) at 10 Hz and linear sweep voltammetry (LSV) at 2 mV s^{-1} of 58d are also shown. Fc* = decamethylferrocene as an internal standard.

Table 3. 11: Electrochemical data of 0.5 mmol dm^{-3} solution of [Rh((Cp-R)Fe(Cp-COCHCOCH$_3$))(cod)] complexes, 58a – 58d, measured in 0.05 mol dm^{-3} [NBu$_4$][B(C$_6$F$_5$)$_4$]/CH$_2$Cl$_2$ on a glassy carbon working electrode at 25 ^{o}C *vs.* Fc/Fc$^+$ at scan rates 100, 200, 300, 400, 500 and 1000 mVs^{-1}.

Ferrocenyl group						Rhodium group				
v mVs^{-1}	E_{pa} /mV	ΔE_p /mV	$E^{o/}$ /mV	i_{pa} /mA	i_{pc}/i_{pa}	E_{pa} /mV	ΔE_p /mV	$E^{o/}$ /mV	i_{pa} /mA	i_{pc}/i_{pa}
58a; R = C$_9$H$_{19}$										
100	79	82	39	2.01	1.02	740	142	686	1.77	0.57
200	84	94	37	2.92	0.86	784	176	705	2.13	0.54
300	86	101	41	3.53	0.83	827	221	708	3.40	0.45
400	90	105	38	3.96	0.83	836	267*	711	2.67	0.32
500	96	111	40	4.48	0.81	850	285*	715	3.09	0.28
1000	110	141	40	6.30	0.78	895	328*	731	4.17	0.20
58b; R = C$_{10}$H$_{21}$										
100	75	68	41	1.50	0.95	763	139	693	1.31	0.55
200	80	79	38	2.14	0.81	785	190	690	1.70	0.59
300	83	90	38	2.57	0.80	799	207*	692	1.95	0.59
400	87	96	39	3.43	0.74	814	240*	694	2.26	1.00
500	90	104	38	3.73	0.76	829	250*	704	2.46	1.21
1000	96	110	41	5.49	0.70	888	352*	712	3.48	1.29
58c; R = C$_{12}$H$_{25}$										
100	73	76	37	2.14	0.90	733	89	689	1.61	0.53
200	85	93	39	2.86	0.91	740	110*	685	2.16	0.23
300	89	98	40	3.79	0.85	769	130*	704	2.60	-
400	93	108	41	4.19	0.84	785	146*	712	2.91	-
500	100	122	39	4.88	0.88	793	150*	718	3.30	-
1000	102	126	37	6.73	0.80	822	162*	741	4.37	-
58d; R = C$_{14}$H$_{29}$										
100	75	84	41	2.18	0.98	753	106	700	2.01	0.38
200	83	100	41	2.90	0.85	765	120*	703	2.86	-
300	86	109	40	3.64	0.83	782	160*	702	3.43	-
400	88	112	40	4.14	0.84	791	178*	702	4.00	-
500	93	123	40	4.57	0.81	805	198*	706	4.57	-
1000	102	142	39	6.64	0.80	831	234*	714	6.45	-

*Values estimated due to poor E_{pc} peak resolution.

Table 3.11: (continued) Electrochemical data of 0.5 mmol dm^{-3} solution of [Rh((Cp-R)Fe(Cp-$COCHCOCH_3$))(cod)] complexes 58e and [Rh($FcCOCHCOCH_3$)(cod)], measured in 0.05 mol dm^{-3} $[NBu_4][B(C_6F_5)_4]/CH_2Cl_2$ on a glassy carbon working electrode at 25 ºC *vs.* Fc/Fc^+ at scan rates 100 – 1000 mVs^{-1}.

	Ferrocenyl group					Rhodium group				
ν mVs^{-1}	**E_{pa} /mV**	**ΔE_p /mV**	**$E^{o/}$ /mV**	**i_{pa} /μA**	**i_{pc}/i_{pa}**	**E_{pa} /mV**	**ΔE_p /mV**	**$E^{o/}$ /mV**	**i_{pa} /μA**	**i_{pc}/i_{pa}**
58e; R = $C_{18}H_{37}$										
100	73	80	33	3.25	0.98	801	148	727	2.68	0.48
200	71	92	25	4.85	0.84	832	204*	711	4.03	-
300	75	100	25	5.87	0.82	855	252*	713	4.96	-
400	81	106	25	6.71	0.86	865	266*	732	5.58	-
500	83	114	26	7.49	0.79	879	290*	734	6.10	-
1000	91	132	25	10.14	0.81	913	354*	736	8.58	-
[Rh(Fc-$COCHCOCH_3$)(cod)] = 24c										
100	168	78	129	2.76	0.94	763	112	707	2.46	0.51
200	169	80	129	4.09	0.64	781	133	714	3.15	0.43
300	173	91	127	5.01	0.61	787	159	707	3.67	0.44
400	178	102	127	5.97	0.61	798	170	713	4.38	0.33
500	186	114	129	6.63	0.58	808	172	720	4.90	0.27
1000	196	136	128	8.90	0.59	844	252	718	6.53	0.16

*Values estimated due to peak broadening at E_{pc}.

As far as the Rh centre is concerned, **Figure 3.31** (right) clearly showed that Rh^{II} formation occurred at increasingly larger formal reduction potentials with longer alkyl substituents. At present this result is considered to be consistent with the possibility that the rhodium center is more effectively masked perhaps *via* encapsulation from the electrode surface with longer alkyl chain substituents on the second cyclopentadienyl ring. Such a scenario would require more electrochemical work to oxidize Rh^I with long chain substituents and imply larger $E^{o/}$ values.

The linear sweep voltammograms trace of **58d**, as representative example for complex series **58** (**Figure 3.30**), confirmed that the ferrocenyl/ferrocenium and Rh^I/Rh^{II} couples both are one-electron transfer processes because the linear sweep voltammogram currents for both processes were approximately equal. Osteryoung square wave voltammograms also demonstrated clearly by peak broadness and low peak currents that the rate of electron transfer for Rh^I nucleus is much slower than for the ferrocenyl centre.

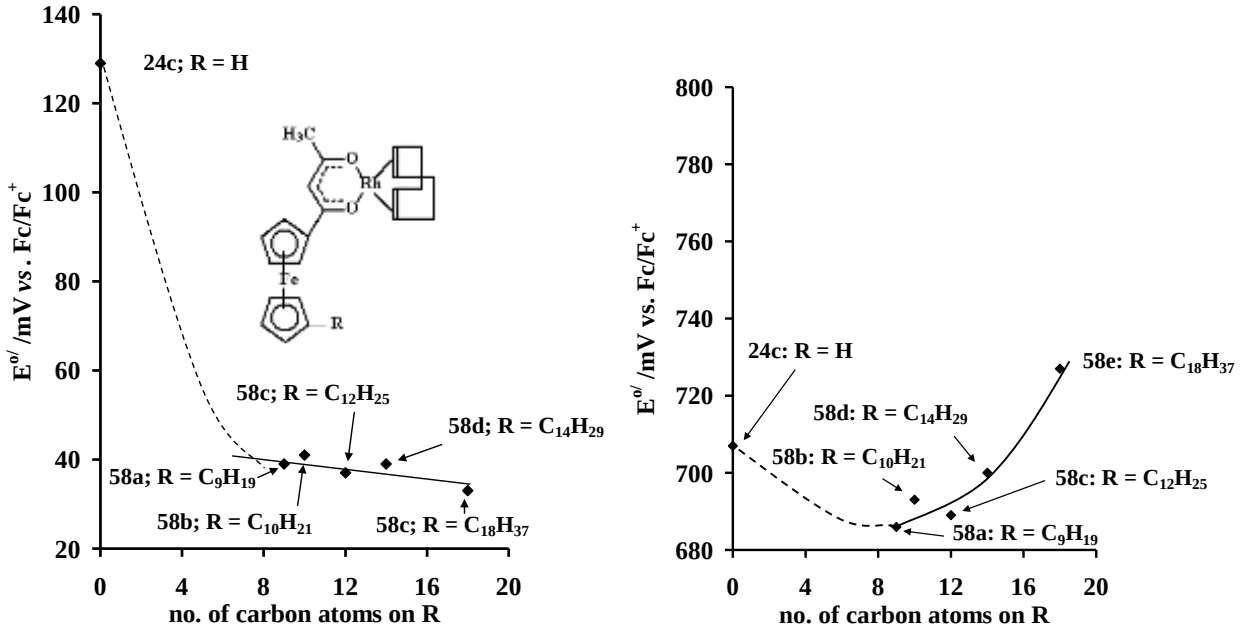

Figure 3. 31: Relationship between the formal reduction potentials, $E^{o/}$, of the ferrocenyl group (left) and rhodium group (right) and the number of carbon atoms on R substituent. The broken line represents a tentative trend for shorter chain alkyl substituent, but experimental data is not yet available.

3.6.3.2. Cyclic voltammetry of [Rh((Cp)Fe(Cp-$C_{10}H_{21}$-COCHCOCH$_3$))(cod)], 59a and [Rh((Cp)Fe(Cp-$C_{12}H_{25}$-COCHCOCH$_3$))(cod)], 59b, complexes

Cyclic voltammograms of rhodium complexes, **59a** and **59b**, (**Figure 3.32, Table 3.12**) show an electrochemically reversible redox wave at $E^{o/} \approx 26 - 33$ mV, which corresponds to the formal reduction potential of the ferrocenyl group of the β-diketonato ligand coordinated to [Rh(β-diketonato)(cod)]. $\Delta Ep < 90$ mV at slow scan rates (100 mVs^{-1}). The rhodium(I) nucleus at 625 – 690 mV exhibited electrochemically and chemically irreversible redox behaviour since $\Delta E_p > 150$ mV even at slow scan rates and $i_{pc}/i_{pa} < 0.6$.

Comparison of formal reduction potentials, $E^{o/} = 1/2(E_{pa} + E_{pc})$, from **Table 3.12** showed that $E^{o/}$ values for the ferrocene-based cyclic voltammograms of wave **59a** and **59b** were in the same range as that of **58b** and **58c** (**Table 3.11,** 100 mVs^{-1} scan rate). They differed at most ~ 5 mV. It was then concluded that it does not matter on which ring the R-substituents on the ferrocenyl group is. The same substituents on different rings have the same influence on the formal reduction potentials of the ferrocenyl group. The same could not be said for the Rh^{II}/Rh^{I} couple.

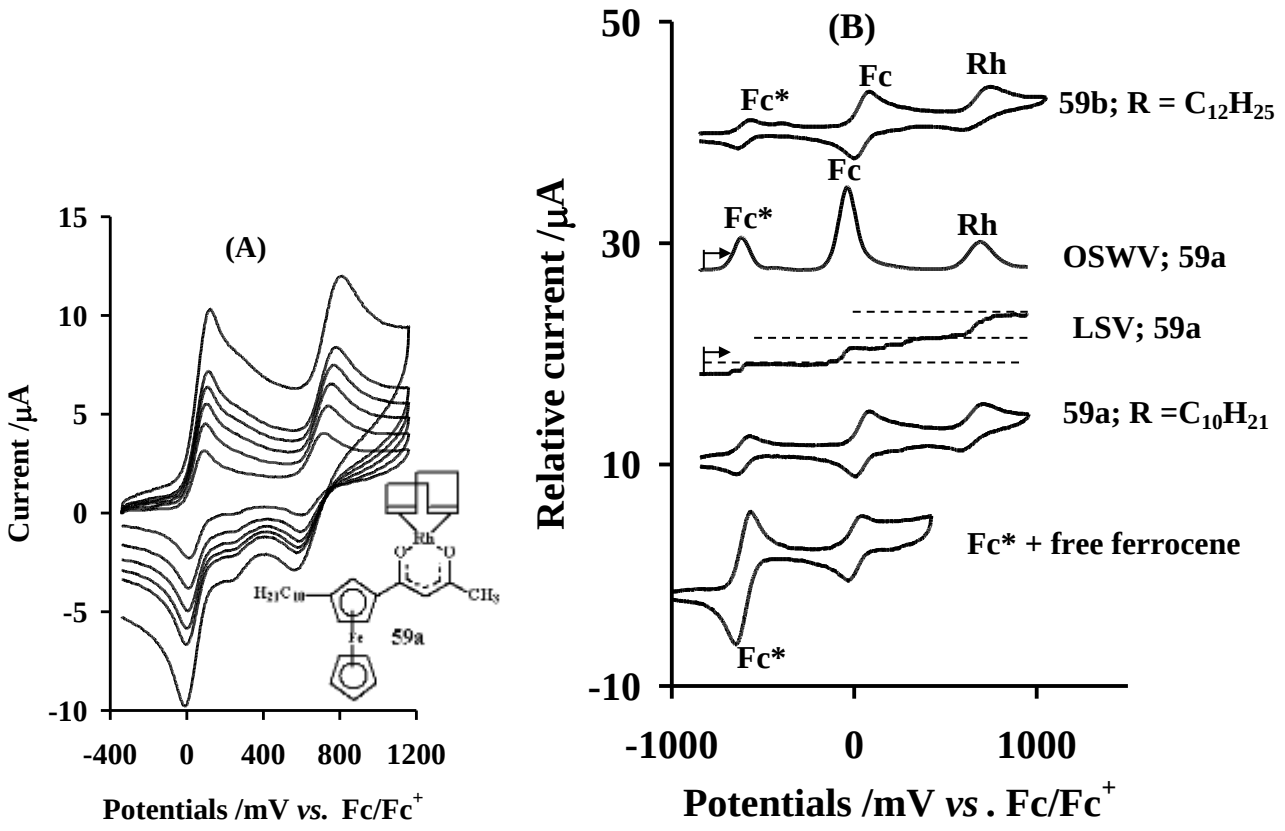

Figure 3. 32: (A) Cyclic voltammograms of 0.5 mmol dm^{-3} solution of 59a measured in 0.05 mol dm^{-3} [NBu$_4$][B(C$_6$F$_5$)$_4$]/CH$_2$Cl$_2$ at a scan rates of 100, 200, 300, 400, 500 and 1000 mVs^{-1} on a glassy carbon working electrode at 25 ºC. (B) Cyclic voltammograms of 0.5 mmol dm^{-3} solutions of [Rh((Cp)Fe(R-Cp-COCHCOCH$_3$)) (cod)] under the same conditions as (A). Osteryoung square wave voltammogram (OSWV) at 10 Hz and linear sweep voltammetry (LSV) at 2 mV s^{-1} of 59a are also shown.

At 100 mVs^{-1} scan rate, for the C_{10} compounds, in moving from the 1,3-homo substituted ferrocenyl complex, **59a**, to the 1,1$^{/}$-hetero-substituted ferrocenyl complex, **58b**, the Rh^{II}/Rh^{I} formal reduction potential increased with *ca*. 40 mV. For the C_{12} complexes, the increase was also *ca*. 40 mV. This implies Rh masking from the electrode is less effective for the 1,3-homo substituted **59** series of compounds than for the 1,1$^{/}$-hetero substituted compound series **58** because more work is required to oxidize Rh^{I} in series **58** than in series **59**.

The linear sweep voltammetry signals of **59a** and **59b** confirmed that the ferrocenyl wave and the rhodium wave both represented a one-electron transfer process, because the currents drawn in both waves were approximately equal. **Figure 3.32(B)**, right, shows this for **59a**. The broadness and low currents of the Osteryoung square wave voltammograms of Rh^{II}/Rh^{I} peak compared to the ferrocenyl wave (**Figure 3.32(B)** shows this for **59a**) is indicative of the fact that the rate of electron transfer for the ferrocenyl redox moiety is much faster than for the rhodium centre. This is also

evident from the cyclic voltammograms. ΔE_p for the ferrocenyl wave at 100 mVs^{-1} is 74 mV, while for the Rh centre it is 106 and 148 mV respectively.

Table 3. 12: Electrochemical data of 0.5 mmol dm^{-3} solutions of [Rh((Cp)Fe(R-Cp-$COCHCOCH_3$)) (cod)] complexes 59a and 59b measured in 0.05 mol dm^{-3} $[NBu_4][B(C_6F_5)_4]/CH_2Cl_2$ on a glassy carbon working electrode at 25 ºC *vs.* Fc/Fc^+ at scan rates indicated in the Table.

	Ferrocenyl group					Rhodium group				
ν mVs^{-1}	**E_{pa} /mV**	**ΔE_p /mV**	**$E^{o/}$ /mV**	**i_{pa} /μA**	**i_{pc}/i_{pa}**	**E_{pa} /mV**	**ΔE_p /mV**	**$E^{o/}$ /mV**	**i_{pa} /μA**	**i_{pc}/i_{pa}**
59a; R = $C_{10}H_{21}$										
100	33	74	47	1.86	0.69	703	106	650	0.68	0.50
200	99	88	55	2.69	0.61	734	135	666	0.93	0.59
300	106	97	55	3.33	0.66	756	162	675	1.11	0.59
400	108	108	54	3.91	0.67	771	187	677	1.28	0.57
500	113	113	56	4.48	0.67	784	208	680	1.38	0.55
1000	125	131	59	6.30	0.69	798	227	684	1.93	0.55
59b; R = $C_{12}H_{25}$										
100	70	74	33	1.80	0.94	723	148	649	0.71	0.39
200	92	90	47	2.56	0.75	750	196*	652	0.89	-
300	105	100	55	3.20	0.82	776	236*	658	1.06	-
400	109	107	54	3.40	0.79	774	244*	672	1.25	-
500	109	107	54	4.01	0.80	794	264*	662	1.35	-
1000	120	135	52	5.46	0.79	829	278*	690	1.85	-

*Values estimated due to peak broadening at E_{pc}.

3.6.3.3. Cyclic voltammetry of [Rh((Cp-$C_{10}H_{21}$)Fe(Cp-$C_{10}H_{21}$-$COCHCOCH_3$))(cod)], 60a and [Rh((Cp-$C_{12}H_{21}$)Fe(Cp-$C_{12}H_{25}$-$COCHCOCH_3$))(cod)], 60b, complexes

Cyclic voltammograms of rhodium complexes, **60a** and **60b**, are shown in **Figure 3.33**. The ferrocenyl wave is observed at $E^{o/}$ *ca.* -39 mV, while the Rh^{II}/Rh^{I} couple is found at $E^{o/} > 600$ mV. At slow scan rates, the ferrocenyl wave exhibits good electrochemical reversibility as ΔE_p is small. With regard to this study, experimentally determined ΔE_p values smaller than 90 mV are assumed to indicate electrochemical reversibility. Theoretically, ΔE_p for one-electron transfer processes should be 59 mV. The ferrocenyl couple becomes progressively more quasi-reversible at higher scan rates. The rhodium nucleus exhibited electrochemically and chemically irreversible behaviour with $\Delta E_p >$ 150 mV at all times. Results are summarized in **Table 3.13**.

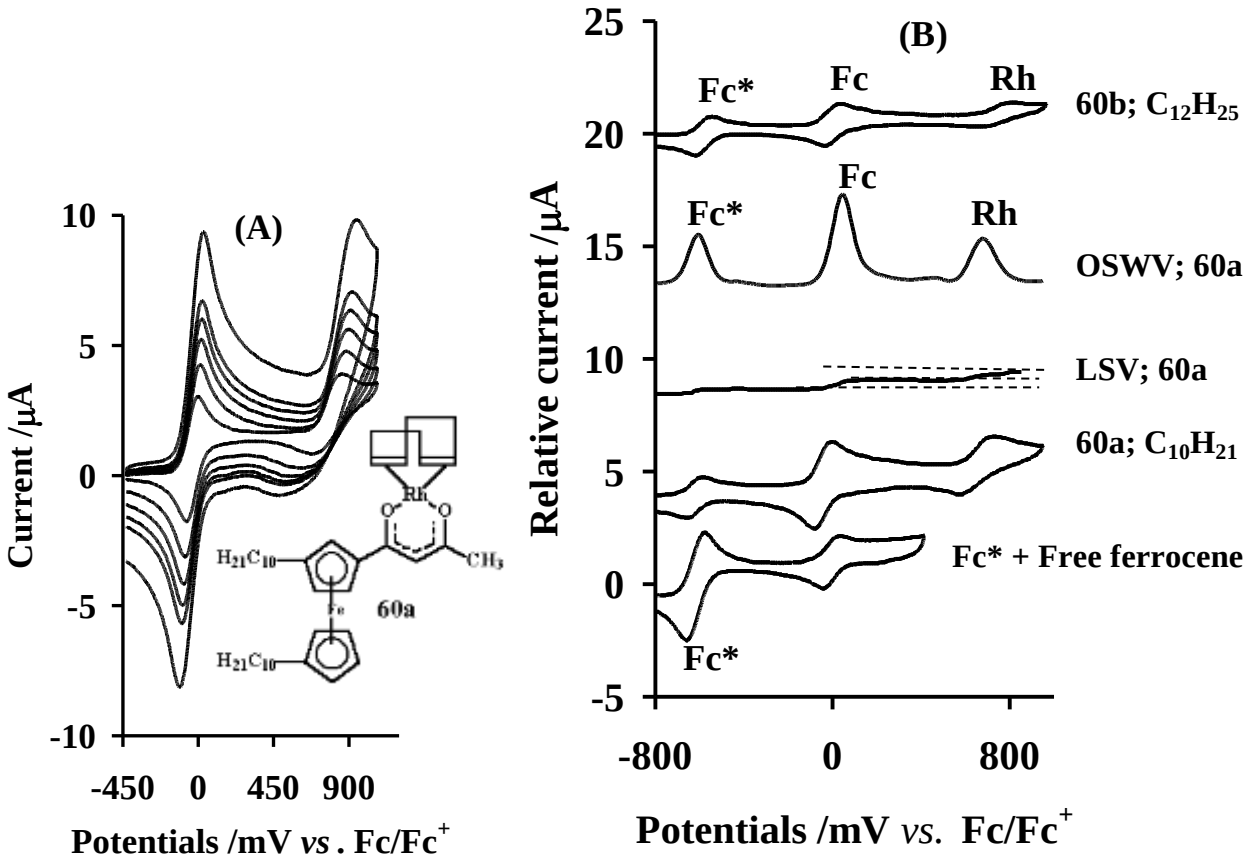

Figure 3. 33: (A) Cyclic voltammograms of 0.5 mmol dm^{-3} solutions of 60a measured in 0.05 mol dm^{-3} [NBu$_4$][B(C$_6$F$_5$)$_4$]/CH$_2$Cl$_2$ at a scan rates of 100, 200, 300, 400, 500 and 1000 mVs^{-1} on a glassy carbon working electrode at 25 ^{o}C *vs*. Fc/Fc$^+$. (B) Cyclic voltammograms of [Rh{(Cp-R)Fe(Cp-COCHCOCH$_3$)}(cod)], 60a and 60b at scan rate 100 mVs^{-1} measured under the same conditions as (A). LSV and OSWV sweeps are also shown. Where Fc* = decamethylferrocene, the internal standard.

From **Table 3.13**, $E^{o/}$ values of the ferrocenyl couple for complexes **60a** and **60b** were found to be about 70 mV more negative compared with those of complexes **58a** and **58b** (**Table 3.11)** and **59a** and **59b** (**Table 3.12**). This result is consistent with the view that two alkyl substituents, both of which are poor electron donors, should make the Fe^{II} nucleus of the ferrocenyl group easier to oxidize resulting in lower $E^{o/}$ values. In contrast, the observation that for the $C_{10}H_{21}$ complexes, the Rh^{II}/Rh^{I} couples were observed at potentials ~ 40 mV **less** positive for compound series **60** than for **58**, and ~ 23 mV **more** positive than for **59** at 100 mVs^{-1} scan rate was completely unexpected.

The effect was much less pronounced in the $C_{12}H_{25}$ series, with an $E^{o/}$ value of 683 mV being only *ca*. 5 mV less positive than for **58c** and *ca*. 30 mV more positive than for **59b**. The reason for this

behaviour is not yet clearly understood. It is doubtful that a mere two carbon chain length elongation from C_{10} to C_{12} in the substituent is the only reason.

Table 3. 13: Electrochemical data of 0.5 mmol dm^{-3} solution of [Rh((Cp-R)Fe(R-Cp-COCHCOCH$_3$))(cod)], complex, 60a, measured in 0.05 mol dm^{-3} [NBu$_4$][B(C$_6$F$_5$)$_4$]/CH$_2$Cl$_2$ on a glassy carbon working electrode at 25 ºC *vs*. Fc/Fc$^+$ at scan rates 100, 200, 300, 400, 500 and 1000 mVs^{-1}.

	Ferrocenyl group					Rhodium group				
ν mVs^{-1}	E_{pa} /mV	ΔE_p /mV	$E^{o/}$ /mV	i_{pa} /μA	i_{pc}/i_{pa}	E_{pa} /mV	ΔE_p /mV	$E^{o/}$ /mV	i_{pa} /μA	i_{pc}/i_{pa}
60a; R = $C_{10}H_{21}$										
100	-2	74	-39	2.93	0.93	722	148	648	1.08	0.26
200	14	92	-32	4.09	0.89	749	230*	649	1.48	-
300	16	100	-34	4.99	0.87	762	239*	642	1.75	-
400	18	112	-38	5.52	0.89	775	246*	652	1.97	-
500	21	120	-39	6.26	0.83	786	276*	648	2.18	-
1000	27	136	-41	8.62	0.83	807	310*	652	2.98	-
60b; R = $C_{12}H_{25}$										
100	-1	64	-33	1.11	0.97	758	151	683	0.91	0.26
200	16	69	-32	1.58	0.92	784	212*	678	1.14	-
300	27	74	-28	1.92	0.91	803	250*	678	1.39	-
400	28	83	-28	2.11	0.88	815	276*	677	1.56	-
500	29	91	-29	2.40	0.88	815	294*	668	1.76	-
1000	31	99	-31	3.46	0.82	823	308*	669	2.38	-

*Values estimated due to poor E_{pc} peak resolution.

As before, for the compound series **60**, it is clear from the linear sweep voltammograms trace in **Figure 3.33** that the ferrocenyl/ferrocenium and Rh^{II}/Rh^{I} couple both are one-electron transfer processes. Osteryoung square wave voltammograms, by virtue of peak broadening, also showed clearly, that the rate of electron transfer for the Rh^{I} nucleus, is much slower than for the ferrocenyl centre.

3.6.3.4. Cyclic voltammetry of [Rh((Cp-C$_{10}$H$_{21}$)Fe(Cp-COCHCO-Cp)Fe(Cp-C$_{10}$H$_{21}$))(cod)] and [Rh((Cp-C$_{12}$H$_{25}$)Fe(Cp-COCHCO-Cp)Fe(Cp-C$_{12}$H$_{25}$))(cod)] complexes.

The cyclic voltammograms of rhodium complex **61a** and **61b**, **Figure 3.34**, each exhibit two Fc/Fc$^+$ couples one at *ca*. 0 mV and the other at 200 mV. Each correspond to a one-electron transfer

process, one for each of the two ferrocenyl groups of the β-diketonato ligand coordinated to the rhodium complex. An electrochemically irreversible one-electron transfer wave which corresponds to the oxidation of rhodium(I) to rhodium(II), is also detected at $E^{o/} > 1000$ mV. The linear sweep voltammogram trace of **61b** shows all three electrochemical processes to represent one-electron transfer redox processes. Reasonable electrochemical reversibility with $\Delta E_p < 90$mV (**Table 3.14**) for the redox couples of the two ferrocenyl groups was observed at slow scan rates.

Osteryoung square wave voltammetry (OSWV) clearly demonstrated the electrochemically inequivalence of the two ferrocenyl groups of **61b** (**Figure 3.34**). To understand the electrochemical inequivalence of the two ferrocenyl groups of [Rh((R-Cp)Fe(Cp-COCHCO-Cp)Fe(Cp-R))(cod)] with R = $C_{10}H_{21}$ and $C_{12}H_{25}$, one should recognize that the first oxidized intermediate species during the oxidation of **61** is the mixed-valent species [Rh((R-Cp)Fe^{+}(Cp-COCHCO-Cp)Fe(Cp-R))(cod)] similarly to what was found for the free β-diketones, **56a** and **56b** (**Figure 3.14**).

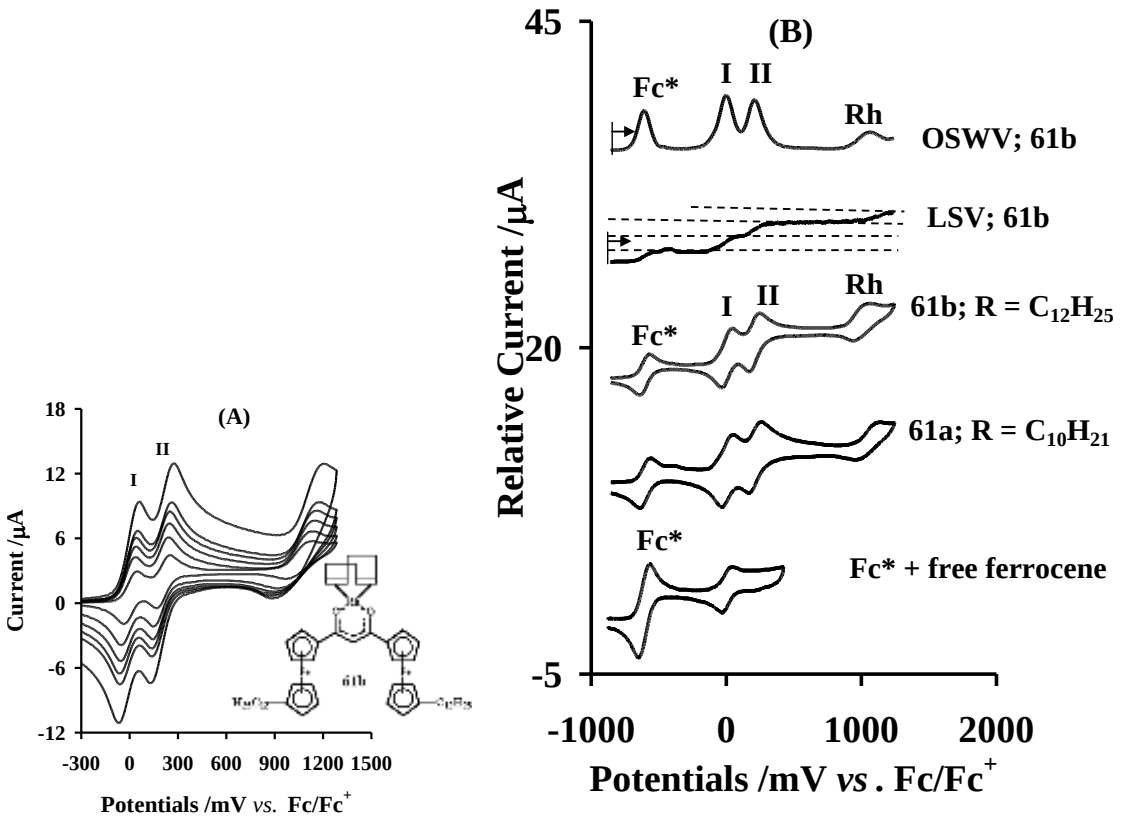

Figure 3. 34: (A) Cyclic voltammograms of 0.5 mmol dm^{-3} solution of 61b measured in CH_2Cl_2/0.05 mol dm^{-3} $[NBu_4][B(C_6F_5)_4]$ at 25 °C utilizing a glassy carbon working electrode at scan rates of 100, 200, 300, 400, 500 and 1000 mVs^{-1}. (B) Cyclic voltammograms of solutions of [Rh((Cp-R)Fe(Cp-COCHCO-Cp)Fe(Cp-R))(cod)] at scan rate of 100 mVs^{-1} under the same conditions as (A). Osteryoung square wave voltammogram (OSWV) at 10 Hz clearly indicates two inequivalent electron transfer processes for the two ferrocenyl groups and linear sweep voltammetry (LSV) at 2 mVs^{-1} of 61b.

As there is good communication (*via* conjugation) between the Fc and Fc^+ β-diketonato pendant side groups on the pseudo-aromatic core of the intermediate [Rh((R-Cp)Fe^+(Cp-COCHCO-Cp)Fe(Cp-R))(cod)], oxidation of the second Fc group to yield the final double ferrocenyl oxidized species [Rh((R-Cp)Fe^+(Cp-COCHCO-Cp)Fe^+(Cp-R))(cod)] takes place at a more positive potential than the one observed for the oxidation of the first ferrocenyl group. Different formal reduction potentials for side groups on symmetrical complexes in which mixed-valent intermediates are generated are well known in systems that allow electron delocalisation.[9,10]

Table 3. 14: Electrochemical data for [Rh((Cp-R)Fe(Cp-COCHCO-Cp)Fe(Cp-R))(cod)] complexes, 61a and 61b, measured in 0.5 mol dm^{-3} $[NBu_4][B(C_6F_5)_4]/CH_2Cl_2$ on a glassy carbon electrode at 25 ^{0}C.

ν mVs^{-1}	E_{pa} /mV	ΔE_p /mV	$E^{o/}$ /mV	i_{pa} /mA	i_{pc}/i_{pa}	E_{pa} /mV	ΔE_p /mV	$E^{o/}$ /mV	i_{pa} /mA	i_{pc}/i_{pa}
61a; R = $C_{10}H_{21}$ ferrocenyl peak I						**61b; R = $C_{12}H_{25}$ ferrocenyl peak I**				
100	46	78	10	1.02	0.96	27	70	-8.0	2.78	0.95
200	49	80	9.0	1.47	0.94	15	74	-22	4.07	0.93
300	54	82	13	1.80	0.94	19	84	-23	4.86	0.93
400	59	92	13	1.95	0.93	21	88	-23	5.53	0.94
500	59	94	12	2.29	0.90	29	96	-19	6.12	0.92
1000	63	102	12	3.12	0.93	39	112	-17	8.48	0.90
61a; R = $C_{10}H_{21}$ ferrocenyl peak II						**61b; R = $C_{12}H_{25}$ ferrocenyl peak II**				
100	252	78	213	1.21	0.90	229	80	189	2.85	0.98
200	257	76	219	1.45	0.90	217	88	174	3.94	0.94
300	259	82	218	1.69	0.92	225	102	174	4.60	0.97
400	264	88	220	1.82	0.92	229	110	174	5.00	0.99
500	267	96	219	2.00	1.00	239	122	178	5.52	1.00
1000	278	120	218	2.91	0.97	253	144	181	7.50	0.99
61a; R =$C_{10}H_{21}$ rhodium peak						**61b; R = $C_{12}H_{25}$ rhodium peak**				
100	1078	126	1015	1.14	0.36	1111	156	1033	2.45	0.31
200	1121	199*	1021	1.56	-	1115	218	1006	3.95	0.15
300	1142	220*	1032	1.88	-	1123	230*	1008	4.01	-
400	1152	238*	1033	2.11	-	1131	254*	1004	4.50	-
500	1165	252*	1039	2.36	-	1149	280*	1009	4.89	-
1000	1198	254*	1079	3.24	-	1187	314*	1030	6.61	-

*Values estimated due to poor E_{pc} peak resolution.

The rhodium complex series **61** showed the highest Rh(I) oxidation potentials, $E^{o/} > 1000$ mV *vs.* Fc/Fc^+ (**Table 3.14, Figure 3.34**). This is much larger compared to complex series, **58, 59** and **60**, which has only one ferrocenyl fragment in their structures. The observed high $E^{o/}$ is explained by recognizing the Rh^I centre is under the electronic influence of two electron withdrawing ferrocenium groups rather than just one as in **58 – 60** group electronegativities are ($\chi_{Fc} = 1.86$ and $\chi_{Fc+} = 2.86$).[11] Rhodium redox processes of **61a** and **61b** also exhibited mostly electrochemically and chemically irreversible behaviour with $\Delta E_p > 150$ mV and $i_{pc}/i_{pa} < 1$, depending on scan rate.

In conclusion, it was demonstrated that all the [Rh(β-diketonato)(cod)] complexes of this study, exhibits a definite electrochemical irreversible system for the Rh^I/Rh^{II} couple, while the ferrocenyl/ferrocenium couple showed electrochemical reversible behaviour at slow scan rates.

3.7. Phase change properties of selected ferrocenyl derivatives

The phase studies of selected ferrocene-containing β-diketones with long alkyl side chains and their corresponding rhodium complexes were expected to show liquid crystal behaviour. To explore this, they were studied utilizing differential scanning calorimetry (DSC). The energy changes from one phase to another were often large and detection of phase changes was often dependent on whether the DSC was on a heating or cooling cycle. The DSC traces of the ferrocenyl derivatives are shown in **Figure 3.35**, which present the results of at least one example of each class of compounds of this study.

3.7.1. Phase studies of ferrocenyl derivatives 44e, 46c, 47c, 48c, 50b, 51b and 52b

Firstly, the alkane substituted ferrocenes, **47c** and **51b** were considered. The transition from solid state to liquid state, peak M at 46.05 ^oC during the heating cycle was clearly observed for compound **47c** (**Figure 3.35**, top left). During the cooling cycle, it was found that **47c** solidified at 10.86 ^oC peak F. The temperature difference between the melting and solidifying peaks is $\Delta T = 46.05 – 10.86 = 35.19\ ^oC$.

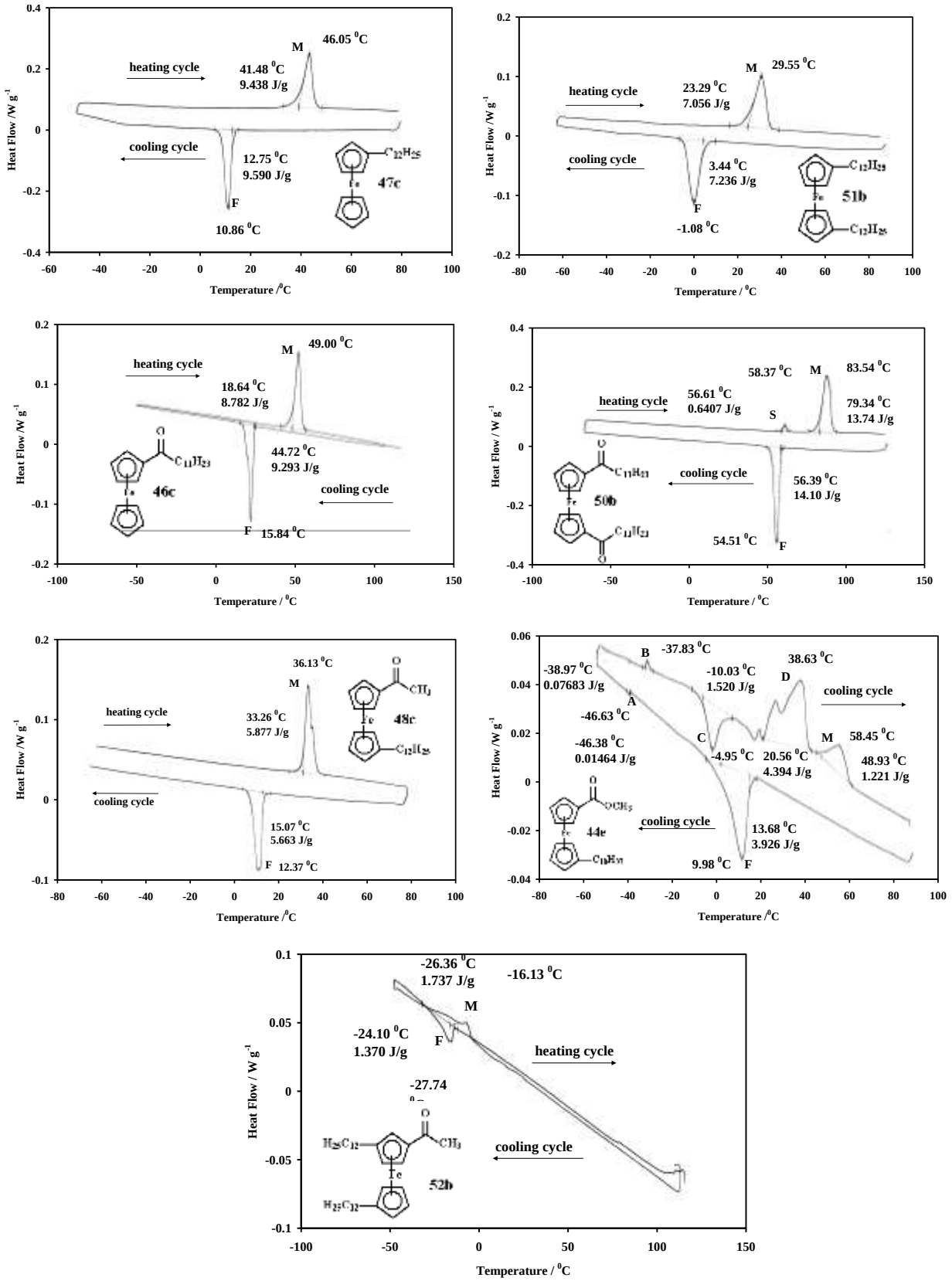

Figure 3. 35: Differential scanning calorimetric thermogram of heat flow *vs.* temperature of ferrocenyl derivatives, 44e, 46c, 47c, 48c, 50b, 51b and 52b respectively. A heating and cooling rate of 10 ^{0}C min^{-1} was used. Three successive heating and cooling cycles were employed. The thermograms shown are from the second cycle.

The observed phase changes are not attributed to the formation of a liquid crystal phase. The typical temperature differences of a liquid crystal transforming into an isotropic liquid and back, defining a liquid crystal phase, is *ca*. 5 ^{o}C.[15] Also, phase transition energies between liquid crystal and isotropic liquid phases are normally very small compared to heats of melting and crystallization. A DSC scan for **51b**, (**Figure 3.35**, top right), with both ferrocenyl rings substituted with alkyl side chains, solidify at -1.08 ^{o}C, peak F, during the cooling cycle and melts at 29.55 ^{o}C at peak M on the heating cycle. Here, $\Delta T = 29.55 - 1.08 = 28.47$ ^{o}C, 6.72 ^{o}C less than for **41c**.

Comparing the ketones, **46c** and **50b**, the heating cycle for **46c** (**Figure 3.35**, middle left) recorded the melting temperature at 49.00 ^{o}C, peak M. During the cooling cycle, crystallization was observed at 15.84 ^{o}C, peak F. A differential scanning calorimetry scan for **50b**, (**Figure 3.35**, middle right), a ferrocenyl derivative substituted with two acyl groups linked to the two separate cyclopentadienyl rings of the molecules, recorded a crystallizing temperature of 54.51 ^{o}C, peak F, during the cooling cycle, 36.67 ^{o}C warmer when compared to the mono substituted ferrocenyl derivative, **46c** (**Figure 3.35**, middle left). Melting occurred at 83.54 ^{o}C during the heating cycle. The peak labeled S during the heating cycle represent a solid state transition from one solid phase s_1 to another solid phase S_2 and probably involves side chain reorganization.

Table 3. 15: Phase transition temperatures and transition energies (ΔH), values are given in brackets observed during DSC studies of ferrocenyl derivatives 44e, 46c, 47c, 48c, 50b, 51b and 52b. Phase transitions are defined and abbreviated as: isotropic liquid → crystalline solid, l →s; crystalline solid → isotropic liquid, s → l; solid phase → new solid phase, $s_i \rightarrow s_{i+1}$ with i = 1, 2, 3, etc. The subscript i is used if more than one solid state phase exist.

Compound	Peak label: Transition Temperatures / ^{0}C (phase transition, heat of conversion, ΔH / J g^{-1})	
	Cooling cycle	Heating cycle
44e	F: 9.98 (l→s_3, 3.93) A: -46.63 (s_3→s_4, 0.0146)	B: -37.83 (s_4→s_3, 0.0768) C: -4.95 (s_3→s_2, 1.52) D: 38.63 (s_2→s_1, 4.39) M: 58.45 (s_1→l, 1.22)
46c	F: 15.84 (l→s, 9.29)	M: 49.00 (s→l, 8.78)
47c	F: 10.86 (l→s, 9.59)	M: 46.05 (s→l, 9.44)
48c	F: 12.37 (l→s, 5.66)	M: 36.13 (s→l, 5.88)
50b	F: 54.51 (l→s_1, 14.10)	S: 58.37 (s_1→s_2, 0.641) M: 83.54 (s_2→l, 13.74)
51b	F: -1.08 (l→s, 7.23)	M: 29.55 (s→l, 7.06)
52b	F: -27.74 (s→l, 1.37)	M: -16.13 (l→s, 1.74)

Upon comparing the alkane derivatives **47c** and **51b**, with the ketone derivatives, **46c** and **50b**, it was observed that the alkanes, especially the disubstituted derivative, became isotropic liquids at lower temperatures compared to the ketone derivatives. The reason for this observation is that polar carbonyl groups enhance intermolecular Van der Waals forces. These forces give rise to larger packing energies in the crystal, which accounts for the ketones melting at higher temperatures.

By comparing the keto-alkane compound **48c** and the ester-alkane derivative **44e**, during the cooling cycle of **48c** (**Figure 3.35**, second from bottom left), the crystallization temperature was recorded at 12.37 ^{o}C, peak F. During the heating cycle, melting was observed at 36.13 ^{o}C, peak M. In contrast, a DSC scan for **44e** (**Figure 3.35**, bottom right), showed the alkyl ester start to solidify at 9.98 ^{o}C peak F, during the cooling cycle. At -46.63 ^{o}C peak A an endothermic solid phase change was also observed. During heating cycle, an exothermic solid phase change was recorded at -37.83 ^{o}C peak B, followed by and endothermic solid state phase change at -4.95 ^{o}C peak C. A further, rather complex exothermic solid phase change was observed at 38.63 ^{o}C peak D and melting sets in at 58.45 ^{o}C peak M.

The large difference in melting and crystallization temperatures for all compounds is an indication of slow kinetics of conformational changes due to the flexibility of the long $C_{18}H_{37}$ side chain of especially **44e**. Excessive supercooling on the cooling cycle is observed.

A DSC scan of compound **52b**, (**Figure 3.35**, bottom), recorded a crystallization phase at -27.74 ^{o}C peak F, 26.70 ^{o}C lower temperatures than for **51b**. During the heating cycle, an exothermic solid phase change occurred at -16.13 ^{o}C peak (M). No further changes were observed for the rest of the cycle. A summary of the phase behaviour for the ferrocenyl derivatives, **44e, 46c, 47c, 48c, 50b, 51b** and **51b**, can be found in **Table 3.15**.

3.7.2. Phase studies of β-diketone derivatives 53e, 54a, 55b and 56b

Regarding the ferrocene-containing β-diketone series, phase studies were also conducted on **53e, 54a, 55b** and **56b** by using differential scanning calorimetry. The four β-diketones were expected to show interesting phase behaviour due to the long chain substituents they possess. Unexpectedly, no thermotropic liquid crystal properties were found for the β-diketone derivatives. They only exhibited different solid state phases as shown in **Figure 3.36**.

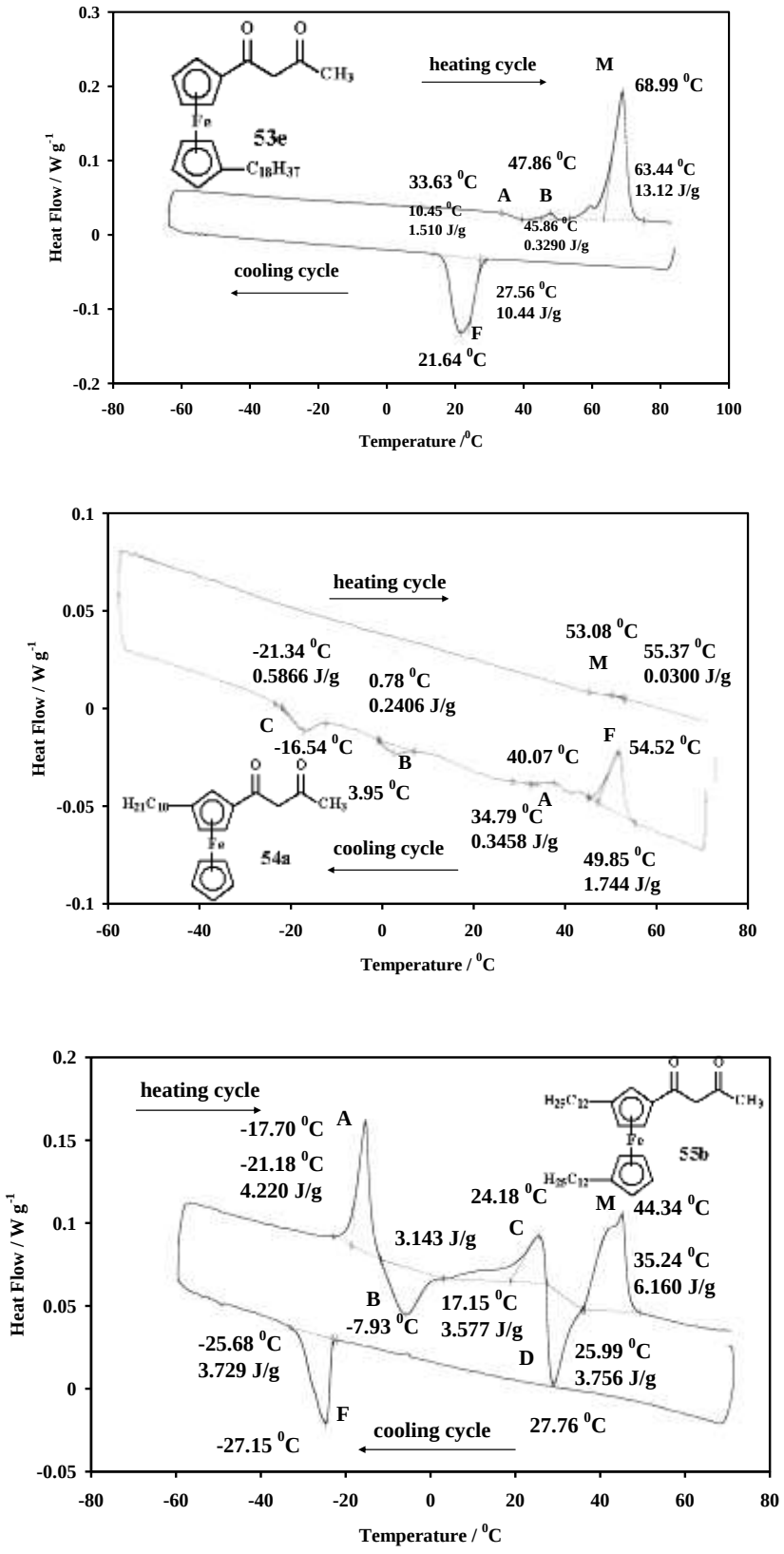

Figure 3. 36: Differential scanning calorimetry thermogram of heat flow *vs.* temperature of new ferrocene-containing β-diketone derivatives, 53e, 54a and 55b. A heating and cooling rate of 10 ^{0}C min^{-1} was used. Three successive heating and cooling cycles were employed. The thermograms shown are from the second cycle.

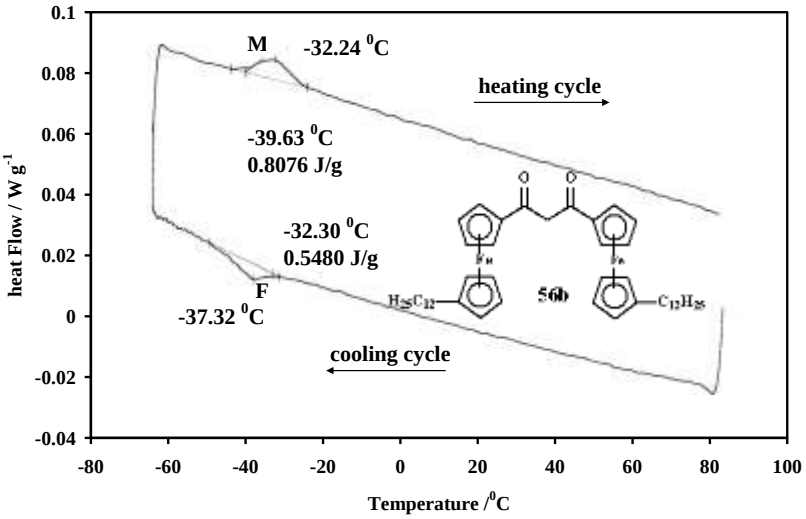

Figure 3.36: (continued) Differential scanning calorimetry thermogram of heat flow *vs.* temperature of new ferrocene-containing β-diketone derivative 56b. A heating and cooling rate of 10 ^{o}C min^{-1} was used. Three successive heating and cooling cycles were employed. The thermograms shown are from the second cycle.

A DSC scan for complex **53e** (**Figure 3.36**, top), shows solid state phase changes during the heating cycle at 33.63 ^{o}C (peak A). This was followed by another solid state phase changes at 47.86 ^{o}C (peak B). The melting temperature was recorded at 68.99 ^{o}C, peak M. During the cooling cycle no other noticeable phase changes was observed apart from crystallization at 21.64 ^{o}C, peak F. From the DSC scan of **54a** (**Figure 3.36**, middle), during the heating cycle, the complex was found to melt at 53.08 ^{o}C (peak M), during the heating cycle. During the cooling cycle, endothermic crystallization starts to take place at 54.52 ^{o}C (peak F). This was followed by another endothermic solid phase at 40.07 ^{o}C peak A. An exothermic solid phase change occurred at 3.95 ^{o}C peak B, and a final solid state phase change at -16.54 ^{o}C, peak C, occurred. The observed phase changes A, B and C are also not attributed to the formation of liquid crystals, but rather to solid state reorganizations. Heat of conversion was recorded between 0.0300 – 1.744 J/g for all phase changes.

The DSC scan for complex **55b**, is shown in **Figure 3.36**, bottom. Crystallization from the melt was observed at -25.68 ^{o}C, peak F, during the cooling cycle. During the heating cycle, an exothermic solid state phase change (peak A) at -17.70 ^{o}C was observed, followed immediately by another endothermic solid state phase change at -7.39 ^{o}C (peak B). Two further solid phase changes were observed at 24.18 ^{o}C (peak C) and 27.76 ^{0}C (peak D). Melting was recorded at 44.34 ^{0}C (peak M). The DSC thermogram for **56b** is shown in **Figure 3.36**. During the cooling cycle,

crystalization was observed to take place at -37.32 ^{0}C (peak F). Melting appeared to occur at -32.34 ^{o}C (peak M) during heating cycle. No other phase changes were observed.

3.7.3. Phase studies of the rhodium complexes 58c, 58e, 60b and 61b

The phase studies of the ferrocene-containing rhodium complexes, **58c, 58e, 60b** and **61b**, with long chain alkyl substituents on the ferrocenyl moiety, all exhibited different solid state crystal phases. However, no liquid crystal stages could be detected. The differential scanning calorimetry traces of the rhodium complexes are shown in **Figure 3.37** and **Figure 3.38**. Melting point peaks, peak M, was confirmed with polarized light optical microscopy.

From the DSC scan for rhodium complex **58c**, (**Figure 3.37**, top), after the first heating cycle has been completed, no further phase changes involving significant amounts of energy could be detected. The two peaks at -27.38 and 18.30 ^{o}C (peaks A and B) involve minute quantities of energy ($\leq$ 0.03 J/g). The absence of any pronounced melting or crystallization peaks in follow-up heating and cooling cycles was thought to be the results of very slow crystallization kinetics for the **58c** derivative. To prove it, a sample was stored overnight at room temperature after the heating cycle was completed. Upon heating this sample the next day, a clear melting phase change was observed at 62.29 ^{o}C (peak M) (**Figure 3.37**, top right insert). However, after this initial melting occurred, no further melting and crystallization peaks could be observed on the DSC time scale during successive heating and cooling cycles.

A DSC scan for **58e**, showed this compound crystalize at -15.55 ^{o}C (peak F) during the cooling cycle (**Figure 3.37**, bottom). During the heating cycle, at -7.73 ^{o}C, an exothermic solid phase change (peak A) was observed. Following this exothermic solid phase change, two endothermic solid phase changes at 37.18 ^{o}C and at 43.55 ^{o}C (peaks B and C) are observed. The broadness of these peaks is an indication of slow kinetics of side chain conformational changes, due to the long $C_{18}H_{37}$ side chain. Eventually melting sets in at 54.22 ^{o}C (peak M). Multiple solid state phase changes in **58e**, is attributed to the long $C_{18}H_{37}$ side chain that settles into different conformation (the exact conformation is not known).

Differential scanning calorimetry for complex **60b**, after the first heating cycle has been completed, showed no phase changes involving significant amounts of energy that could be detected (**Figure 3.38**, top).

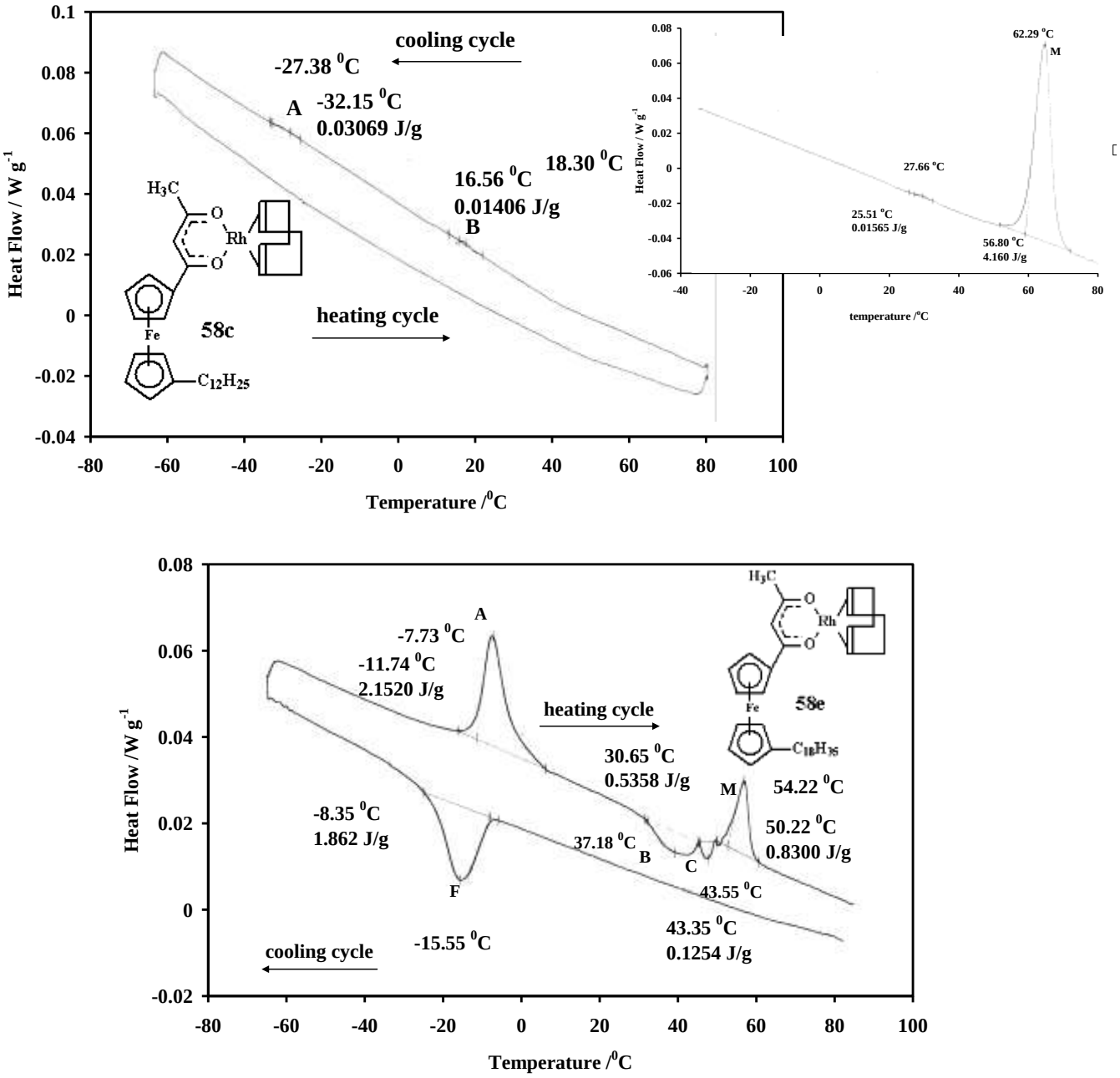

Figure 3. 37: Differential scanning calorimetry thermogram of heat flow *vs.* temperature of new ferrocene-containing rhodium complexes 58c and 58e. Insert thermogram (top right) shows a clear melting phase change after 24h storage. A heating and cooling rate of 10 ^{0}C min^{-1} was used. Three successive heating and cooling cycles were employed. The thermograms shown are from the second cycle.

The three peaks at - 42.52, 1.68 and 7.53 ^{o}C (peaks A, B and M) involves minute quantities of energy (≤ 0.04 J/g). The absence of any pronounced melting or crystallization peaks in follow-up heating and cooling cycles was thought to be very slow crystallization kinetics for **60b** derivative. No phase change was observed during the cooling cycle, (**Figure 3.38**, top). A DSC scan for compound **61b** showed no significant phase change during the cooling and the heating cycles (**Figure 3.38**, bottom).

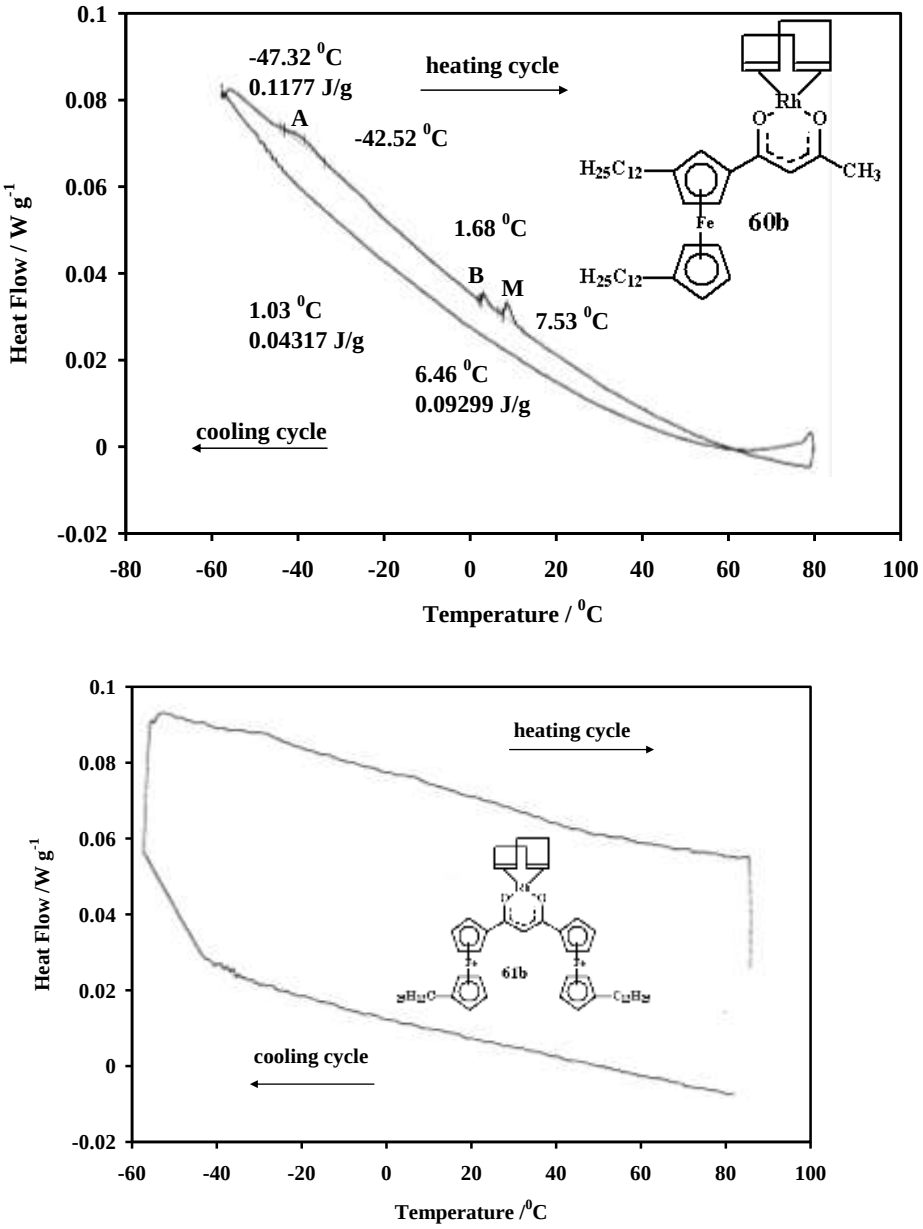

Figure 3. 38: Differential scanning calorimetry thermogram of heat flow *vs.* temperature of new ferrocene-containing rhodium complexes, 60b and 61b. A heating and cooling rate of 10 °C min^{-1} was used. Three successive heating and cooling cycles were employed. The thermograms shown are from the second cycle.

3.8. Cytotoxic studies

The experimental part of the cytotoxic studies described in this thesis was performed by Mrs Elle Kreft from the Department of Immunology, Institute for pathology at the University of Pretoria. The author thanks her for her efforts.

3.8.1. Introduction

The cytotoxic properties in terms of potential anticancer applications of the present new ferrocene-containing β-diketones and their rhodium(I) complexes are discussed in this section. It has been shown before that in β-diketones of the type (Cp)Fe(Cp-COCHCO-R) and their rhodium complexes of the type [Rh((Cp)Fe(Cp-COCHCO-R))(cod)], the R group drastically influences antineoplastic activity.[16] It was observed that the complex with R = CF_3 was dramatically more active than, for example, R = Ph, in killing cancer cells. This research program has as its target according to goal 7 of chapter 1 an investigation to determine what is the effect of long chain alkyl substituents on the ferrocenyl group. In previous studies, the IC_{50} (50 % lethal dosage values) of Fc-$COCH_2COCH_3$, **13c**, was 57.1 μmol dm^{-3} against CoLo and 66.6 μmol dm^{-3} against HeLa cells, **Table 3.16**. For the rhodium complex [Rh(Fc$COCHCOCH_3$)(cod)], **24c**, it was 56.6 (CoLo) and 64.4 (HeLa) μmol dm^{-3} respectively. HeLa is a human cervix epitheloid cancer cell line, while CoLo is an intrinsically multidrug resistant human colorectal cell line.

3.8.2. Cytotoxicity of β-diketones 53b and 54a and their rhodium complexes 58b and 59a

The author acknowledges Prof. Medlen and Mrs Elle Kreft for performing the experimental part of the cytotoxic studies and for constructing survival curves. The cytotoxicity of ferrocene-containing β-diketone derivatives, **53b** and **54a**, and their rhodium(I) complexes, **58b** and **59a**, were determined by observing their effects *in vitro* on cultured HeLa and CoLo cancer cell lines for 24 hours of continuous drug exposure. After incubation at 37 °C, for 24 hours, cell survival was measured as a percentage of living cells in relation to a control that was not exposed to the drug by means of the colorometric 3-(4,5-dimethylthiazol-2-yl)-diphenyltetrasodium bromide (MTT) assay.

Survival curves indicating percentage cell survival were plotted as a function of drug dose (in μmol dm^{-3}). **Figures 3.39** and **3.40** show a set of these survival curves after 24 hours of incubation with the β-diketone derivatives and their rhodium complexes. IC_{50} values (drug dose required for 50% cell death) were estimated by extrapolation and are summarized in **Table 3.16**. From the survival curves and IC_{50} values tabulated in **Table 3.16**, it is clear that rhodium complexes and the free β-diketones are about equally toxic for each cancer cell line. This was expected as the same trend was observed for other ferrocene-containing rhodium complexes studied in this laboratory.[16]

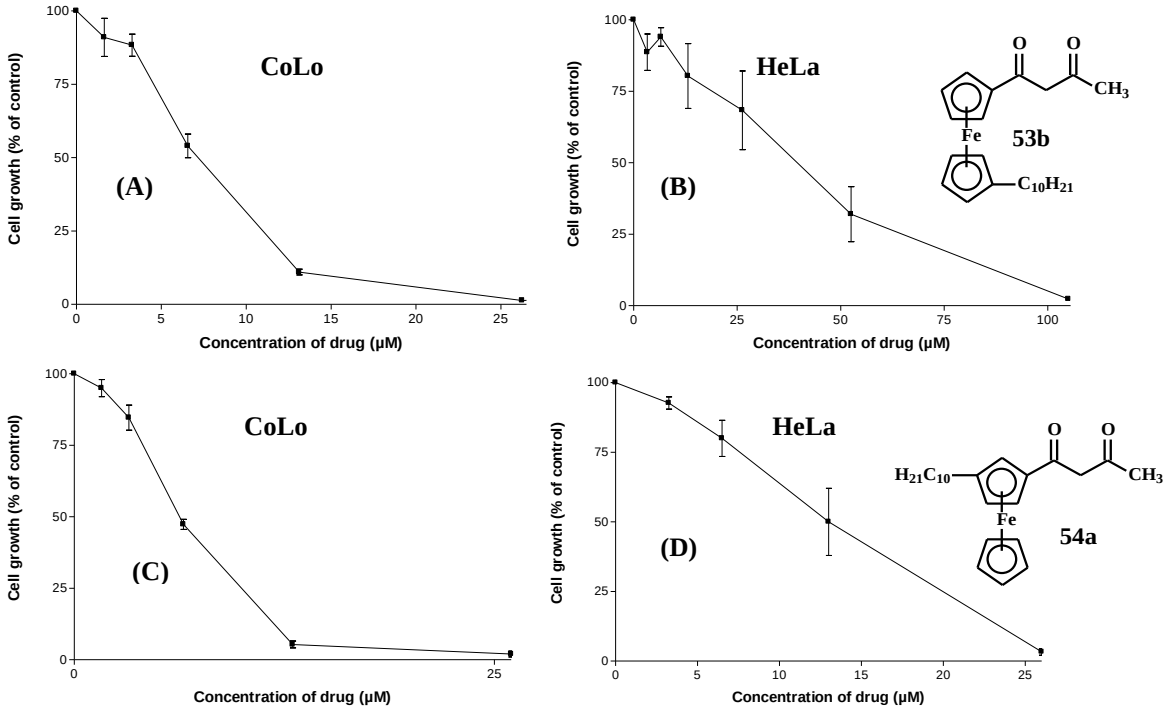

Figure 3. 39 Plots of the percentage survival of cells for CoLo cancer cell line (A) and (C), with HeLa cancer cell line (B) and (D) against concentration (μmol dm^{-3}) of β-diketones, (Cp-$C_{10}H_{21}$)Fe(Cp-$COCHCOCH_3$) and (Cp)Fe(Cp-$C_{10}H_{21}$-$COCHCOCH_3$) after 24 hours incubation.

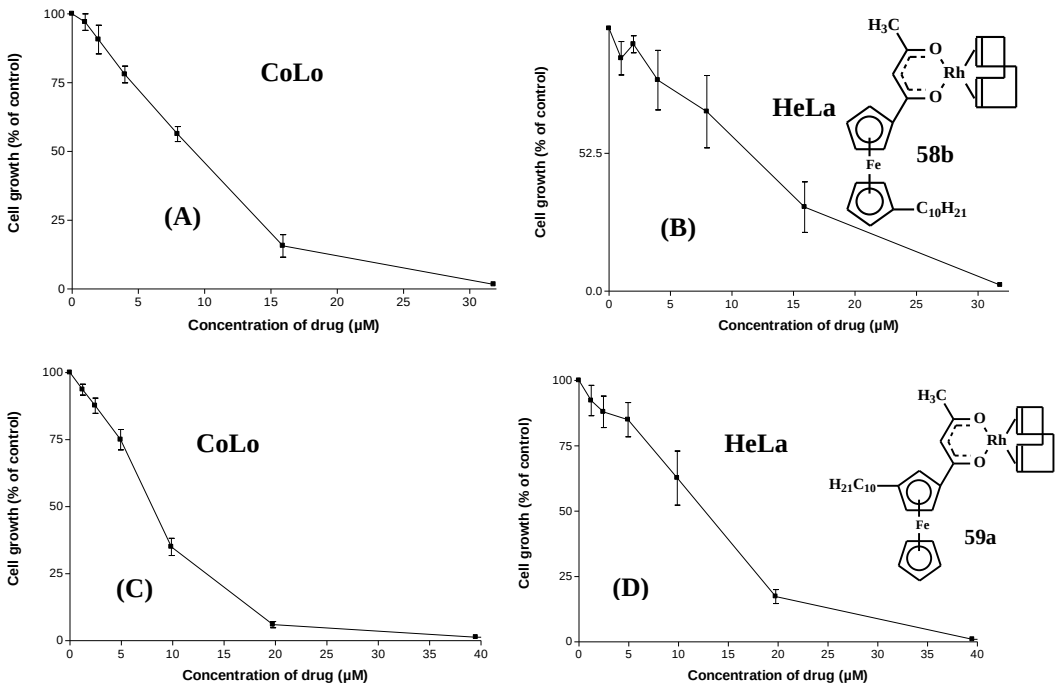

Figure 3. 40 Plots of the percentage survival of cells for CoLo cancer cell line (A) and (C), with HeLa cancer cell line (B) and (D) against concentration (μmol dm^{-3}) of [Rh((Cp-$C_{10}H_{21}$)Fe(Cp-$COCHCOCH_3$))(cod)] and [Rh((Cp)Fe(Cp-$C_{10}H_{21}$-$COCHCOCH_3$))(cod)] after 24 hours incubation.

However, the rhodium complexes without the long chain alkyl substituents β-diketone **13c** and its rhodium complex **24c** were previously shown to be much less toxic. Of special importance to this study was the observation that the activity of β-diketones of the type (Cp-R^2)Fe(R^1-Cp-$COCH_2COCH_3$), **53b** and **54a**, and the [Rh((Cp-R^2)Fe(R^1-Cp-$COCHCOCH_3$))(cod)] complexes, **58b** and **59a**, against CoLo and HeLa cell lines, are almost 10 times more active in killing cancer cells than Fc-$COCH_2CO$-CH_3, **13c** and the [Rh(Fc-$COCHCO$-CH_3))(cod)], **24c** in (**Table 3.16**).

It is strikingly evident that the free β-diketones **53b** and **54a** are about twice more effective in killing the multi drug resistant CoLo cell line than the HeLa cell line. Rhodium(I) complexes, **58b** and **59a** toxicity is approximately in the same range for both cancer cell lines. This is an unusual observation as most drugs are more active against HeLa than CoLo cancer cells. It is concluded that it does not matter on which cyclopentadienyl ring of complexes **53, 54, 58** and **59** alkyl substitution has occurred, as all complexes were about equally active in killing cancer cells.

In comparing the activity of the β-diketones and rhodium complexes, with the IC_{50} values of *cisplatin*, it was found that in CoLo cancer cell lines the β-diketones, **53b** and **54a**, are five times less effective, while the rhodium(I) complexes, **58b** and **59a** toxicity is approximately six times less active than *cisplatin*. In HeLa cell lines the activity of the free β-diketones and their rhodium complexes was found to be similar. This is consistent with **53, 54, 58** and **59** being more lypophilic than **13c** and **24c** because of the long alkyl side chains. Higher lypophilicity implies better cell entry in cell entry mechanism designed for lipids. Here it resulted in more effective cancer cell deaths.

Table 3. 16 IC_{50} values of CoLo and HeLa cancer cell lines, with formal reduction potentials, $E^{o\prime}$, for ferrocene-containing β-diketones and their rhodium complexes. The second-order rate constants, k_2, for the substitution of (Cp-R^2)Fe(R^1-Cp-$COCHCOCH_3$) in [Rh((Cp-R^2)Fe(R^1-Cp-$COCHCOCH_3$))(cod)] with 1,10-phenanthroline are also indicated.

Compounds	$E^{o\prime}$ /mV *vs*. Fc/Fc^+	k_2 /dm^3 mol^{-1} s^{-1}	IC_{50} /μmol dm^{-3}	
			CoLo	HeLa
53b; R^1 =H, R^2 = $C_{10}H_{21}$	150	-	6.9	11.0
54a; R^2 =H, R^1 = $C_{10}H_{21}$	151	-	6.3	13.0
58b; R^1 =H, R^2 = $C_{10}H_{21}$	41	1157	9.0	12.7
59a; R^2 =H, R^1 = $C_{10}H_{21}$	44	1594	8.1	12.0
cisplatin	-	-	1.3	0.97
13c	209	-	57.1	66.6[(a)]
24c	129	18	56.6	64.4[(a)]

(a) data from reference 16.

The mechanism of action of rhodium complexes in chemotherapy for [Rh(Fc-COCHCO-R)(cod)] complexes were previously proven to involve a substitution reaction between rhodium-containing drug and cytocin and thymin DNA fragments, while the mechanism of action of the ferrocenyl moiety in chemotherapy is based on electron transfer.[16] It is not expected that the new ligands and complexes of this research program will be different. It is of importance to note that the rate of β-diketonato substitution in **58b** and **59b** is three orders of magnitude faster than **24c**. This is partially the reason why **58b** and **59b** is one order of magnitude more effective in killing cancer cells than **24c**. Cytotoxicity was found to be independent of ferrocenyl formal reduction potentials.

[1] Goldberg, S. I., Keith, L. H. and Prokopov, T. S., *J. Org. Chem.*, **28**, 850, (1963).

[2] Donnio, B., Seddon, J. M. and Deschenaux, R., *Organometallics*, **19**, 3077, (2000).

[3] Vogel, M., Rausch, M. D. and Rosenberg, H., *J. Org. Chem.*, **22**, 1016, (1957).

[4] Chatt, J. and Venanzi, L. M., *J. Chem. Soc.*, **A**, 4735, (1957).

[5] Du Plessis, W. C., Vosloo, T. G. and Swarts, J. C., *J. Chem. Soc., Dalton Trans.*, 2507, (1998).

[6] Du Plessis, W. C., Davis, W. L., Cronje, S. L. and Swarts, J. C., *Inorg. Chim. Acta*, **314**, 97, (2001).

[7] Swart, J. C., unpublished results with permission.

[8] Du Plessis, W. C., Erasmus, J. J. C., Lamprecht, G. J., Conradie, J. C., Cameron, T. S., Aquino, M. A. S. and Swarts, J. C., *Can. J. Chem.*, **77**, 378, (1999).

[9] Gritzner, G. and Kuta, J., *Pure Appl. Chem.*, **56**, 461, (1984).

[10] (a) Creutz, C. and Taube, H., *J. Am. Chem. Soc.*, **91**, 3988, (1969); (b) Geiger, W. E., Van Order, N., Pierce, D. T., Bitterwolf, T. E., Rheingold, A. L. and Chasteen, N. D., *Organometallics*, **10**, 2403, (1991); (c) Van Order, N., Geiger, W. E. Bitterwolf, T. E. and Reingold, A. L, *J. Am. Chem. Soc.*, **109**, 5680, (1987); (d) Pierce, D. T. and Geiger, W. E., *Inorg. Chem.*, **33**, 373, (1994); (e) Conradie, J., Cameron, T. S., Aquino, M. A. S., Lamprecht, G. J. and Swarts, J. C., *Inorg. Chim. Acta*, **358**, 2530, (2005).

[11] Du Plessis, W. C., Vosloo, T. G. and Swarts, J. C., *J. Chem. Soc.*,*Dalton Trans.*, 2507, (1998).

[12] Wilkinson, R. G., *Kinetics and mechanism of reactions of Transition Metal Complexes, 2nd* thoroughly revised edition, CVH, Weinhein, p. 103, 232, (1991).

[13] Maron, S. H and Lando, J. B., *Fundamentals of Physical Chemistry*, Macmillan Publishing Co. Inc., New York, Chapter 16, p. 677, (1974).

[14] Helm, L., MINSQ, Non-linear parameter estimation and model development, least squares parameter optimisation V3. 12, MicroMath Scientific Software, Salt Lake City, UT (1990).

[15] Van Camp, L. and Rosenbrg, B., *Advances in Antimicrobia and Antineoplatis Chemotherapy*, Univ. Park Press, Baltimore, p. 239, (1972).

[16] Swarts, J. C., and van Rensburg, C. E. J., A Substrate or Composition for the Treatment of Cancer, Patent PCT/IB01/02258 in PCT Countries, European Patent 1345951, p. 1, (2004).

Chapter 4

Experimental

4.1. Materials

Solid reagents and liquid reactants (esters) were purchased from Merck and Aldrich, and used without further purification. Solvents were distilled prior to use and water was double distilled. Reactions requiring anhydrous conditions were performed using oven-dried glassware under nitrogen atmosphere. Solvents such as THF, dichloromethane, and acetone were dried in accordance with standard protocols,[1] or purchased from Aldrich or Merck in Sure/Seal^{TM} bottles. Flash column chromatography was performed on Silica gel 60 of particle size 0.040-0.063mm, using eluent hexane-ether 4:1 v/v unless otherwise stated. Melting points (m.p.) were determined with a Reichert Thermopan microscope with a Koffler hot-stage and are uncorrected.

4.2. Techniques and calculations

4.2.1. Spectroscopy

^{1}H NMR measurements were recorded on a Bruker Advance DPX 300 NMR spectrometer at 292K. The chemical shifts are reported relative to $SiMe_4$ at 0.00 ppm. UV spectra of [Rh((Cp-R)Fe(Cp-$COCHCOCH_3$))(cod)] and [Rh(phenanthroline)(cod)]$^+$ were recorded in a Cary 50 probe UV/Visible spectrophotometer.

4.2.2. Observed acid dissociation constant, $pK_a^/$, determination

The $pK_a^/$ values were obtained by measuring the absorbance at different pH during an acid-base titration in water-containing 10 % acetonitrile mixture and water-containing 9 % acetonitrile/1 % THF mixture, μ = 0.100 mol dm^{-3} ($NaClO_4$). A linear response by the pH meter (Hanna instruments model HI 9321), fitted with a glass electrode, was ensured by calibration with buffers at pH = -log α_H = 4.00, 7.02 and 12.00 respectively, α_H = activity of H^+. A test $pK_a^/$ determination was performed by titrating $FcCOCH_2COCH_3$, which was previously characterized.[2] The titrations

were performed with $HClO_4$ from high pH, adjusted with NaOH, to low pH. The least square fit of the observed absorbance/pH data for this calibrating titration using equation

$$A_T = \frac{A_{HA}10^{-pH} + A_A10^{-pKa}}{10^{-pH} + 10^{-pKa}}$$

resulted in a $pK_a^{/}$ of 9.98 ± 0.09. This was within the experimental error of the published $pK_a^{/}$ of 10.01 ± 0.02. It was therefore concluded that our electrode system was calibrated to measure hydrogen ion activity under the conditions used. The fitting program MINSQ,[3] was used for non-linear fitting of data to the above equation.

4.2.3. Calculation of % keto isomer and determination of K_c

^{1}H NMR spectra of β-diketone series **53, 54, 55** and **56** were recorded at 293 K with concentrations ranging between 1.0 and 1.7 mmol dm^{-3} in $CDCl_3$. Integrations of spectra were done in such a way that the methine proton, (Cp-R)Fe(Cp-CO-C**H**=C(OH)CH_3 at *ca*. δ_H 5.65 – 5.80 ppm was always assigned a integral value of one. The % keto was calculated from the relationship;

$$\% \text{ keto isomer} = (\text{I of keto signal})/\{(\text{I of keto signal}) + (\text{I of enol signal})\} \times 100$$

with I = integral value of ^{1}H NMR signal. Once the % keto isomer is known, the equilibrium constant

$$K_c = \frac{[(\text{Cp-R})\text{Fe}(\text{Cp-CO-CH}_2\text{-CO-CH}_3)]}{[(\text{Cp-R})\text{Fe}(\text{Cp-CO-CH=C(OH)-CH}_3)]}$$

for the equilibrium

$$(\text{Cp-R})\text{Fe}(\text{Cp-CO-CH=C(OH)-CH}_3) \underset{}{\overset{K_c}{\rightleftharpoons}} (\text{Cp-R})\text{Fe}(\text{Cp-CO-CH}_2\text{-CO-CH}_3)$$

was obtained from the relationship

K_c = [keto form]/[enol form]
= (% keto isomer) / (% enol isomer)
= (% keto isomer) / (100 - % keto isomer)
= k_1/k_{-1}

Once the % keto isomer was known, a plot of % keto isomer *vs* time was constructed. The rate constant from this plot was extracted by constructing a graph of ln[(%keto isomer at t = 0)/(%keto isomer at time t)] against time. The slope of this graph gave $k_{obs} = k_1 + k_{-1}$. The equilibrium constant K_c was obtained from the relationship, K_c = (% enol isomer)/(% keto isomer). Once K_c was known, k_1 and k_{-1} could be determined by simultaneous solution of $k_{obs} = k_1 + k_{-1}$ and $K_c = k_1/k_{-1}$.

4.2.4. Substitution kinetics

The Beer-Lambert law, $A = \varepsilon c \ell$ with A = UV/Vis absorbance, ε = molar extinction coefficient, c = concentration and ℓ = path length = 1 cm, was found to be valid for all complexes within the concentration range of 0.0002 mol dm^{-3} that was used for the kinetic studies. Pseudo-first-order rate constants, k_{obs}, were determined by monitoring the substitution of β-diketonato ligands from the [Rh((Cp-R^2)Fe(R^1-Cp-$COCHCOCH_3$))(cod)] with 1,10-phenanthroline at wavelengths indicated in **Table 3.8** (Chapter 3, page 101) on a computer controlled Applied Photophysics SX.18MV stopped flow spectrophotometer. 1,10-Phenanthroline concentrations were between 0.002 and 0.025 mol dm^{-3}. "Volt"-time data was collected and k_{obs} values were determined from a non-linear fit data according to:

$$\ln \frac{(C_0 - C_\infty)}{(C_t - C_\infty)} = \ln \left[\frac{k_v (V_0 - V_\infty)}{k_v (V_t - V_\infty)} \right] = \ln \left(\frac{V_0 - V_\infty}{V_t - V_\infty} \right) = k_{obs} t$$

Here k_v is the proportionality constant that links V with C. The second-order rate constant, k_2, was determined (slope) from the relationship between the k_{obs} and different 1,10-phenanthroline concentrations according to the following equation

$$k_{obs} = \frac{k_2 K[1,10 - phenanthroline]}{1 + K[1,10 - phenanthroline]}$$

The activation parameters ΔH*, ΔS* and ΔG* were obtained by fitting second order kinetic data collected at 5 ºC, 15 ºC, 25 ºC and 35 ºC to the following equations:

$$\ln \frac{k}{T} = -\frac{\Delta H^*}{RT} + \frac{\Delta S^*}{R} + \ln \frac{R}{Nh}$$

$$\Delta G^* = \Delta H^* - T\Delta S^*$$

Here ΔS* is entropy of activation, ΔH* is activation enthalpy and the Gibbs activation free energy ΔG*. Utilizing the fitting program MINSQ.[3] Temperatures were kept constant within 0.01 ºC.

4.2.5. Cyclic Voltammetry

Measurements on *ca.* 0.5 mmol dm^{-3} analyte in dichloromethane with 0.05 mol dm^{-3} tetrabutylammonium tetrakispentafluorophenylborate as supporting electrolyte were conducted under a blanket of argon at 25 ºC utilising BAS model 100 voltammograph interfaced with a personal computer. A three-electrode cell, which utilized a Pt auxiliary electrode, a glassy carbon (surface area = 2 mm) working electrode, and an in-house constructed Ag/AgCl reference electrode are employed. The reference electrode was prepared as follows: Two silver wires were connected to the positive and negative poles of a DC power source and submerged into a dilute HCl (0.1 mol dm^{-3}) solution. A 700 mA current was passed through the solution with the evolution of H_2 gas at the cathode. After the anode has acquired a uniform dark colour (deposition of AgCl), the wire was removed and washed with water, methanol and acetone-now being ready for use. After obtaining cyclic voltammograms of a series of compounds, the AgCl is removed from the reference electrode by washing with concentrated ammonia, and following the same procedure as described above for the next set of cyclic voltammograms. Experimentally potentials were referenced against a Ag/AgCl reference electrode, but results are presented referenced against ferrocene and decamethylferrocene as an internal standard. To achieve this, each experiment was performed first in the absence of decamethylferrocene and then repeated in the presence of < 0.5 mmol dm^{-3} decamethylferrocene. In a separate experiment decamethylferrocene was reference against ferrocene in the absence of any compound. Data were then manipulated on a Microsoft excel worksheet to set the formal reduction potentials of Fc/Fc^+ couple at 0 mV. Data, uncorrected for junction potentials, were collected with an Adalab-PC™ and Adapt™ data acquisition kit

(Interactive Microwave. Inc.) with a locally developed software. All temperatures were kept constant to within 0.1 ^{o}C.

4.2.6. Differential Scanning Calorimetry (DSC)

Transitions from solid phase to liquid phase states were studied by DSC. For enthalpy changes, 2.5 – 6 mg samples at heating and cooling rates of 10 ^{o}C min^{-1} between -60 ^{o}C and a convenient maximum temperature at least 30 ^{o}C higher than the melting point of the compounds were used. Measurements were done on a TA Instruments DSC 10 thermal analyzer fitted with Du-Pont Instruments mechanical cooling accessory and a TA Instruments Thermal Analyst 2000 data processing unit.

4.2.7. Cytotoxic Results

The author acknowledges Mrs. Elke Kreft from the Department of Immunology, Institute for Pathology at the University of Pretoria for performing these experiments.

Sample preparations: Rhodium complexes, **58b** and **59a**, were dissolved in water giving stock concentration of 50 mg/ml. β-diketones (**53b** and **54a** respectively), were dissolved in DMSO to give stock concentration of 10 mg/cm^3 and diluted in the appropriate growth medium supplemented with fetal calf serum (FCS) to give final DMSO concentrations not exceeding 0.5% and drug concentrations of 1-3000 μg/cm^3 prior to cell experiments.

Cell cultures: A human colorectal cell line, CoLo (ATCC CCL-220), was grown as a suspended culture in RPMI 1640. The human cervix epitheloid cancer cell line, HeLa (ATCC CCL-2), was grown as a monolayer culture in MEM. Growth media was at 37°C under 5 % CO_2 and fortified with 10 % FCS, and 1 % penicillin and streptomycin. Appropriate solvent control systems were included. Cells were seeded at 2000 cells/well for 24 h incubation experiments in 96 well microtiter plates in a final volume of 200 μl of growth medium in the presence or absence of different concentrations of experimental drugs. Wells without cells and with cells but without drugs were included as controls. After incubation at 37°C for 1 day cell survival was measured by means of the colometric 3-(4,5-dimethylthiazol-2-yl)-diphenyltetrasodium bromide (MMT) assay.[4]

4.3. Synthesis

4.3.1. Tetrabutylammonium tetrakispentafluorophenylborate

In a 50 cm^3 beaker, lithium tetrakis(pentafluorophenyl) borate etherate (10 g, 18.20 mmol) was dissolved in 20 cm^3 methanol (AR). In another 50 cm^3 beaker tetrabutylammonium bromide (5.10 g, 15.80 mmol) was dissolved in 10 cm^3 methanol (AR) and was added dropwise to the solution of tetrakis salt using a pasteur pipette over 15 min while stirring at room temperature (precipitate forms). The beaker was then sealed (covered with septum) and left for 30 min at 0 ^oC and then overnight at 25 ^oC. An off-white precipitate from a brown liquid was obtained by filtration and washed with methanol (10 cm^3) at 25 ^oC and air-dried for 2 hours. Then the solid residue was dissolved in excess dry CH_2Cl_2 (30 cm^3) and further dried over $MgSO_4$ (covered with a septum) while stirring for 2 hours at room temperature. The $MgSO_4$ was filtered and washed with CH_2Cl_2 and evaporated to give a white solid (8.52 g, 9.423 mmol, 51 %). Further purification by recrystallization was achieved by dissolving the crude product (8.52 g, 9.423 mmol) in CH_2Cl_2 (9.91 cm^3) first and then diethyl ether (48 cm^3) was added dropwise over 20 minutes (at 24 cm^3 precipitate begin showing and salt start crashing down). The beaker was then sealed (closed with a septum) and cooled for an hour at 0 ^oC and then overnight at 25 ^oC. The precipitate was filtered and rinsed with distilled hexane (30 cm^3) and air-dried for 2 hours to give white crystals. Recrystallization process was repeated and the product was air-dried for 24 h to give pure white crystals (7.32 g, 44 %). Characterization data: m. p. = 160 ^oC; δ_H (300 MHz, $CDCl_3$)/ppm: 0.98 (t; 12H; 4 x CH_3); 1.36 (q, 8H; 4 x CH_2); 1.56 (q, 8H; 4 x CH_2); 3.03 (t, 8H; 4 x CH_2).

4.3.2. Acylferrocenyl esters

The synthesis of 1-carbomethoxy-1′-nonanoylferrocene is provided as a representative example.

4.3.2.1. 1-Carbomethoxy-1′-nonanoylferrocene, 42a [Scheme 3.1, p 69]

In a 250 cm^3 two-necked round bottom flask, zinc powder (5.36 g, 82 mmol) and aluminium chloride (1.64 g, 12.3 mmol) were added to a stirred solution of methylferrocenoate (2.34 g, 12.3

mmol) in dichloromethane (CH_2Cl_2) (60 cm^3) cooled to 0 ^oC. Nonanoyl chloride (2.17 g, 12.3 mmol) in CH_2Cl_2 (40 cm^3) was added dropwise to the suspension which was stirred at 0 ^oC for 3 hours. The mixture was allowed to warm to room temperature. The crude was recovered by filtration and washed thoroughly with CH_2Cl_2. The organic phase was hydrolyzed with water (50 cm^3), washed with a dilute $NaHCO_3$ solution to neutral pH, and dried over $MgSO_4$. The solvent was evaporated to dryness and purified by column chromatography (CH_2Cl_2 as eluent) to give an oily 1-carbomethoxy-1$^/$-nonanoylferrocene (4.06 g, 48 %) yield. R_f = 0.68. δ_H (300 MHz, $CDCl_3$/ppm): 0.90 (3 H, t, (CH_3), 1.30 (12 H, m, $(CH_2)_6$, 1.70 (2H, s, CH_2), 2.70 (2H, m, $COCH_2$), 3.85 (3H, s, CO_2CH_3), 4.40 (2H, t, HCp), 4.50 (2 H, t, HCp), 4.83 (4H, t, HCp).

Characterization data of the other carboxylic acids is as follows.

4.3.2.2. 1-Carbomethoxy-1$^/$-decanoylferrocene, 42b [Scheme 3.1, p 69]

Yield: 86 % as dark red oil. R_f = 0.64. δ_H (300 MHz, $CDCl_3$/ppm): 0.90 (3 H, t, (CH_3), 1.30 (10 H, m, $(CH_2)_6$), 1.60 (2H, s, (CH_2), 1.70 (2H, s, CH_2), 2.70 (2H, m, $COCH_2$), 3.85 (3H, s, CO_2CH_3), 4.40 (2H, t, HCp), 4.50 (2 H, t, HCp), 4.83 (4H, t, HCp).

4.3.2.3. 1-Carbomethoxy-1$^/$-dodecanoylferrocene, 42c [Scheme 3.1, p 69]

Yield: 86 % as a red solid. R_f = 0.68. Melting point = 42 ^oC δ_H (300 MHz, $CDCl_3$/ppm): 0.90 (3 H, t, (CH_3), 1.30 (18 H, m, $(CH_2)_9$), 1.70 (2H, s, CH_2), 2.70 (2H, m, $COCH_2$), 3.85 (3H, s, CO_2CH_3), 4.40 (2H, t, HCp), 4.50 (2 H, t, HCp), 4.83 (4H, t, HCp).

4.3.2.4. 1-Carbomethoxy-1$^/$-tetradecanoylferrocene, 42d [Scheme 3.1, p 69]

Yield: 51 % as red solid. R_f = 0.47. Melting point = 70 ^oC. δ_H (300 MHz, $CDCl_3$/ppm): 0.90 (3 H, t, (CH_3), 1.30 (20H, m, $(CH_2)_{10}$), 1.70 (2H, s, CH_2), 2.70 (2H, m, $COCH_2$), 3.85 (3H, s, CO_2CH_3), 4.40 (2H, t, HCp), 4.50 (2 H, t, HCp), 4.80 (4H, t, HCp).

4.3.2.5. 1-Carbomethoxy-1′-octadecanoylferrocene, 42e [Scheme 3.1, p 69]

Yield: 48 % as brownish solid. R_f = 0.62. Melting point = 66 °C. δ_H (300 MHz, $CDCl_3$/ppm): 0.90 (3 H, t, (CH_3), 1.30 (32H, m, $(CH_2)_{16}$), 2.70 (2H, m, $COCH_2$), 3.85 (3H, s, CO_2CH_3), 4.40 (2H, t, HCp), 4.52 (2 H, t, HCp), 4.80 (4H, t, HCp).

4.3.2.6. 1-Carbomethoxy-3,1′-di(decanoyl)ferrocene, 43a [Scheme 3.1, p 69]

Yield: 54 % as brownish solid. R_f = 0.73. Melting point = 58 °C δ_H (300 MHz, $CDCl_3$/ppm): 0.88 (3 H, t, (CH_3), 1.30 (28 H, m, $(CH_2)_{14}$), 1.65 (4H, s, $(CH_2)_2$), 2.35 (2H, s, $COCH_2$), 2.70 (2H, t, $COCH_2$), 3.85 (3 H, s, CO_2CH_3), 4.40 (2H, t, HCp), 4.52 (2 H, t, HCp), 4.80 (4H, s, HCp).

4.3.2.7. 1-Carbomethoxy-3,1′-di(dodecanoyl)ferrocene, 43b [Scheme 3.1, p 69]

Yield: 70 % as red solid. R_f = 0.66. Melting point = 40 °C. δ_H (300 MHz, $CDCl_3$/ppm): 0.90 (6 H, t, $(CH_3)_2$), 1.30 (36 H, m, $(CH_2)_{18}$), 1.65 (4H, s, $(CH_2)_2$), 2.35 (2H, s, $COCH_2$), 2.70 (2H, t, $COCH_2$), 3.85 (3 H, s, CO_2CH_3), 4.40 (2H, t, HCp), 4.52 (2 H, t, HCp), 4.80 (4H, s, HCp).

4.3.3. Alkylferrocenyl esters

All the alkylferrocenyl esters were synthesized from a general procedure.[5]

4.3.3.1. 1-Carbomethoxy-1′-(nonyl)ferrocene, 44a [Scheme 3.1, p 69]

A mixture of zinc powder (10.36 g, 160 mmol), mercury chloride (0.72 g, 2.65 mmol), water (20 cm^3) and concentrated HCl (4 cm^3) was stirred at room temperature for 5 min. The aqueous phase was removed and replaced by water (35 cm^3) and concentrated HCl (16 cm^3). Then a solution of 1-carbomethoxthy -1'-nonanoylferrocene (1.2 g, 3.122 mmol) in methanol (40 cm^3) was added. The suspension was refluxed overnight. The mixture was cooled to room temperature and the organic phase was recovered, diluted with methanol (100 cm^3), washed with water to neutral pH, dried over $MgSO_4$ and evaporated to dryness under reduced pressure. Purification of the residue by column chromatography (CH_2Cl_2 as eluent) gave 1-carbomethoxthy-1′-(nonyl)ferrocene (1.013 g, 88 %) as

a red oil. Characterization data: R_f = 0.68. δ_H (300 MHz, $CDCl_3$/ppm): 0.88 (6 H, t, $(CH_3)_2$), 1.30 (18 H, m, $(CH_2)_9$), 1.43 (4 H, s, $(CH_2)_2$), 2.26 (4 H, m, $(CH_2)_2$), 4.10 (4 H, s, HCp), 4.46 (2 H, t, HCp), 4.70 (2H, t, HCp).

4.3.3.2. 1-Carbomethoxy-1′-(decyl)ferrocene, 44b [Scheme 3.1, p 69]

1-Carbomethoxy-1′-(decyl)ferrocene was prepared in yields up to 55 % as a red oil. Characterization data: R_f = 0.76. δ_H (300 MHz, $CDCl_3$/ppm): 0.90 (3 H, t, (CH_3), 1.30 (14H, m, $(CH_2)_7$), 1.45 (2H, s, CH_2), 2.25 (2H, m, CH_2), 3.80 (3H, s, CO_2CH_3), 4.10 (4H, t, HCp), 4.35 (2H, t, HCp), 4.73 (2H, t, HCp).

4.3.3.3. 1-Carbomethoxy-1′-(dodecyl)ferrocene, 44c [Scheme 3.1, p 69]

1-Carbomethoxy-1′-(dodecyl)ferrocene was prepared in yields up to 54 %. Characterization data: R_f = 0.70. Melting point = 28 ºC. δ_H (300 MHz, $CDCl_3$/ppm): 0.88 (6 H, t, $(CH_3)_2$), 1.30 (36 H, m, $(CH_2)_{18}$), 1.43 (4 H, s, $(CH_2)_2$), 2.26 (4 H, m, $(CH_2)_2$), 4.10 (4 H, s, HCp), 4.46 (H, s, HCp), 4.70 (2H, t, HCp).

4.3.3.4. 1-Carbomethoxy-1′-(tetradecyl)ferrocene, 44d [Scheme 3.1, p 69]

1-Carbomethoxy-1′-(tetradecyl)ferrocene was prepared in yields up to 51. Characterization data: R_f = 0.47. Melting point = 53 ºC. δ_H (300 MHz, $CDCl_3$/ppm): 0.88 (6 H, t, $(CH_3)_2$), 1.30 (18 H, m, $(CH_2)_9$), 1.43 (4 H, s, $(CH_2)_2$), 2.26 (4 H, m, $(CH_2)_2$), 4.10 (4 H, s, HCp), 4.46 (2 H, t, HCp), 4.70 (2H, t, HCp).

4.3.3.5. 1-Carbomethoxy-1′-(octa)decylferrocene, 44e [Scheme 3.1, p 69]

1-Carbomethoxy-1′-(octa)decylferrocene was prepared in yields up to 56 %. Characterization data: R_f = 0.71. Melting point = 50 ºC. δ_H (300 MHz, $CDCl_3$/ppm): 0.88 (6 H, t, $(CH_3)_2$), 1.30 (30H, m, $(CH_2)_{15}$), 1.45 (2H, s, CH_2), 2.25 (2H, m, $(CH_2)_2$), 3.80 (3H, s, CO_2CH_3), 4.10 (4H, s, HCp), 4.35 (2H, t, HCp), 4.73 (2H, t, HCp).

4.3.4. Alkylferrocenyl carboxylic acids

All the alkylferrocenyl carboxylic acids were synthesized from a general procedure.

4.3.4.1. 1-Carboxy-1′-(nonyl)ferrocene, 45a [Scheme 3.1, p 69]

In a two-necked flask, a solution of 1-carbomethoxy-1′-(nonyl)ferrocene (1.00 g, 2.70 mmol) and potassium hydroxide (0.8762 g, 15.62 mmol) in ethanol (50 cm^3) was stirred under reflux for 4 h. The solution was cooled to room temperature and poured onto a stirred ice-water mixture. Concentrated HCl was added slowly to acid pH. The formed precipitate was recovered by filtration and washed thoroughly with water to give a brown solid 1-carboxy-1′-(nonyl)ferrocene, (0.63 g, 66 %). Characteristic data: Melting point = 48 °C. δ_H (300 MHz, $CDCl_3$): 0.90 (3H, t, CH_3), 1.25 (12H, m, $(CH_2)_6$), 1.50 (2H, s, CH_2), 2.32 (2H, s, CH_2), 4.10 (2H, s, HCp), 4.22 (2H, t, HCp), 4.40 (2H, t, HCp). 4.80 (2H, t, HCp).

Characterization data of the other carboxylic acids is as follows.

4.3.4.2. 1-Carboxy-1′-(decyl)ferrocene, 45b [Scheme 3.1, p 69]

Yield: 52 % as a yellowish solid. Melting point = 52 °C. δ_H (300 MHz, $CDCl_3$/ppm): 0.90 (3H, t, CH_3), 1.30 (14H, m, $(CH_2)_7$), 1.50 (2H, s, CH_2), 2.28 (2H, s, CH_2), 4.10 (4H, t, HCp), 4.40 (2H, t, HCp). 4.78 (2H, t, HCp).

4.3.4.3. 1-Carboxy-1′-(dodecyl)ferrocene, 45c [Scheme 3.1, p 69]

Yield: 69 % as a brownish solid. Melting point = 65 °C. δ_H (300 MHz, $CDCl_3$/ppm): 0.90 (3H, t, CH_3), 1.20 (18H, m, $(CH_2)_9$), 1.55 (2H, s, CH_2), 2.30 (2H, s, CH_2), 4.15 (4H, t, HCp), 4.50 (2H, t, HCp). 4.80 (2H, t, HCp).

4.3.4.4. 1-Carboxy-1′-(tetradecyl)ferrocene, 45d [Scheme 3.1, p 69]

Yield: 62 % as a yellowish solid. Melting point = 73 °C. δ_H (300 MHz, $CDCl_3$/ppm): 0.90 (3H, t, CH_3), 1.24 (24H, m, $(CH_2)_{12}$), 1.50 (2H, s, CH_2), 2.27 (2H, s, CH_2), 4.10 (4H, t, HCp), 4.40 (2H, t, HCp). 4.77 (2H, t, HCp).

4.3.4.5. 1-Carboxy-1′-(octadecyl)ferrocene, 45e [Scheme 3.1, p 69]

Yield: 86 % as a yellow solid. Melting point = 79 – 82 ºC. δ_H (300 MHz, $CDCl_3$/ppm): 0.90 (3H, t, CH_3), 1.25 (30H, m, $(CH_2)_{15}$), 1.45 (2H, s, CH_2), 2.25 (2H, s, CH_2), 4.20 (4H, t, HCp), 4.45 (2H, t, HCp). 4.82 (2H, t, HCp).

4.3.5. Ferrocenyl ketones

General procedure for the preparation of ferrocenyl ketones.[6]

In a clean oven-dried 250 cm^3 round-bottom flask immersed in an ice bath, and flushed with nitrogen gas, ferrocene (2.00g, 10.75mmol, 1.0 equiv.) was added to a stirred suspension of the acyl chloride (1.1 equiv. for the monoketones and 2.2 equiv. for diketones) and aluminum chloride (1.1 equiv. for the monoketones and 2.2 equiv. for diketones) in dichloromethane (22 cm^3.). The appearance of a deep blue colour indicates that the reaction was taking place. The resulting mixture was stirred for 30 min in the ice bath and then overnight at room temperature. The reaction mixture was cooled in ice, ice water (200 cm^3) was cautiously added, and the resulting heterogeneous mixture stirred vigorously for 30 min before the separated aqueous layer was extracted with dichloromethane (3 x 200 cm^3). The dichloromethane extracts were combined with the original organic layer before it was first washed with an equal volume of water, with 10% aqueous NaOH (2 x 100 cm^3), and dried over $MgSO_4$. Removal of the solvent under reduced pressure gave the crude product which was purified by column chromatography (ether:hexane = 1:4) on silica gel to give the ferrocenyl ketone.

Characterisation data is as follows:

4.3.5.1. 1-Nonanoylferrocene, 46a [Scheme 3.2, p 70]

Yield: 91 % as a dark brown oil; R_f = 0.63. δ_H (300 MHz, $CDCl_3$/ppm) 0.90 (3 H, t, CH_3), 1.31 (10 H, m, $(CH_2)_5$), 1.71 (2 H, s, CH_2), 2.70 (2 H, m, $COCH_2$), 4.20 (5 H, s, HCp), 4.50 (2 H, t, HCp), 4.80 (2H, t, HCp).

4.3.5.2. 1-Decanoylferrocene, 46b [Scheme 3.2, p 70]

Yield: 95 % as a brown solid; melting point = 37 ^{o}C; R_f = 0.55. δ_H (300 MHz, $CDCl_3$/ppm): 0.90 (3 H, t, CH_3), 1.31 (14 H, m, $(CH_2)_6$), 1.71 (2 H, s, CH_2), 2.70 (2 H, m, $COCH_2$), 4.20 (5 H, s, HCp), 4.50 (2 H, t, HCp), 4.80 (2H, t, HCp).

4.3.5.3. 1-Dodecanoylferrocene, 46c [Scheme 3.2, p 70]

Yield: 92 % as a yellow solid; melting point = 43 ^{o}C; R_f = 0.50. δ_H (300 MHz, $CDCl_3$/ppm): 0.90 (3 H, t, CH_3), 1.31 (16 H, m, $(CH_2)_8$), 1.71 (2 H, s, CH_2), 2.70 (2 H, m, $COCH_2$), 4.20 (5 H, s, HCp), 4.50 (2 H, t, HCp), 4.80 (2H, t, HCp).

4.3.5.4. 1-Tetradecanoylferrocene, 46d [Scheme 3.2, p 70]

Yield: 79 % as a brown solid; melting point = 48 ^{o}C, R_f = 0.50. δ_H (300 MHz, $CDCl_3$/ppm): 0.90 (3 H, t, CH_3), 1.31 (20 H, m, $(CH_2)_{10}$), 1.71 (2 H, s, CH_2), 2.70 (2 H, m, $COCH_2$), 4.20 (5 H, s, HCp), 4.50 (2 H, t, HCp), 4.80 (2H, t, HCp).

4.3.5.5. 1-Octadecanoylferrocene, 46e [Scheme 3.2, p 70]

Yield: 59 % as a yellow solid; melting point = 64 ^{o}C, R_f = 0.54. δ_H (300 MHz, $CDCl_3$/ppm): 0.90 (3 H, t, CH_3), 1.31 (12 H, m, $(CH_2)_{14}$), 1.71 (2 H, s, CH_2), 2.70 (2 H, m, $COCH_2$), 4.20 (5 H, s, HCp), 4.50 (2 H, t, HCp), 4.80 (2H, t, HCp).

4.3.5.6. 1,1$^{/}$-Di(decanoyl)ferrocene, 50a [Scheme 3.2, p 70]

Yield: 50 % as a brown solid; melting point = 67 ^{o}C, R_f = 0.34. δ_H (300 MHz, $CDCl_3$/ppm): 0.90 (6 H, t, $(CH_3)_2$), 1.31 (24 H, m, $(CH_2)_{12}$), 1.71 (4 H, s, $(CH_2)_2$), 2.70 (4 H, m, $(COCH_2)_2$), 4.20 (4 H, s, HCp), 4.50 (2 H, t, HCp), 4.80 (2H, t, HCp).

4.3.5.7. 1,1′-Di(dodecanoyl)ferrocene, 50b [Scheme 3.2, p 70]

Yield: 41 % as a red solid; melting point = 68 °C, R_f = 0.38. δ_H (300 MHz, $CDCl_3$/ppm): 0.90 (6 H, t, $(CH_3)_2$), 1.31 (32 H, m, $(CH_2)_{16}$), 1.71 (4 H, s, $(CH_2)_2$), 2.70 (4 H, m, $(COCH_2)_2$), 4.20 (4 H, s, HCp), 4.50 (2 H, t, HCp), 4.80 (2H, t, HCp).

4.3.6. Alkylferrocene

4.3.6.1. 1-Nonylferrocene, 47a [Scheme 3.2, p 70]

The synthesis of 1-nonylferrocene is provided as a representative example.

First zinc amalgam was prepared by washing 20 g of zinc dust with 2 mol dm^{-3} HCl after which 27 cm^3 water, 2 g mercuric chloride and 1.1 cm^3 concentrated HCl were added. The mixture was left for 10 min after which all liquids were decanted from the gray solid residue. The newly formed amalgam was then washed with water (10 cm^3), methanol (15 cm^3), 2 mol dm^{-3} HCl (10 cm^3) and again with water (20 cm^3).

1-Nonylferrocene, (7.37 g, 22.59 mmol) was refluxed in a mixture of concentrated HCl (40 cm^3), methanol (20 cm^3) and water (20 cm^3) in the presence of zinc amalgam under nitrogen for 42 hours. Concentrated HCl (2 cm^3 aliquots) was added to the mixture at 12 hours intervals. The ice cooled product was diluted with ice water (150 cm^3) and extracted with diethyl ether. The ether extracts were combined and washed thoroughly with water, and dried over $MgSO_4$. Solvent removal under reduced pressure gave a brownish solid (6.2 g, 88 %). Characterization data: Melting point = 33 °C; R_f = 0.61 (hexane). δ_H (300 MHz, $CDCl_3$): 0.88 (3 H, t, CH_3/ppm), 1.30 (12 H, m, $(CH_2)_6$), 1.43 (2 H, s, CH_2), 2.26 (2 H, m, CH_2), 4.10 (5 H, s, HCp), 4.46 (2 H, t, HCp), 4.70 (2H, t, HCp).

Characterization data for the other alkyl ferrocenes are given below.

4.3.6.2. 1-Decylferrocene, 47b [Scheme 3.2, p 70]

Yield: 86 % as a brownish solid; melting point = 35 °C; R_f = 0.59. δ_H (300 MHz, $CDCl_3$/ppm): 0.88 (3 H, t, CH_3), 1.30 (14 H, m, $(CH_2)_7$), 1.43 (2 H, s, CH_2), 2.26 (2 H, m, CH_2), 4.10 (5 H, s, HCp), 4.46 (2 H, t, HCp), 4.70 (2H, t, HCp).

4.3.6.3. 1-Dodecylferrocene, 47c [Scheme 3.2, p 70]

Yield: 80 % as a yellow solid; melting point = 36 ^{o}C; R_f = 0.60. δ_H (300 MHz, $CDCl_3$/ppm): 0.88 (3 H, t, CH_3), 1.30 (18 H, m, $(CH_2)_9$), 1.43 (2 H, s, CH_2), 2.26 (2 H, m, CH_2), 4.10 (5 H, s, HCp), 4.46 (2 H, t, HCp), 4.70 (2H, t, HCp).

4.3.6.4. 1-Tetradecylferrocene, 47d [Scheme 3.2, p 70]

Yield: 76 % as a brown solid; melting point = 43 ^{o}C; R_f = 0.61. δ_H (300 MHz, $CDCl_3$/ppm): 0.88 (3 H, t, CH_3), 1.30 (22 H, m, $(CH_2)_{11}$), 1.43 (2 H, s, CH_2), 2.26 (2 H, m, CH_2), 4.10 (5 H, s, HCp), 4.46 (2 H, t, HCp), 4.70 (2H, t, HCp).

4.3.6.5. 1-Octadecylferrocene, 47e [Scheme 3.2, p 70]

Yield: 94 % as a yellow powder; melting point = 54 ^{o}C; R_f = 0.71. δ_H (300 MHz, $CDCl_3$/ppm): 0.88 (3 H, t, CH_3), 1.30 (30 H, m, $(CH_2)_{15}$), 1.43 (2 H, s, CH_2), 2.26 (2 H, m, CH_2), 4.10 (5 H, s, HCp), 4.46 (2 H, t, HCp), 4.70 (2H, t, HCp).

4.3.6.6. 1,1$^{/}$-Di(decanyl)ferrocene, 51a [Scheme 3.2, p 70]

Yield: 92 % as a dark brown oil; R_f = 0.70. δ_H (300 MHz, $CDCl_3$/ppm): 0.88 (6 H, t, $(CH_3)_2$), 1.30 (28 H, m, $(CH_2)_{14}$), 1.43 (4 H, s, $(CH_2)_2$), 2.26 (2 H, m, $(CH_2)_2$), 4.10 (4 H, s, HCp), 4.46 (2 H, t, HCp), 4.70 (2H, t, HCp).

4.3.6.7. 1,1$^{/}$-Di(dodecyl)ferrocene, 51b [Scheme 3.2, p 70]

Yield: 86 % as a dark brown oil; R_f = 0.71. δ_H (300 MHz, $CDCl_3$/ppm): 0.88 (6 H, t, $(CH_3)_2$), 1.30 (36 H, m, $(CH_2)_{18}$), 1.43 (4 H, s, $(CH_2)_2$), 2.26 (4 H, m, $(CH_2)_2$), 4.10 (4 H, s, HCp), 4.46 (2 H, t, HCp), 4.70 (2H, t, HCp).

4.3.7. Acetyl-alkylferrocene

4.3.7.1. 1-Acetyl-1′-nonylferrocene, 48a [Scheme 3.2, p 70]

1-Acetyl-1′-nonylferrocene is provided as a representative example.

In a clean oven-dried 250 cm^3 round-bottom flask immersed in an ice bath, and flushed with nitrogen gas, 1-nonylferrocene (4.00g, 12.26mmol.) was added to a stirred suspension of the acetylchloride (0.9624g, 12.26 mmol) and aluminium chloride (1.635g, 12.26 mmol) in dichloromethane (45 cm^3). The appearance of a deep blue colour indicates that the reaction was taking place. The resulting mixture was stirred for 30 min in the ice bath and then overnight at room temperature. The reaction mixture was cooled in ice, ice water (200 cm^3) was cautiously added, and the resulting heterogeneous mixture stirred vigorously for 30 min before the separated aqueous layer was extracted with dichloromethane (3 x 200 cm^3). The dichloromethane extracts were combined with the original organic layer before it was first washed with an equal volume of water, with 10% aqueous NaOH (2 x 100 cm^3), and dried over $MgSO_4$. Removal of the solvent under reduced pressure gave the crude product which was purified by column chromatography (ether:hexane = 1:2) on silica gel to give the 1-acetyl-1′-nonylferrocene in yields up to 53 % as dark brown oil. R_f =0.38. δ_H (300 MHz, $CDCl_3$/ppm): 0.90 (3 H, t, CH_3), 1.30 (12 H, m, $(CH_2)_6$), 1.45 (2 H, s, CH_2), 2.25 (2 H, m, CH_2), 2.40 (3H, s, $COCH_3$), 4.10 (4 H, s, HCp), 4.45 (2 H, t, HCp), 4.70 (2H, t, HCp).

Characterization data for the other 1-acetyl-1′-alkylferrocenes are given below.

4.3.7.2. 1-Acetyl-1′-decylferrocene, 48b [Scheme 3.2, p 70]

Yield: 62 % as a dark red oil, R_f = 0.41. δ_H (300 MHz, $CDCl_3$/ppm): 0.90 (3 H, t, CH_3), 1.27 (14 H, m, $(CH_2)_7$), 1.45 (2 H, s, CH_2), 2.22 (2 H, m, CH_2), 2.35 (3H, s, $COCH_3$), 4.15 (4 H, s, HCp), 4.50 (2 H, t, HCp), 4.78 (2H, t, HCp).

4.3.7.3. 1-Acetyl-1′-dodecylferrocene, 48c [Scheme 3.2, p 70]

Yield: 59 % as brown oil, R_f = 0.44. δ_H (300 MHz, $CDCl_3$/ppm): 0.90 (3 H, t, CH_3), 1.30 (18 H, m, $(CH_2)_9$), 1.45 (2 H, s, CH_2), 2.25 (2 H, m, CH_2), 2.40 (3H, s, $COCH_3$), 4.05 (4 H, s, HCp), 4.50 (2 H, t, HCp), 4.70 (2H, t, HCp).

4.3.7.4. 1-Acetyl-1′-tetradecylferrocene, 48d [Scheme 3.2, p 70]

Yield: 47 % as a yellow solid, melting point = 41 °C, R_f = 0.39. δ_H (300 MHz, $CDCl_3$/ppm): 0.88 (3 H, t, CH_3), 1.30 (22 H, m, $(CH_2)_{11}$), 1.43 (2 H, s, CH_2), 2.26 (2 H, m, CH_2), 4.10 (5 H, s, HCp), 4.46 (2 H, t, HCp), 4.70 (2H, t, HCp).

4.3.7.5. 1-Acetyl-1′-octadecylferrocene, 48e [Scheme 3.2, p 70]

Yield: 39 % as a red solid, melting point = 51 °C, R_f = 0.48. δ_H (300 MHz, $CDCl_3$/ppm: 0.90 (3 H, t, CH_3), 1.28 (30 H, m, $(CH_2)_{15}$), 1.43 (2 H, s, CH_2), 2.25 (2 H, m, CH_2), 2.40 (3H, s, $COCH_3$), 4.10 (4 H, s, HCp), 4.46 (2 H, t, HCp), 4.70 (2H, t, HCp).

4.3.7.6. 1-Acetyl-3-decylferrocene, 49a [Scheme 3.2, p 70]

Yield: 49 % as a brown solid, melting point = 46 °C, R_f = 0.33. δ_H (300 MHz, $CDCl_3$): 0.90 (3 H, t, CH_3), 1.30 (14 H, m, $(CH_2)_7$), 1.52 (2 H, s, CH_2), 2.38 (5H, s, $CH_2CpCOCH_3$), 4.20 (4 H, s, HCp), 4.50 (2 H, t, HCp), 4.75 (2H, t, HCp).

4.3.7.7. 1-Acetyl-3-dodecylferrocene, 49b [Scheme 3.2, p 70]

Yield: 55 % as a brown solid, melting point = 53 °C, R_f = 0.35. δ_H (300 MHz, $CDCl_3$/ppm): 0.90 (3 H, t, CH_3), 1.30 (18 H, m, $(CH_2)_9$), 1.50 (2 H, s, CH_2), 2.35 (5H, s, $CH_2CpCOCH_3$), 4.20 (4 H, s, HCp), 4.46 (2 H, t, HCp), 4.70 (2H, t, HCp).

4.3.7.8. 1-Acetyl-3,1′-di(decyl)ferrocene, 52a [Scheme 3.2, p 70]

Yield: 33 % as a dark red oil, R_f = 0.54. δ_H (300 MHz, $CDCl_3$/ppm): 0.90 (6 H, t, $(CH_3)_2$), 1.30 (28 H, m, $(CH_2)_{14}$), 1.50 (2 H, s, CH_2), 2.26 (2H, m, CH_2), 2.38 (5H, s, $CH_2CpCOCH_3$), 4.00 (4 H, s, HCp), 4.33 (H, t, HCp), 4.60 (H, t, HCp).

4.3.7.9. 1-Acetyl-3,1′-di(dodecyl)ferrocene, 52b [Scheme 3.2, p 70]

Yield: 37 % as a dark red oil, R_f = 0.68. δ_H (300 MHz, $CDCl_3$/ppm): 0.90 (6 H, t, $(CH_3)_2$), 1.30 (36 H, m, $(CH_2)_{18}$), 1.50 (4 H, s, $(CH_2)_2$), 2.26 (2H, m, CH_2), 2.35 (5H, s, $CH_2CpCOCH_3$), 4.00 (4 H, s, HCp), 4.35 (2 H, t, HCp), 4.60 (2H, t, HCp).

4.3.8. β-Diketones

All the β-diketones were synthesized from a general procedure as described for 1-[1-(nonyl)ferrocenyl-1′-]-butane-1,3-dione.

4.3.8.1. 1-[1-(nonyl)ferrocenyl-1′-]-butane-1,3-dione, 53a [Scheme 3.3, p 72]

A flask charged with 1-acetyl-1′-nonylferrocene (1.00 g, 2.821 mmol) and dry THF (5 cm^3) was degassed with nitrogen for an hour. Lithiumdiisopropylamide (LDA) (2 cm^3) was added at 0 ^oC and the solution was stirred for 30 minutes before a solution of ethyl acetate (distilled prior to use) (0.2880 g, 2.821 mmol) in 1 cm^3 dry THF was added. The resulting dark red suspension was stirred under nitrogen atmosphere for 16 hours, followed by treatment with HCl (100 cm^3, 0.5 mol dm^{-3}). After extraction of the product with ether, purification was effected by column chromatography on silica gel (hexane:ether (4:1) as the eluent) and dried over $MgSO_4$. Solvent removal under reduced pressure yielded 1-[1-(nonyl)ferrocenyl-1′-]-butane-1,3-dione (0.39 g, 33 %) as dark red oil. Characterization data: R_f = 0.53 (ether:hexane = 1:4); δ_H (300 MHz, $CDCl_3$/ppm): 0.90 (3H, t, CH_3), 1.30 (12H, m, $(CH_2)_6$), 1.45 (2H, s, CH_2), 2.10 (3H, s, enol CH_3), 2.25 (2H, t, CH_2), 2.35 (3H, s, keto CH_3), 3.85 (2H, s, keto CH_2), 4.10 (4H, t, enol + keto HCp), 4.45 (2H, s, enol HCp), 4.52 (2H, s, keto HCp), 4.72 (2H, s, enol + keto HCp), 5.70 (1H, s, enol CH).

Characterization data for the other β-diketones.

4.3.8.2. 1-[1-(decyl)ferrocenyl-1′-]-butane-1,3-dione, 53b [Scheme 3.3, p 72]

Yield: 37 % as a dark red oil; R_f = 0.48. δ_H (300 MHz, $CDCl_3$/ppm): 0.90 (3H, t, CH_3), 1.27 (14H, m $(CH_2)_7$), 1.45 (2H, s, CH_2), 2.10 (2H, s, enol CH_3), 2.30 (2H, t, CH_2), 2.32 (3H, s, keto CH_3), 3.82 (2H, s, keto CH_2), 4.05 (4H, t, enol HCp), 4.15 (4H, s, keto HCp), 4.45 (2H, s, enol HCp), 4.58

(2H, s, keto HCp), 4.70 (2H, s, enol HCp), 4.80 (2H, s, keto HCp), 5.70 (1H, s, enol CH). $C_{24}H_{34}FeO_2$ requires: C, 70.23 %; H, 8.35 %. Found: C, 69.23 %; H, 7.60 %.

4.3.8.3. 1-[1-(dodecyl)ferrocenyl-1′-]-butane-1,3-dione, 53c [Scheme 3.3, p 72]

Yield: 34 % as a dark red solid; melting point = 39 °C, R_f = 0.56. δ_H (300 MHz, $CDCl_3$/ppm): 0.90 (3H, t, CH_3), 1.27 (18H, m $(CH_2)_9$), 1.44 (2H, s, CH_2), 2.08 (3H, s, enol CH_3), 2.22 (2H, t, CH_2), 2.32 (3H, s, keto CH_3), 3.83 (2H, s, keto CH_2), 4.05 (4H, t, enol HCp), 4.15 (4H, s, keto HCp), 4.43 (2H, s, enol HCp), 4.52 (2H, s, keto HCp), 4.67 (2H, s, enol HCp), 4.78 (4H, s, HCp), 5.70 (1H, s, enol CH).

4.3.8.4. 1-[1-(tetradecyl)ferrocenyl-1′-]-butane-1,3-dione, 53d [Scheme 3.3, p 72]

Yield: 41 % as a dark red solid, melting point = 41 - 43 °C; R_f = 0.59. δ_H (300 MHz, $CDCl_3$/ppm): 0.90 (3H, t, CH_3), 1.28 (12H, m $(CH_2)_{11}$), 1.47 (2H, s, CH_2), 2.10 (3H, s, enol CH_3), 2.25 (2H, t, CH_2), 2.32 (3H, s, keto CH_3), 3.83 (2H, s, keto CH_2), 4.05 (4H, t, enol HCp), 4.15 (4H, s, keto HCp), 4.48 (2H, s, enol HCp), 4.52 (2H, s, keto HCp), 4.70 (2H, s, enol HCp), 4.78 (2H, s, HCp), 5.70 (1H, s, enol CH).

4.3.8.5. 1-[1-(octadecyl)ferrocenyl-1′-]-butane-1,3-dione, 53e [Scheme 3.3, p 72]

Yield: 34 % as a red solid; melting point = 63 °C, R_f = 0.56. δ_H (300 MHz, $CDCl_3$/ppm): 0.90 (3H, t, CH_3), 1.30 (30H, m $(CH_2)_{15}$), 1.45 (2H, s, CH_2), 2.10 (3H, s, enol CH_3), 2.22 (2H, t, CH_2), 2.32 (3H, s, keto CH_3), 3.82 (2H, s, keto CH_2), 4.05 (4H, t, enol HCp), 4.15 (4H, s, keto HCp), 4.47 (2H, s, enol HCp), 4.53 (2H, s, keto HCp), 4.71 (2H, s, enol HCp), 4.82 (2H, s, HCp), 5.70 (1H, s, enol CH).

4.3.8.6. 1-[3-(decyl)ferrocenyl-1-]-butane-1,3-dione, 54a [Scheme 3.3, p 72]

Yield: 37 % as a red solid; melting point = 51 °C, R_f = 0.58. δ_H (300 MHz, $CDCl_3$/ppm): 0.90 (3H, t, CH_3), 1.25 (14H, m $(CH_2)_7$), 1.45 (2H, s, CH_2), 2.10 (3H, s, enol CH_3), 2.20 (2H, t, CH_2), 2.32 (3H, s, keto CH_3), 3.82 (2H, s, keto CH_2), 4.05 (4H, t, enol HCp), 4.15 (4H, s, keto HCp), 4.45

(2H, s, enol HCp), 4.52 (2H, s, keto HCp), 4.70 (2H, s, enol + keto HCp), 5.70 (1H, s, enol CH). $C_{24}H_{34}FeO_2$ requires: C, 70.23 %; H, 8.35 %. Found: C, 70.10 %; H, 7.98 %.

4.3.8.7. 1-[3-(dodecyl)ferrocenyl-1′-]-butane-1,3-dione, 54b [Scheme 3.3, p 72]

Yield: 37 % as red oil, R_f = 0.42. δ_H (300 MHz, $CDCl_3$/ppm): 0.90 (3H, t, CH_3), 1.25 (18H, m $(CH_2)_9$), 1.43 (2H, s, CH_2), 2.10 (3H, s, enol CH_3), 2.22 (2H, t, CH_2), 2.32 (3H, s, keto CH_3), 3.85 (2H, s, keto CH_2), 4.05 (4H, t, enol HCp), 4.15 (4H, s, keto HCp), 4.45 (2H, s, enol HCp), 4.52 (2H, s, keto HCp), 4.65 (2H, s, enol HCp), 4.80 (4H, s, HCp), 5.70 (1H, s, enol CH).

4.3.8.8. 1-[1,1′-di(decyl)ferrocenyl-3-]-butane-1,3-dione, 55a [Scheme 3.3, p 72]

Yield: 35 % as red oil, R_f = 0.55; δ_H (300 MHz, $CDCl_3$/ppm): 0.90 (6H, t, $(CH_3)_2$), 1.30 (28H, m $(CH_2)_{14}$), 1.43 (2H, t, CH_2), 1.54 (2H, t,CH_2), 2.07 (3H, s, enol CH_3), 2.20 (2H, t, CH_2), 2.35 (2H, t, CH_2), 2.52 (3H, s, keto CH_3), 3.80 (2H, s, keto CH_2), 4.05 (4H, t, enol + keto HCp), 4.38 (1H, s, enol HCp), 4.48 (2H, s, keto HCp), 4.60 (2H, s, keto HCp), 4.71 (2H, s, enol HCp) , 5.70 (1H, s, enol CH). $C_{34}H_{54}FeO_2$ requires: C, 74.65 %; H, 9.88 %. Found: C, 74.78 %; H, 9.20 %.

4.3.8.9. 1-[1,1′-di(dodecyl)ferrocenyl-3-]-butane-1,3-dione, 55b [Scheme 3.3, p 72]

Yield: 33 % as a red solid; melting point = 41 ^oC, R_f = 0.55. δ_H (300 MHz, $CDCl_3$/ppm): 0.90 (6H, t, $(CH_3)_2$), 1.27 (32H, m $(CH_2)_{16}$), 1.40 (2H, t, CH_2), 1.52 (2H, t,CH_2), 2.07 (3H, s, enol CH_3), 2.20 (2H, t, CH_2), 2.35 (2H, t, CH_2), 2.52 (3H, s, keto CH_3), 3.75 (2H, s, keto CH_2), 4.05 (4H, t, enol + keto HCp), 4.34 (1H, s, enol HCp), 4.60 (2H, s, enol + keto HCp), 5.66 (1H, s, enol CH).

4.3.8.10. 1,3-di-[-(1-decyl)ferrocenyl-1′-]-propane-1,3-dione, 56a [Scheme 3.3, p 72]

Yield: 41 % as a dark red oil, R_f = 0.67; δ_H (300 MHz, $CDCl_3$/ppm): 0.85 (6H, t, $(CH_3)_2$), 1.30 (28H, m $(CH_2)_{14}$), 1.45 (4H, t, $(CH_2)_2$), 2.10 (3H, s, enol CH_3), 2.25 (4H, t, $(CH_2)_2$), 2.40 (3H, s, keto CH_3), 3.75 (2H, s, keto CH_2), 4.05 (8H, t, enol + keto 2HCp), 4.40 (4H, s, enol 2HCp), 4.50 (4H, s, keto 2HCp), 4.72 (4H, s, enol 2HCp), 4.85 (4H, s, keto 2HCp), 5.92 (1H, s, enol CH). $C_{43}H_{60}Fe_2O_2$ requires: C, 71.79 %; H, 9.10 %. Found: C, 71.39 %; H, 8.62 %.

4.3.8.11. 1,3-di-[-(1-dodecyl)ferrocenyl-1′-]-propane-1,3-dione, 56b [Scheme 3.3, p 72]

Yield: 30 % as a dark red oil, R_f = 0.65; δ_H (300 MHz, $CDCl_3$/ppm): 0.90 (6H, t, $(CH_3)_2$), 1.30 (36H, m $(CH_2)_{18}$), 1.50 (4H, t, $(CH_2)_2$), 1.52 (2H, t,CH_2), 2.05 (3H, s, enol CH_3), 2.20 (2H, t, CH_2), 2.35 (2H, t, CH_2), 2.52 (3H, s, keto CH_3), 3.75 (2H, s, keto CH_2), 4.00 (4H, t, enol + keto HCp), 4.35 (1H, s, enol HCp), 4.40 (2H, s, keto HCp), 4.60 (2H, s, enol + keto HCp), 5.68 (1H, s, enol CH).

4.3.9. Di-μ-chloro-bis(η-cycloocta-1,5-diene)dirhodium(I) [Rh_2Cl_2(cod)]

$RhCl_3.H_2O$ (0.50 g, 2.200 mmol) was dissolved with few drops of water, and ethanol (11 cm^3) was added while stirring the solution. Cyclooctadiene (3.25 cm^3) was added dropwise and the dark red solution was refluxed at 78 ^oC for 2.5 h. Then the mixture was cooled down on an ice bath. The yellow precipitate was filtered off and washed with methanol. Then di-μ-chloro-bis(η-cycloocta-1,5-diene)dirhodium(I) (0.72 g, 65 % yield) was the left overnight in the cupboard to dry. Characterization data: Melting point = 256 ^oC; δ_H (300 MHz, $CDCl_3$/ppm) 1.80 (4H, m, half of $4CH_2$), 2.50 (4H, m, half of $4CH_2$) and 4.42 (4H, m, half of $4CH_2$).

4.3.10. [Rh(β-diketone)(cod)] complexes

The general procedure for all rhodium complexes was as follows: In a 20 cm^3 round bottom flask, [Rh_2Cl_2(cod)] (0.20 g, 0.4056 mmol) was dissolved in 2 cm^3 DMF. $NaHCO_3$ (0.8112 mmol) was added followed by the β-diketone (0.8112 mmol). After stirring at room temperature for 16 h, the product was precipitated with an excess of ice cold water, filtered off and then extracted with ether. The ethereal extracts were washed with water, dried over $MgSO_4$ followed by solvent removal under reduced pressure. Purification by column chromatography (using hexane:ether (4:1) as eluent) gave the pure products with yields up to 85 %.

Characterization data for all the rhodium complexes are given below.

4.3.10.1. (η^4-1,5-cyclooctadiene){(1-((1-nonyl)ferrocenyl-1′-)-butane-1,3-dionato-κ^2O,O')}rhodium (I), 58a [Scheme 3.4, p 73]

Red oil (45 % yield), R_f = 62. δ_H (300 MHz, $CDCl_3$/ppm): 0.90 (3H, t, CH_3), 1.35 (12H, m, $(CH_2)_6$), 1.48 (2H, t, CH_2), 1.85 (4H, m, half of aliphatic C_8H_{12} protons), 2.00 (3H, t, CH_3), 2.30 (2H, t, CH_2), 2.50 (4H, m, other half of aliphatic C_8H_{12} protons), 4.02 (4H, m, four olefinic protons of C_8H_{12}), 4.12 (4H, t, HCp), 4.35 (2H, s, HCp), 4.55 (2H, s, HCp), 5.58 (1H, s, CH).

4.3.10.2. (η^4-1,5-cyclooctadiene){(1-((1-decyl)ferrocenyl-1′-)-butane-1,3-dionato-κ^2O,O')}rhodium (I), 58b [Scheme 3.4, p 73]

Red oil (75 % yield), R_f = 0.70. δ_H (300 MHz, $CDCl_3$/ppm): 0.90 (3H, t, CH_3), 1.30 (14H, m, $(CH_2)_7$), 1.50 (2H, t, CH_2), 1.85 (4H, m, half of aliphatic C_8H_{12} protons), 2.00 (3H, t, CH_3), 2.30 (2H, t, CH_2), 2.50 (4H, m, other half of aliphatic C_8H_{12} protons), 4.10 (8H, m, four olefinic protons of C_8H_{12} + four protons of HCp), 4.32 (2H, s, HCp), 4.55 (2H, s, HCp), 5.58 (1H, s, CH). $C_{32}H_{45}FeO_2Rh$ requires: C, 62.34 %; H, 6.70 %. Found: C, 61.77 %; H, 7.25 %.

4.3.10.3. (η^4-1,5-cyclooctadiene){(1-((1-dodecyl)ferrocenyl-1′-)-butane-1,3-dionato-κ^2O,O')}rhodium (I), 58c [Scheme 3.4, p 73]

Dark red powder (77 % yield), melting point = 58 ^oC, R_f = 77. δ_H (300 MHz, $CDCl_3$/ppm): 0.90 (3H, t, CH_3), 1.30 (18H, m, $(CH_2)_9$), 1.48 (2H, t, CH_2), 1.85 (4H, m, half of aliphatic C_8H_{12} protons), 2.00 (3H, t, CH_3), 2.28 (2H, t, CH_2), 2.50 (4H, m, other half of aliphatic C_8H_{12} protons), 4.00 (4H, m, four olefinic protons of C_8H_{12}), 4.10 (4H, m, HCp), 4.30 (2H, s, HCp), 4.52 (2H, s, HCp), 5.58 (1H, s, CH).

4.3.10.4. (η^4-1,5-cyclooctadiene){(1-((1-tetradecyl)ferrocenyl-1′-)-butane-1,3-dionato-κ^2O,O')}rhodium (I), 58d [Scheme 3.4, p 73]

Red oil (86 % yield), R_f = 0.78. δ_H (300 MHz, $CDCl_3$/ppm): 0.90 (3H, t, CH_3), 1.29 (22H, m, $(CH_2)_{11}$), 1.50 (2H, t, CH_2), 1.87 (4H, m, half of aliphatic C_8H_{12} protons), 2.00 (3H, t, CH_3), 2.30

(2H, t, CH_2), 2.50 (4H, m, other half of aliphatic C_8H_{12} protons), 3.98 (4H, m, four olefinic protons of C_8H_{12}), 4.10 (4H, m, HCp), 4.32 (2H, s, HCp), 4.55 (2H, s, HCp), 5.59 (1H, s, CH).

4.3.10.5. (η^4-1,5-cyclooctadiene){(1-((1-octadecyl)ferrocenyl-1$^{/}$-)-butane-1,3-dionato-$\kappa^2O,O^{/}$)}rhodium (I), 58e [Scheme 3.4, p 73]

Red powder (78 % yield), melting point = 57 ^oC, R_f = 0.77. δ_H (300 MHz, $CDCl_3$/ppm): 0.90 (3H, t, CH_3), 1.31 (30H, m, $(CH_2)_{15}$), 1.50 (2H, t, CH_2), 1.87 (4H, m, half of aliphatic C_8H_{12} protons), 2.01 (3H, t, CH_3), 2.29 (2H, t, CH_2), 2.50 (4H, m, other half of aliphatic C_8H_{12} protons), 4.01 (4H, m, HCp), 4.10 (4H, m, four olefinic protons of C_8H_{12}), 4.30 (2H, s, HCp), 4.55 (2H, s, HCp), 5.59 (1H, s, CH).

4.3.10.6. (η^4-1,5-cyclooctadiene){(1-((3-decyl)ferrocenyl-1-)-butane-1,3-dionato-$\kappa^2O,O^{/}$)}rhodium (I), 59a [Scheme 3.4, p 73]

Red oil (77 % yield), R_f = 0.75. δ_H (300 MHz, $CDCl_3$/ppm): 0.90 (3H, t, CH_3), 1.30 (14H, m, $(CH_2)_7$), 1.50 (2H, t, CH_2), 1.85 (4H, m, half of aliphatic C_8H_{12} protons), 2.00 (3H, t, CH_3), 2.30 (2H, t, CH_2), 2.51 (4H, m, other half of aliphatic C_8H_{12} protons), 4.10 (8H, m, four olefinic protons of C_8H_{12} + four protons of HCp), 4.29 (2H, s, HCp), 4.55 (2H, s, HCp), 5.58 (1H, s, CH). $C_{32}H_{45}FeO_2Rh$ requires: C, 62.34 %; H, 6.70 %. Found: C, 61.50 %; H, 7.08 %.

4.3.10.7. (η^4-1,5-cyclooctadiene){(1-((3-dodecyl)ferrocenyl-1-)-butane-1,3-dionato-$\kappa^2O,O^{/}$)}rhodium (I), 59b [Scheme 3.4, p 73]

Red powder (52 % yield), melting point = 45 ^oC, R_f = 0.77. δ_H (300 MHz, $CDCl_3$/ppm): 0.90 (3H, t, CH_3), 1.30 (18H, m, $(CH_2)_9$), 1.50 (2H, t, CH_2), 1.85 (4H, m, half of aliphatic C_8H_{12} protons), 2.00 (3H, t, CH_3), 2.30 (2H, t, CH_2), 2.50 (4H, m, other half of aliphatic C_8H_{12} protons), 4.10 (8H, m, four olefinic protons of C_8H_{12} + four protons of HCp), 4.30 (1H, s, HCp), 4.53 (2H, s, HCp), 5.60 (1H, s, CH).

4.3.10.8. (η^4-1,5-cyclooctadiene){(1-((1,1′-di(decyl))ferrocenyl-3-)-butane-1,3-dionato-κ^2O,O')}rhodium (I), 60a [Scheme 3.4, p 73]

Red oil (71 % yield), R_f = 0.86. δ_H (300 MHz, $CDCl_3$/ppm): 0.90 (6H, t, CH_3), 1.30 (28H, m, $(CH_2)_{14}$), 1.48 (4H, t, $(CH_2)_2$), 1.85 (4H, m, half of aliphatic C_8H_{12} protons), 2.00 (3H, t, CH_3), 2.30 (4H, t, $(CH_2)_2$), 2.50 (4H, m, other half of aliphatic C_8H_{12} protons), 3.95 (4H, m, four olefinic protons of C_8H_{12}), 4.10 (4H, m, HCp), 4.20 (1H, s, HCp), 4.45 (2H, s, HCp), 5.55 (1H, s, CH). $C_{42}H_{65}FeO_2Rh$ requires: C, 66.66 %; H, 8.12 %. Found: C, 66.47 %; H, 8.10 %.

4.3.10.9. (η^4-1,5-cyclooctadiene){(1-((1,1′-di(dodecyl))ferrocenyl-3-)-butane-1,3-dionato-κ^2O,O')}rhodium (I), 60b [Scheme 3.4, p 73]

Red oil (75 % yield), R_f = 0.87. δ_H (300 MHz, $CDCl_3$/ppm): 0.90 (6H, t, CH_3), 1.30 (36H, m, $(CH_2)_{18}$), 1.50 (4H, t, $(CH_2)_2$), 1.85 (4H, m, half of aliphatic C_8H_{12} protons), 2.00 (3H, t, CH_3), 2.30 (4H, t, $(CH_2)_2$), 2.50 (4H, m, other half of aliphatic C_8H_{12} protons), 3.95 (4H, m, four olefinic protons of C_8H_{12}), 4.10 (4H, m, HCp), 4.20 (1H, s, HCp), 4.45 (2H, s, HCp), 5.55 (1H, s, CH).

4.3.10.10. (η^4-1,5-cyclooctadiene){(1-((1,3-[-di-(1-decyl))ferrocenyl-3-)]-propane-1,3-dionato-κ^2O,O')}rhodium (I), 61a [Scheme 3.4, p 73]

Dark red oil (71 % yield), R_f = 0.83. δ_H (300 MHz, $CDCl_3$/ppm): 0.90 (6H, t, CH_3), 1.30 (28H, m, $(CH_2)_{14}$), 1.50 (4H, t, $(CH_2)_2$), 1.90 (4H, m, half of aliphatic C_8H_{12} protons), 2.32 (4H, t, $(CH_2)_2$), 2.55 (4H, m, other half of aliphatic C_8H_{12} protons), 4.02 (8H, m, 2HCp), 4.15 (4H, m, four olefinic protons of C_8H_{12}), 4.30 (4H, s, 2HCp), 4.60 (4H, s, 2HCp), 5.90 (1H, s, CH). $C_{51}H_{72}Fe_2O_2Rh$ requires: C, 67.21 %; H, 7.69 %. Found: C, 67.48 %; H, 7.71 %.

4.3.10.11. (η^4-1,5-cyclooctadiene){(1-((1,3-[-di-(1-dodecyl))ferrocenyl-3-)]-propane-1,3-dionato-κ^2O,O')}rhodium (I), 61b [Scheme 3.4, p 73]

Dark red oil (78 % yield), R_f = 0.83. δ_H (300 MHz, $CDCl_3$/ppm): 0.90 (6H, t, CH_3), 1.32 (36H, m, $(CH_2)_{18}$), 1.43 (4H, t, $(CH_2)_2$), 1.90 (4H, m, half of aliphatic C_8H_{12} protons), 2.32 (4H, t, $(CH_2)_2$), 2.53 (4H, m, other half of aliphatic C_8H_{12} protons), 4.03 (8H, m, 2HCp), 4.12 (4H, m, four olefinic protons of C_8H_{12}), 4.30 (4H, s, 2HCp), 4.60 (4H, s, 2HCp), 5.90 (1H, s, CH).

[1] Furniss, B. S., Hannaford, A. J., Smith, P. W. G. and Tatchell, A. R., *Vogel's Textbook of Practical Organic Chemistry*, 5th Ed., Longman, Harlow, p.399, (1989).

[2] Du Plessis, W. C., Vosloo, T. G. and Swarts, J. C., *J. Chem. Soc., Dalton Trans.*, 2507 (1998).

[3] Helm, L., MINSQ, Non-linear parameter estimation and model development, least squares parameter optimisation V3.12, MicroMath Scientific Software, Salt lake City, UT (1990).

[4] Keppler, B. K., Henn, M., Juhl, U. M., Berger, M. R., Niebl, R. and Wagner, F. E., *Progress in Clinical Biochemistry and Medicine*, **10**, 41, (1989).

[5] Donnio, B., Seddon, J. M. and Deschenaux, R., *Organometallics*, **19**, 3077, (2000).

[6] Reeves, P. C., *Org. Synthesis*, **5**, p. 28.

Chapter 5

Summary, conclusions and future perspectives

5.1. Synthesis

In this study, the syntheses of acyl ferrocene derivatives were first performed. Acylation was achieved with the acyl chloride, RCOCl where R = C_8H_{17}, C_9H_{19}, $C_{11}H_{23}$, $C_{13}H_{27}$ and $C_{17}H_{35}$ under Friedel-Crafts reaction conditions to give 1,1′-acylferrocene esters as well as the 1,3,1′-acyl substituted ferrocene esters in good yields. The substitution pattern achieved included the 1,1′-(Cp-COOMe)Fe(Cp-R) and 1,3,1′-(R^2-Cp-COOMe)Fe(Cp-R^1) substituent positions by an acyl and/or long chain alkyl substituents. Clemmensen reduction of the 1,1′-acylferrocenyl esters gave the corresponding alkyl derivatives. However, Clemmensen reduction was unsuccessful in obtaining the 1,3,1′-substituted dialkyl ferrocene ester derivatives. The carboxylic acid derivatives were obtained in good yields by the hydrolysis of the methyl ester precursors, under alkaline alcoholic conditions.[1] All these compounds were characterized by both infrared and ^{1}H NMR spectroscopy.

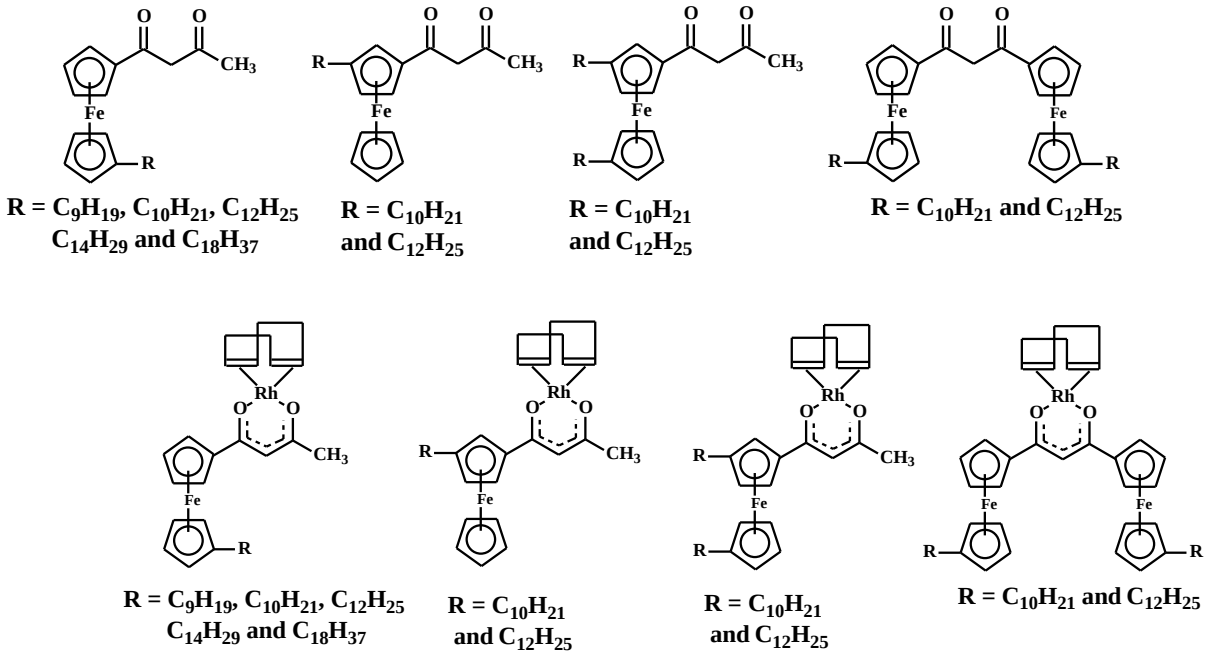

Figure 5. 1: Structures of the β-diketone series (top) and rhodium complex series (bottom) of key compounds synthesized in this study.

A series of mixed mono- and diacyl derivatives of alkylated ferrocenes, were then prepared. In the first step, ferrocene, was treated with a suspension of the appropriate acyl chloride RCOCl (R = C_8H_{17}, C_9H_{19}, $C_{11}H_{23}$, $C_{13}H_{27}$ and $C_{17}H_{35}$).[2] The diacyl ferrocenes were obtained by treating ferrocene with 2

equivalents of RCOCl and 2 equivalents of $AlCl_3$, while the mono-acetylated series were obtained by using a 1:1 stoichiometric quantity of acyl chloride and $AlCl_3$ over ferrocene. The acyl and diacyl ferrocene derivatives were then reduced by Clemmensen reduction reaction to the corresponding alkyl and dialkylated ferrocenes in good yields. The mixed acetyl-alkylferrocene derivatives were synthesized utilizing Friedel-Crafts acylation techniques as described in the above paragraph.

Claisen condensation of acetyl-alkylferrocene derivatives with an appropriate ester under the influence of the strong base lithium diisopropylamide (LDA) yielded eleven new alkylferrocene-containing β-diketones of the type $(Cp\text{-}R^2)\text{-}Fe(R^1\text{-}Cp\text{-}COCH_2COCH_3)$ (**Figure 5.1**, top row). Complexation of all the β-diketones with $[RhCl_2(cod)_2]$ in DMF gave the rhodium β-diketones of the type $[Rh((Cp\text{-}R^2)\text{-}Fe(R^1\text{-}Cp\text{-}COCHCOCH_3))(cod)]$ (**Figure 5.1**, bottom row).

5.2. Physical studies

The physical properties of the new compounds were investigated with kinetic, thermodynamic phase study and electrochemical techniques. Some of the new compounds were also evaluated as potentially new anti-cancer drugs by determining IC_{50} values on CoLo and HeLa human cancer cell lines.

Having synthesized the new β-diketone derivatives, their $pK_a^{/}$ values were determined. $pK_a^{/}$ values were determined spectroscopically in water containing 10 % acetonitrile (v/v). It was observed during pH titration that at pH > 12, compound stability was erratic. $pK_a^{/}$ values for all the β-diketones varied from 9.97 to 10.89. This meant that the effect substituent alkyl chain lengths have in the range C_9H_{19} – $C_{18}H_{37}$ on thermodynamic $pK_a^{/}$ values are minimal.

The isomerization kinetics of all new β-diketones was studied in $CDCl_3$ by ^1H NMR spectroscopy. The keto-enol equilibrium constant, K_c, was independent of alkyl chain length in the region C_9H_{29} – $C_{18}H_{37}$ as well as of the position of the R-substituent.

Electrochemical studies in dichloromethane/0.05 mol dm^{-3} $[NBu_4][B(C_6F_5)_4]$ utilizing cyclic voltammetry, linear sweep voltammetry and Oster Young square wave voltammetry revealed that the electrochemistry of the ferrocenyl groups are one-electron transfer redox process and were considered

electrochemically reversible with ΔE_p values smaller than 90 mV at scan rate 100 mVs^{-1} and chemically reversible with current ratios approximately one. The redox active centre of all the β-diketones exhibited $E^{o/}$ values that are independent on the alkyl chain length of the ferrocene-containing β-diketones due to the lack of conjugation between the ferrocenyl group and the alkyl R groups. Di-ferrocene-containing β-diketones, showed multiple oxidation and reduction peaks.

The electrochemical study of all the rhodium complexes investigated had two or three redox centres: the iron centre(s) of the ferrocenyl group(s) as well as the square planar rhodium centre. Fc/Fc^+ couple for all the complexes is an electrochemically and chemically reversible one-electron transfer process with $\Delta E_p \leq 90$ mV and current ratios approached one at slow scan rate 100 mVs^{-1}. The Rh^I nucleus showed an electrochemically quasi reversible process in which it was oxidized to Rh^{II} at $E_{pa} > 500$ mV. Current ratios i_{pc}/i_{pa} was < 0.60 and $90 \leq \Delta E_p \leq 150$ at scan rates 100 – 1000 mVs^{-1}. Cyclic voltammograms clearly showed that, Rh^{II} formation occurred at increasingly larger formal reduction potentials with longer alkyl substituents. This result was considered to be consistent with the possibility that the rhodium center was more effectively masked perhaps *via* encapsulation from the electrode surface with longer alkyl chain substituents on the second cyclopentadienyl ring.

Substitution reactions investigated in this study involved the substitution of the β-diketonato ligands, $(Cp\text{-}R^2)Fe(R^1\text{-}Cp\text{-}COCHCOCH_3)^-$ from rhodium complexes $[Rh((Cp\text{-}R^2)Fe(R^1\text{-}Cp\text{-}COCHCOCH_3))(cod)]$ by 1,10-phenanthroline to give $[Rh(phen)(cod)]^+$. These studies were conducted utilizing a stopped-flow spectrophometer. All the rhodium(I) complexes obeyed the Beer-Lambert law, which allowed substitution kinetics to be studied by optical methods. Saturation kinetics was observed. To accommodate saturation kinetics, the general substitution mechanism in **Scheme 5.1** was proposed:

Unique to the proposed mechanism is the concept that the compounds in equilibrium (ii) does not represent a transition state but a stable intermediate with lifetime long enough to be considered finite, *i.e.* long enough to lead to the observed saturation kinetic effect.

The general rate law applicable to this substitution was as follows.[3]

$$\text{Rate} = \frac{k_2 K[1,10-phenanthroline][Rh(\beta-diketonato]}{1+K[1,10-phenanthroline]}$$

$$= k_{obs}[Rh(\beta-diketonato)(cod)]$$

$$\text{with } k_{obs} = \frac{k_2 K[1,10-phenanthroline]}{1 + K[1,10-phenanthroline]}$$

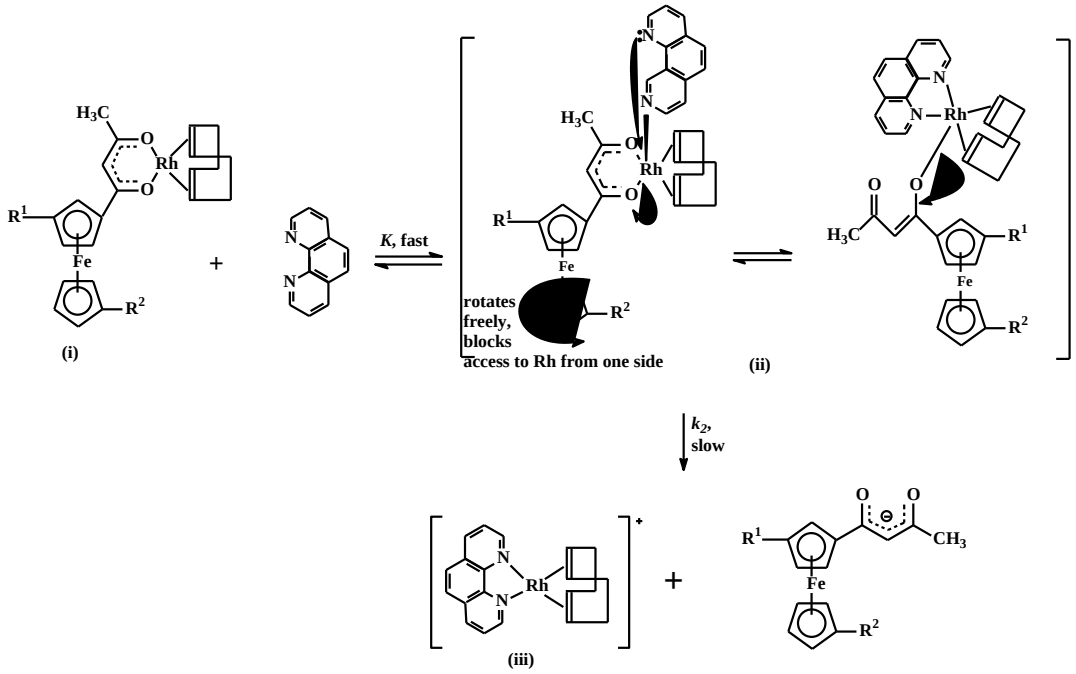

Scheme 5. 1 Schematic representation of the substitution mechanism

The non-linear k_{obs}-1,10-phenanthroline relationship (i.e. saturation kinetics) were further confirmed by obtaining linear plots of $1/k_{obs}$ against 1/[1,10-phenanthroline]. None of the substitution reactions showed a noticeable solvent related pathway. The second-order rate constants, k_2, measured for all rhodium(I) complexes of this study varied between 612 and 2678 $dm^3\,mol^{-1}\,s^{-1}$ and that K values were also in the same range (0.0158 – 0.0742). This implied that R-substituents with chain length varying from C_9H_{19}– $C_{18}H_{37}$, and with one or more than one R-group substituent, had very little effect on the reaction rate. A solvent study showed the substitution of the β-diketonato ligand $(Fc\text{-}COCHCOCH_3)^-$ (*i.e.* no long chain alkyl substituents) from $[Rh(Fc\text{-}COCHCOCH_3)(cod)]$ by 1,10-phenanthroline in acetone do not show saturation kinetics. A non-zero intercept for the linear plot of k_{obs} *vs.* [1,10-phenanthroline] was, however, observed. This means that acetone provides a solvent route to the substitution mechanism in the absence of long chain alkyl substituents. In contrast, the long-chain alkyl substituted complexes of this study showed zero intercepts and saturation kinetics. This observation was considered consistent with the view that the long chain alkyl substituted complexes are so lipophylic that they tend to form minute micelles which interact favourably with 1,10-phenanthroline, but not with hydrophilic acetone.

The activation entropy values obtained from the temperature study of all the substitution reactions was large negative. The negative activation entropy values suggested an association mechanism, thus providing more credibility to the mechanism suggested in **Scheme 5.1**. The values obtained for the Gibbs free activation energy were also found to be roughly in the same range (88.72 – 118.64 kJ mol^{-1}) for all the compounds indicating the intermediates in (ii) in **Scheme 5.1** forms with almost equal ease in every reaction and is virtually independent of side chain length and substitution position for complexes having long alkyl chain substituents.

Phase studies showed that none of the selected ferrocene-containing long-chain alkyl substituted β-diketones (Cp-$C_{18}H_{37}$)Fe(Cp-$COCH_2COCH_3$), (Cp)Fe($C_{10}H_{21}$-Cp-$COCH_2COCH_3$), (Cp-$C_{12}H_{25}$)Fe($C_{12}H_{25}$-Cp-$COCH_2COCH_3$) and (Cp-$C_{12}H_{25}$)Fe(Cp-$COCH_2CO$-Cp)Fe(Cp-$C_{12}H_{25}$) or the rhodium(I) complexes [Rh((Cp-$C_{12}H_{25}$)Fe(Cp-$COCHCOCH_3$)(cod))], [Rh((Cp-$C_{18}H_{37}$)Fe(Cp-$COCHCOCH_3$)(cod))], [Rh((Cp-$C_{12}H_{25}$)Fe($C_{12}H_{25}$-Cp-$COCHCOCH_3$)(cod))] and [Rh((Cp-$C_{12}H_{25}$)Fe(Cp-COCHCO-Cp)Fe(Cp-$C_{12}H_{25}$)(cod))] exhibits liquid-crystal properties. The ferrocenyl derivatives and free β-diketones exhibited solid state phase changes while the rhodium(I) complexes showed no pronounced melting or crystallisation peaks due to a very slow crystallisation kinetics.

5.3. Medical studies

The potential anticancer applications of selected β-diketones and their rhodium complexes were probed by determining the cytotoxicity of these complexes with respect to human colorectal (CoLo) and human cervix epitheloid (HeLa) cancer cell lines. The free β-diketones **53b** and **54a** were about twice as effective in killing the multi drug resistant CoLo cell line (with IC_{50} values = 6.9 and 6.3 μmol dm^{-3} respectively) than the HeLa cell line (with IC_{50} values = 11.0 and 13.0 μmol dm^{-3} respectively). Rhodium(I) complex toxicity was found to be approximately in the same range for both cancer cell lines. The β-diketones were five times less effective in killing cancer cells than *cisplatin* (IC_{50} = 1.84 μmol dm^{-3}, while the rhodium(I) complexes' toxicity was approximately six times less than that of *cisplatin*. All the drugs that were investigated in this study had a lower IC_{50} value (*i.e.* it is more toxic) than the rhodium complexes without the long chain alkyl substituents, [Rh(Fc-$COCHCOCH_3$)(cod)], (IC_{50} = 56.6 μmol dm^{-3}). This makes them all potentially more effective anti-cancer drugs than [Rh(Fc-$COCHCOCH_3$)(cod)].

5.4. Future perspective

In this study, a series of ferrocene-containing long-chain alkyl derivatives, β-diketones and their rhodium complexes were synthesized and subjected to $pK_a^{/}$, keto-enol kinetic, substitution kinetic, electrochemical studies, thermal phase change as well as cyctotoxic studies. Future studies on similar systems may include varying the ferrocenyl group with a variety of other metallocenes including ruthenocene, osmocene, titanocene and cobaltocene. Other metallic centres than rhodium may also be considered, these include iridium, platinum and palladium. Applications of these novel complexes in terms of catalysis as well as possible synergistic antineoplastic effects should also be addressed.

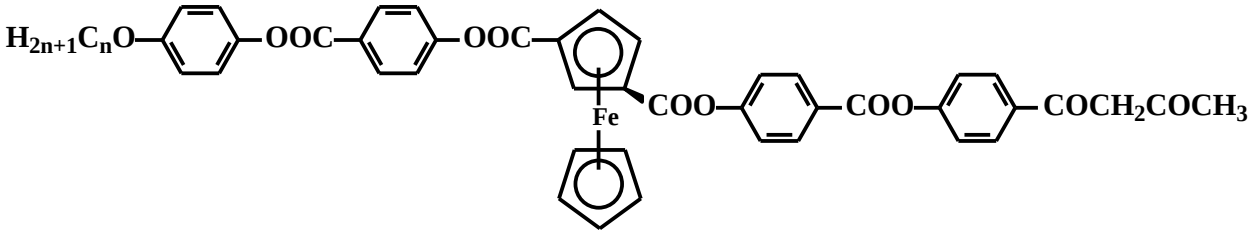

n = 10, 11, 12, 13, 14, 16 and 18

Figure 5. 2: Structure of liquid crystal ferrocene derivative reported by Deschenaux.

The long-chain alkyl substituents of the ferrocenyl group of the present β-diketones complexes were aimed at introducing liquid crystalline properties into the complexes. It failed because the β-diketonato aromatic core did not stabilize columnar mesophases enough to introduce liquid crystal properties. By extending conjugated aromatic patterns, new materials with liquid crystal properties may be obtained (see **Figure 5.2**).[4,5]

A clarification study as to what mode of action the present complexes has in killing cancer cells needs to be performed. The cytotoxic properties with respect to HeLa and CoLo cancer cell lines were reported in this study, the toxicity on healthy cells in comparison with the cancer cells should still be investigated. This will show the specificity, if any, that the present series of compounds may have for cancer cells. The influence different metal centres in the metallocenyl group such as Ru, Co, Os and Ti, may have on cytotoxicity should also be investigated.

[1] Donnio, B., Seddon, J. M. and Deschenaux, R., *Organometallics,* **19**, 3077, (2000).

[2] Vogel, M., Rausch, M. D. and Rosenberg, H., *J. Org. Chem.*, **22**, 1016, (1957).

[3] Wilkinson, R. G., *Kinetics and mechanism of reactions of Transition Metal Complexes, 2nd* thoroughly revised edition, CVH, Weinheim, p. 103, 232, (1991).

[4] Deschenaux, R, Rama, M and Santiago, J., *Tet. Lett.*, **34**, 3293, (1993).

[5] Deschenaux, R. and Santiago, J., *Tet. Lett.*, **35**, 2169, (1994).

Appendix

^{1}H NMR Spectra

Ferrocene derivatives:

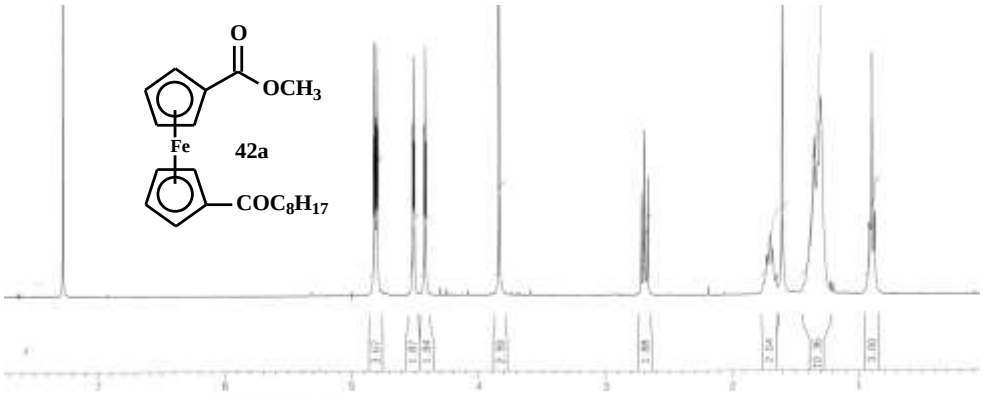

Spectrum 1: 1-Carbomethoxy-1/-(nonanoyl)ferrocene, 42a.

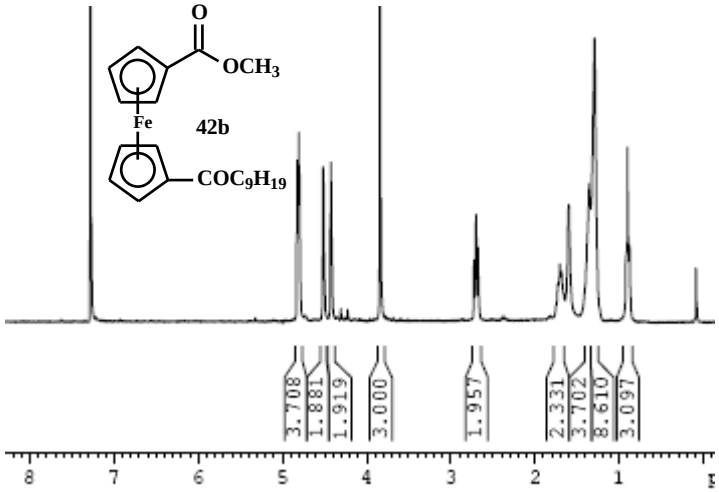

Spectrum 2: 1-Carbomethoxy-1/-(decanoyl)ferrocene, 42b.

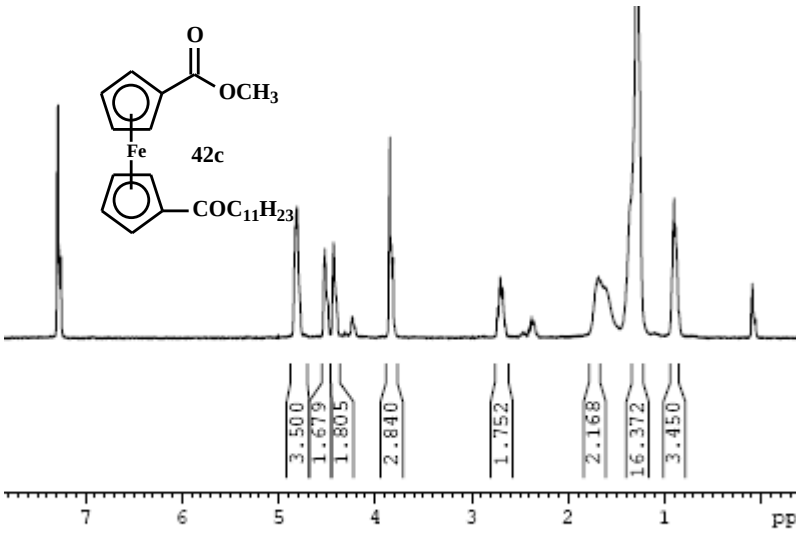

Spectrum 3: 1-Carbomethoxy-1/-(dodecanoyl)ferrocene, 42c

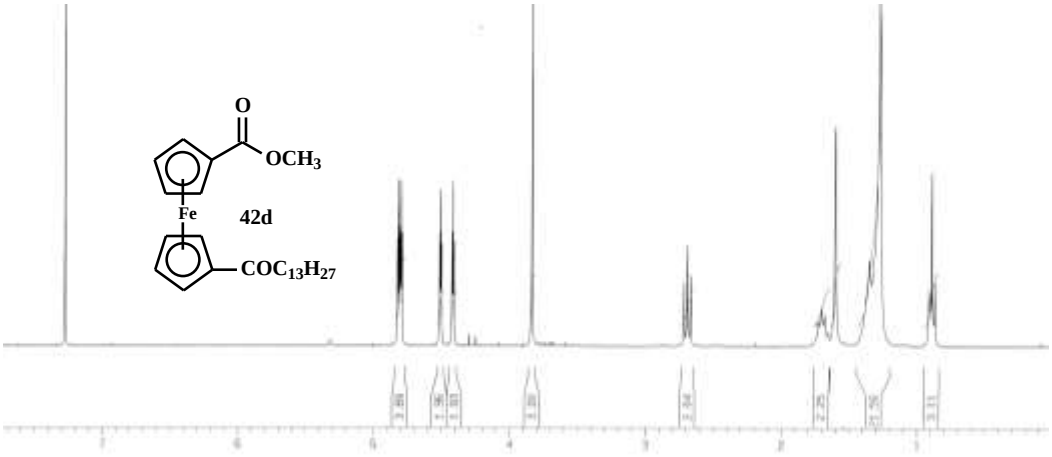

Spectrum 4: 1-Carbomethoxy-1$^{/}$-(tetradecanoyl)ferrocene, 42d

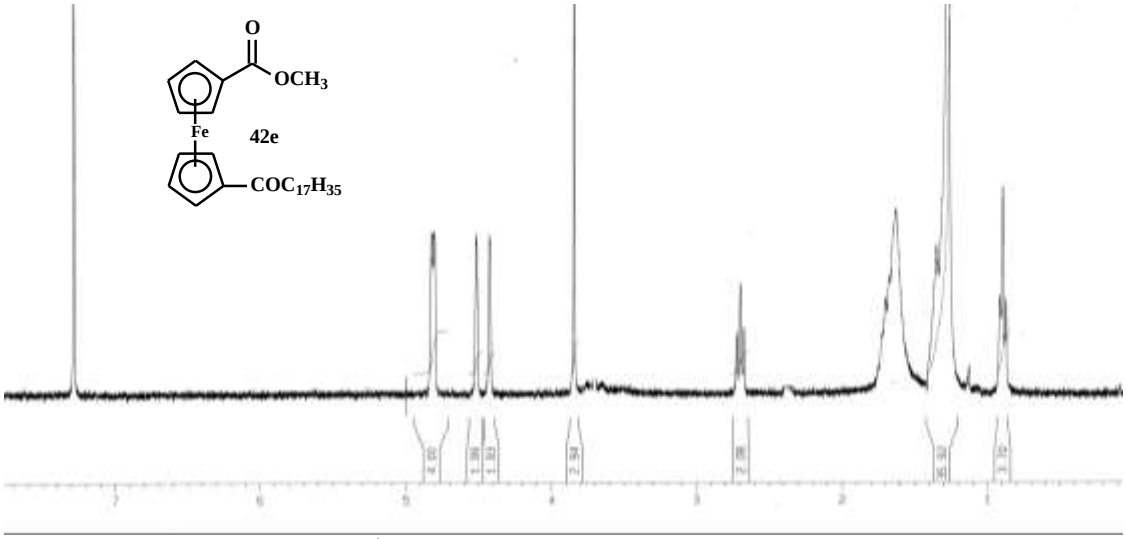

Spectrum 5: 1-Carbomethoxy-1$^{/}$-(octadecanoyl)ferrocene, 42d

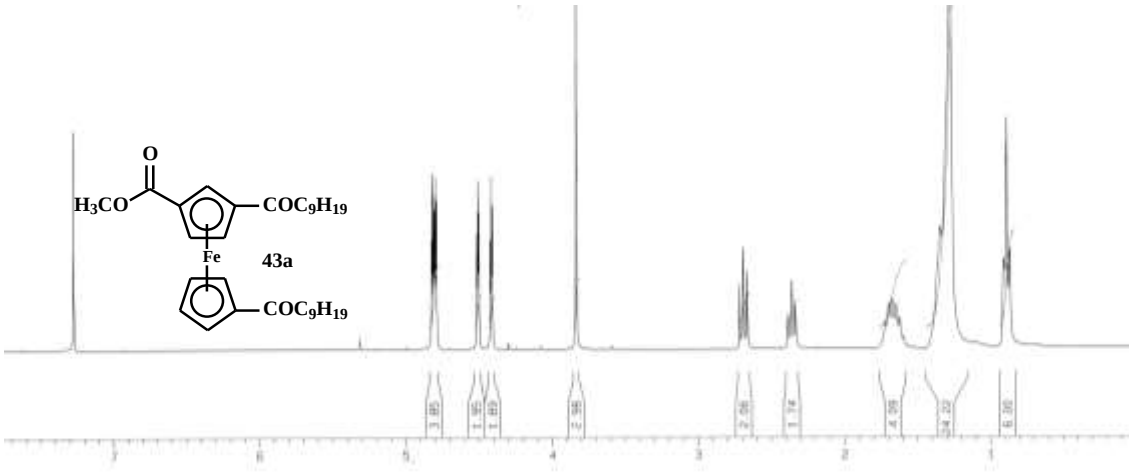

Spectrum 6: 1-Carbomethoxy-3,1$^{/}$-di(decanoyl)ferrocene, 43a

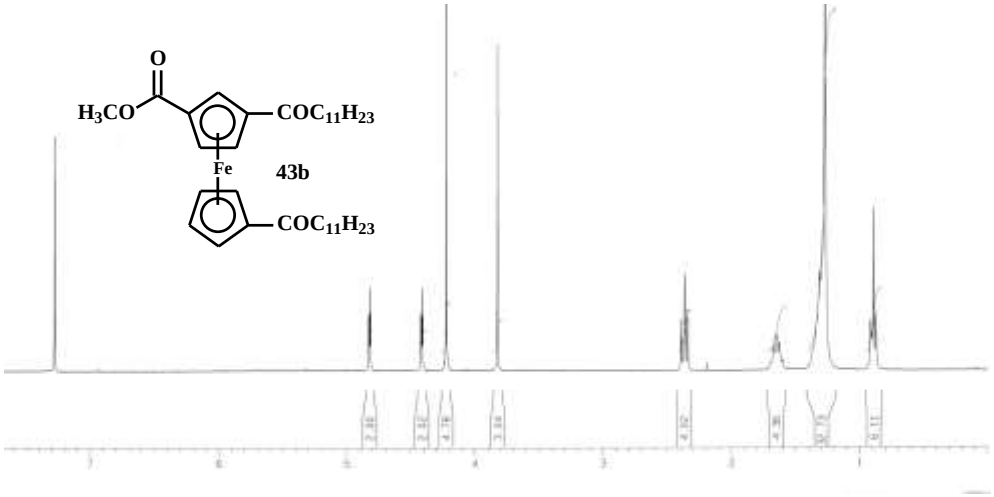

Spectrum 7: 1-Carbomethoxy-3,1′-di(dodecanoyl)ferrocene, 43b

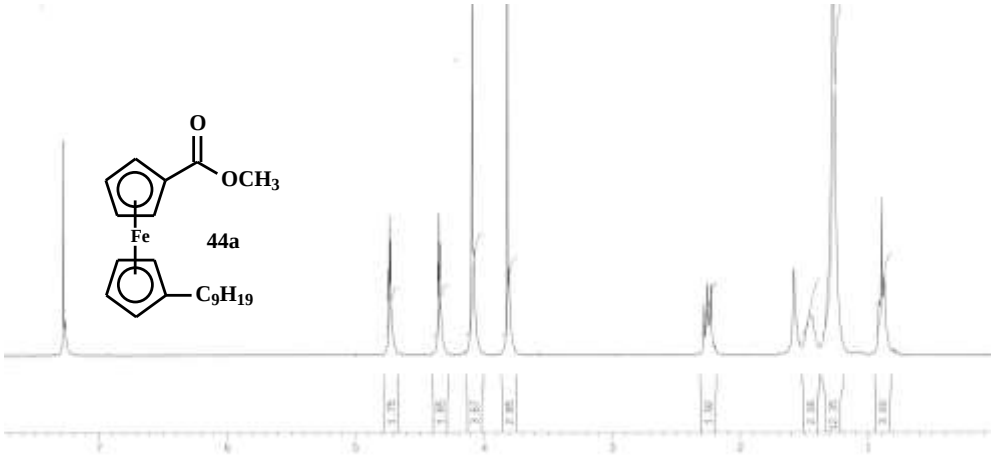

Spectrum 8: 1-Carbomethoxy-1′-(nonyl)ferrocene, 44a

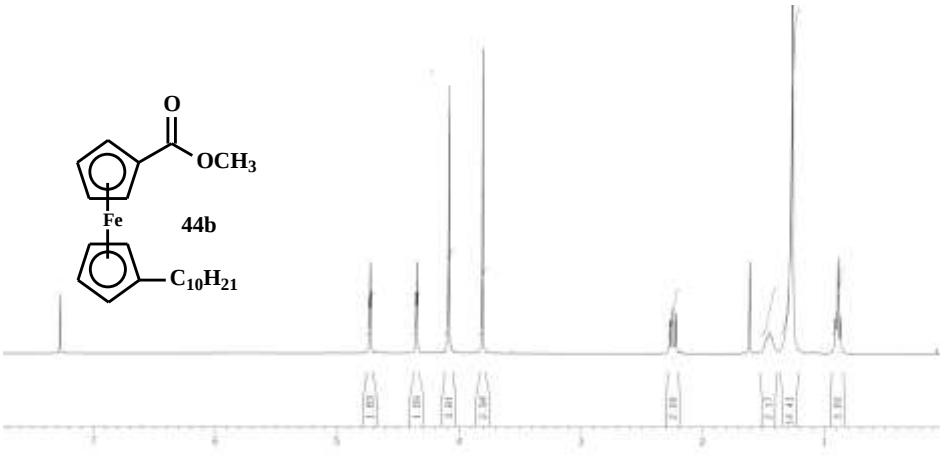

Spectrum 9: 1-Carbomethoxy-1′-(decyl)ferrocene, 44b

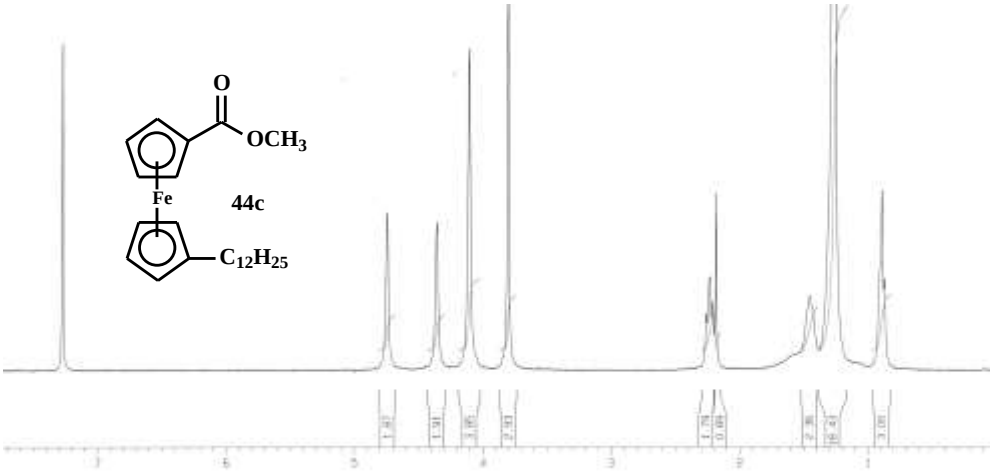

Spectrum 10: 1-Carbomethoxy-1′-(dodecyl)ferrocene, 44c

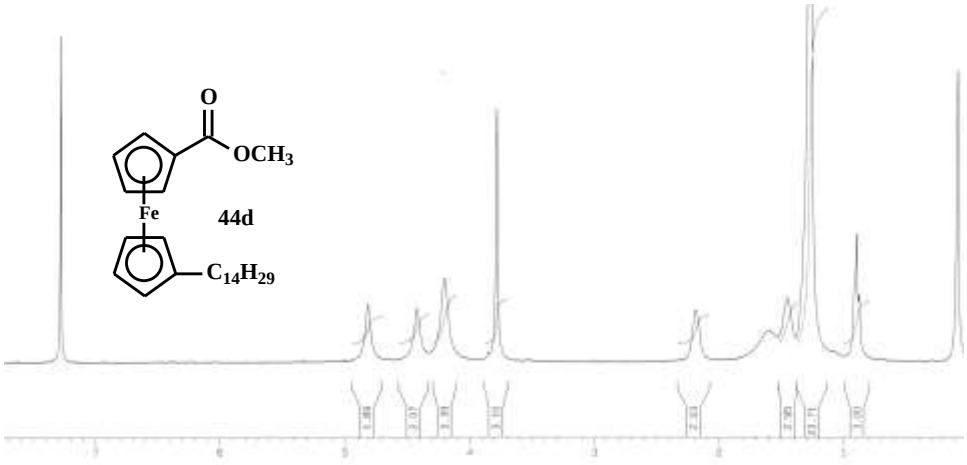

Spectrum 11: 1-Carbomethoxy-1′-(tetradecyl)ferrocene, 44d

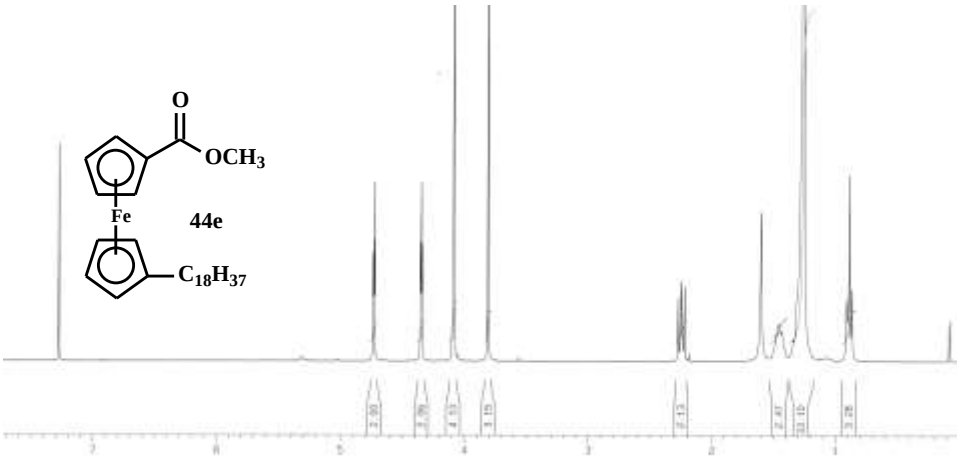

Spectrum 12: 1-Carbomethoxy-1′-(octadecyl)ferrocene, 44e

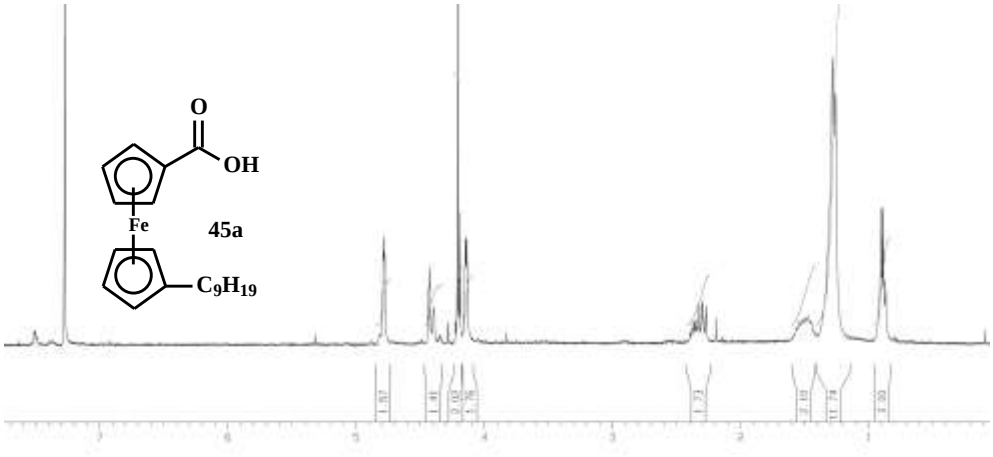

Spectrum 13: 1-Carboxy-1′-(nonyl)ferrocene, 45a

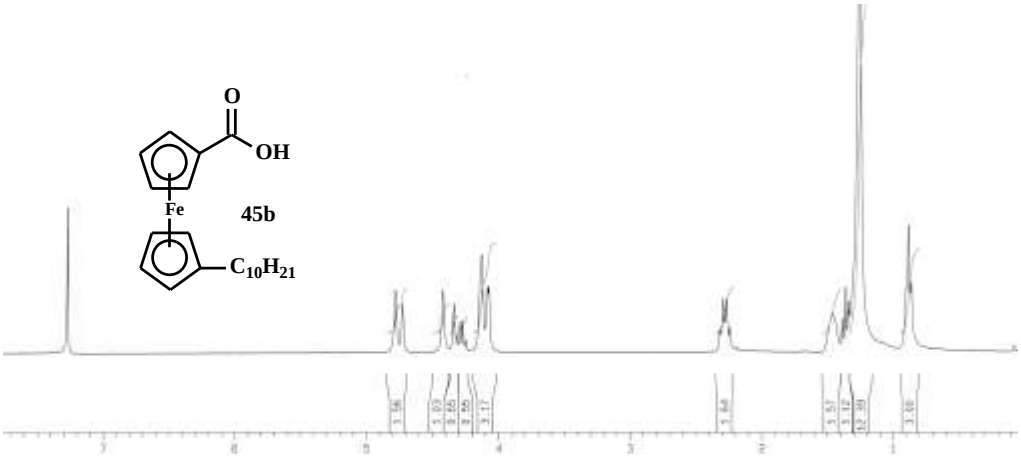

Spectrum 14: 1-Carboxy-1′-(decyl)ferrocene, 45b

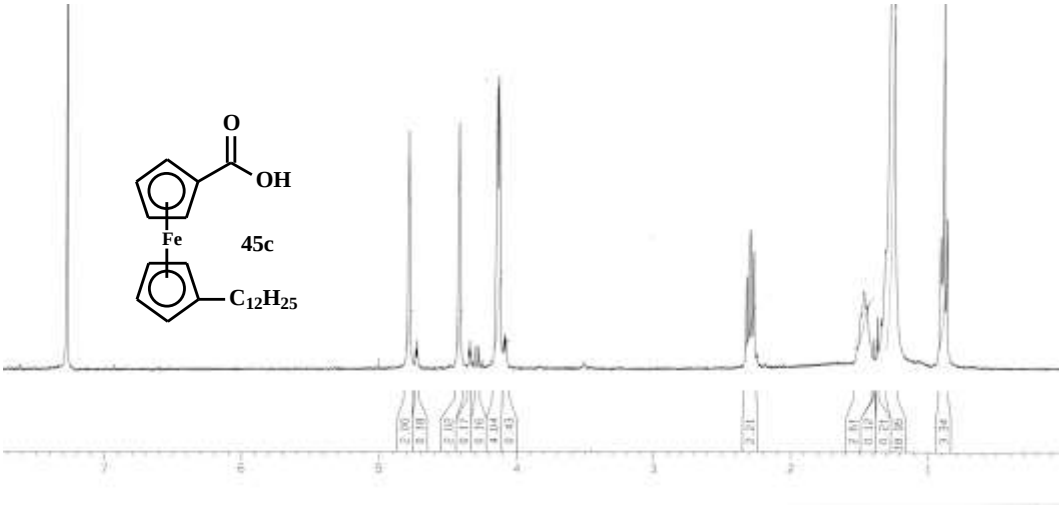

Spectrum 15: 1-Carboxy-1′-(dodecyl)ferrocene, 45c

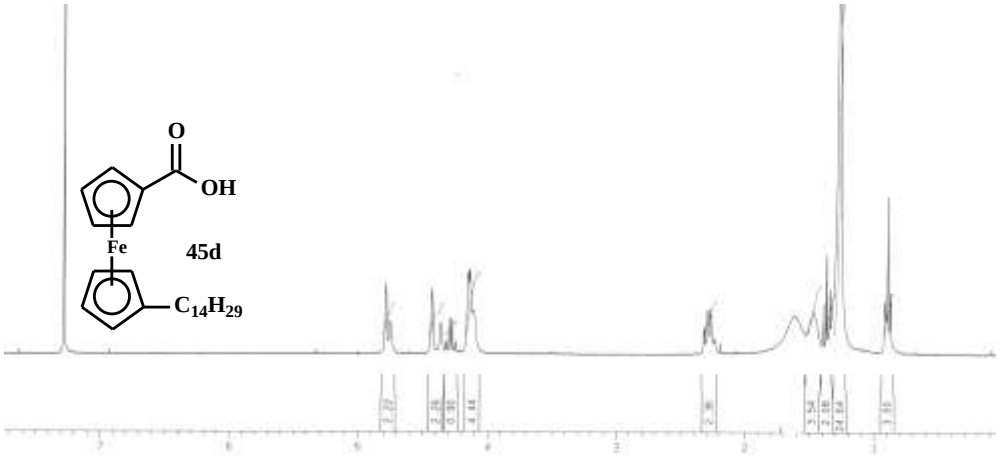

Spectrum 16: 1-Carboxy-1′-(tetradecyl)ferrocene, 45d

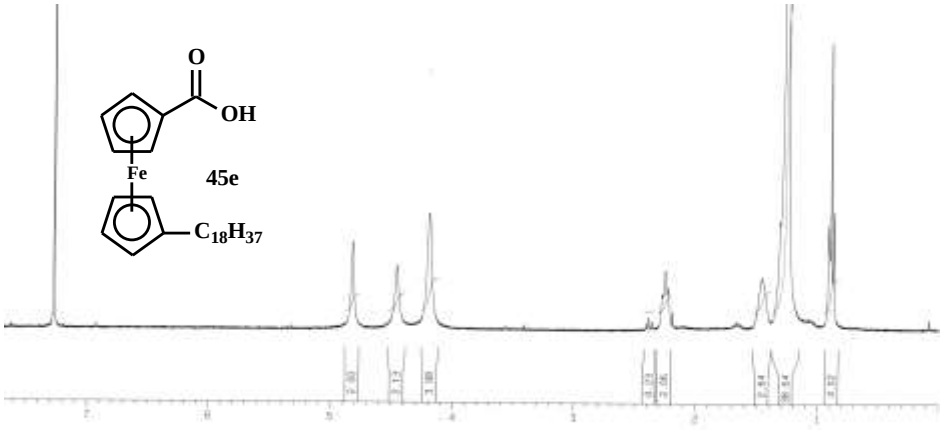

Spectrum 17: 1-Carboxy-1′-(octadecyl)ferrocene, 45d

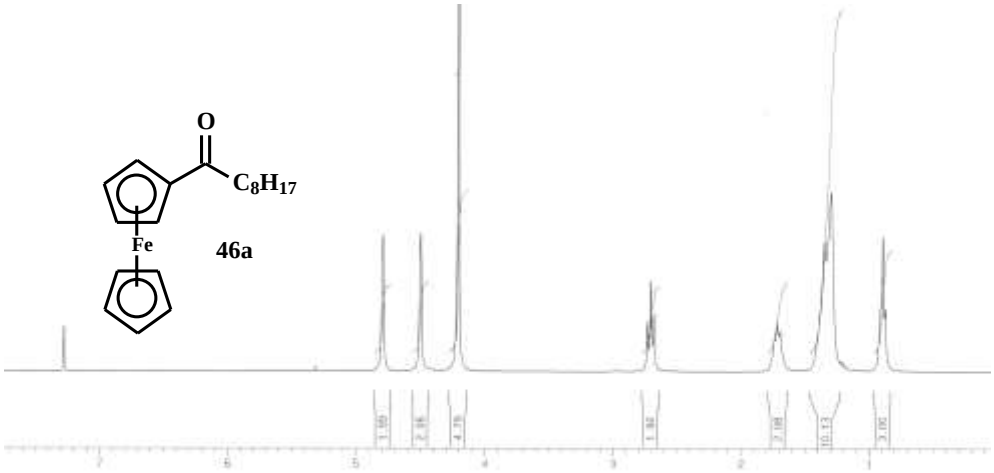

Spectrum 18: 1-Nonanoylferrocene, 46a.

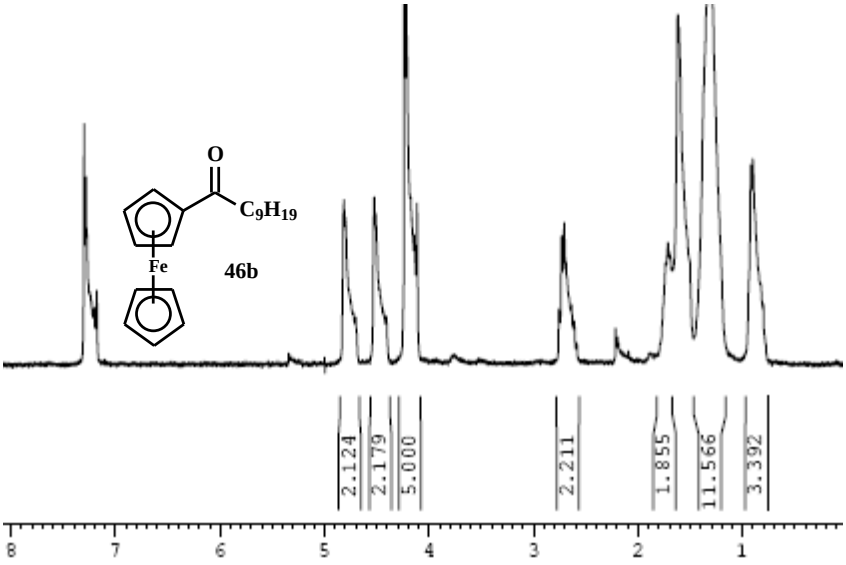

Spectrum 19: 1-Decanoylferrocene, 46b.

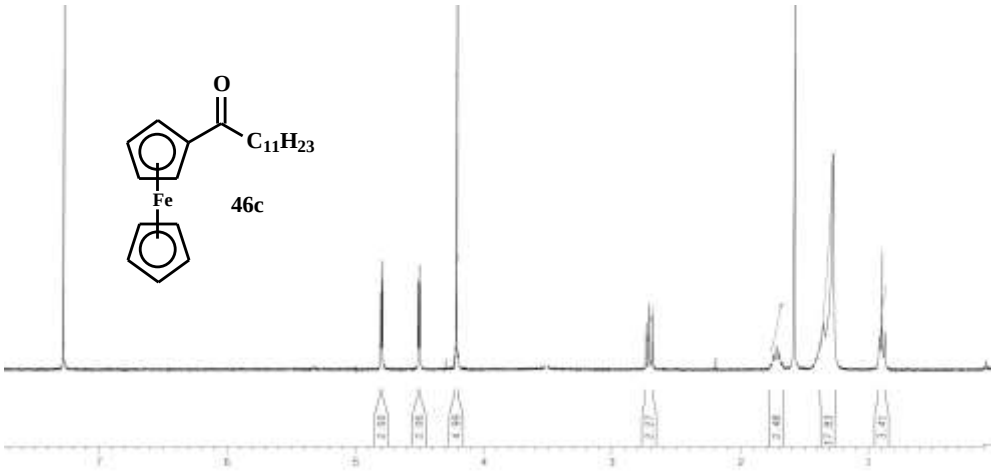

Spectrum 20: 1-dodecanoylferrocene, 46c.

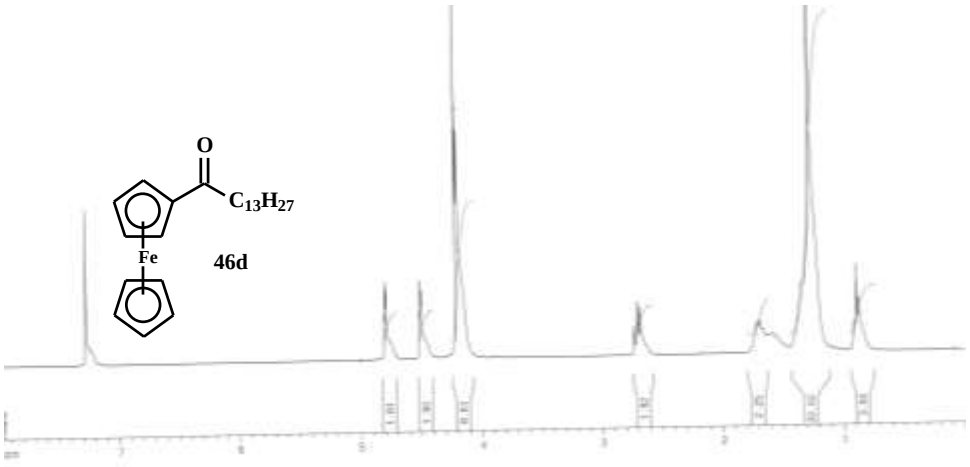

Spectrum 21: 1-Tetradecanoylferrocene, 46d.

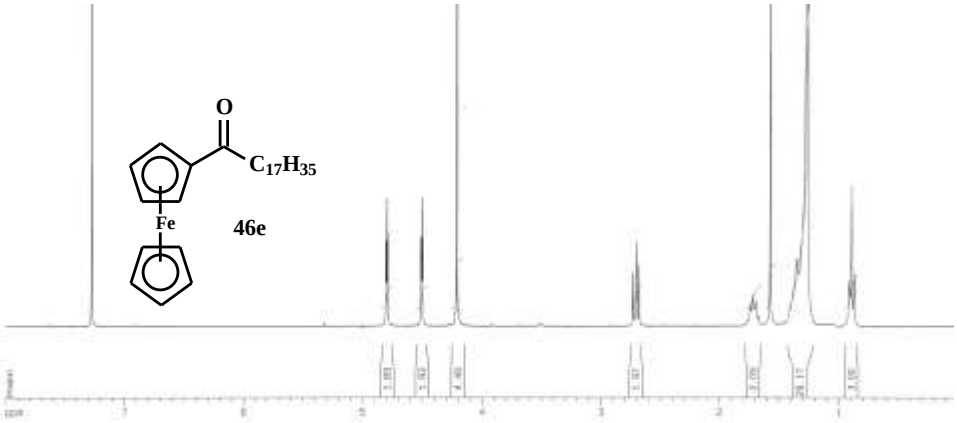

Spectrum 22: 1-Octadecanoylferrocene, 46e.

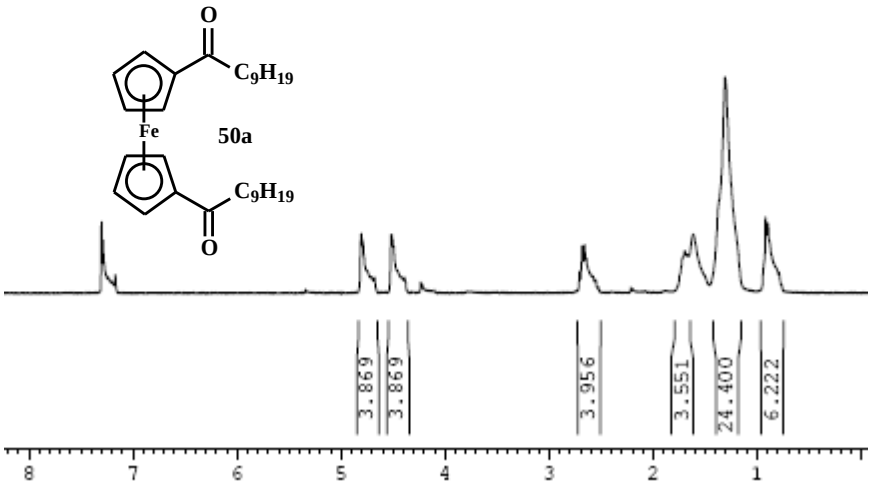

Spectrum 23: 1,1$^{/}$-di(decanoyl)ferrocene, 50a.

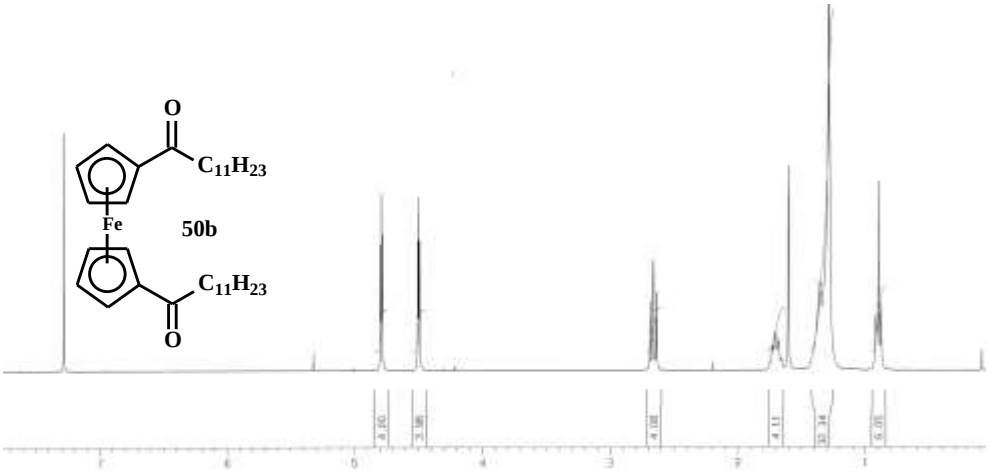

Spectrum 24: 1,1$^{/}$-di(dodecanoyl)ferrocene, 50b.

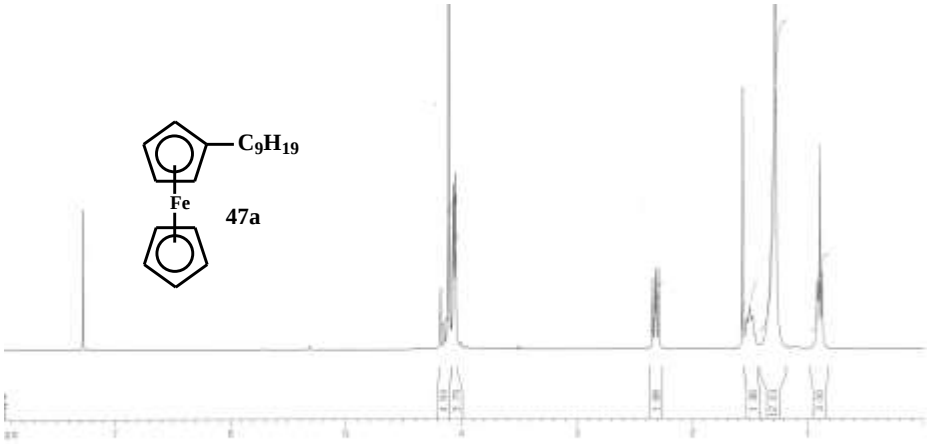

Spectrum 25: 1-Nonylferrocene, 47a.

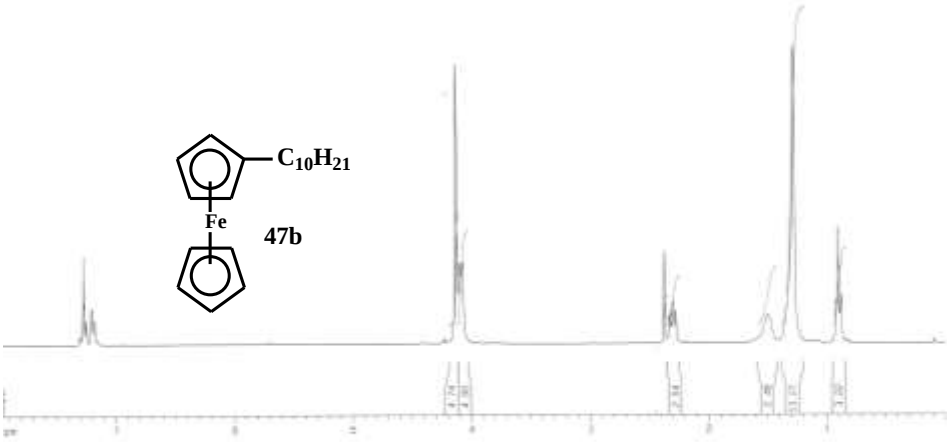

Spectrum 26: 1-Decylferrocene, 47b.

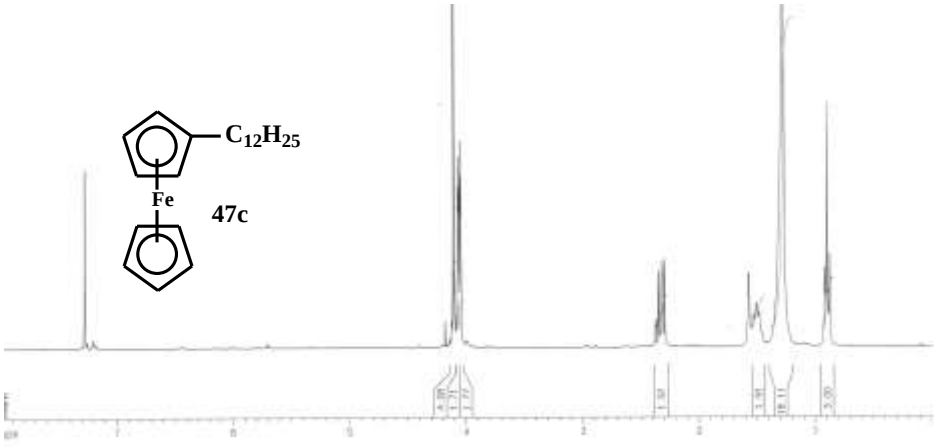

Spectrum 27: 1-Dodecylferrocene, 47c.

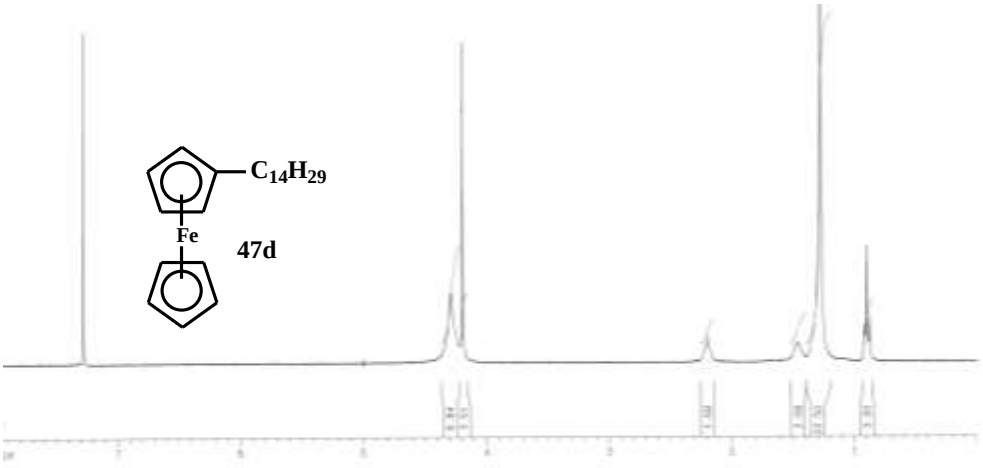

Spectrum 28: 1-Tetradecylferrocene, 47d.

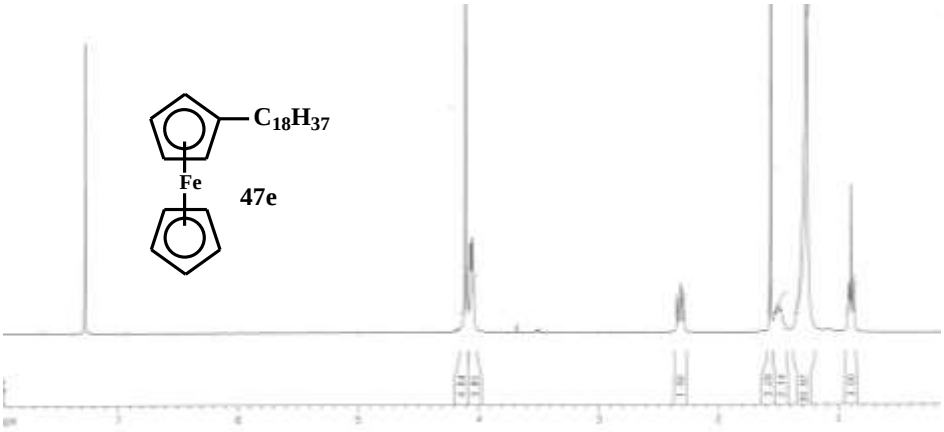

Spectrum 27: 1-Octadecylferrocene, 47e.

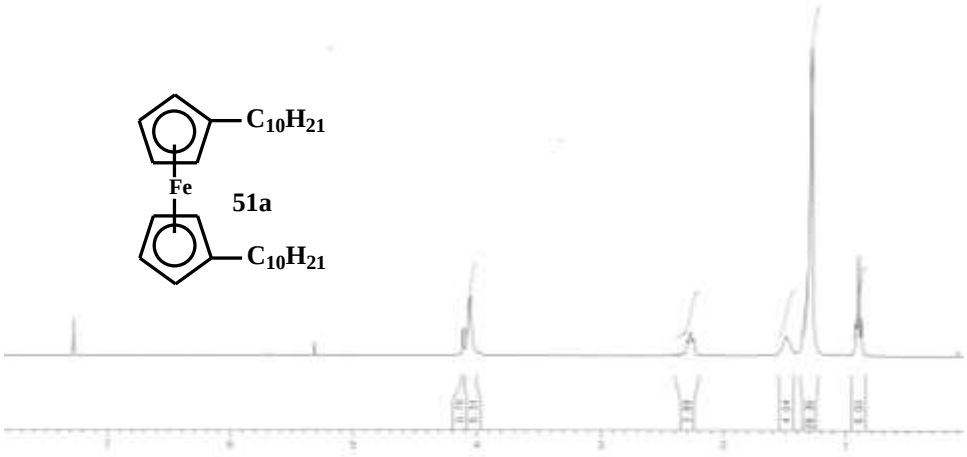

Spectrum 28: 1,1$^/$-Di(decyl)ferrocene, 51a.

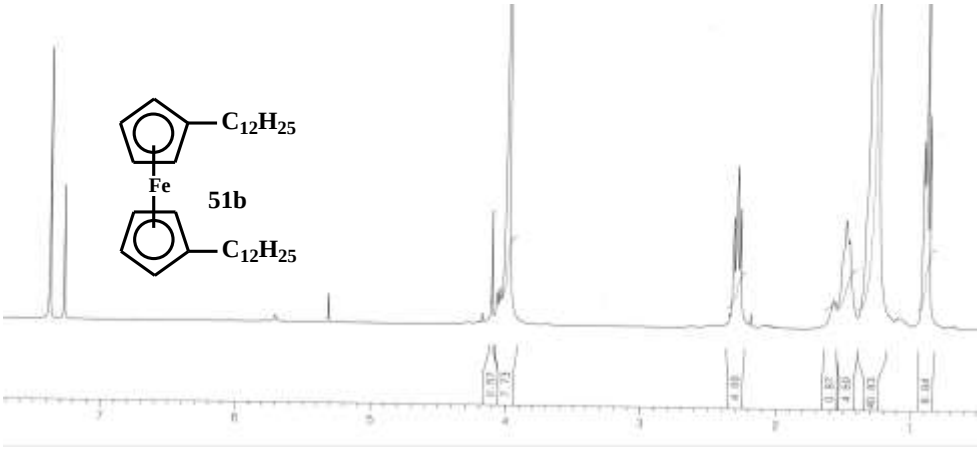

Spectrum 29: 1,1$^/$-Di(dodecyl)ferrocene, 51b.

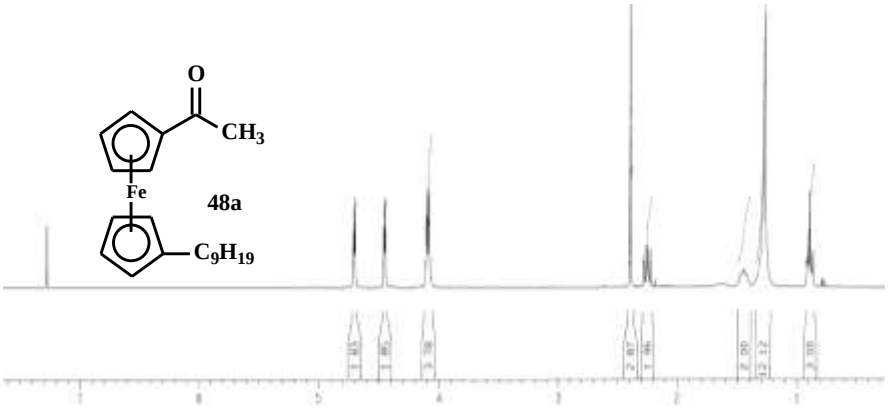

Spectrum 30: 1-Acetyl-1$^/$-nonylferrocene, 48a.

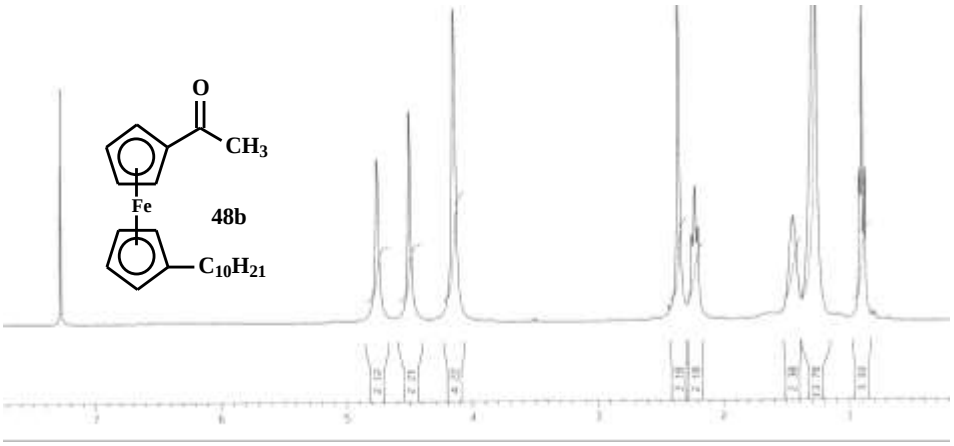

Spectrum 31: 1-Acetyl-1$^/$-decylferrocene, 48b.

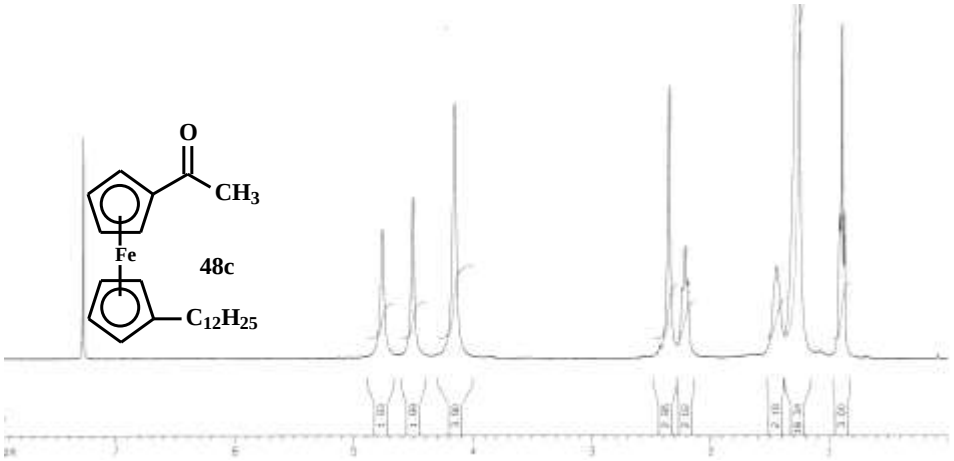

Spectrum 32: 1-Acetyl-1′-dodecylferrocene, 48c.

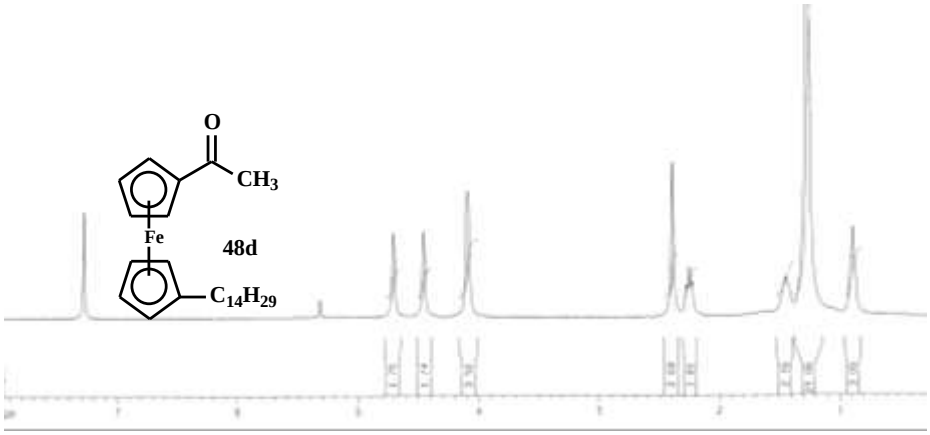

Spectrum 33: 1-Acetyl-1′-tetradecylferrocene, 48d.

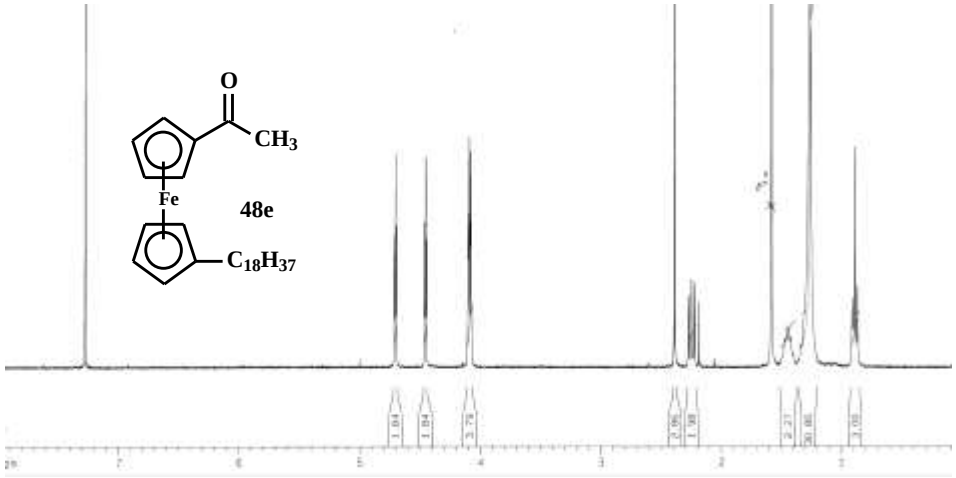

Spectrum 34: 1-Acetyl-1′-octadecylferrocene, 48e

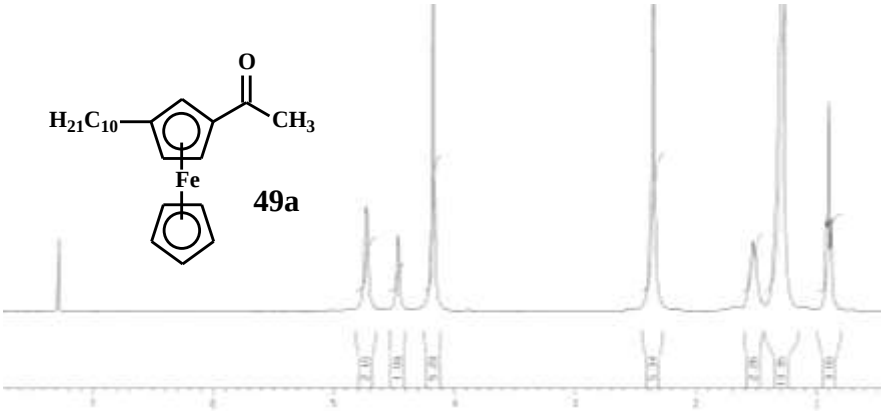

Spectrum 35: 1-Acetyl-3-decylferrocene, 49a.

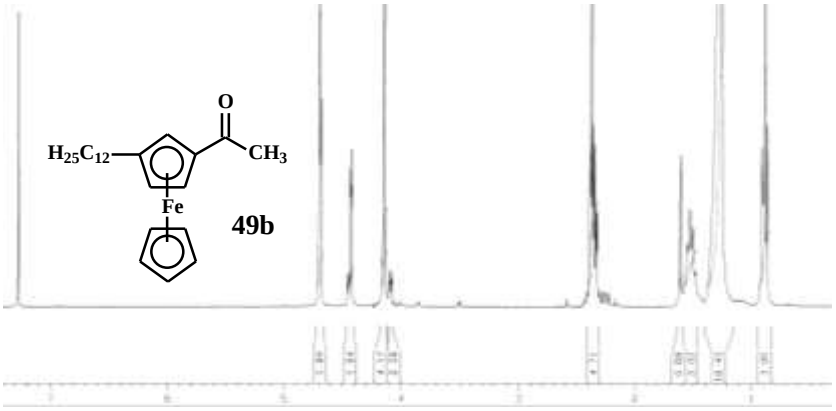

Spectrum 36: 1-Acetyl-3-dodecylferrocene, 49b.

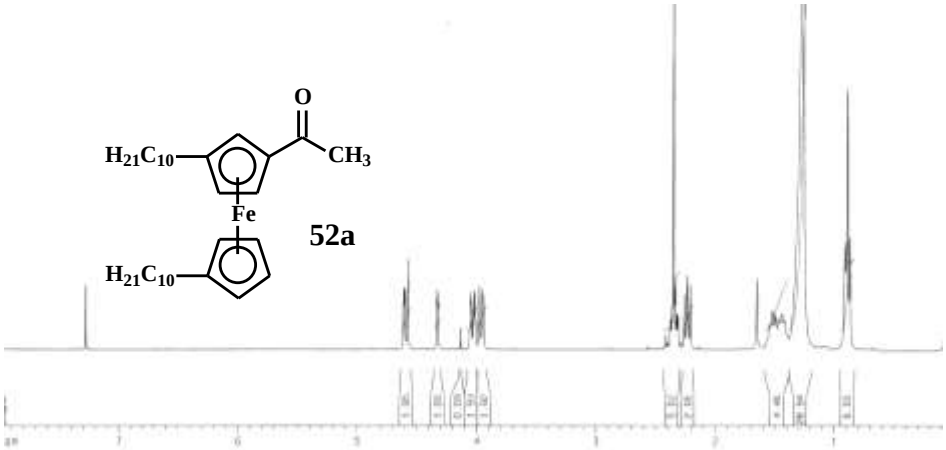

Spectrum 37: 1-Acetyl-3,1$^/$-di(decyl)ferrocene, 52a.

Spectrum 38: 1-Acetyl-3,1′-di(dodecyl)ferrocene, 52b.

β-Diketones:

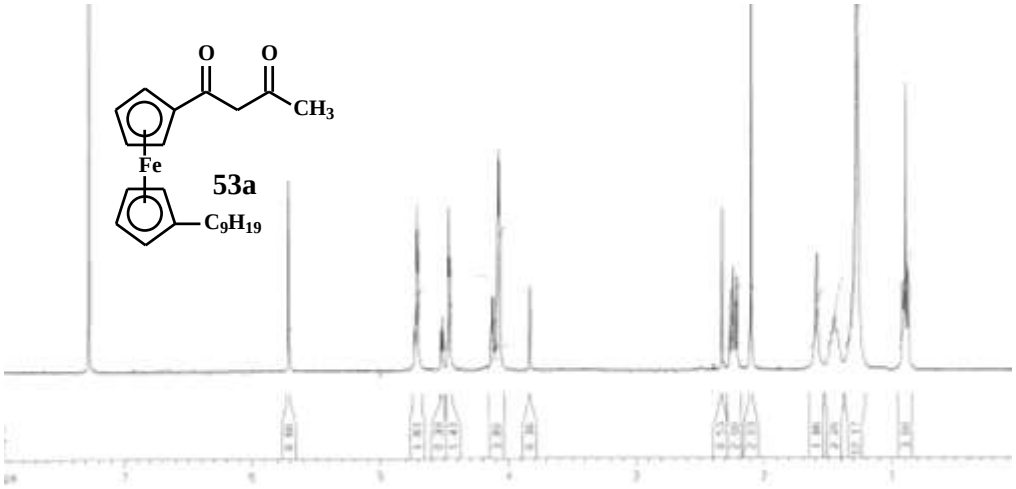

Spectrum 39: 1-[1-(Nonyl)ferrocenyl-1′-]-butane-1,3-dione, 53a

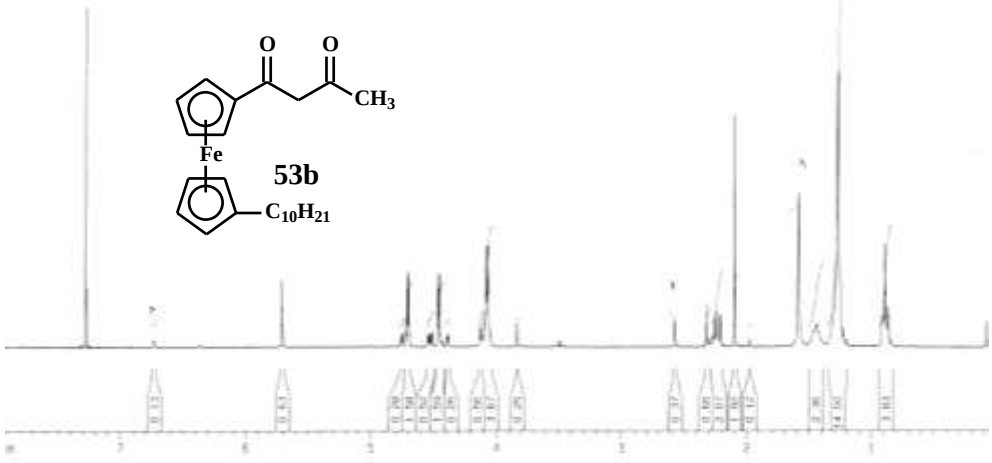

Spectrum 40: 1-[1-(Decyl)ferrocenyl-1′-]-butane-1,3-dione, 53b

Spectrum 41: 1-[1-(Dodecyl)ferrocenyl-1′-]-butane-1,3-dione, 53c.

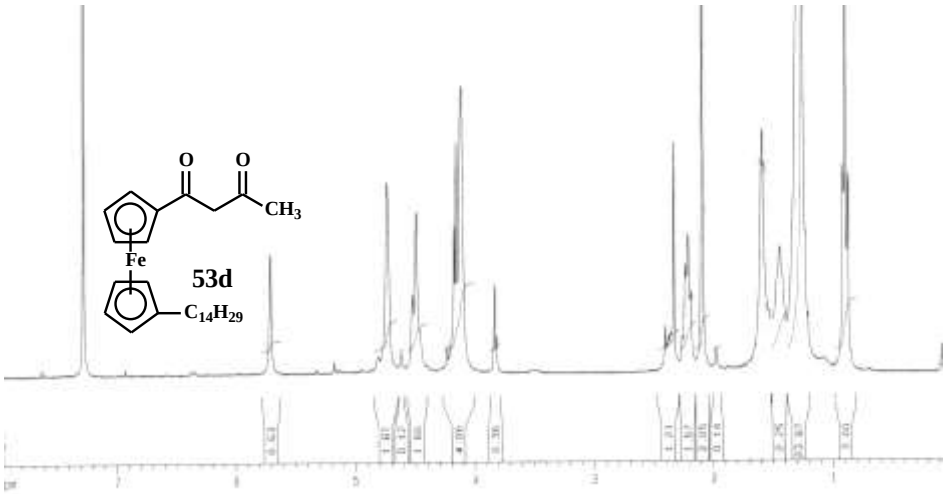

Spectrum 42: 1-[1-(Tetradecyl)ferrocenyl-1′-]-butane-1,3-dione, 53d.

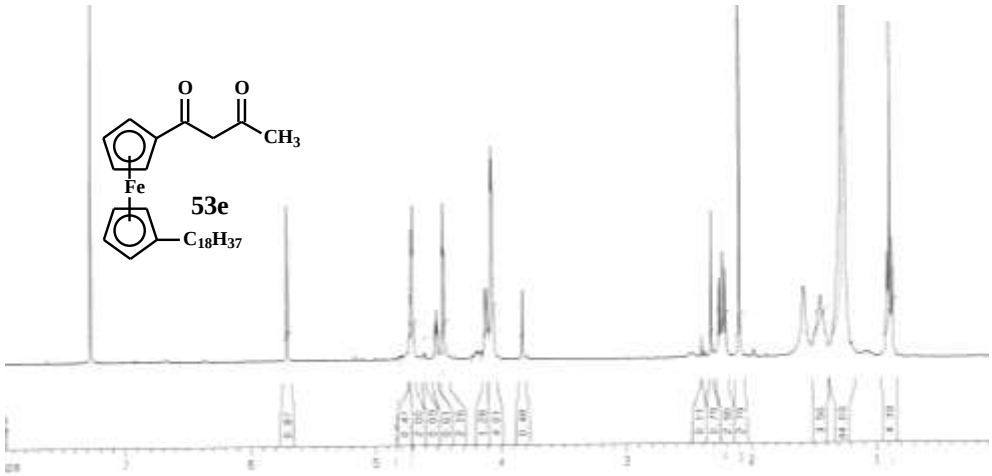

Spectrum 43: 1-[1-(Octadecyl)ferrocenyl-1′-]-butane-1,3-dione, 53e.

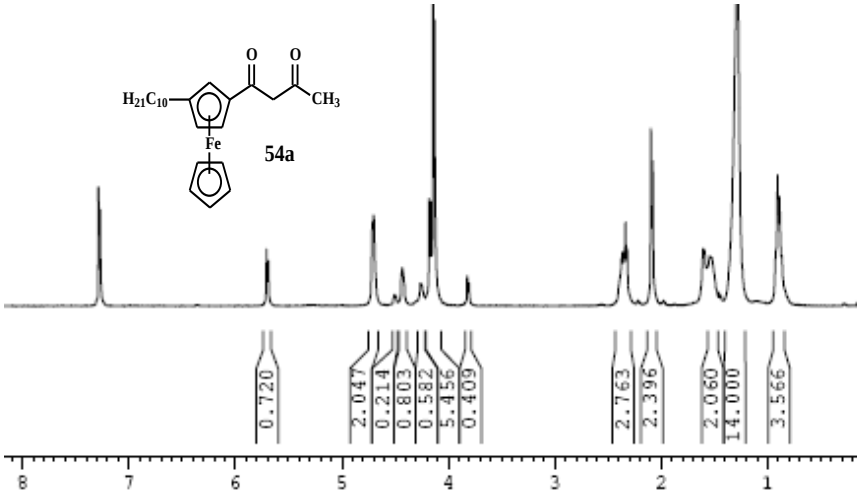

Spectrum 44: 1-[3-(decyl)ferrocenyl-1-]-butane-1,3-dione, 54a.

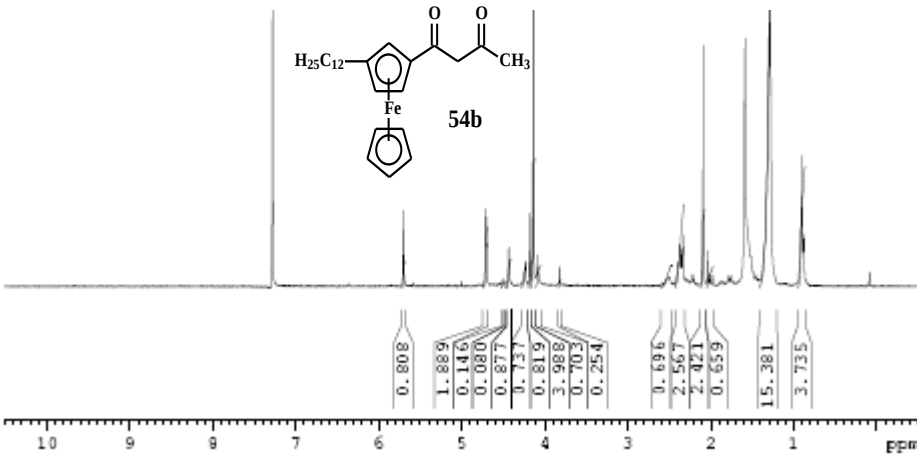

Spectrum 45: 1-[3-(decyl)ferrocenyl-1-]-butane-1,3-dione, 54b.

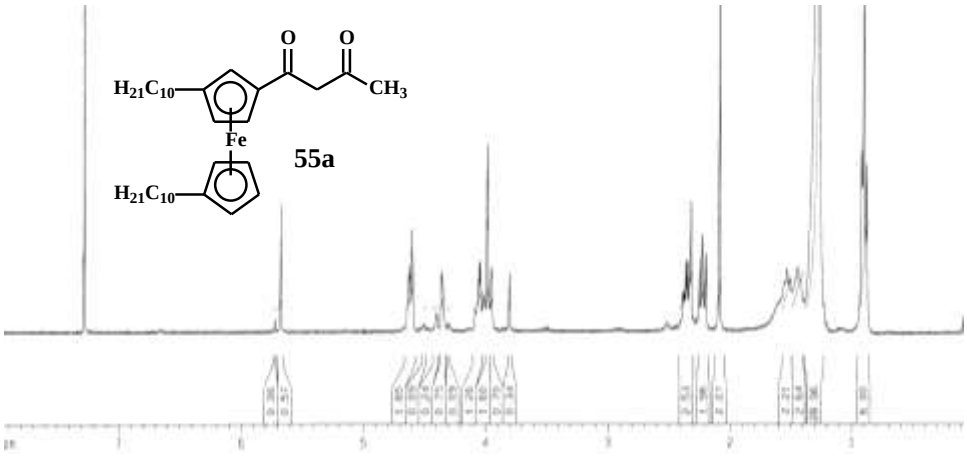

Spectrum 46: 1-[1,1′-di(decyl)ferrocenyl-3-]-butane-1,3-dione, 55a.

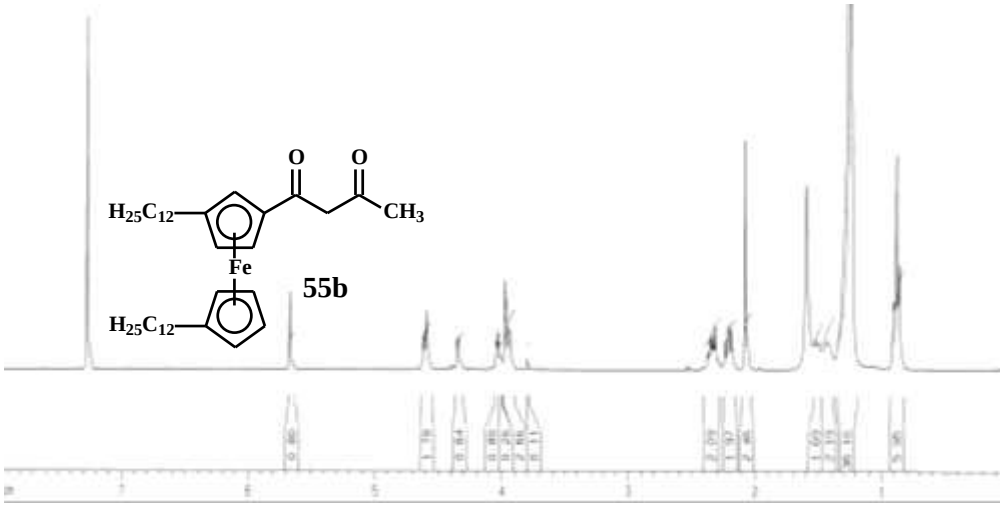

Spectrum 47: 1-[1,1′-di(dodecyl)ferrocenyl-3-]-butane-1,3-dione, 55b.

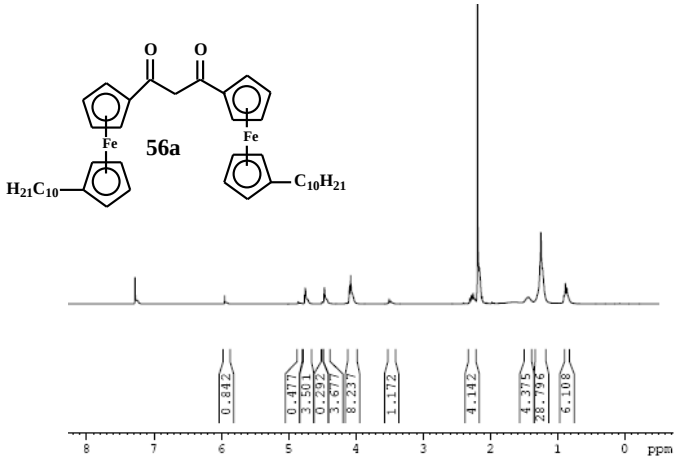

Spectrum 48: 1,3-di-[-(1-decyl)ferrocenyl-1′-]-propane-1,3-dione, 56a.

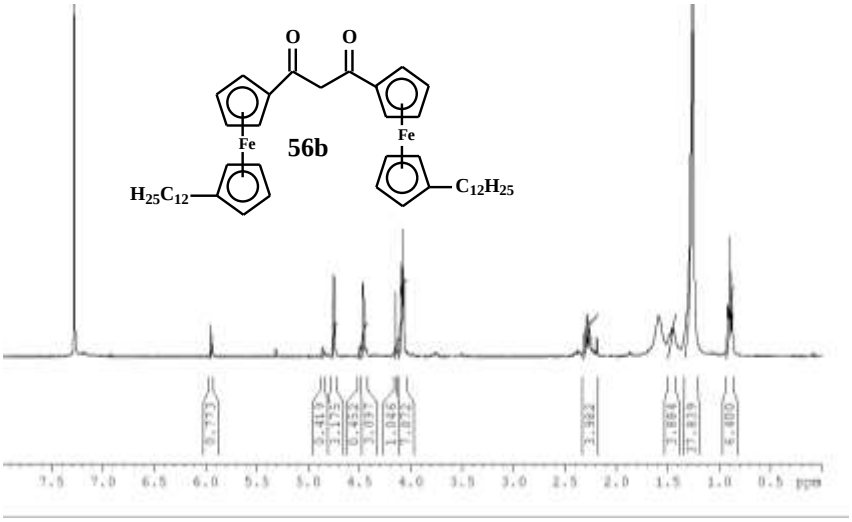

Spectrum 49: 1,3-di-[-(1-dodecyl)ferrocenyl-1′-]-propane-1,3-dione, 56b.

Rhodium complexes:

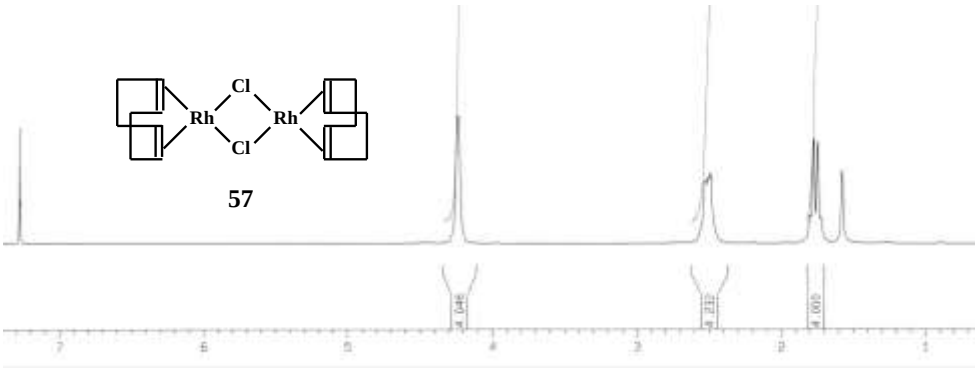

57

Spectrum 50: Di-μ-chloro-bis(η-cycloocta-1,5-diene)dirhodium(I) [Rh_2Cl_2(cod)], 57.

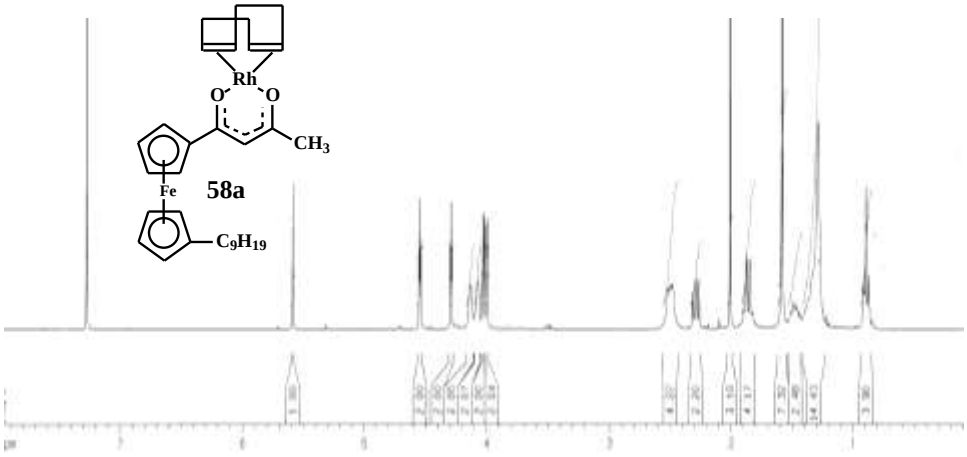

58a

Spectrum 51: [(η^4-1,5-cyclooctadiene){(1-((-1-nonyl)ferrocenyl-1′-)-butane-1,3-dionato-κ^2*O*,*O*′)}rhodium(I)], 58a.

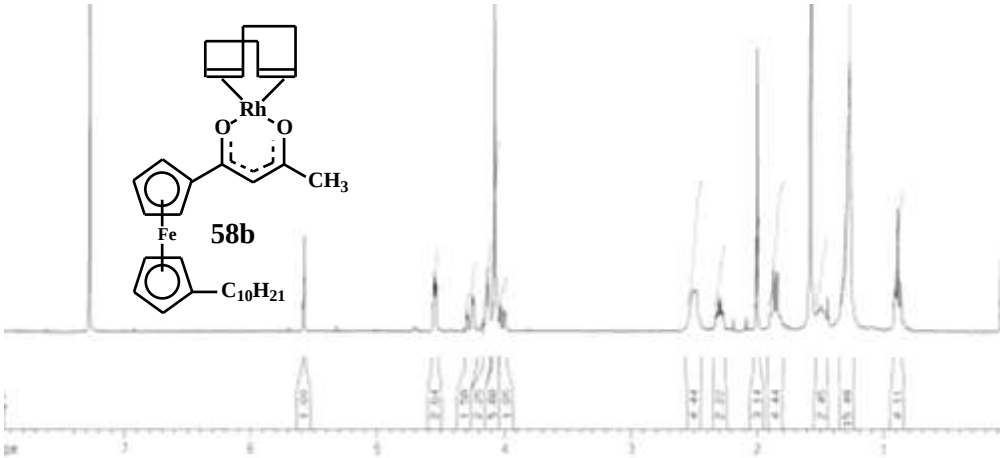

58b

Spectrum 52: [(η^4-1,5-cyclooctadiene){(1-((-1-decyl)ferrocenyl-1′-)-butane-1,3-dionato-κ^2*O*,*O*′)}rhodium(I)], 58b.

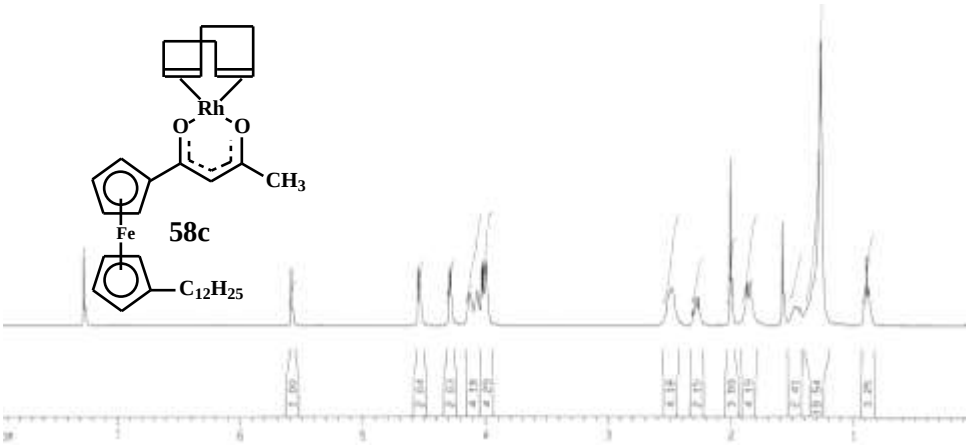

Spectrum 53: [(η^4-1,5-cyclooctadiene){(1-((-1-dodecyl)ferrocenyl-1′-)-butane-1,3-dionato-κ^2*O*,*O*′)}rhodium(I)], 58c.

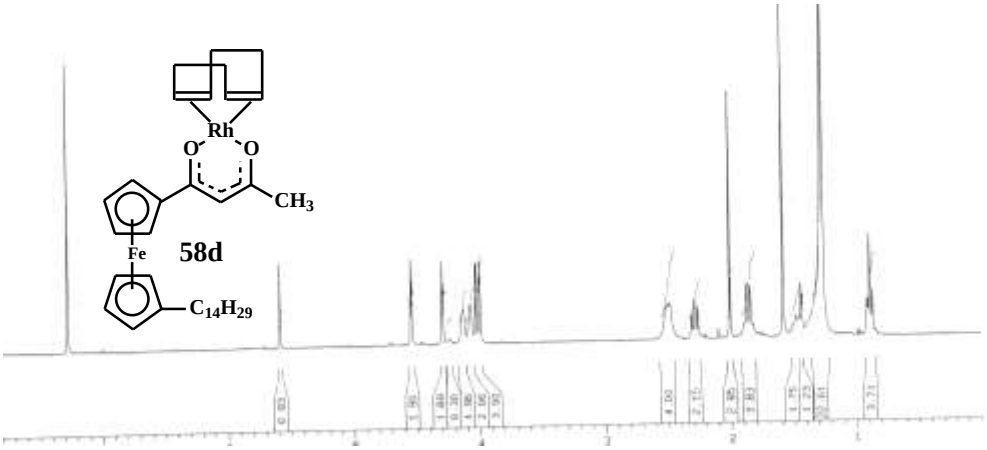

Spectrum 54: [(η^4-1,5-cyclooctadiene){(1-((-1-tetradecyl)ferrocenyl-1′-)-butane-1,3-dionato-κ^2*O*,*O*′)}rhodium(I)], 58d.

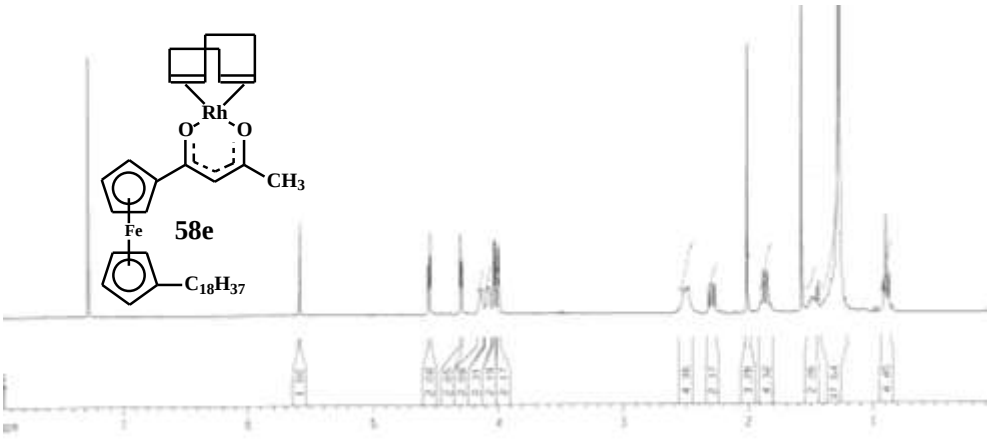

Spectrum 55: [(η^4-1,5-cyclooctadiene){(1-((-1-octadecyl)ferrocenyl-1′-)-butane-1,3-dionato-κ^2*O*,*O*′)}rhodium(I)], 58e.

Spectrum 56: [(η^4-1,5-cyclooctadiene){(1-((-3-decyl)ferrocenyl-1-)-butane-1,3-dionato-κ^2*O*,*O*′)}rhodium(I)], 59a.

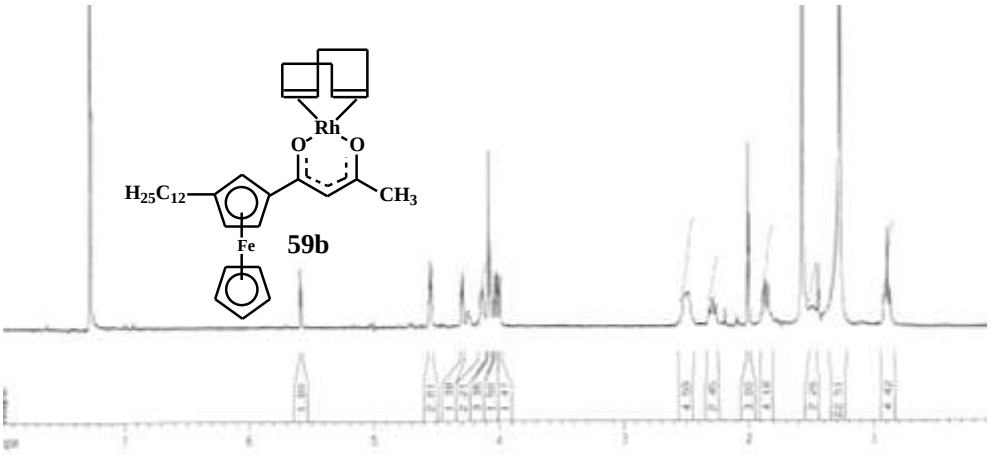

Spectrum 57: [(η^4-1,5-cyclooctadiene){(1-((-3-dodecyl)ferrocenyl-1-)-butane-1,3-dionato-κ^2*O*,*O*′)}rhodium(I)], 59b.

Spectrum 58: [(η^4-1,5-cyclooctadiene){(1-((-1,1′-di(decyl))ferrocenyl-3-)-butane-1,3-dionato-κ^2*O*,*O*′)}rhodium(I)], 60a.

Spectrum 59: [(η^4-1,5-cyclooctadiene){(1-((-1,1′-di(dodecyl))ferrocenyl-3-)-butane-1,3-dionato-κ^2*O*,*O*′)}rhodium(I)], 60b.

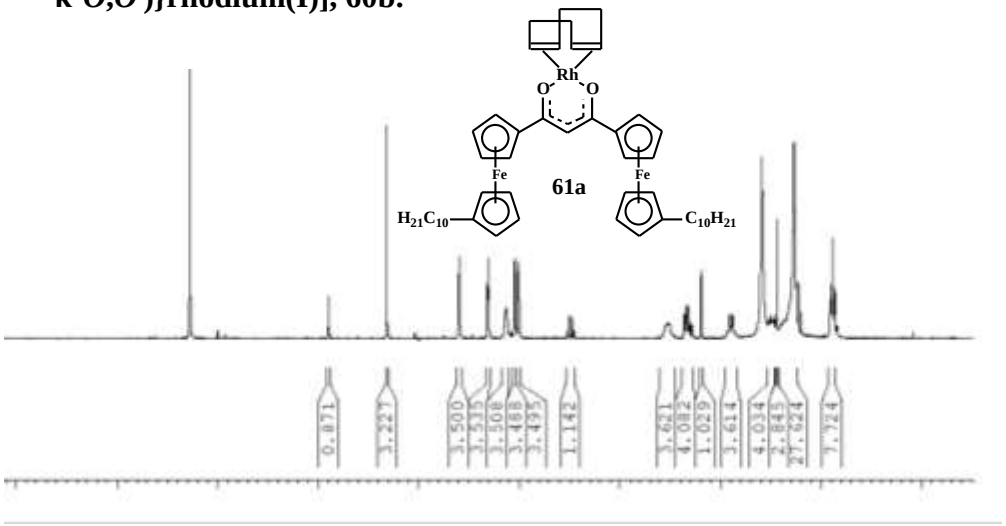

Spectrum 60: [(η^4-1,5-cyclooctadiene){(1-((-1,3-[-di-(1-decyl))ferrocenyl-3-)]-propane-1,3-dionato-κ^2*O*,*O*′)}rhodium(I)], 61a.

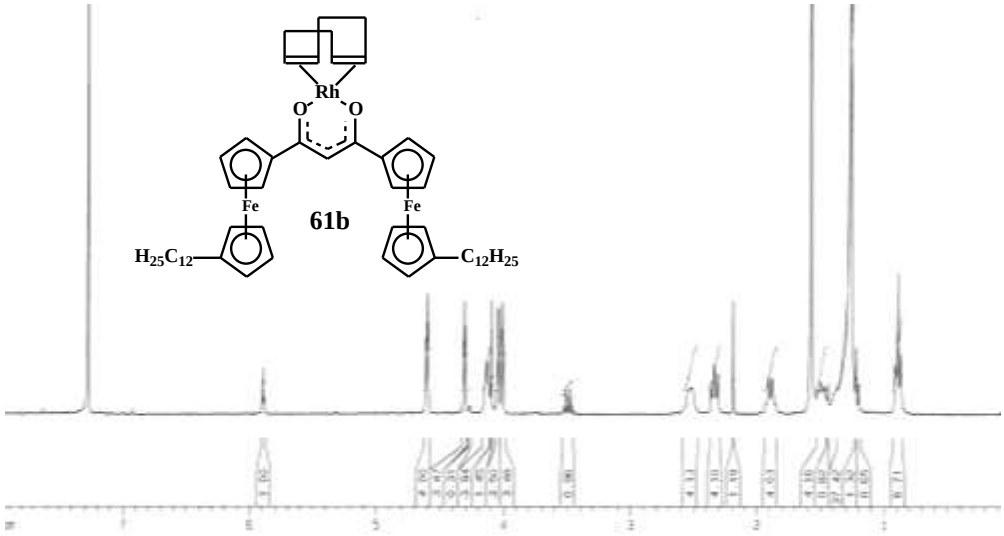

Spectrum 61: [(η^4-1,5-cyclooctadiene){(1-((-1,3-[-di-(1-dodecyl))ferrocenyl-3-)]-propane-1,3-dionato-κ^2*O*,*O*′)}rhodium(I)], 61b.

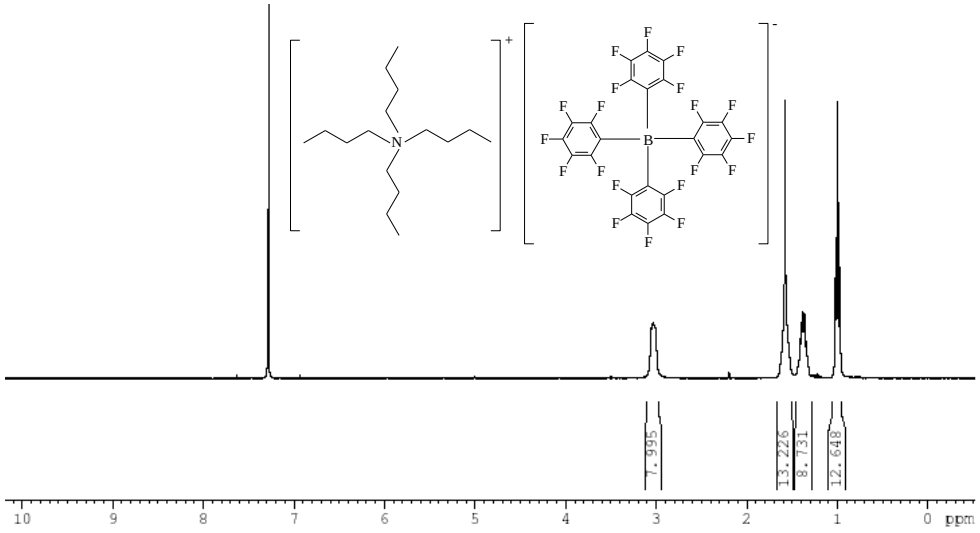

Spectrum 62: Tetrabutylammonium tetrakis[pentafluorophenyl]borate.

I, Patrick Thabo Ndaba Nonjola, declare that the thesis hereby submitted by me for the Philosophiae Doctor degree at the University of the Free State is my own independent work and has not previously been submitted by me at another university/facility. I further more cede copyright of the thesis in favour of the University of the Free State.

Signed …….. Date ……...